The background of the cover features a stylized mass spectrum. It consists of several vertical bars of varying heights, with the tallest bar in the center. The bars are rendered in a dark teal color against a lighter teal background. The overall design is modern and scientific.

# **INTEGRATED BIORECOGNITION MASS SPECTROMETRY APPROACHES**

**Ariadni Geballa-Koukoul**

# Propositions

1. Chromatographic separation is not necessary to achieve specificity in food safety contaminants monitoring. (this thesis)
2. Portable mass spectrometry is the future of on-site food safety testing. (this thesis)
3. For the development of consumer-operable biosensors, end-users must be involved throughout all stages; from research to deployment.
4. Inclusive and reproducible science is impossible without true open science.
5. The solution to the emergence of pseudosciences is science communication.
6. Political correctness in comedy could lead to self-censorship practices.
7. Euripides' concept of "appearance and reality" is now more relevant than ever.

Propositions belonging to the thesis, entitled:  
***Integrated biorecognition-mass spectrometry approaches***  
**Ariadni Geballa-Koukoul**  
Wageningen, 29 November 2022

# **Integrated Biorecognition – Mass Spectrometry Approaches**

Ariadni Geballa-Koukoulou

## **Thesis committee**

### **Promotor**

Prof. Dr M.W.F. Nielen

Special professor, Analytical Chemistry, with special emphasis on the detection of chemical food contaminants

Wageningen University & Research

### **Co-promotor**

Dr A. Gerssen

Program Manager WOT Food Safety Enforcement

Wageningen University & Research

### **Other members**

Prof. Dr H. A. Schols, Wageningen University & Research

Prof. Dr A. M. Rijs, VU Amsterdam

Prof. Dr M. Suman, Barilla & Università Cattolica del Sacro Cuore, Italy

Prof. Dr M.P. Marco, IQAC-CSIC, Barcelona, Spain

This research was conducted under the auspices of the Graduate School VLAG (Advanced studies in Food Technology, Agrobiotechnology, Nutrition and Health Sciences).



# **Integrated Biorecognition – Mass Spectrometry Approaches**

Ariadni Geballa-Koukoulou

## **Thesis**

Submitted to fulfilment of the requirements for the degree of doctor  
At Wageningen University  
by the authority of the Rector Magnificus,  
Prof. Dr A. P. J. Mol,  
in the presence of the  
Thesis Committee appointed by the Academic Board  
to be defended in public  
on Tuesday 29 November 2022  
at 4 p.m. in the Omnia Auditorium.

Ariadni Geballa-Koukoura  
Integrated Biorecognition – Mass Spectrometry Approaches  
178 pages

PhD thesis, Wageningen University, Wageningen, NL (2022)  
With references, with summary in English  
DOI: [10.18174/576841](https://doi.org/10.18174/576841)  
ISBN: 978-94-6447-402-2

*It always seems impossible until it's done.*

Nelson Mandela



# Table of Contents

<b>1</b>	<b>General Introduction</b>	<b>9</b>
<b>2</b>	<b>Direct Analysis of Lateral Flow Immunoassays for Deoxynivalenol Using Electrospray Ionization Mass Spectrometry</b>	<b>39</b>
<b>3</b>	<b>Development and Validation of a Semi-quantitative Direct Analysis in Real Time Tandem Mass Spectrometry (DART-MS/MS) Approach to the Analysis of Lateral Flow Immunoassay for Deoxynivalenol</b>	<b>61</b>
<b>4</b>	<b>Immuno-enriched Microspheres - Magnetic Blade Spray Tandem Mass Spectrometry for Domoic Acid in Mussels</b>	<b>87</b>
<b>5</b>	<b>Immunoaffinity Plastic Blade Spray Mass Spectrometry for Rapid Confirmatory Analysis of Food Contaminants</b>	<b>115</b>
<b>6</b>	<b>General Discussion &amp; Future Perspectives</b>	<b>133</b>
	<b>Summary</b>	<b>157</b>
	<b>Acknowledgments</b>	<b>161</b>
	<b>Curriculum Vitae</b>	<b>169</b>
	<b>Overview of Completed Training Activities</b>	<b>173</b>



## **General Introduction**







## 1.1 Preface

"The art and science of determining what matter is and how much of it exists" (1) is one definition of analytical chemistry. Fine arts and analytical chemistry alike employ techniques and means that undergo trends. Just like "Pablo Picasso," "Salvador Dali," and "Vincent van Gogh" are known for the use of classic artistic tools, mass spectrometry, spectroscopy, and biosensors or bioassays are classic tools that dominate analytical chemistry. But what about the artistic trends of the 21<sup>st</sup> century? We meet "Melissa McCracken," "Kara Walker," or even "Benjamin Shine," who combine diverse classic artistic traits and techniques to create contemporary art. Then why not apply the same approach to the "art" of analytical chemistry by combining the "classics" to form a new era?

This thesis in analytical chemistry illustrates combinations of classic analytical techniques, i.e., mass spectrometry and biorecognition elements conventionally used in bioassays or biosensors. Led by "artistic" and scientific impulse and curiosity, the inspiration for this innovative scientific approach is to form contemporary analytical methods with many potential applications in future monitoring systems.

## 1.2 Future of monitoring systems

Bioassays and biosensors are employed as screening tests in monitoring systems. They are ideal for frequent, fast, and on-demand testing of substances above a specified cut-off level. Suitable screening assays are characterized by a false-compliant rate of lower than or equal to 5%. Nonetheless, screening assays do not identify a specific substance in the sample (2, 3), and because of this uncertainty, confirmatory testing should follow, identifying (and quantifying) the specific substance causing the positive screening result (3). Confirmation is typically done with chromatography coupled to mass spectrometry (MS), providing an absolute and unequivocal identification. Despite this, confirmation is expensive, requires energy-laboring machinery, and is time-consuming, because of the extensive sample preparation and chromatographic separation needed (4–6).

In an ever-changing world, it is doubtful that the monitoring systems will remain stable. Production, processing, distribution, and consumption of goods (and services) are changing due to an unparallel confluence of exogenous pressure and trends (7). Socioeconomic shifts, including the rising population, the broad awareness of environmental and equity issues, and new technological approaches, including citizen science, are prevalent changes affecting peoples' lives. By 2050, it is estimated that two-thirds of the population will be residing in cities, and megacities with ten million people will not be rare (8). Current monitoring systems and approaches will prove inefficient to the increased demand if adjustment is not achieved in due time. The necessity for alternative methods is also underlined by the United Nations 2030 agenda for sustainable development goals (SDGs); a call for people, countries, and

stakeholders to act on improving natural resources and ensure enduring socio-economic growth and planet protection (9).

Another trend that might shape the future structure of monitoring systems is citizen science, i.e., collaboration and participation of citizens in scientific practices and research, for instance with the development of consumer-operable testing devices (10). Decentralized consumer-based testing provides individuals with the possibility of personalized point-of-care (POC) testing and screening diagnostics in many fields (11), including, but not limited to, food safety (12) and clinical applications (13, 14). On top of that, use of a ubiquitous readout system, such as smartphones, potentially in combination with wearable sensors, induces semi-quantitative possibilities and increases confidence in interpreting the result (15). Apart from the described citizen science approach during product deployment, crowdsourcing in science during the research and development (R&D) stage can improve practices and results, influencing directly the targeted population (10).

An additional challenge for the future monitoring systems is climate change-induced changes. Results of climate change vary from extreme drought to rise of sea levels, which amend the quality of life of individuals worldwide (16). Especially in terms of monitoring systems, the food safety sector, involving farming, crop production, and the nutritional content of crops, has already been impacted by long-term variations in temperature, humidity, and the frequency of extreme weather phenomena (17). Climate change may alter crops' susceptibility to germs, toxin-producing bacteria and mycotoxin-producing fungi, risking consumers' health. Even marine species are in danger because of the proliferation of toxin-producing algae because of increased temperatures (18). The results of climate change on crop production are already evident in literature where a 25% of global agricultural crop contamination with mycotoxin is estimated to be above the legal limits (19), underlining the need for fast, unambiguous identification and quantification of food contaminants.

It is safe to assume that current monitoring protocols will be insufficient in the future because of the increased demand for official control from monitoring laboratories that will be caused due to the aforementioned changes. Already, despite its elaborate monitoring procedures, the food-safety system has been stressed, with incidences of food safety-related scandals and contaminated commodities reaching the market (20, 21). Combining screening and confirmation methods, two seemingly incompatible orthogonal techniques, provides improved and accurate methods with high throughput, sensitivity, robustness, and ease of use, which are necessary for future monitoring systems. To offer an elaborate background and understanding, the following parts of the introduction describe the classic analytical chemistry techniques that are coupled in order to develop the novel approaches discussed in the research chapters.

### 1.3 Biorecognition

Since the description of the first-ever biosensor by Clark and Lyon in 1962, an amperometric glucose meter (22), the field has expanded a lot, with the modern

glucose-meter biosensor being the most common commercial sensor (23). Biosensors and bioassays allow for highly sophisticated applications and POC diagnostics with an increased impact on the lives of individuals and multiple citizen science applications (24). Especially during the COVID-19 pandemic, the increased use of bioassays in self-tests for fast, sensitive, and specific POC applications has proven necessary (25, 26).

Biosensors' and bioassays' "heart" is the biorecognition element, which is used for the detection of a specific target analyte. The principal function of biorecognition elements in biosensors is analyte specificity for the application by having a selective and robust affinity towards the analyte. Due to the binding affinity towards an analyte, biorecognition is also named bio-affinity.

Various biorecognition elements exist, each with unique features, enabling different performances. Antibodies and enzymes are naturally/biologically derived biorecognition elements. Contrary, molecularly imprinted polymers (MIP) are artificially manufactured cavities that mimic specific biomolecular interactions. An intermediate that shares features of both categories are pseudo-natural modalities, i.e., tailor-made supramolecular structures from natural subunits, such as aptamers, synthetic enzymes and synthetic antibodies (27).

### 1.3.1 Immunorecognition

Immunorecognition is the biorecognition originating from antibodies. Antibodies (Immunoglobulins - Ig) are naturally occurring proteins of five primary classes (IgG, IgM, IgA, IgD, and IgE) and having a characteristic "Y"-shaped three-dimensional (3D) structure, consisting of two light and two heavy chains (28). Owing to that exact 3D shape, antibodies demonstrate a uniquely specific and accurate recognition pattern based on affinity between the antigen/analyte that binds at the fragment antigen-binding (Fab) region, forming an immunocomplex, and the fragment crystalline (Fc) region of the antibody which interacts with the respective cell receptors activating the immune response (29, 30) (Figure 1.1)

Among the many different types of antibodies, monoclonal antibodies (mAb) are identical clones produced using a hybridoma technology. Briefly, mice are immunized with the targeted analyte (that acts as antigen), and then the antibody-producing cells (B lymphocytes) are isolated. Consecutively, the isolated cells are fused with immortal myeloma cell lines forming hybrid cells, which are then cultured to produce mAb. Due to the use of an individual hybrid cell line, monoclonal antibodies are selective towards a specific antigen and less cross-reacting with other co-occurring analytes (31). Owing to this high selectivity, mAb dominate the biosensors field with various applications, even though their production is costly, laborious due to the extensive purification needed, and controversial because of the usage of laboratory animals (32).

Many methods have been developed for antibody immobilization in immunoassays, ranging from simple physical adsorption involving hydrophobic interactions, to a comparatively more intricate chemistry involving active groups (e.g., amine covalent coupling using 1-Ethyl-3-(3-dimethylaminopropyl)carbodiimide / N-

Hydroxysuccinimide (EDC/NHS)) (35, 36). Using different immobilization procedures, antibodies have been employed in various immunoassay formats, including lateral flow immunoassays (LFIA), surface plasmon resonance (SPR) based immunoassays and microsphere-based immunoassays, which are used in the experimental section of the thesis and are described in general terms in the following sections.

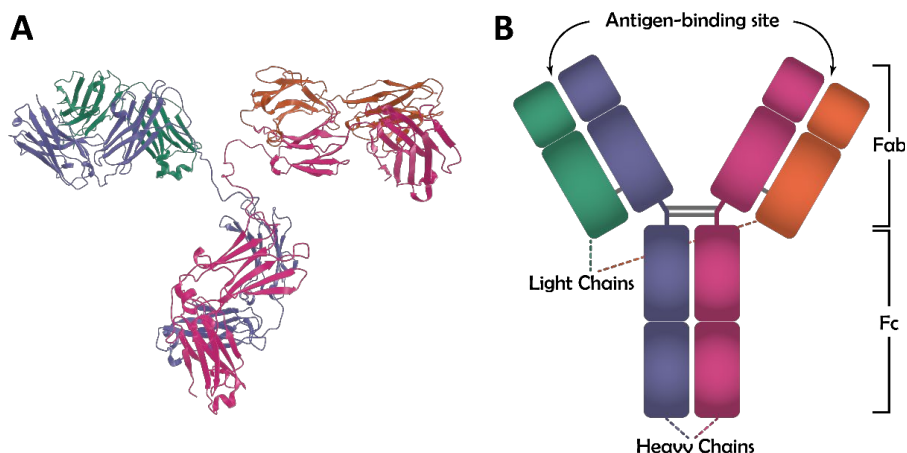


**Figure 1.1.** (A) Crystal structure of antibody (IgG type) showing its characteristic Y shape (33, 34) (B) Annotated figure showing the regions of the antibody. The heavy chains are in pink and purple, and the light chains in green and orange.

Additionally, different immunoassay formats can be chosen, depending on the targeted application. The format of an immunoassay is defined by interactions between the targeted analyte, which acts as an antigen, and the components of the immunoassay, i.e., antibodies and/or (analyte-protein) conjugates that can act as capture agents and/or detection agents (37). The most straightforward format to use for big-sized molecules with many antigenic sites is a "direct immunoassay". In direct immunoassays, a measurable signal is produced when the analyte binds directly with a capture antibody immobilized on the assay surface, forming an immunocomplex. If the immunocomplex does not produce a measurable signal alone, a detection antibody can be employed that binds to a separate antigenic site of the targeted analyte, leading to the configuration of a "direct sandwich immunoassay". In the described formats, the signal attained is proportional to the concentration of the analyte in the sample (Figure 1.2) (38, 39).

For small-sized molecules with a single antigenic site, the case is reversed to that of big-sized molecules, since the attained signal is inversely proportional to the concentration of the analyte in the samples. The main format used for small-sized molecules is a competitive assay, where the analyte competes with an (analyte-)conjugate for binding with the antibody. In the absence of the analyte from the sample, the conjugate binds with the antibody, leading to a measurable signal production, while, in the presence of the analyte, the conjugate and the analyte compete for

binding with the antibody. Two main formats can be generated with the given interactions; (i) "competitive immunoassay," where the antibodies are immobilized on the assay surface, and the conjugate acts as a detection agent, and (ii) "inhibition immunoassay" where the conjugate is immobilized on the surface, and the antibody act as the detection agent (*Figure 1.2*).

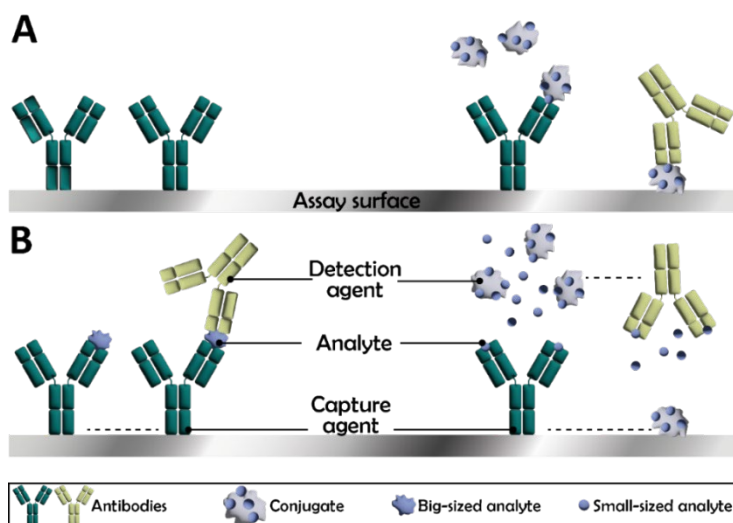


**Figure 1.2.** Schematic demonstrating the different types of immunoassay formats from left to right: direct immunoassay, direct sandwich immunoassay, competitive immunoassay and inhibition immunoassay. (A) in the absence of analyte, and (B) in the presence of analyte

### Lateral flow immunoassays (LFIAs)

LFIAs are generally fast, easy-to-use, affordable paper-based immunoassays for qualitative and occasionally semi-quantitative detection of specific analytes. The principle of the LFIA detection is relatively simple; a liquid sample or a sample extract, diluted with the assay buffer, passively wicks through the porous substrate, most commonly a nitrocellulose paper, due to capillary action, while reacting with molecules immobilized on the substrate, forming a test and a control line. For an optical signal attainment, the detection agent is labeled with labels such as dyed polystyrene beads, carbon nanoparticles, or gold nanoparticles. After LFIA development, the appearance of a control line indicates that the assay has been performed correctly. However, the presence or absence of a test line depends on the chosen immunoassay format. A positive result is indicated by the appearance of the test line, for a sandwich immunoassay format, while, for a competitive assay format, a positive result is indicated by the absence of the test line (40, 41) (as also described in 1.3.1) (*Figure 1.3*).

LFIAs' distinct user-friendliness has led the LFIA market to grow exponentially with a plethora of applications, ranging from medical diagnostics (42–46), food safety (47–50), forensics (51–53), and many more (54). Also, the on-site usability of LFIAs, without the need for a sophisticated operational and readout system or refrigeration

for their storage, makes them attractive for use in low-resource settings, thereby yielding a potential positive social impact (24,53–56). Despite all those advantages, it should not be overlooked that LFIA development still faces scientific challenges, such as the correct choice of label and format, or false negatives/positives occurrence, that analysts should overcome during the R&D process (59).

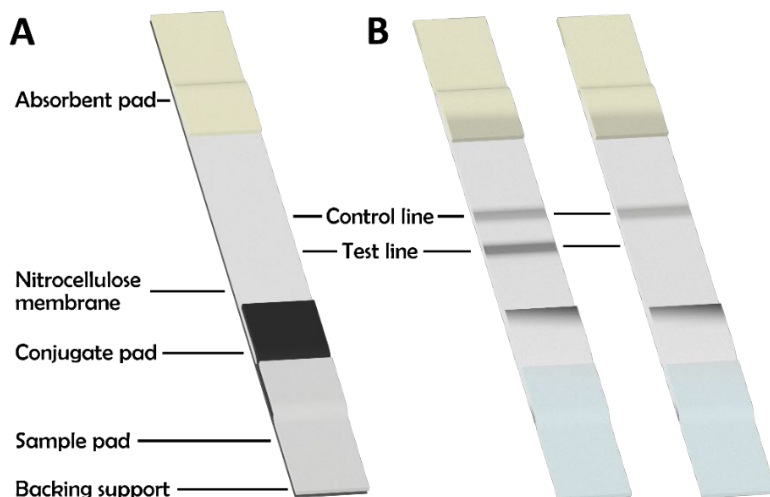


**Figure 1.3.** (A) The structure of a typical singleplex (i.e., detecting one analyte) LFIA strip before assay development. The different constituents of the LFIA are indicated. (i) backing support on top of which the different elements are deposited, (ii) sample pad where the sample is deposited, (iii) conjugate pad enriched with the labeled/signaling antibody, (iv) nitrocellulose membrane with immunorecognition areas, and (v) absorbent pad by the end of the LFIA that the non-reacting molecules are collected after traveling through the different zones of the LFIA. (B) Direct sandwich LFIA after assay development, demonstrating a positive result (presence of test and control line) and a negative result (presence of control line).

An extension of the classic LFIAs are LFIAs with smartphone readout, which take advantage of the optical components of a smartphone, i.e., camera and flash-light, for the interpretation of the optical result. Smartphones provide homogeneity of the readout by eliminating ambient light differences, either by the in-built ambient light sensor (ALS) of the smartphone and performing color calibration (60) or by an instrumental interface (e.g. 3D-printed attachment/enclosure) (61), adding confidence to the user for correctly interpreting the LFIA result (62, 63). Moreover, they offer more accurate quantification prospects, automated input processing, network connectivity with sharing capabilities, online data handling, geo-positioning, and result storage (64, 65). The immense market size of smartphones proves a well-adopted system (66, 67), and smartphone-based LFIAs offer laypersons the possibility of a democratizing and decentralized approach to healthcare and food safety by personal, accurate analysis, and confident interpretation of the screening result (68). Nonetheless, operating system differences between smartphone models and constant need

for smartphone software upgrades, hinder broader adaptation with the need for individualized design of smartphone application. Also, in many scientific reports on smartphone-based LFIA, it is indicated that the images are processed after the acquisition and on a separate device (e.g. a personal computer), losing the aim of fast, on-site testing (69). Ideally, consumer-friendliness could be enhanced with the development of smartphone applications with a simplified interface for offline data handling (70). Despite those limitations, various food safety (71–73) and medical-related (74, 75) applications have been developed thus far and made commercially available.

### SPR-based immunorecognition

Surface Plasmon Resonance (SPR) occurs when a monochromatic and plane-polarized light (incident light) strikes a thin metal layer at a certain angle. Part of the light is absorbed, and the rest is reflected, giving rise to an evanescent field and wave perpendicular to the metal. From the evanescent wave, excitation of free electrons of the metal gives rise to the wave of surface plasmons. The angle that triggers the generation of plasmons depends on the material's refractive index. Minor changes in the surface properties lead to analyte detection by measuring the intensity of the reflected light or the shift in the resonance angle.

In most SPR biosensor applications, the phenomenon occurs on an SPR chip, consisting of a glass surface coated with metal. The metal typically employed is gold because of its chemical inertia to the measurement conditions and because it provides reflectance angle and wavelength signal within measurable rates (76). On top of the metal layer, a self-assembled monolayer is deposited and is further activated to act as a linker for a functional antifouling layer, e.g., dextran. After chemical activation, the desirable molecule can be immobilized on the layer, thus creating an immunorecognition-capable surface (*Figure 1.4*).

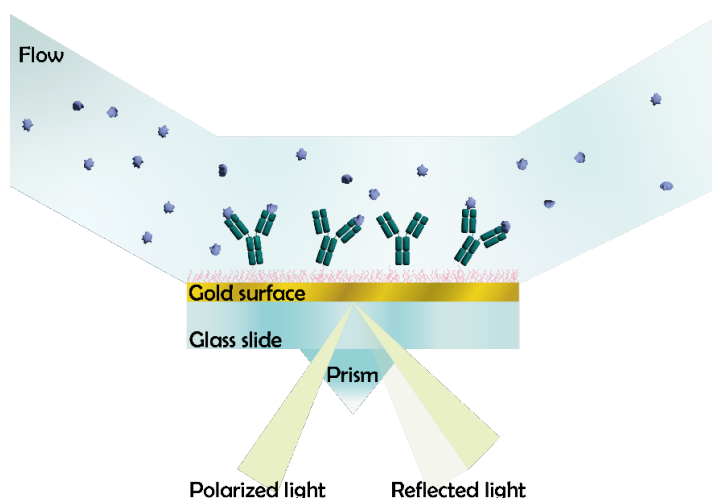


**Figure 1.4.** Schematic illustration of a direct SPR-based immunoassay, highlighting the different components of an SPR chip. The analyte is indicated with light blue inside the liquid flow on top of the SPR chip, and the surface is enriched with antibodies.

After introducing the analyte on the surface through liquid flow, an immuno-complex with sufficient mass difference is formed, and the refractive index of the polarized light shifts, generating the SPR signal. The SPR signal is recorded over time in a sensogram (Figure 1.5). The intensity of the signal is measured in response units (RUs), and it is proportional to the number of immunocomplexes formed at the surface, which permits quantitative analysis. Same as with the LFIA, different formats of SPR methods can be employed depending on the type of the targeted analyte (77, 78)

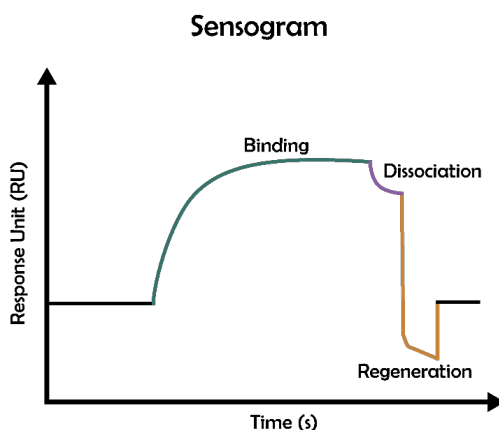


**Figure 1.5.** SPR signal recorded on a sensogram based on differences in the surface properties due to the immunocomplex formation.

SPR studies allow for label-free exploration of biomolecular interactions (79–81), elucidation of the binding kinetics, and qualitative assessment of the immunorecognition specificity, sensitivity, and speed (82–84). SPR has many bio-analytical applications (13, 85–88); however, the bulky instrumentation does not enable on-site detection or consumer-operable simplified analysis (89). An alternative to those limitations is the use of smartphone-based SPR. Similar to the smartphone-based LFIA, smartphone-based SPR uses the light source, the photodetector, the processor, and the device interface to produce miniaturized-portable SPR systems with similar potentials as the benchtop SPR instrumentation (90–92).

### Microsphere-based immunorecognition

Microspheres, typically used in suspension or planar array systems, come in different types suitable for different applications. All microspheres are internally dyed with different proportions of red and infrared fluorophores, which can be excited using a red classification laser at 635 nm and correspond to a distinct spectral signature. Further, a fluorescently-labeled detection antibody is excited by the presence of a green reporter laser at 525–532 nm. This double fluorescent detection provides options for simultaneously detecting at different wavelengths, thus facilitating multiplexing. The microspheres typically used in immunoassays are 5.6  $\mu\text{m}$  size polystyrene beads whose surfaces have approximately  $10^8$  carboxyl groups that can



covalently bind molecules, modifying the surface with the desired bio-recognition element according to the targeted application. An alternative version of standard microspheres is paramagnetic microspheres, which are slightly larger because of an extra paramagnetic layer of magnetite (*Figure 1.6*). The paramagnetic properties of those microspheres enable attachment on a surface using a strong magnet, which eases washing that eliminates unwanted sample constituents.

Microsphere-based immunorecognition is well adopted in the xMAP technology, where x stands for analyte and MAP for Multi-Analyte Profiling. With xMAP, analysis of a 96-well plate takes less than 60 minutes, corresponding to an analysis time of less than 1 minute per sample (93–95). The bottleneck of microsphere-based immunorecognition assays is that the procedure for surface enhancement/modification of the microspheres is elaborate because of the covalent binding (96, 97). Further, limited alternatives bypass the benchtop instrumentation to move towards applied on-site experimentation (98) and citizen science using smartphones (99, 100).

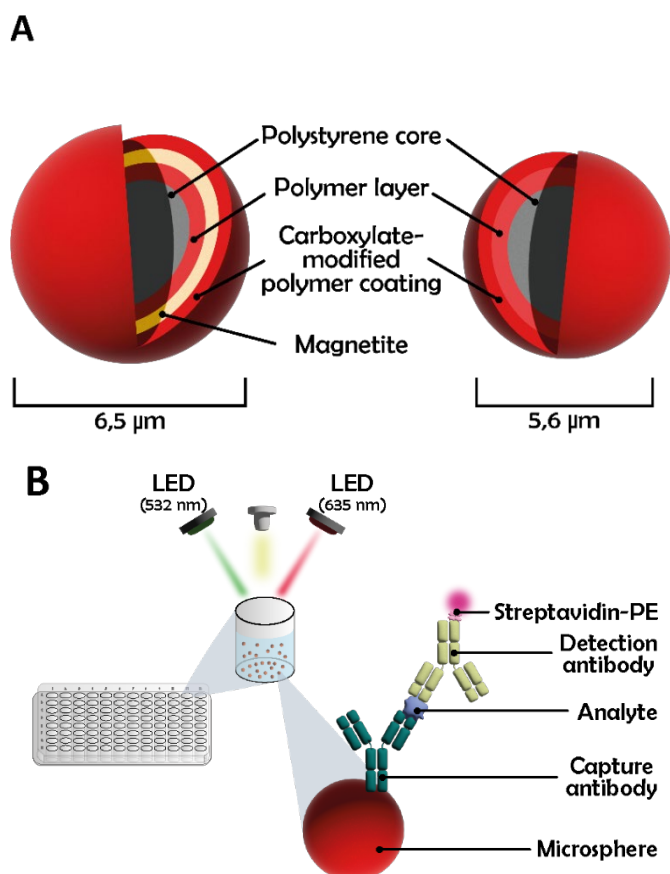


**Figure 1.6.** Illustration of (A) a microsphere and a paramagnetic microsphere with their distinct layers, and (B) the biorecognition-based principle for analyte detection using sandwich-based immunoassay demonstrating the different detection parameters.

## 1.4 Mass spectrometry

Mass spectrometry (MS) is a fundamental analytical technology proven by its applications ranging from clinical (100–102), food (103–105), environmental (106,107), and even forensics, airport security, and space missions (108–110). As early as the beginning of the 20<sup>th</sup> century, J.J. Thomson developed the parabola spectrograph, the first-ever mass spectrometer, which operated under the same main principles as the modern mass spectrometers (111,112). MS principles are based on the generation of ions of molecules, separation based on their mass-to-charge ratio ( $m/z$ ), i.e., the molecular mass of molecules or their fragments divided by their charge, detect the separated ions and qualitative or quantitative record them based on the different  $m/z$  and their (relative) abundance. A mass spectrum results from this process, with the  $m/z$  values on the x-axis and the relative or absolute abundance on the y-axis. The MS identification principle dictates the three main components of an MS instrument: the ionization source, the mass analyzer, and the detector (113,114). Below, the ionization sources and analyzers used in this thesis are discussed (Figure 1.7).

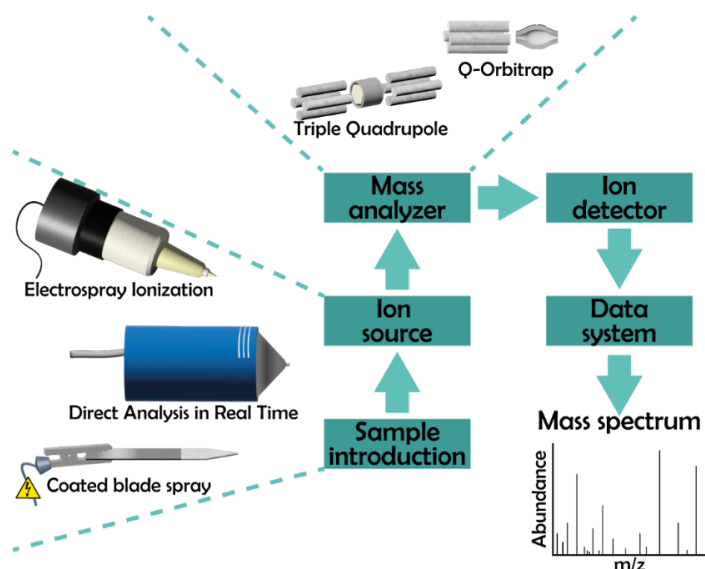


**Figure 1.7.** Schematic illustration of the main components of a mass spectrometer focusing on the ionization sources and the mass analyzers that are used in the experimental section of the thesis.

### 1.4.1 Ionization sources

So far, various ionization sources have been developed differentiating in many aspects including the transfer of the internal energy or the analyte compatibility. For instance, ionization sources using hard ionization methods are very energetic and induce fragmentation, whereas soft ionization techniques only produce ions of the molecular species. In general terms, ions are formed by electron ejection or capture,

protonation, deprotonation, adduct formation, or transfer of charged species to neutral molecules in the gas phase (116–118).

### Conventional ionization sources – Electrospray Ionization (ESI)

The story behind developing the first electrospray ionization (ESI) source starts with the study of the electrospray process as early as 1882 by Lord Rayleigh (119). However, it was not until a century later, in 1989, that John B. Fenn and his group studied biomolecules by combining ESI with MS detection (120,121). For this contribution to science, John B. Fenn was awarded the Nobel Prize in Chemistry in 2002, underlying the impact ESI has on science (122). All initial applications of ESI focused on the analysis of large biomolecules. However, the use of ESI has expanded to other fields, including analyzing smaller molecules in clinical (123–126), food safety (127–129), anti-doping control (130), environmental applications (131–134), and structural elucidation (135–137).

Ion generation in ESI begins when liquid containing the target analyte is introduced in the ionization source which is at atmospheric pressure, through a narrow metal capillary that is on high voltage. Due to the difference in potential between the capillary and the inlet of the mass spectrometer the liquid is dispersed into charged droplets. At first the so-called Taylor cone (138) is formed from the end of the liquid due to an increase in the electrostatic force as a result of the accumulation of ionic charge. Subsequently, smaller charged droplets are ejected from the cone. Further gas-aided solvent evaporation leads to an increase in the charge per volume unit where Coulomb repulsive surface forces are too strong (Rayleigh limit) (119), leading to droplet fission. After a few generations of subsequent fission events, the charged droplets reach nanometer scale, generating gas-phased ions and ejecting the charged analyte (138, 139) (Figure 1.8).

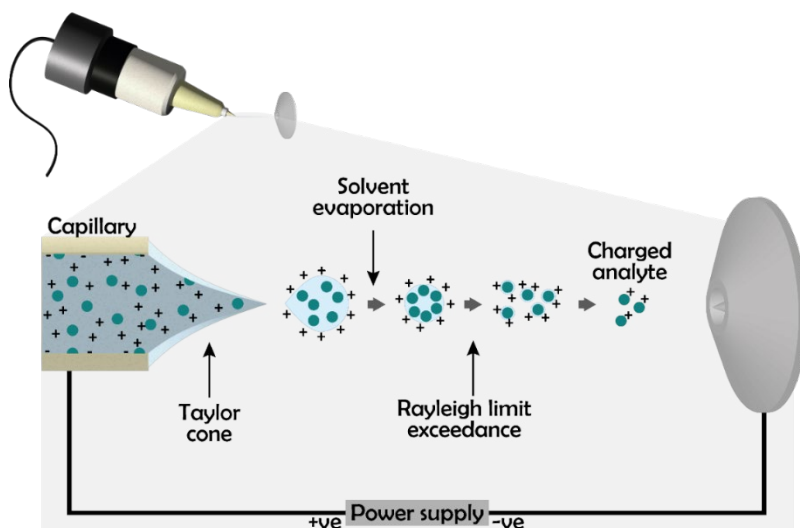


**Figure 1.8.** Illustration of ESI process for an analyte (teal spheres) - positive ionization mode.

ESI is a soft ionization technique, producing ions of the molecular species, with minimum fragmentation during ionization. For the ejection of charged analytes, multiple theoretical mechanisms have been described, namely, the ion evaporation model (IEM) for small molecule ionization, the charged residue model (CRM) for large globular species, and the chain ejection model (CEM) for disordered polymer ionization. A detailed description of each model can be studied in the feature article of 2013 from Konermann et al. (140, 141).

Following the ionization mechanism, it is clear that the constituents of the liquid sample solution are essential for ionization efficiency. Namely, solvents with lower surface tension and vaporization enthalpy promote ionization. However, non-volatile constituents, such as residues of non-volatile salts, or large co-eluting compounds, will hinder ionization causing ion suppression, i.e., reduction in the ionization efficiency and the produced signal (142, 143). Many mechanisms have been proposed to explain the ion suppression, most of which interpret the influence of constituents of an analytical workflow on the ionization. Main explanation for the ion suppression phenomenon is the reduction of analyte access to the gas phase emission stage, which can be done by: (i) increasing the viscosity and the surface tension of the droplets, so the droplets are unable to surpass the Rayleigh limit, (ii) competition between the targeted analyte and interfering compound for charge availability, (iii) co-precipitation of analyte after binding with the interfering matrix compounds, or (iv) neutralization of the targeted analyte ions due to the presence of a higher proton affinity co-existing compound (for positive ionization mechanism) (144–146). So, apart from carefully choosing the solvents used for ESI, it is crucial to minimize interferences with sample pre-treatment using extraction techniques (142, 143). Separation systems, such as liquid chromatography (LC), effectively allow co-eluting substances to separate in time. With LC-MS, data are acquired in a chromatogram, a graph of the time on the x-axis and the (relative) abundance on the y-axis, while a characteristic peak corresponding to a retention time appears when a substance elutes from the chromatographic column. The retention time is characteristic for an analyte under the specific separation conditions (147). Alternatively, to avoid chromatographic separation, a direct infusion can be used, jeopardizing, though, the ionization efficiency in case of an insufficiently cleaned sample (148–150).

### Ambient Ionization Sources

Ambient ionization mass spectrometry (AIMS) sources were developed in response to the demand for increased throughput analysis and the need for direct analysis without excessive sample pre-treatment and analyte chromatographic separation (151) (Figure 1.9). The first-ever AIMS source published was desorption electrospray ionization (DESI) in 2004 by the Cooks' research group (152), followed by direct analysis in real time (DART) in 2005 by Cody et al. (153). Ever since, more than 90 AIMS sources have been reported, each with its unique ionization mechanism, analyte compatibility, and applications which complicate their classification with a single categorization scheme (151, 154–156). The most comprehensive categorization of AIMS is based on the basic ionization principle into: (i) spray desorption/ionization-based

(ii) laser ablation/desorption-based (iii) thermal desorption-based, (iv) plasma-based, (v) substrate-based, and (vi) hybrid or other methods (157).

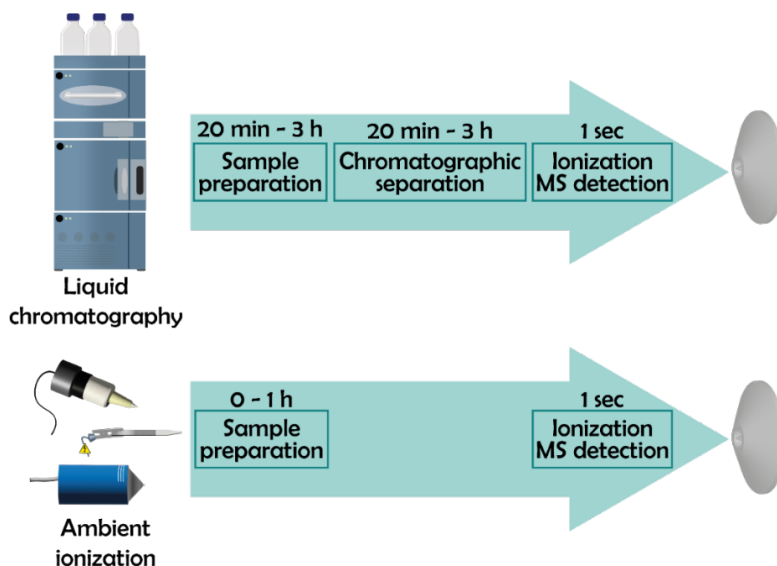


**Figure 1.9.** Indication of a time frame for a complete analysis using conventional (liquid) chromatography-MS compared to the time for a complete analysis using AIMS.

For an ionization source to be categorized as ambient, it must adhere to three basic rules. First, the ions are generated and maintained under atmospheric pressure before introducing them to the mass spectrometer. Second, no or minimal sample pre-treatment is required. Last, the analytes are directly desorbed or ionized from a sample surface or a sample extract. AIMS does not require chromatographic separation; thus, the data is retrieved not in a chromatogram but in a chronogram, which is, a graph of the time on the x-axis and the (relative) abundance on the y-axis, for which, however, unlike chromatograph the concept of retention time does not apply (158, 159). Lastly, AIMS sources are suitable for on-site applications because of the minimum sample preparation and solvent use, making them an excellent option for coupling with miniaturized, portable or transportable MS instrumentation for fast on-the-spot analysis (160–162).

#### **Direct Analysis in Real Time (DART)**

For DART ionization, a gas, usually helium (He) or nitrogen (N<sub>2</sub>), is subjected to corona discharge producing electrons, ions, and excited-state (metastable) atoms. In this way, an excited cold (50–60 °C) plasma is generated, which then undergoes removal of charged species by passing through a series of electrodes, generating plasma consisting of metastable electronically excited neutral species. Finally, the metastable plasma is (optionally) heated (up to 500 °C) (Figure 1.10). After the plasma is generated, it exits the DART chamber where it induces penning ionization of

ambient air constituents (reagents). For Helium (He) gas, the main reagents generated are: hydronium ion ( $\text{H}_3\text{O}^+$ ), superoxide ( $\text{O}_2^-$ ), hydroxyl radical ( $\text{HO}^\cdot$ ), ozone ( $\text{O}_3$ ), and slow electrons. Those active reagents subsequently lead to desorption and ionization of the analytes (153).

DART ionization is a soft ionization method, ionizing the analytes mainly via protonation and deprotonation. Additionally, DART is more efficient when increased plasma temperatures are used for the analysis of thermally stable, both polar and non-polar, volatile analytes with a molecular weight of no more than 1000 Da (156). DART has many applications, including food (163), forensics (161,162), environmental (166), and drug (167, 168) analysis.

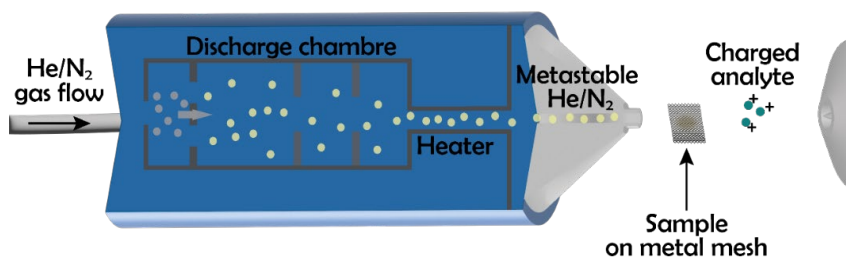


**Figure 1.10.** Illustration of DART and its functional parts that enable sample ionization.

### Coated Blade Spray (CBS)

CBS is an integrated sampling, sample preparation, sample introduction, and ionization method developed in 2014 by Gomez-Rios and Pawliszyn (169). CBS consists of a conductive stainless steel sheet in the form of a blade with a pointy edge covered by a coating. The sharp point of the blade is optimally angled at 45°. The geometry and coating of the blade allows for pre-concentration of the analyte through a solid-phase microextraction (SPME)-like mechanism on the coated substrate, followed by online desorption with less than 20  $\mu\text{L}$  of desorption solvent (170). Finally, by voltage application, an electric field is created between the blade and the MS inlet, which induces charge accumulation at the vertex of the blade, leading to an ESI-like ionization of the analytes (169). Details of ESI ionization process can be retrieved earlier in section 1.4.1. CBS is a time-saving method because the sample extraction and ionization happen from the same surface, and it requires minimum solvent usage (171), (Figure 1.11) while reaching detection and quantification limits similar to ESI (172).

Due to its simplicity of operation, without an external gas or liquid flow requirement, CBS has been used in various applications despite being at its early stages. Applications include: drugs (173), biofluids (174), wastewater (175), pesticide (176), and potential portable MS analysis (162), and Restek Corp (PA, USA) has already commercialized coated blades (177), which could pave the path for further applications.

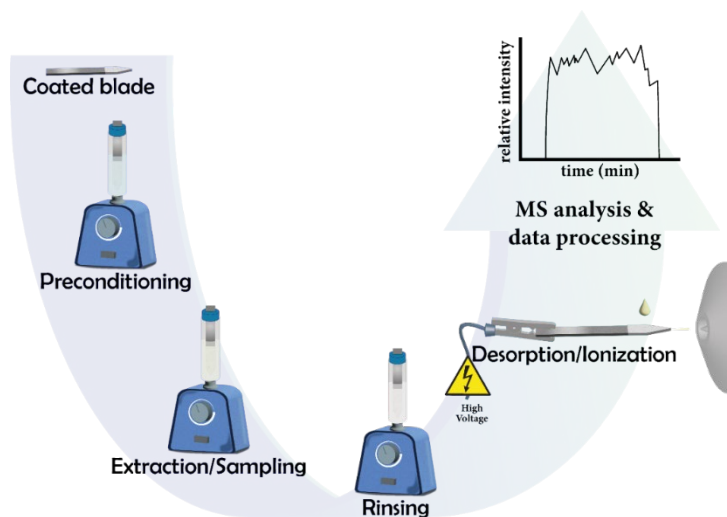


**Figure 1.11.** Schematic representation of a CBS-MS complete analytical protocol with all stages from sample to MS detection.

## 1.4.2 Mass analyzers

After analyte ionization in the ion source, the gas-phase ions move towards the mass analyzer in vacuum and are separated based on their mass-to-charge ratio ( $m/z$ ). Many available mass analyzers operate under different principles; magnetic or electric fields are applied, alone or in combination. The main attributes that characterize mass analyzers are the mass range, the speed of analysis (or scan speed), the ion transmission, the mass accuracy, and the mass resolution (118). The greater the resolution, the greater the ability of the mass analyzer to distinguish ions with a slight mass difference, so depending on the application, we can choose between low and high-resolution MS instrumentation. For instance, high resolution MS (hrMS) instrumentation is preferred for structural elucidation in full scan mode (118). In contrast, structural elucidation with a low resolution MS instrumentation requires fragmentation (MS/MS mode) of a precursor ion and monitoring of the characteristic product ion (115). Below, the instruments used in the experimental section of this thesis are described.

### Low resolution - Triple Quadrupole mass analyzer

Linear quadrupole mass analyzers consist of four hyperbolic or circular, parallel rod electrodes. Each opposing rod is paired and homogeneously charged using a radio frequency (RF) and a direct current (DC) offset voltage. When ions move inside the quadrupole analyzers, they develop an oscillating trajectory. Depending on the DC and RF settings, only ions with a specific  $m/z$  will develop a stable trajectory and reach the detector, while the rest will develop unstable trajectories, collide with the rods, and de-charge. Upon changing the settings (scanning), different ions can

consecutively pass the quadrupole filter. A series of three consecutive linear quadrupoles is called a triple quadrupole. Combining three quadrupoles provides a variety of detection capabilities; refined mass spectra of a specific mass range defined by the 1<sup>st</sup> and the 3<sup>rd</sup> quadrupole settings and fragmentation in the 2<sup>nd</sup> quadrupole (115, 178) (Figure 1.12).

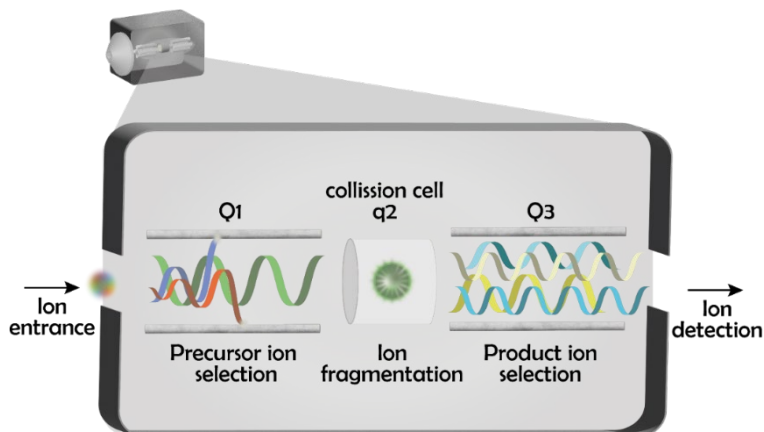


**Figure 1.12.** Triple quadrupole analyzer and trajectory of ions. The inserted ions to the first quadrupole will develop an oscillating trajectory, and the selected  $m/z$  (demonstrated in green) will move to the second quadrupole (collision cell), while the rest will collide with the rod and de-charge. In the collision cell the selected ion will fragment and its product ions (yellow and blue), will be further refined in the third quadrupole, and will reach the detector.

Even though initial instrumentations had poor resolution and a limited mass range (1-200  $m/z$ ), a modern linear quadrupole MS can reach up to 4000  $m/z$  range and a resolution of 0.2 Da FWHM (full width half maximum). Additionally, linear quadrupoles were the first to be commercialized; they are relatively affordable compared to other instrumentation, easily connected with various ion sources, and offer high transmission in single ion monitoring (SIM) mode and scan speeds. For those reasons, triple quadrupole mass analyzers are the gold standards for routine MS analytical laboratories and monitoring specific analytes with defined  $m/z$  values and fragmentation patterns (179–184).

### High resolution – (Q) Orbitrap mass analyzer

The initial design of orbitrap was introduced in 1923 by Kingdon (185), but the commercialized design of the final orbitrap instrumentation came by Makarov (186). The orbitrap has a spindle-shaped central electrode inside a barrel-shaped outer electrode. After ionization, the ions enter the space between the two electrodes and develop a tangentially oscillating spiral trajectory around the inner electrode. Their oscillating movement is defined by a centrifugal and an electrostatic force generated by voltage application. The frequency of the axial oscillating movement is detected by the barrel-like electrodes, and after Fourier transform application, specific  $m/z$  values



are obtained (Figure 1.13) (186, 187). Due to this movement, high resolving power can be achieved with orbitrap instrumentation (185–187). The full functionality of the orbitrap was explored in hybrid instrumentations, one of which combines a linear quadrupole (Q) preceding the orbitrap analyzer (Q-Orbitrap, also named QExactive). Due to the high resolving power and accuracy of measurement in (Q)Orbitrap analyzers, many successful research applications include untargeted analysis and omics studies (115, 187).

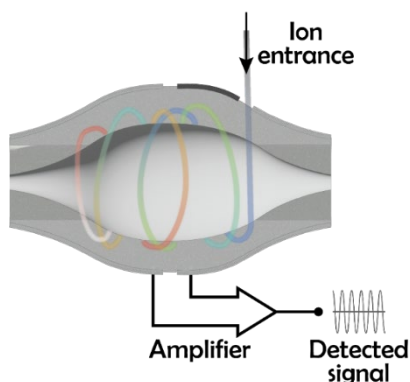


**Figure 1.13.** Schematic representation of Orbitrap and the movement of ions in the analyzer. The movement of an ion is indicated with a continuous color change (from black to white)

## 1.5 Integration of Biorecognition to Ambient MS

Biorecognition components in biosensors and bioassays might identify a set of analytes with similar backbone structure and physicochemical features, so cross-reaction and false-positive results are possible (29). For this reason, bioassays and biosensors are solely used for screening, and further confirmation is required for positive and suspect results (147). This strategy for confirming the original result is not restricted only to food safety but is rather a standard procedure. For instance, when a COVID-19 self-test is positive, a PCR is used to confirm or reject the positive result.

Depending on the application, several confirmatory tools might be utilized. MS is the preferred confirmatory approach in food safety (147). According to the EU regulation, confirmatory methods must provide information on the structural chemical composition of the analyte (3), and MS can be adequate for elemental identification and determining a molecular formula of an analyte (118). Nonetheless, MS is used in conjunction with a separation method, such as gas or liquid chromatography (GC- or LC-MS and MS/MS), for definitive identification of material under regulatory frameworks. Chromatography adds an identification criterion; the substance's retention time versus a standard, despite often being generic (providing general retention time

that are not specifically assigned to one analyte) and not sufficiently specific on its own (188).

Combining screening and confirmation by incorporating ambient MS analysis and biorecognition elements in a single technique improves the quality and specificity of the acquired data (189). Biorecognition elements enable the rapid separation of a set of analytes with excellent selectivity, which is more specific than a generic chromatographic separation. Subsequent sensitive MS detection and identification based on the characteristic  $m/z$  is possible, removing the need for time-consuming chromatography and the extensive pre-treatment necessary for sample introduction on a chromatography column. Additionally, liquid chromatography demands an excessive volume of organic solvents that can be detrimental to the environment and the analyst (190), and, gas chromatography requires carrier gas, which raises the cost of individual measurements (191). The development of **integrated biorecognition - mass spectrometry approaches** has been enabled by advances in ambient ionization sources. As discussed above, the development of smartphone-based bioassays has facilitated their use by laypersons, which could increase the need for confirmatory analysis, especially in the food safety sector. Such integrated biorecognition - mass spectrometry approaches can improve throughput in future regulatory settings and alleviate stress for increased analysis in routine analysis laboratories.

## 1.6 Method Validation and Maximum Limits

Validation is a frequent practice performed prior to broad implementation of a newly developed method. Validation is carried out to confirm that the method fits its intended purpose and performs as expected. Many validation methodologies exist, depending on the intended application, the type of technique, and the authority that certifies the validation rules (192).

In the European Union for food safety-related methods, the European Commission is the authority that establishes the rules for method validation. The document 2021/808 (amending 2002/657/EC) is the one used for assessing the performance of analytical procedures (3). There, detailed method performance requirements, acceptance limits, and criteria are listed. The criteria include; selectivity/specificity, trueness, recovery, stability, decision limit ( $CC\alpha$ ), and detection capability ( $CC\beta$ ). Additionally, the European Commission establishes maximum limits (ML) for which food contaminants are still considered acceptable in food commodities (193). The ML vary depending on the type of food commodity, the physicochemical properties and known toxicological effect of the contaminant. For instance, the marine biotoxin domoic acid (DA) that causes amnesic shellfish poisoning (ASP) has an ML of 20.0 mg/kg (194, 195). Stricter ML applies for the mycotoxin deoxynivalenol (DON), which causes gastrointestinal problems including vomiting and diarrhea (190,191). The highest ML for DON is 1.75 mg/kg in unprocessed durum wheat, and the lowest is 0.20 mg/kg in baby foods (193). Regardless of the ML for those compounds, their structural analogs, kainic acid (KA) for DA and AcetylDON and DON-glucoside for DON, are not regulated, underlining the significance of specific confirmation of contaminants; those

contaminants could cross-react with the biorecognition element on the screening assay, but they would be identified only using MS.

## 1.7 Thesis Outline

Numerous scientific challenges need to be addressed to integrate biorecognition elements with ambient MS analysis that provide different isolation and ionization capabilities. Several approaches were tested to answer these challenges and provide alternatives for effective immunocapture and ionization (*Table 1.1*). **Chapter 2** addresses the incompatibility of LFIA and ESI-MS; for MS analysis, an insufficient amount of analyte is trapped on the LFIA, and necessary buffers for the proper development of LFIA are involatile, causing MS ion suppression. In response to these limitations, the identification LFIA (ID-LFIA) was developed. The ID-LFIA consists of several lines of mAb to increase the absolute amount of trapped analyte. Moreover, ID-LFIA washing during analyte isolation minimizes buffer residues, thus decreasing ion suppression. **Chapter 3** explores the utilization of the ID-LFIA in combination with a different MS ionization source, i.e., DART, for the ionization of analytes that were not MS-amenable with the ESI approach in **Chapter 2**. Additionally, validation of the method proves its fit-for-purpose, its superiority over the screening assay in substance identification, and its performance similarity to the official confirmatory method. Next, **Chapter 4** examines the isolation and online ionization of the analyte from microspheres. Antibody-enriched paramagnetic microspheres, conventionally used in suspension planar assays, were magnetically immobilized on a stainless steel blade for direct blade spray MS analysis enabling antibody-based surface enhancement in CBS for the first time. The last research chapter, **Chapter 5**, introduces the novel concept of conductive polystyrene as an alternative substrate for blade spray MS. Conductive polystyrene allows for simple physical immobilization of antibodies, which eases blades' production, allows for fast online ionization, and promotes high throughput analysis. Finally, **Chapter 6** contains an overarching summary of the methods developed within the framework of this thesis, provides a critical reflection on **Chapters 2-5** while discussing persisting challenges, and reflects on future perspectives and potential applications for the development of integrated biorecognition MS approaches.

**Table 1.1.** Challenges of integrating biorecognition elements with direct MS analysis and solutions provided by this thesis.

### Aim

Combination of:

- Biorecognition elements for selective analyte isolation, with;
- Ambient ionization MS for rapid confirmation, avoiding time-consuming chromatographic separation.

Challenges	Developed method	Solution
<b>Chapter 2</b>		
1. Insufficient amount of analyte trap on the biorecognition element in conventional LFIA.	ID-LFIA ESI-Q-Orbitrap-MS	1. Development of identification LFIA (ID-LFIA) consisting of 15 lines of mAb to trap a sufficient amount of MS amenable analyte.
2. In conventional LFIA, the analyte is lost in the absorbent pad.	&	2. Elimination of labeled antibody - the mAb of the ID-LFIA act as a bioaffinity trapping zone.
3. Incompatibility of bioassays and MS ionization – ion suppression from bioassay buffer residues (involatile salts).	ID-LFIA ESI-QqQ-MS/MS	3. Washing of the ID-LFIA prior to the MS analysis to minimize involatile buffer residues.
<b>Chapter 3</b>		
1. Inability to detect all analytes trapped on the mAb with ESI-MS and ESI-MS/MS.	ID-LFIA DART-QqQ-MS/MS	1. DART ionization employs a different ionization mechanism that ionizes different MS amenable analytes than ESI.
2. Prove the integrated approach is fit for the intended purpose in the food safety framework.		2. Presented validation to demonstrate performance for the intended use.

(Continued on next page)

**Table 1.1. Continued**

Challenges	Developed method	Solution
<b>Chapter 4</b> Isolating the trapped analyte before MS analysis – need for online isolation and MS ionization of the analyte from the same surface.	iMBS-QqQ-MS/MS	Paramagnetic microspheres are enriched with mAb, and the immuno-enriched microspheres are immobilized on a stainless steel blade with the aid of a magnet, followed by blade spray-MS ionization and analysis.
<b>Chapter 5</b> Time-consuming surface antibody immobilization involving intricate surface activation chemistry increasing the preparation time of the method.	iBS-QqQ-MS/MS	Immunoaffinity conductive polystyrene blades enable physical adsorption for immobilization of mAb. The total analysis time from sample to result is less than 5 minutes.

## 1.8 References

1. American Chemical Society, Analytical Chemistry, (available at <https://www.acs.org/content/acs/en/careers/chemical-sciences/areas/analytical-chemistry.html>).
2. A. Gerssen, T.H.F. Bovee, L.A. van Ginkel, M.L.P.S. van Iersel, R.L.A.P. Hoogenboom, *Food Control*. **98**, 9-18 (2018).
3. European Commission. *Off. J. Eur. Union*. **180**, 84–109 (2021).
4. S. J. Lehotay, Y. Sapozhnikova, H. G. J. Mol, *TrAC*. **69**, 62–75 (2015).
5. C. Yuan, D. Chen, S. Wang, *Clin. Chim. Acta*. **438**, 119–125 (2015).
6. K. Aziz, *Clin. Lab. Med.* **10**, 493–502 (2010).
7. FAO and WHO, Technical summary (available at <https://www.fao.org/documents/card/en/c/ca8386en>).
8. United Nations, World Population Prospects 2019: Highlights, (available at <https://www.un.org/development/desa/publications/world-population-prospects-2019-highlights.html>).
9. United Nations, Transforming our world: the 2030 Agenda for Sustainable Development, (available at <https://sdgs.un.org/2030agenda>).
10. EU-Citizen. Science, Citizen Science, (available at <https://eu-citizen.science/>).
11. A. Irwin, *Nature*. **562**, 480–482 (2018).
12. J. R. Choi, K. W. Yong, J. Y. Choi, A. C. Cowie, *Sensors*. **19**, 1-31 (2019).
13. C. Wang *et al.*, *Nano Today*. **37**, 101092 (2021).
14. A. Gowri, N. Ashwin Kumar, B. S. Suresh Anand, *TrAC*. **137**, 116205 (2021).
15. H. Kholafazad-Kordasht, M. Hasanzadeh, F. Seidi, *TrAC*. **145**, 116455 (2021).
16. J. A. Rising, C. Taylor, M. C. Ives, R. E. T. Ward, *Ecol. Econ*. **197**, 107437 (2022).
17. M. C. Tirado, R. Clarke, L. A. Jaykus, A. McQuatters-Gollop, J. M. Frank, *Food Res. Int.* **43**, 1745–1765 (2010).
18. H. J. van der Fels-Klerx, J.E. Olesen, L.J. Naustvoll, Y. Friocourt, M.J.B. Mengelers, J.H. Christensen, *Food Addit. Contam.* **29**, 1647–1659 (2012).
19. R. J. Kubiak, L. Zhang, J. Zhang, Y. Zhu, N. Lee, F.F. Weichold, H. Yang, V. Abraham, P.F. Akufongwe, L. Hewitt, S. Robinson, W. Liu, X. Liu, M.M. Patnaik, S. Spitz, Y. Wu, L.K. Roskos, *J. Pharm. Biomed. Anal.* **74**, 235–245 (2013).
20. H. Montgomery, S. A. Haughey, C. T. Elliott, *Glob. Food Sec.* **26**, 100447 (2020).
21. K. Chen, X. xin Wang, H. ying Song, *J. Integr. Agric.* **14**, 2203–2217 (2015).
22. L. C. Clark, C. Lyons, *Ann. N. Y. Acad. Sci.* **102**, 29–45 (1962).
23. Grand View Research, Biosensors Market Size Worth (available at <https://www.grandviewresearch.com/press-release/global-biosensors-market>).
24. M. Urdea, L.A. Penny, S.S. Olmsted, M.Y. Giovanni, P. Kaspar, A. Shepherd, P. Wilson, C.A. Dahl, S. Buchsbaum, G. Moeller, D.C. Hay Burgess, *Nature*. **444**, 73–79 (2006).
25. W. W.-W. Hsiao, T.-N. Le, D.M. Pham, H.-H. Ko, H.-C. Chang, C.-K.C.-C. Lee, N. Sharma, C.-K.C.-C. Lee, W.-H. Chiang, *Biosensors*. **11**, 1-26 (2021).
26. B. Pérez-López, M. Mir, *Talanta*. **225**, 121898 (2021).
27. M. A. Morales, J. M. Halpern, *Bioconjug. Chem.* **29**, 3231–3239 (2018).
28. J. Jay, B. Bray, Y. Qi, E. Igbini, H. Wu, J. Li, G. Ren, *Antibodies*. **7**, 1-20 (2018).
29. I. Sela-Culang, V. Kunik, Y. Ofra, *Front. Immunol.* **4**, 1-13 (2013).
30. N. G. Welch, J. A. Scoble, B. W. Muir, P. J. Pigram, *Biointerphases*. **12**, 1-13 (2017).
31. 3D View: 1IGT - structure of immunoglobulin, (available at <https://www.rcsb.org/3d-view/1IGT/1>).
32. D. Sehnal, S. Bittrich, M. Deshpande, R. Svobodová, K. Berka, V. Bazgier, S. Velankar, S.K. Burley, J. Koča, A.S. Rose, *Nucleic Acids Res.* **49**, 431–437 (2021).

33. A. Singh, A. Mishra, A. Verma, *Anim. Biotechnol. Model. Discov. Transl.* **8**, 327–352 (2020).
34. D. S. Chahar, S. Ravindran, S. S. Pisal, *Biologicals*. **63**, 1–13 (2020).
35. S. Gao, J. M. Guisán, J. Rocha-Martin, *Anal. Chim. Acta*. **1189**, 338907 (2022).
36. Q. Yu, Q. Wang, B. Li, Q. Lin, Y. Duan, *Crit. Rev. Anal. Chem.* **45**, 62–75 (2015).
37. H. Ye, Y. Liu, L. Zhan, Y. Liu, Z. Qin, *Theranostics*. **10**, 4359–4373 (2020).
38. E. B. Bahadır, M. K. Sezgintürk, *TrAC*. **82**, 286–306 (2016).
39. R. B. M. Schasfoort, *Handb. Surf. Plasmon Reson.*, **1**, 1–26 (2017).
40. K. M. Koczula, A. Gallotta, *Essays Biochem.* **60**, 111–120 (2016).
41. Q. Zhang, L. Fang, B. Jia, N. Long, L. Shi, L. Zhou, H. Zhao, W. Kong, *TrAC*. **144**, 1–17 (2021).
42. T. Salminen, A. Knuutila, A. M. Barkoff, J. Mertsola, Q. He, *Vaccine*. **36**, 1429–1434 (2018).
43. M. Xu, F. Lu, C. Lyu, Q. Wu, J. Zhang, P. Tian, L. Xue, T. Xu, D. Wang, *BMC Microbiol.* **21**, 1–10 (2021).
44. T. Wen, C. Huang, F.-J. Shi, X.-Y. Zeng, T. Lu, S.-N. Ding, Y.-J. Jiao, *Analyst*. **145**, 5345–5352 (2020).
45. S. Bayoumy, H. Hyttiä, J. Leivo, S.M. Talha, K. Huhtinen, M. Poutanen, J. Hynninen, A. Perheentupa, U. Lamminmäki, K. Gidwani, K. Pettersson, *Commun. Biol.* **3**, 1–7 (2020).
46. D. Huang, H. Ying, D. Jiang, F. Liu, Y. Tian, C. Du, L. Zhang, X. Pu, *Anal. Biochem.* **588**, 1–17 (2020).
47. W. Jawaid, J. Meneely, K. Campbell, M. Hooper, K. Melville, S. Holmes, J. Rice, C. T. Elliott, *Talanta*. **116**, 663–669 (2013).
48. C. S. Bever Id, C.A. Adams, R.M. Hnasko, L.W. Cheng, L.H. Stanker, *PLoS One*, **15**, 1–18 (2020).
49. N. A. Byzova, T.S. Serchenya, I.I. Vashkevich, A. V. Zherdev, O. V. Sviridov, B.B. Dzantiev, *Microchem. J.* **156**, 104884 (2020).
50. C. Wang, R. Xiao, S. Wang, X. Yang, Z. Bai, X. Li, Z. Rong, *Biosens. Bioelectron.* **146**, 111754 (2019).
51. F. S. Romolo, E. Ferri, M. Mirasoli, M. D'Elia, L. Ripani, G. Peluso, R. Risoluti, E. Maiolini, S. Girotti, *Forensic Sci. Int.* **246**, 25–30 (2015).
52. D. J. Angelini, T.D. Biggs, A.M. Prugh, J.A. Smith, J.A. Hanburger, B. Llano, R. Avelar, A. Ellis, B. Lusk, A. Naanaa, M.G. Feasel, J.W. Sekowski, *Forensic Chem.* **23**, 100309 (2021).
53. D. J. Angelini, T.D. Biggs, A.M. Prugh, J.A. Smith, J.A. Hanburger, B. Llano, R. Avelar, A. Ellis, B. Lusk, A. Malik Naanaa, E. Sisco, J.W. Sekowski, *J Forensic Sci.* **66**, 758–765 (2021).
54. F. Di Nardo, M. Chiarello, S. Cavallera, C. Baggiani, L. Anfossi, K. Wang, *Sensors*. **21**, 1–33 (2021).
55. T. Salminen, F. Mehdi, D. Rohila, M. Kumar, M. Talha, J. Antony, J. Prakash, N. Khanna, K. Pettersson, G. Batra, *Anal. Chem.* **92**, 15766–15772 (2020).
56. S. J. Yoo, H. S. Shim, | Sumi Yoon, H.-W. Moon, *J Med Virol.* **92**, 1040–1046 (2020).
57. I. Martiskainen, E. Juntunen, T. Salminen, K. Vuorenperä, S. Bayoumy, T. Vuorinen, N. Khanna, K. Pettersson, G. Batra, S.M. Talha, *Sensors*. **330**, 1–17 (2021).
58. J. Liu, S. Zanardi, S. Powers, M. Suman, *Food Control*. **26**, 88–91 (2012).
59. B. G. Andryukov, *AIMS Microbiol.* **6**, 280–304 (2020).
60. S. Dutta, *TrAC*. **110**, 393–400 (2019).
61. A. Roda, E. Michellini, M. Zangheri, M. Di Fusco, D. Calabria, P. Simoni, *TrAC*. **79**, 317–325 (2016).
62. K. J. Merazzo, J. Toticaguena-Gorriño, E. Fernández-Martín, F. Javier Del Campo, E. Baldrich, *Diagnostics*. **11**, 1–13 (2021).
63. U. M. Jalal, G. J. Jin, J. S. Shim, *Anal. Chem.* **89**, 13160–13166 (2017).
64. M. Ilesh Shah, J. Joseph, U. Sriharsha Sanne, M. Sivaprakasam, *39th Annual Int. Conf. of the IEEE Eng. in Med. and Bio. Soc. (EMBC)*, 4247–4250 (2017).
65. S. Lee, G. Kim, J. Moon, *J. Nanosci. Nanotechnol.* **14**, 8453–8457 (2014).

66. Statista, Number of smartphone users from 2016 to 2021, (available at <https://www.statista.com/statistics/330695/number-of-smartphone-users-worldwide/>).
67. Statista, Penetration rate of smartphones in selected countries 2020, (available at <https://www.statista.com/statistics/539395/smartphone-penetration-worldwide-by-country/>).
68. K. Kalinowska, W. Wojnowski, M. Tobiszewski, *Trends Food Sci. Technol.* **111**, 271–279 (2021).
69. G. M. S. Ross, M. G. E. G. Bremer, M. W. F. Nielen, *Anal. Bioanal. Chem.* **410**, 5353–5371 (2018).
70. X. Xu, X. Wang, J. Hu, Y. Gong, L. Wang, W. Zhou, X. Li, F. Xu, *Electrophoresis*. **40**, 914–921 (2019).
71. S. Lee, G. Kim, J. Moon, *Sensors*. **13**, 5109–5116 (2013).
72. Z. Liu, Q. Hua, J. Wang, Z. Liang, J. Li, J. Wu, X. Shen, H. Lei, X. Li, *Biosens. Bioelectron.* **158**, 1–8 (2020).
73. M. Zangheri, F. Di Nardo, D. Calabria, E. Marchegiani, L. Anfossi, M. Guardigli, M. Mirasoli, C. Baggiani, A. Roda, *Anal. Chim. Acta.* **1163**, 338515 (2021).
74. M. Zangheri, L. Cevenini, L. Anfossi, C. Baggiani, P. Simoni, F. Di Nardo, A. Roda, *Biosens. Bioelectron.* **64**, 63–68 (2015).
75. Z. Rong, Q. Wang, N. Sun, X. Jia, K. Wang, R. Xiao, S. Wang, *Anal. Chim. Acta.* **1055**, 140–147 (2019).
76. S. Nivedha, P. Ramesh Babu, K. Senthilnathan, *Curr. Sci.* **115**, 56–63 (2018).
77. H. H. Nguyen, J. Park, S. Kang, M. Kim, *Sensors*. **15**, 10481–10510 (2015).
78. X. Guo, *J. Biophotonics*. **5**, 483–501 (2012).
79. V. Kodoyianni, *Biotechniques*. **50**, 32–40 (2011).
80. D. G. Drescher, M. J. Drescher, N. A. Ramakrishnan, *Methods Mol. Biol.* **493**, 323–332 (2009).
81. F. C. Dudak, I. H. Boyaci, *Biotechnol. J.* **4**, 1003–1011 (2009).
82. F. Fathi, J. Ezzati Nazhad Dolatanbadi, M. R. Rashidi, Y. Omid, *Int. J. Biol. Macromol.* **91**, 1045–1050 (2016).
83. N. M. Nunes, H.M.C. de Paula, Y.L. Coelho, L.H.M. da Silva, A.C.S. Pires, *Food Chem.* **297**, 125022 (2019).
84. M. B. Medina, *Int. J. Food Microbiol.* **93**, 63–72 (2004).
85. C. S. Pundir, A. Malik, Preeti, *Biosens. Bioelectron.* **140**, 111348 (2019).
86. J. Zhou, Q. Qi, C. Wang, Y. Qian, G. Liu, Y. Wang, L. Fu, *Biosens. Bioelectron.* **142**, 111449 (2019).
87. A. Rezabakhsh, R. Rahbarghazi, F. Fathi, *Biosens. Bioelectron.* **167** (2020).
88. A. Azzouz, L. Hejji, K.H. Kim, D. Kukkar, B. Souhail, N. Bhardwaj, R.J.C. Brown, W. Zhang, *Biosens. Bioelectron.* **197**, 113767 (2022).
89. C. Chen, J. Wang, *Analyst.* **145**, 1605–1628 (2020).
90. C. Lertvachirapaiboon, A. Baba, K. Shinbo, K. Kato, *Anal. Methods.* **10**, 4732–4740 (2018).
91. J. Zhang, I. Khan, Q. Zhang, X. Liu, J. Dostalek, B. Liedberg, Y. Wang, *Biosens. Bioelectron.* **99**, 312–317 (2018).
92. C. Xiao, J. Eriksson, A. Suska, D. Filippini, W. C. Mak, *Anal. Chim. Acta.* **1201**, 339606 (2022).
93. N. Reslova, V. Michna, M. Kasny, P. Mikel, P. Kralik, *Front. Microbiol.* **8**, 1–17 (2017).
94. H. Graham, D. J. Chandler, S. A. Dunbar, *Methods.* **158**, 2–11 (2019).
95. S. A. Dunbar, M. R. Hoffmeyer, *The Immunoassay Handbook*, 157–174 (2013).
96. J. Peters, A. Cardall, W. Haasnoot, M. W. F. Nielen, *Analyst.* **139**, 3968–3976 (2014).
97. P. Carl, I. I. Ramos, M. A. Segundo, R. J. Schneider, *PLoS One*, **8**, 1–18 (2019).
98. J. Peters, J. H. W. Bergervoet, W. Haasnoot, M. W. F. Nielen, in *Mycotoxin multiplex microsphere immunoassays: screening from ingredients to beer* 132–147 (2022).
99. G. Rateni, P. Dario, F. Cavallo, *Sensors.* **17**, 1453 (2017).



100. S. F. Parsa, A. Vafajoo, A. Rostami, R. Salarian, M. Rabiee, N. Rabiee, G. Rabiee, M. Tahriri, A. Yadegari, D. Vashaei, L. Tayebi, M.R. Hamblin, *Anal. Chim. Acta.* **1032**, 1-23 (2018).
101. C. Seger, L. Salzmann, *Clin. Biochem.* **82**, 2–11 (2020).
102. I. Mahmud, T. J. Garrett, *J. Am. Soc. Mass Spectrom.* **31**, 2013–2024 (2020).
103. J. Klingberg, B. Keen, A. Cawley, D. Pasin, S. Fu, *Arch. Toxicol.* **96**, 949–967 (2022).
104. M. Valletta, S. Ragucci, N. Landi, A. Di Maro, P.V. Pedone, R. Russo, A. Chambery, *Food Chem.* **365**, 130456 (2021).
105. G. Cao, K. Li, J. Guo, M. Lu, Y. Hong, Z. Cai, *J. Agric. Food Chem.* **68**, 6956–6966 (2020).
106. T. Sun, X. Wang, P. Cong, J. Xu, C. Xue, *Compr. Rev. food Sci. food Saf.* **19**, 2530–2558 (2020).
107. C. Kim, H.D. Ryu, E.G. Chung, Y. Kim, J. kwan Lee, *J. Environ. Manage.* **217**, 629–645 (2018).
108. W. Shi, W. E. Zhuang, J. Hur, L. Yang, *Water Res.* **188**, 116406 (2021).
109. K. Evans-Nguyen, A. R. Stelmack, P. C. Clowser, J. M. Holtz, C. C. Mulligan, *Mass Spectrom. Rev.* **40**, 628–646 (2021).
110. R. Ueki, E. Fukusaki, S. Shimma, *J. Biosci. Bioeng.* **133**, 89–97 (2022).
111. T. Vazquez, S. Vuppala, I. Ayodeji, L. Song, N. Grimes, T. Evans-Nguyen, *Mass Spectrom. Rev.* **40**, 670–691 (2021).
112. J. J. Thomson, *London, Edinburgh, Dublin Philos. Mag. J. Sci.* **13**, 561–575 (1907).
113. G. Münzenberg, *Int. J. Mass Spectrom.* **349–350**, 9–18 (2013).
114. C. Murayama, Y. Kimura, M. Setou, *Biophys. Rev.* **1**, 131–139 (2009).
115. A. M. Haag, *Adv. Exp. Med. Biol.* **919**, 157–169 (2016).
116. C. Bhardwaj, L. Hanley, *Nat. Prod. Rep.* **31**, 756–767 (2014).
117. W. P. Peng, S. W. Chou, A. A. Patil, *Analyst.* **139**, 3507–3523 (2014).
118. A. G. Marshall, C. L. Hendrickson, *Annu. Rev. Anal. Chem.* **1**, 579–599 (2008).
119. L. F. R. S. Rayleigh, *Philos. Mag. J. Sci.* **14**, 184–186 (1882).
120. J. B. Fenn, M. Mann, C. K. Meng, S. F. Wong, C. M. Whitehouse, *Science.* **246**, 64–71 (1989).
121. M. Zhou, T. D. Veenstra, *Biotechniques.* **44**, 667–670 (2008).
122. John B. Fenn – Facts - NobelPrize.org, (available at <https://www.nobelprize.org/prizes/chemistry/2002/fenn/facts/>).
123. A. Geballa-Koukoulou, I. Panderi, K. Zervas, K. Geballa-Koukoulas, E. Kavvalou, E. Panteri-Petratou, P. Vourna, D. Gennimata, *J. Chromatogr. B.* **1084**, 175–184 (2018).
124. W. Smyth, *Curr. Pharm. Anal.* **2**, 299–311 (2006).
125. R. Kanneti, D. Bhavesh, D. Paramar, R. Shivaprakash, P.A. Bhatt, *Biomed. Chromatogr.* **25**, 458–465 (2011).
126. X. Hu, Y. Zheng, G. Wu, J. Liu, M. Zhu, H. Zhou, Y. Zhai, L. Wu, J. Shen-Tu, *J. Chromatogr. B.* **951–952**, 1–6 (2014).
127. P. He, Y. Ling, W. Yong, M. Yao, Y. Zhang, X. Feng, Y. Zhang, F. Zhang, *J. Chromatogr. A*, **1669**, 462916 (2022).
128. L. Valdemiro Alves de Oliveira, C. Rafael Kleemann, L. Molognoni, H. Daguer, R. Barcellos Hoff, E. Schwinden Prudencio, *Food Res. Int.* **156**, 111140 (2022).
129. R. Liu, X. Tang, R. Xiong, L. Li, X. Du, L. He, *J. Chromatogr. B.* **1193**, 123169 (2022),
130. T. Zhu, X. Tang, R. Xiong, L. Li, X. Du, L. He, *Rapid Commun. Mass Spectrom.* **36**, 1-15 (2022).
131. H. John, H. Thiermann, *J. mass Spectrom. Adv. Clin. lab.* **19**, 20–31 (2021).
132. E. O. Omotola, O. S. Olatunji, *Heliyon.* **6**, 1-10 (2020).
133. C. Mirasole, M. Di Carro, S. Tanwar, E. Magi, *J. Mass Spectrom.* **51**, 814–820 (2016).
134. H. Matsukami, H. Takemori, T. Takasuga, H. Kuramochi, N. Kajiwaru, *Chemosphere.* **244**, 125531 (2020).
135. S. Limjiasahapong, K. Kaewnarin, N. Jariyasopit, S. Hongthong, N. Nuntasaen, J.L. Robinson, I. Nookaew, Y. Sirivatanauksorn, C. Kuhakarn, V. Reutrakul, S. Khoomrung, *Front. Plant Sci.* **11**, 602993 (2021).
136. T. Shama Yamin, H. Prihed, M. Madmon, M. Blanca, A. Weissberg, *J. Mass Spectrom.* **55**,

- 34-43 (2020).
137. M. Madmon, A. Weissberg, *J. Mass Spectrom.* **56**, 1-18 (2021).
138. C. S. Ho, C.W.K. Lam, M.H.M. Chan, R.C.K. Cheung, L.K. Law, L.C.W. Lit, K.F. Ng, M.W.M. Suen, H.L. Tai, *Clin. Biochem. Rev.* **24**, 3-21 (2003).
139. S. Banerjee, S. Mazumdar, *Int. J. Anal. Chem.* **2012**, 1-40 (2012).
140. L. Konermann, E. Ahadi, A. D. Rodriguez, S. Vahidi, *Anal. Chem.* **85**, 2-9 (2013).
141. H. Metwally, Q. Duez, L. Konermann, *Anal. Chem.* **90**, 10069-10077 (2018).
142. A. Kageyama, A. Motoyama, M. Takayama, *Mass Spectrom.* **8**, 1-9 (2019).
143. P. Liigand, J. Liigand, K. Kaupmees, A. Kruve, *Anal. Chim. Acta.* **1152**, 238117 (2021).
144. R. King, R. Bonfiglio, C. Fernandez-Metzler, C. Miller-Stein, T. Olah, *J. Am. Soc. Mass Spectrom.* **11**, 942-950 (2000).
145. C. R. Mallet, Z. Lu, J. R. Mazzeo, *Rapid Commun. Mass Spectrom.* **18**, 49-58 (2004).
146. T. M. Annesley, *Clin. Chem.* **49**, 1041-1044 (2003).
147. A. S. Tsagkaris, J.L.D. Nelis, G.M.S. Ross, S. Jafari, J. Guercetti, K. Kopper, Y. Zhao, K. Rafferty, J.P. Salvador, D. Migliorelli, G.I. Salentijn, K. Campbell, M.P. Marco, C.T. Elliot, M.W.F. Nielen, J. Pulkabova, J. Hajslova, *TrAC.* **121**, 115688 (2019).
148. F. Versace, J. Déglon, P. Mangin, C. Staub, *Bioanalysis.* **6**, 2043-2055 (2014).
149. E. M. McBride, G. F. Verbeck, *Forensic Sci. Int.* **288**, 278-282 (2018).
150. S. G. Musharraf, A. J. Siddiqui, S. Mazhar, *Bioanalysis.* **6**, 2057-2070 (2014).
151. R. Javanshad, A. R. Venter, *Anal. Methods.* **9**, 4896-4907 (2017).
152. Z. Takáts, J. M. Wiseman, B. Gologan, R. Graham Cooks, *Science.* **306**, 471-473 (2004).
153. R. B. Cody, J. A. Laramée, H. D. Durst, *Anal. Chem.* **77**, 2297-2302 (2005).
154. A. Venter, M. Nefliu, R. Graham Cooks, *TrAC Trends Anal. Chem.* **27**, 284-290 (2008).
155. G. A. Harris, A. S. Galhena, F. M. Fernández, *Anal. Chem.* **83**, 4508-4538 (2011).
156. M. Z. Huang, S. C. Cheng, Y. T. Cho, J. Shiea, *Anal. Chim. Acta.* **702**, 1-15 (2011).
157. M. E. Monge, F. M. Fernández, *An Introduction to Ambient Ionization Mass Spectrometry.* **1**, 1-22 (2014).
158. C. L. Feider, A. Krieger, R. J. DeHoog, L. S. Eberlin, *Anal. Chem.* **91**, 4266-4290 (2019).
159. T. H. Kuo, E. P. Dutkiewicz, J. Pei, C. C. Hsu, *Anal. Chem.* **92**, 2353-2363 (2020).
160. W. R. De Araujo *et al.*, *Anal Chim Acta.* **1034**, 1-21 (2018).
161. X. Ma, Z. Ouyang, *TrAC.* **85**, 10-19 (2016).
162. J. Jager, A. Gerssen, J. Pawliszyn, S.S. Sterk, M.W.F. Nielen, M.H. Blokland, *J. Am. Soc. Mass Spectrom.* **31**, 2243-2249 (2020).
163. T. Guo, W. Yong, Y. Jin, L. Zhang, J. Liu, S. Wang, Q. Chen, Y. Dong, H. Su, T. Tan, *Mass Spectrom. Rev.* **36**, 161-187 (2017).
164. M. J. Pavlovich, B. Musselman, A. B. Hall, *Mass Spectrom. Rev.* **37**, 171-187 (2018).
165. L. Watt, E. Sisco, *J. Forensic Sci.* **66**, 172-178 (2021).
166. R. Chen, J. Deng, L. Fang, Y. Yao, B. Chen, X. Wang, T. Luan, *Trends Environ. Anal. Chem.* **15**, 1-11 (2017).
167. Y. Liu, C. Su, Y. Zhang, D. Zhang, Y. Li, J. Gu, E. Wang, D. Sun, *Anal. Biochem.* **635**, 114435 (2021).
168. W. L. Shelver, S. Chakrabarty, D. J. Smith, *ACS Food Sci. Technol.* **2**, 195-205 (2022).
169. G. A. Gómez-Ríos, J. Pawliszyn, *Angew. Chemie - Int. Ed.* **53**, 14503-14507 (2014).
170. G. A. Gómez-Ríos, M. Tascon, J. Pawliszyn, *Bioanalysis.* **10**, 257-271 (2018).
171. A. Kasperkiewicz, G. A. Gómez-Ríos, D. Hein, J. Pawliszyn, *Anal. Chem.* **91**, 13039-13046 (2019).
172. A. Kasperkiewicz, J. Pawliszyn, *Food Chem.* **339**, 127815 (2021).
173. A. Khaled, G. A. Gómez-Ríos, J. Pawliszyn, *Anal. Chem.* **92**, 5937-5943 (2020).
174. M. Tascon, G.A. Gómez-Ríos, N. Reyes-Garcés, J. Poole, E. Boyaci, J. Pawliszyn, *J. Pharm. Biomed. Anal.* **144**, 106-111 (2017).

175. J. J. Poole, G. A. Gómez-Ríos, E. Boyaci, N. Reyes-Garcés, J. Pawliszyn, *Environ. Sci. Technol.* **51**, 12566–12572 (2017).
176. A. Kasperkiewicz, J. Pawliszyn, *Talanta*. **225**, 122036 (2021).
177. Restek Corp., Coated Blade Spray Blades, (available at <https://www.restek.com/row/products/sample-preparation--air-sampling/coated-blade-spray-cbs-products/blades/107677/>).
178. A. Raffaelli, A. Saba, *Mass Spectrom. Rev.* 1-22 (2021).
179. C. Duchateau, M. Canfyn, B. Desmedt, J.M. Kauffmann, C. Stévigny, K. De Braekeleer, E. Deconinck, *J. Pharm. Biomed. Anal.* **205**, 114344 (2021).
180. E. Hewawasam, G. Liu, D. W. Jeffery, B. S. Muhlhausler, R. A. Gibson, *Prostaglandins, Leukot. Essent. Fat. Acids.* **137**, 12–18 (2018).
181. M. Creydt, B. Wegner, A. Gnauck, R. Hörner, C. Hummert, M. Fischer, *Food Control.* **135**, 108690 (2022).
182. A. Bibi, N. Rafique, S. Khalid, A. Samad, K. Ahad, F. Mehboob, *Food Chem.* **369**, 130914 (2022).
183. S. Benito, A. Sánchez-Ortega, N. Unceta, M. A. Goicolea, R. J. Barrio, *J. Pharm. Biomed. Anal.* **169**, 82–89 (2019).
184. M. Degreef, E. M. Berry, K. E. K. Maudens, A. L. N. van Nuijs, *J. Chromatogr. B.* **1179**, 122867 (2021).
185. K. H. Kingdon, *Phys. Rev.* **21**, 408 (1923).
186. A. Makarov, *Anal. Chem.* **72**, 1156–1162 (2000).
187. S. Eliuk, A. Makarov, *Annual Rev. of Anal. Chem.* **8**, 61–80 (2015).
188. B. J. A. Berendsen, L. A. M. Stolker, M. W. F. Nielen, *J. Am. Soc. Mass Spectrom.* **24**, 154–163 (2013).
189. S. Joshi, H. Zuilhof, T. A. Van Beek, M. W. F. Nielen, *Anal. Chem.* **89**, 1427–1432 (2017).
190. M. Sajid, J. Plotka-Wasyłka, *Talanta*. **238**, 123046 (2022).
191. E. Hinterberger, E. Ackerly, Y. Chen, Y. C. Li, *J. Chem. Educ.* **98**, 4074–4077 (2021).
192. M. Rambla-Alegre, J. Esteve-Romero, S. Carda-Broch, *J. Chromatogr. A.* **1232**, 101–109 (2012).
193. European Commission. *Off. J. Eur. Union*, **364**, 558–577 (2006).
194. K. A. Lefebvre, A. Robertson, *Toxicon.* **56**, 218–230 (2010).
195. European Commission, *Off. J. Eur. Union.* **139**, 1–14 (2004).
196. P. Sobrova, V. Adam, A. Vasatkova, M. Beklova, L. Zeman, R. Kizek, *Interdiscip. Toxicol.* **3**, 94–99 (2010).
197. A. Pierzgałski, M. Bryła, J. Kanabus, M. Modrzewska, G. Podolska, *Toxins.* **13**, 1-33 (2021).





## **Direct Analysis of Lateral Flow Immunoassays for Deoxynivalenol Using Electrospray Ionization Mass Spectrometry**

*Adapted from:*

A. Geballa-Koukoulou, A. Gerssen, M.W.F. Nielen, *Direct analysis of lateral flow immunoassays for deoxynivalenol using electrospray ionization mass spectrometry*, *Anal. Bioanal. Chem.* 412 (2020) 7547–7558. <https://doi.org/10.1007/s00216-020-02890-4>.

### *Abstract*

Lateral flow immunoassays (LFIA) are widely used for rapid food safety screening analysis. Owing to the simplified protocols and smartphone readouts, LFIAs are expected to be increasingly used on-site, even by non-experts. As a typical follow-up in EU regulatory settings, samples that were marked as "suspect" by such on-site screening are sent to laboratories for confirmatory analysis by liquid chromatography-tandem mass spectrometry (LC-MS/MS). However, re-analysis by LC-MS/MS is laborious and time-consuming. In this work, an identification LFIA (ID-LFIA) approach followed by streamlined quadrupole-orbitrap MS or triple quadrupole (QqQ) MS/MS analysis was developed to expedite that cumbersome process. As a first step, a dedicated ID-LFIA was developed for the mycotoxin deoxynivalenol (DON) following its initial screening by a commercial smartphone LFIA. The ID-LFIA can be simply immersed in the same sample extract used for the smartphone LFIA screening. Upon positive screening, as the second step, DON is retrieved from the monoclonal antibody with a dissociation solution consisting of methanol/ammonia and the solution thus obtained is analyzed directly with MS to rapidly confirm the presence of DON and any cross-reacting species. The protocol was designed to cope with severe ion suppression otherwise caused by LFIA buffers and nitrocellulose substrate residues. Initial analysis of blank, spiked, and incurred samples showed that the newly developed ID-LFIA MS method was able to confirm the presence or absence of mycotoxins in the samples previously analyzed by LFIA and also differentiate between DON and DON 3-glucoside after obtaining a positive screening result. The concept and technique developed are envisaged to complement on-site screening and confirmation of any low molecular weight contaminant in future food control frameworks.

## 2.1 Introduction

The EU General Food Law stipulates that in order to reassure safety within the food and feed chain, producers are responsible for conducting all necessary tests so that their products comply with the legislation. Also, regulatory authorities perform inspections to ensure compliance with the current regulations (1). The effective strategy for food contaminants monitoring consists of a two-step approach. First, a rapid initial screening is performed, and second, confirmatory analysis of the suspect samples is carried out by instrumental analysis that provides unequivocal identification and quantification, if needed (2).

Many (bio)analytical techniques can be used as screening tools, such as biorecognition-based assays using antibodies, receptors, enzymes, or aptamers (3–5). An example of a bioassay that employs antibodies is a lateral flow immunoassay (LFIA). LFIA is widely used for on-site screening, with many applications reported, such as detecting antibiotic residues, mycotoxins, or allergens (6–8). Screening LFIA is relatively cheap, can be performed on-site, are fast, and an LFIA can be read out visually or with a smartphone camera for a more reliable and semi-quantitative result (9). Smartphones offer a variety of opportunities for user-friendly diagnostics, providing easy-to-read results, wireless data transfer to the cloud, and, most notably, for on-site testing, time, and location data of the sampling (10). The potential of smartphone-based diagnostics is highlighted by Rateni et al. that recorded 27 studies using smartphone-based diagnostics solely on food safety and only within five years (2012–2017) (11). Despite their extensive usage, a significant drawback of LFIA is that the antibodies used can only recognize a specific part of the targeted molecule, which could be shared among structural analogs, making antibodies unable to differentiate between molecules of similar physicochemical characteristics and structure (12–14). This uncertainty is the main reason why LFIA is used solely for rapid screening, and if the result of the screening is ambiguous or suggests an exceeding of regulatory limits, then confirmation is necessary. The methods primarily used for confirmation are liquid or gas chromatography followed by tandem mass spectrometry (LC- or GC-MS/MS) (2, 15). However, the confirmatory analysis is time-consuming because tedious sample preparation, extraction, clean-up step, and chromatographic separation are necessary (16–18).

Nonetheless, an LFIA itself can be considered an immunochromatographic device capable of selectively extracting analytes of interest, thus providing the necessary analyte selection and isolation step prior to instrumental analysis. In this study, the concept of an identification LFIA (ID-LFIA) has been developed in combination with direct MS analysis. With the ID-LFIA, the analytes are immuno-extracted, dissociated, and subsequently directly analyzed by MS without prior time-consuming chromatographic separation. Such a concept was far from trivial due to the general incompatibility of the LFIA with MS; the presence of involatile buffer salts and detergents in the LFIA buffer, and the nitrocellulose substrate hamper the MS ionization (19). The concept has been developed targeting the mycotoxin deoxynivalenol (DON);

consequently, the ID-LFIA contains monoclonal antibodies (mAbs) against DON. The model analyte, DON, is a mycotoxin produced by the *Fusarium* sp. fungi. Because of the toxicity of DON, maximum residue limits (MRLs) for DON in food and feed have been established to protect consumers (20). Apart from DON, conjugated forms, such as DON 3-glucoside (DON-3G), may occur in contaminated cereal crops, such as wheat, barley, and maize, as well as products thereof (21, 22).

Although a few approaches, using antibodies as a biorecognition element, and ambient ionization mass spectrometry identification, have been reported previously (23–26), to the best of our knowledge, this is the first successful attempt to simply analyze an LFIA with direct ESI-MS.

## 2.2 Material and Methods

### 2.2.1 Chemicals and reagents

Acetonitrile (ACN), methanol (MeOH), and water (H<sub>2</sub>O), all of UHPLC-MS purity grade, as well as hydrochloric acid (HCl), sodium hydroxide (NaOH), ammonia solution (25% v/v) (NH<sub>3</sub>) and formic acid (98% v/v) (HCOOH) were purchased from Merck (Darmstadt, Germany). Milli-Q water of 18.3 MΩ/cm conductivity was obtained using a water purification system from Merck (Amsterdam, The Netherlands). Bovine serum albumin (BSA) and bromothymol blue sodium salt solution in water were purchased from Sigma-Aldrich (Zwijndrecht, The Netherlands). A stock solution of 10× Phosphate Buffered Saline (PBS) containing 137 mM sodium chloride (NaCl), 2.7 mM potassium chloride (KCl), 10 mM sodium hydrogen phosphate (Na<sub>2</sub>HPO<sub>4</sub>), and 1.8 mM potassium dihydrogen phosphate (KH<sub>2</sub>PO<sub>4</sub>) (Merck, Darmstadt, Germany) and having a pH of 7.4 was prepared in Milli-Q water. Tenfold dilution of the stock solution to 1× PBS in Milli-Q water and addition of different percentages of Tween-20 (Sigma-Aldrich, Zwijndrecht, The Netherlands) provided different running buffer compositions for surface plasmon resonance (SPR) and LFIA experiments.

For SPR experiments, an amine coupling kit was obtained from GE Healthcare (Uppsala, Sweden), containing 1 M Ethanolamine, 1-ethyl-3-(3-(dimethylamino)propyl)-carbodiimide hydrochloride (EDC), and N-hydroxysuccinimide (NHS). Also, a carboxymethylated dextran-coated gold chip (CM5) (GE Healthcare, Uppsala, Sweden) having four flow channels was used.

A commercially available DON smartphone-based LFIA kit, RIDA QUICK DON, including DON extraction buffer, was obtained from r-Biopharm (Darmstadt, Germany). RosaFast DON screening tests for DON and its running buffer were purchased from Charm Sciences Inc. (Lawrence, UK).

Standard stock solutions of 100 µg/mL DON, 25 µg/mL <sup>13</sup>C-DON, and 50 µg/mL DON-3G, all in ACN, and wheat flour "DON blank certified reference material" (Joint Research Centre) were all purchased from LGC standards (Wesel, Germany). A contaminated beer sample was kindly provided by the Institute of Chemical Technology (Prague, CZ), and a naturally incurred wheat sample was purchased from Trilogly Analytical Laboratories (Arnhem, The Netherlands). Blank grounded, and slurry



grounded wheat and grounded barley samples, previously analyzed by confirmatory LC-MS/MS analysis, were provided in-house. Spiked samples were produced by spiking parts of the blank sample extracts at 200 ng/mL with DON or DON-3G. Two mouse mAbs for DON, clone 2, clone 4, and DON conjugate with BSA (DON-BSA) were purchased from Aokin AG (Berlin, Germany).

## 2.2.2 ID-LFIA development

### SPR measurements – Biosensor Chip Preparation

To develop the ID-LFIA approach, appropriate biorecognition conditions were determined using surface plasmon resonance (SPR). SPR measurements were conducted to evaluate the mAb binding affinity, sensitivity, and analyte dissociation. All measurements were performed on a Biacore 3000 (GE Healthcare, Uppsala, Sweden) with a CM5 chip. DON-BSA and BSA were immobilized on flow channels 1 and 2, using a slightly modified method from the previously described by Joshi et al. (27). First, immobilization of DON-BSA and BSA was done, instead of DON-OVA and OVA. Also, PBS with Tween-20 (0.02% v/v) was used as a running buffer at a flow rate of 5  $\mu$ L/min, in order to simulate better the conditions of the LFIA development. The immobilization starts by first activating the carboxymethylated surface of the CM5 chip, with a 1:1 mixture of EDC/NHS for 7 min, followed by a 7 min injection of DON-BSA 50  $\mu$ g/mL or BSA 50  $\mu$ g/mL, diluted in 10 mM acetate buffer pH 4.5. Following the immobilization, the remaining free carboxymethylated groups of flow channels 1 and 2 were blocked with ethanolamine 1 M injection for 7 min. Finally, the chips were stored at 4–8 °C until further use. All SPR results were processed with Biaevaluate (GE Healthcare, Uppsala, Sweden).

### ID-LFIA Construction

The ID-LFIA was constructed using an XYZ3060 BioJet & AirJet instrument (Biodot Inc., Irvine, CA, USA) with a spraying speed of 1  $\mu$ L/cm. The selected mAb diluted in 1x PBS was sprayed at the center of a nitrocellulose (NC) membrane (HiFlow Plus HF13502, Millipore, Carrigtwohill, Ireland). To capture a high quantity of DON, fifteen identical lines of the same antibody type and dilution were sprayed, thus forming a rectangle zone of mAb on the NC membrane. The NC membrane was then secured on plastic backing (G & L, San Jose, CA, USA). After drying the ID-LFIAs at room temperature, an absorbent pad (Schleicher & Schuell, Dassel, Germany) of 3 cm length was incorporated, slightly overlapping at the end with the NC membrane. In contrast to regular LFIAs, the ID-LFIA lacks visible test and control lines. So, to assure that the running buffer moved correctly through the NC membrane, the indicator bromothymol blue was incorporated into the absorbent pad as follows: the absorbent pad was soaked in the indicator solution and air-dried overnight at room temperature. The indicator changes color from yellow (pH < 6) when dry, to light green (pH > 7.4) when in contact with the running buffer, and keeps the light green color when the ID-LFIA is dry again after sampling. Finally, the ID-LFIAs were cut at a 5 mm width using a CM4000 BioDot Guillotine (Biodot Inc., Irvine, CA, USA). The final ID-LFIA were packed

in aluminum pouches with silica desiccation packs, heat-sealed, and stored in the fridge at 4 °C until further use.

## 2.2.3 Mass spectrometry

### Quadrupole-orbitrap MS

Initial experiments for optimizing ionization conditions were performed on a model Exactive orbitrap high resolution (HR) MS (Thermo Fisher Scientific, San Jose, CA, USA). The heated electrospray ionization (HESI) source parameters for the ionization of DON in negative ESI were optimized with direct infusion of a standard solution of DON 1 µg/mL in MeOH/NH<sub>3</sub> (2% v/v) at a constant flow rate of 20 µL/min. Then, the same optimized HESI source conditions were used for ionizing DON in the model Q-Exactive Focus quadrupole orbitrap hr-MS (Thermo Fisher Scientific). The following settings were used: sheath gas/aux gas 35/10 arbitrary units, spray voltage 2.5 kV, capillary temperature 270 °C, and capillary voltage -50 V. Single ion monitoring (SIM) and MS-MS fragmentation (ddMS<sup>2</sup>) with a normalized collision energy of 10 for DON and 15 for the conjugated form DON-3G were used as data acquisition methods. Spectra were recorded at a resolution of 70000 FWHM at a 3 Hz scan rate with a maximum ion injection time of 1500 ms. The theoretical exact masses of the model analytes and the experimentally obtained *m/z* values for [M-H]<sup>-</sup> precursor ions and fragment ions thereof are given in Table 2.1. Xcalibur software (Thermo Scientific) was used to obtain reconstructed ion chromatograms (RIC) of the selected ions with 5 ppm mass accuracy, as well as the full scan mass spectra in the *m/z* range of 100-600 Da.

**Table 2.1.** Ions monitored for DON and its conjugated forms in Quadrupole-Orbitrap MS and the ion transitions in Triple Quadrupole MS.

Analyte	Theoretical exact mass	Ion (negative ion mode)	Elemental composition	Q-Orbitrap-MS ( <i>m/z</i> )	QqQ-MS/MS ( <i>m/z</i> )
DON	296.1260	[M-H] <sup>-</sup>	[C <sub>15</sub> H <sub>20</sub> O <sub>6</sub> -H] <sup>-</sup>	295.1187	
		Fragment 1	[C <sub>14</sub> H <sub>18</sub> O <sub>5</sub> -H] <sup>-</sup>	265.1081	295.1 > 265.1
		Fragment 2	[C <sub>14</sub> H <sub>16</sub> O <sub>4</sub> -H] <sup>-</sup>		295.1 > 247.1
<sup>13</sup> C-DON	311.1763	[M-H] <sup>-</sup>	[C <sub>15</sub> H <sub>20</sub> O <sub>6</sub> -H] <sup>-</sup>	310.1690	
		Fragment 1	[C <sub>14</sub> H <sub>18</sub> O <sub>5</sub> -H] <sup>-</sup>	279.1551	310.2 > 279.2
DON-3G	458.1788	[M-H] <sup>-</sup>	[C <sub>21</sub> H <sub>30</sub> O <sub>11</sub> -H] <sup>-</sup>	457.1715	
		Fragment 1	[C <sub>20</sub> H <sub>28</sub> O <sub>10</sub> -H] <sup>-</sup>	427.1610	457.0 > 427.0
		Fragment 2	[C <sub>14</sub> H <sub>16</sub> O <sub>4</sub> -H] <sup>-</sup>		457.0 > 247.1

### Triple Quadrupole (QqQ) MS/MS

The conditions of the ESI source were optimized on a Xevo TQ-XS QqQ-MS system (Waters Corporation, Milford, MA, USA) in full scan mode ( $m/z$  100-600) using direct infusion of 1  $\mu\text{g/mL}$  DON in  $\text{MeOH/NH}_3$  (2%  $v/v$ ) with a constant flow rate of 20  $\mu\text{L/min}$ . Fragmentation conditions were optimized in product ion scan mode using 100 ng/mL solutions in  $\text{MeOH/NH}_3$  (2%  $v/v$ ) of DON and DON-3G. Optimized conditions were as follows: capillary voltage 2.5 kV, cone voltage 5 V, source temperature 120  $^\circ\text{C}$ , desolvation temperature 200  $^\circ\text{C}$ , cone gas  $\text{N}_2$  flow 150 L/h, desolvation gas  $\text{N}_2$  flow 300 L/h, collision gas Ar flow 0.16 mL/min. Data were acquired in multiple reaction monitoring (MRM) mode with a collision energy of 11 eV for DON and 15 eV for DON-3G. The final sample analysis was performed using flow injection analysis (FIA) with a 10  $\mu\text{L}$  loop and  $\text{MeOH/NH}_3$  (2%  $v/v$ ) as mobile phase at a flow rate of 80  $\mu\text{L/min}$ ; total runtime was only 0.6 min. For data acquisition and processing of the MS data, MassLynx software (Waters) was used.

### 2.2.4 Sample preparation

The extraction protocol from the r-Biopharm smartphone-based LFIA was used for wheat and barley samples: 1 g of grounded wheat sample was extracted using 15 mL of extraction buffer from the assay kit. Slight agitation is needed, followed by centrifugation to facilitate sedimentation of the sample. For the extraction of the contaminated beer sample, a method previously developed by Pagkali et al. was used (28), because the r-Biopharm protocol was not developed for the analysis of liquid samples. The degassed beer sample was simply diluted 8 times with the r-Biopharm extraction buffer.

In the r-Biopharm LFIA, the extraction buffer doubles as a running buffer so directly after extraction, 100  $\mu\text{L}$  is pipetted onto the sample port of the LFIA. After 5 min, the result can be read visually or by using the smartphone app for a semi-quantitative result. For the development of the ID-LFIA, 200  $\mu\text{L}$  of the same sample extract is used for immersing the ID-LFIA, without any additional sample preparation and extraction needed. Next, the rectangle zone of mAb on the ID-LFIA is isolated and placed in an Eppendorf tube to wash with 500  $\mu\text{L}$  of Milli-Q and slight agitation. The washing step aids non-specifically bound analytes removal and minimizes the ion suppression effects of assay buffer and NC membrane residues. Afterward the rectangle zone of mAb on the ID-LFIA is placed in an Eppendorf tube filled with 200  $\mu\text{L}$  dissociation solution of  $\text{MeOH/NH}_3$  (2%  $v/v$ ). After vortexing for 5 min and adding 40 ng/mL  $^{13}\text{C}$ -DON internal standard (IS), to compensate for the ion suppression, the final solution is ready for analysis by direct ESI-MS.

To demonstrate the efficiency of this protocol in coping with ion suppression, the extraction protocol from a second LFIA provider, Charm Sc., was used in which 10 g of ground wheat sample was extracted with 50 mL of Milli-Q water, shaken for 1 min and centrifuged. 100  $\mu\text{L}$  of the extract was mixed with 1 mL of assay buffer, yielding the final solution used to develop the ID-LFIA according to the above protocol.

## 2.3 Results

### 2.3.1 General concept

Direct coupling of a (smartphone-based) screening LFIA and MS is not straightforward. For low molecular weight analytes, such as the model analyte, DON, the most common LFIA format is a competitive assay. This assay format does not allow direct ionization of the analyte of interest because it is found by the end of the LFIA (in the absorbent pad) (29). Therefore, a complementary ID-LFIA was developed, with anti-DON mAb, immobilized directly on the NC membrane for the subsequent detection and identification of DON by direct MS analysis. In this concept, the end-user may perform on-site a (smartphone-based) LFIA and, in the case of a suspect result, immediately immerse the newly designed ID-LFIA into the same sample extract. The ID-LFIA can be sent for confirmation in the lab with direct MS analysis (Figure 2.1).

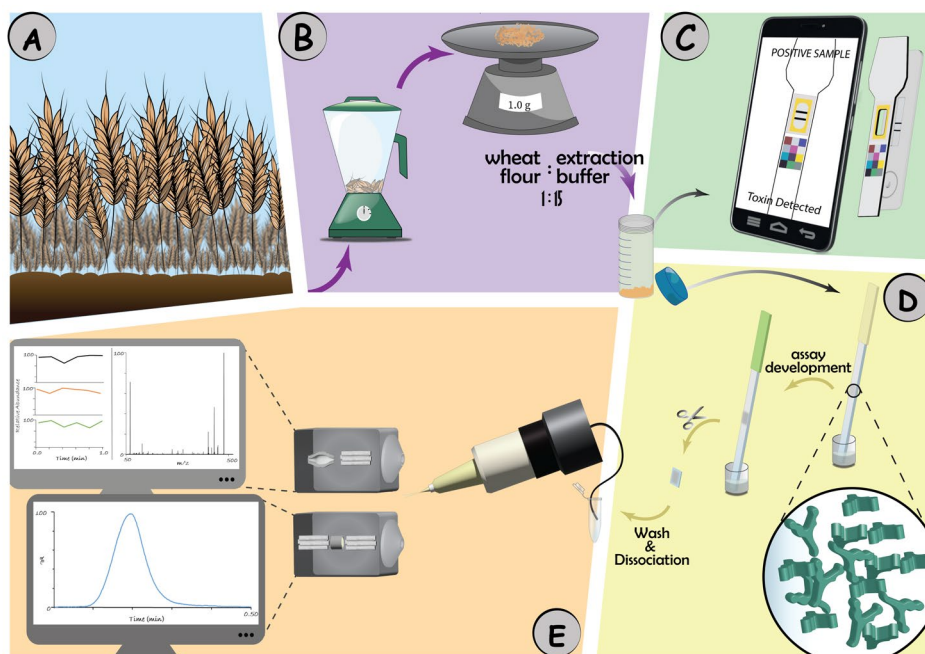


**Figure 2.1.** General concept of the ID-LFIA direct MS approach. (A) Sampling of the selected food commodity (wheat) on-site. (B) Homogenization and simplified extraction, (C) performance of a smartphone-based screening LFIA. If the result is suspect ('positive'), then (D) the same extract is used to develop the ID-LFIA. After development of the ID-LFIA, the mAb trapping zone is isolated, followed by washing, and dissociation. (E) Finally, the retrieved solution is directly analyzed by Q-Orbitrap MS, or QqQ MS/MS.

The main benefit of this concept is the very rapid confirmation of the analytes causing the suspect LFIA screening result. No laborious conventional LC-MS/MS is needed to check for false positive LFIA screening results. Only if more specification and/or a more accurate quantification is needed then conventional time-consuming LC-MS/MS analysis follows, for example for the purpose of specific regulatory requirements. When, in the future, LFIAs are increasingly used on-site by non-experts, it is essential to overcome increased confirmatory analysis time and costs spent in the lab on increasing false positive screening samples.

### 2.3.2 ID-LFIA development

To develop the ID-LFIA approach, appropriate the mAb were evaluated using SPR. DON-BSA and BSA diluted to 50  $\mu\text{g/mL}$  in 10 mM acetate buffer of pH 4.5, were immobilized on a CM5 chip to serve as assay and reference channels, respectively. The mAbs (clone 2 and 4 diluted in running buffer at a concentration of 20  $\mu\text{g/mL}$ ) were screened for their affinity towards immobilized DON-BSA. According to the RU values in the SPR sensograms obtained (Figure 2.2), we can conclude that mAb clone 2 is binding with a higher affinity to DON-BSA immobilized on the surface than clone 4. We observed that clone 2, was not dissociating; in contrast, clone 4 dissociated rapidly from the DON-BSA chip, demonstrating a stronger binding of the former.

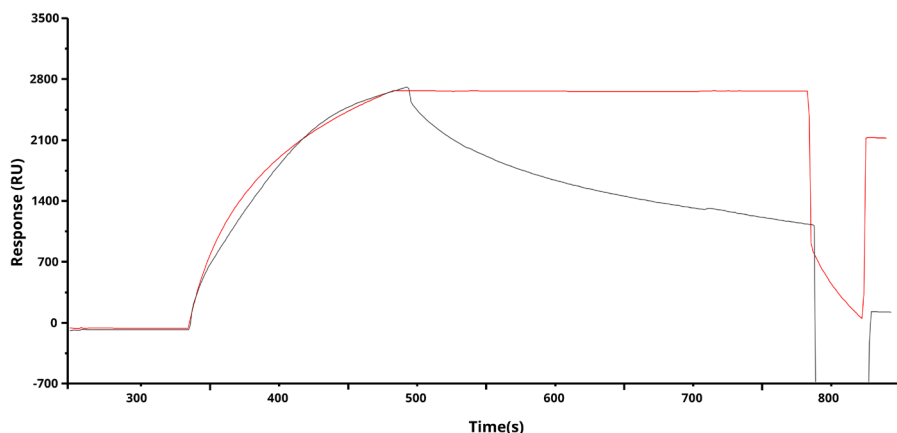


**Figure 2.2.** SPR sensograms comparing the binding of mAb clones 2 (red) and 4 (green) to immobilized DON-BSA on the flow channel of the SPR chip. Conditions: running buffer of PBS with Tween-20 (0.02% v/v) at a flow rate of 5  $\mu\text{L/min}$ . Injection of 35  $\mu\text{L}$  of each mAb. Regeneration of the SPR chip surface by injecting 25 mM NaOH at a flow rate of 100  $\mu\text{L/min}$ .

To assess the sensitivity of the selected antibody, an inhibition method was implemented as described in literature (30). A 35  $\mu\text{L}$  mixture of mAb 2  $\mu\text{g/mL}$  together with increasing concentrations of DON standard solutions diluted in running buffer (1:1 v/v) were injected in the flow channels 1 and 2. The concentration of DON ranged

from 0.0001  $\mu\text{g/mL}$  to 10  $\mu\text{g/mL}$ , with steps of a tenfold concentration increase. The experiment was performed in duplicate, with four blank solvent injections, two at the beginning and two at the end of the method (Figure 2.3).

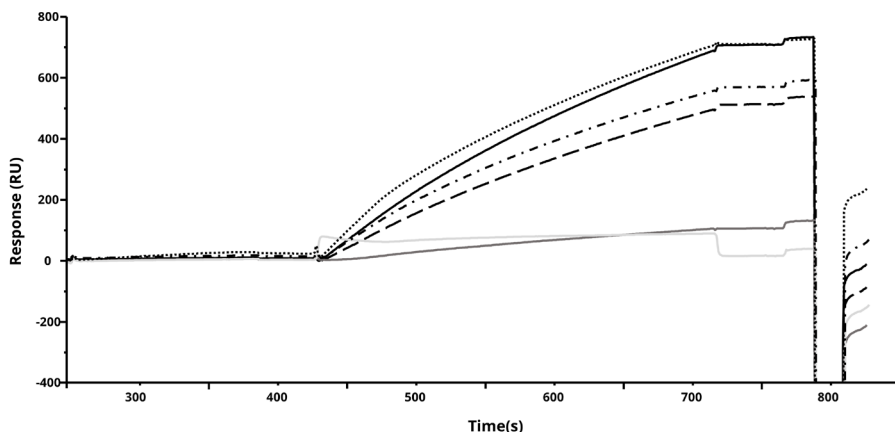


**Figure 2.3.** Overlay SPR sensograms obtained from the inhibition assay for DON.

### 2.3.3 Direct electrospray MS of dissociated DON

For the MS experiments, we first optimized the ionization conditions for DON using different standard solutions. Secondly, the compatibility of the dissociating solution of the ID-LFIA with ESI-MS and the matrix effects from both the LFIA assay buffers and the ID-LFIA material residues were investigated in detail.

Dissociation of antibody binding can be achieved, among others, under acidic or alkaline conditions. Therefore, for evaluating the MS sensitivity of DON, we tested both 1  $\mu\text{g/mL}$  DON in solutions of HCOOH (0.1% v/v),  $\text{NH}_3$  (0.1% v/v) and ammonium acetate/acetic acid buffer and in different solvents such as MeOH and ACN, as well as mixtures of the organic solvents with  $\text{H}_2\text{O}$  in 50/50 (v/v). The solution that yielded the highest MS intensity at optimized ionization conditions is MeOH/ $\text{NH}_3$  for the deprotonated ion of DON in negative ESI mode (Figure 2.4). Compared with the most intense ion in positive ESI mode, there was a 50-fold or higher increase in signal. Moreover, the final negative ESI conditions of 2.5 kV spray and -50 V capillary voltages showed to be very robust, as only minor differences were observed for the intensity of the deprotonated ion of DON at the various capillary and spray voltages tested. Next, we tested different percentages of  $\text{NH}_3$ , and 2% v/v of  $\text{NH}_3$  in MeOH was sufficient for optimal ionization, without altering the appearance of the spectra.

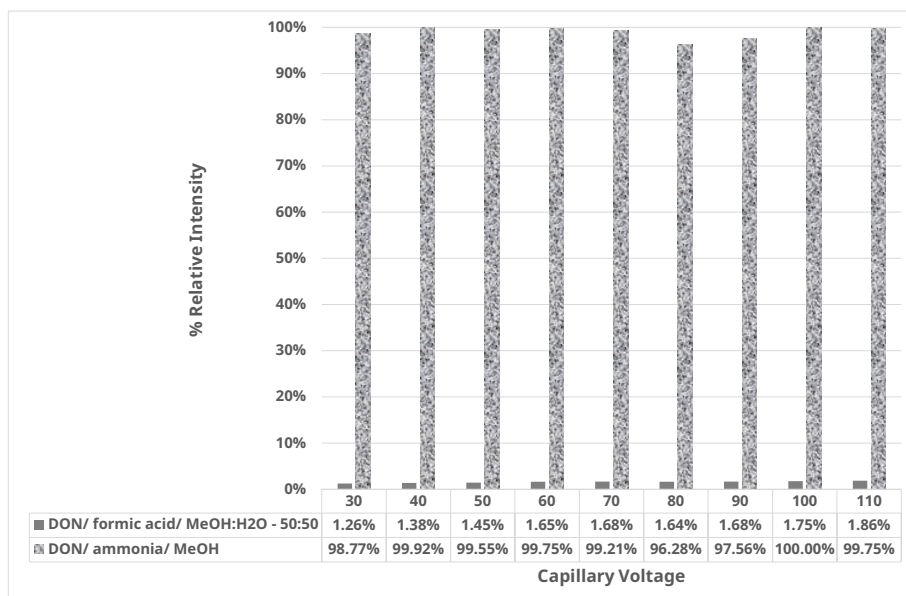


**Figure 2.4.** Relative intensity of DON 1  $\mu\text{g/mL}$   $[\text{M-H}]^-$  and  $[\text{M+H}]^+$  in Methanol/ ammonia 0.1% v/v and methanol/ water/ formic acid 50/50/0.1 v/v/v, shown in grey and black bars, respectively. From all the different solutions of DON tested, those are the optimum for the ionization in negative and positive mode, recorded at 2.5 kV spray voltage, resolution of 50000 FWHM and 4.5 kV spray voltage, resolution of 100000 FWHM, respectively.

To assess the effective dissociation of mAb-DON binding in the optimized solution of  $\text{NH}_3$  2%v/v in MeOH, an SPR measurement was conducted. In a CM5 SPR chip, with immobilized DON-BSA, using PBS with Tween-20 (0.02% v/v), as a running buffer with a flow rate of 5  $\mu\text{L/min}$ , 35  $\mu\text{L}$  of clone 2 antiDON mAb was injected, followed by a 20  $\mu\text{L}$  regeneration injection of MeOH/ $\text{NH}_3$  (2% v/v). According to the RU values in the SPR sensogram obtained before and after the regeneration (Figure 2.5), we can conclude that the selected MeOH/ $\text{NH}_3$  (2% v/v) dissociation solution, is effective for rapid and complete dissociation. The regeneration of the SPR chip requires approximately 3 min, so a total vortex time of 5 min and a 200  $\mu\text{L}$  volume was chosen in the final ID-LFIA protocol to reassure complete dissociation of the analyte from the mAb.

### 2.3.4 Ion suppression study

Different types and percentages of LFIA buffers, commonly used in screening assays, such as 1x PBS, were tested to assess the effect of residual buffer salts and detergents on the MS signal. Buffers used in immunoassays typically contain various non-volatile salts, such as sodium chloride or potassium phosphate (31), known to cause severe ion suppression in ESI-MS (19). As expected, a higher percentage of buffers showed increased ion suppression, as well as, increased background, regardless of the type of the buffer used (Figure 2.6).

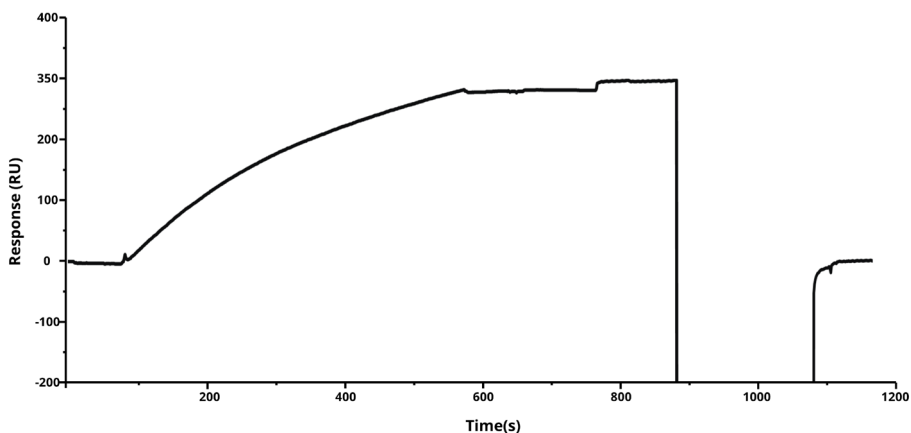


**Figure 2.5.** SPR sensograms of the binding of mAb clones 2 to immobilized DON-BSA on the flow channel of the SPR chip, followed by regeneration with the dissociation solution MeOH/NH<sub>3</sub> 2%. The RU value reaches the baseline after the regeneration.

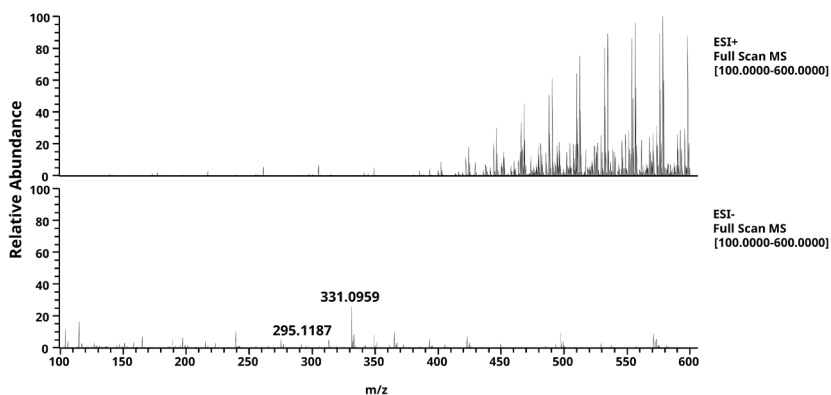


**Figure 2.6.** Full scan mass spectra ( $m/z$  100-600), normalized on the highest intensity, of DON 1  $\mu\text{g/mL}$  in MeOH/NH<sub>3</sub> (2% v/v) solution containing *r*-Biopharm running buffer (10% v/v) in positive ESI mode (above) and negative ESI mode (below).

As can be seen in Figure 2.6, the background caused by the surfactant is significantly higher in positive ion mode compared with the negative ion mode. In the negative ion spectra, both the  $[\text{M}-\text{H}]^-$  ion at  $m/z$  295.1187 and the  $[\text{M}+\text{Cl}]^-$  ion of DON at  $m/z$  331.0954 can be clearly observed, despite the ion suppression caused by the assay buffer. Aiming for a robust rapid analysis protocol, a washing step using 500  $\mu\text{L}$  of Milli-Q water was incorporated to remove the excess LFIA buffer components prior to dissociation with MeOH/NH<sub>3</sub> (2% v/v).



However, ion suppression may be caused not only by the LFIA buffer but also by residues from the NC membrane. During the production of NC membranes for LFIA use, proprietary additives are being used by manufacturers. And since nitrocellulose dissolves partly in MeOH/NH<sub>3</sub> (2% v/v) during the dissociation step, membrane-embedded additives that cannot be entirely removed in the aqueous washing step may end up in the final solution for MS analysis. To evaluate the overall ion suppression caused by assay buffer and the nitrocellulose residues, we conducted a matrix-matched ion suppression study by comparing the intensity of the [M-H]<sup>-</sup> ion of 40 ng/mL DON spiked in MeOH/NH<sub>3</sub> (2% v/v) (reference solution) to DON in a solution of a MeOH/NH<sub>3</sub> (2% v/v) extract from a blank ID-LFIA developed with the assay buffer according to the ID-LFIA protocol. The results of the comparison showed an 80% drop in the intensity of DON in the extract from blank ID-LFIA (Figure 2.7). In order to achieve still adequate sensitivity for the identification of DON in the less sensitive Q-Orbitrap MS, the ratio of captured DON molecules versus buffer/NC substrate background was successfully managed by increasing the number of mAb lines on the ID-LFIA to 15, thereby creating a rectangular affinity trapping zone. By cutting that mAb zone from the ID-LFIA prior to the dissociation with MeOH/NH<sub>3</sub> (2% v/v), we minimized the interference caused by dissolved nitrocellulose residues. As a result, in the final ID-LFIA MS protocol and despite the lack of additional clean-up steps and chromatography, the sensitivity of DON to <sup>13</sup>C-DON ratio, dropped only by a factor of 2.5 and the linear regression only from 0.999 to 0.994 in the concentration range of 8-40 ng/mL. Remember that the <sup>13</sup>C-DON is added just prior to the MS analysis and will compensate, at least partly, for ionization interferences but not for incomplete recovery from the immunocapturing and dissociation steps. The final sensitivity for DON thus obtained in ID-LFIA MS is adequate for identification at regulatory limits.

Assuming 100% recovery from the mAb, an absolute quantity of 0.28 ng of DON is captured on a single line of mAbs. The number of lines increased the absolute quantity of analytes trapped by the mAb and the concentration of analytes in the sample solution for MS analysis. Calculations were made based on (i) the sensitivity of the orbitrap MS taking into account the ion suppression conditions, (ii) the maximum mAb loading and trapping capacity per line, and (iii) the required regulatory limits. Based on these calculations, an immunocapturing area composed of a number of 15 lines was found to be fit-for-purpose. In the final protocol, a 200 μL MeOH solution containing 2 % v/v NH<sub>3</sub> solution was used for the dissociation and recovery of DON from the mAb on the ID-LFIA. The calculated theoretical concentration of DON, assuming an extracted sample containing 1750 μg/kg DON and 100% recovery of DON from the 15 lines of mAb following dissociation from the mAb and aqueous washing, will be approximately 100 ng/mL in the absence ion suppression. In combination with the expected ion suppression from the substrate, we expect a signal beyond the LOD and LOQ (13 and 38 ng/mL, respectively) of the orbitrap MS. This will allow MS identification of DON and/or its conjugates in samples previously screened suspect by smartphone-based LFIA but not a precise and accurate quantification.

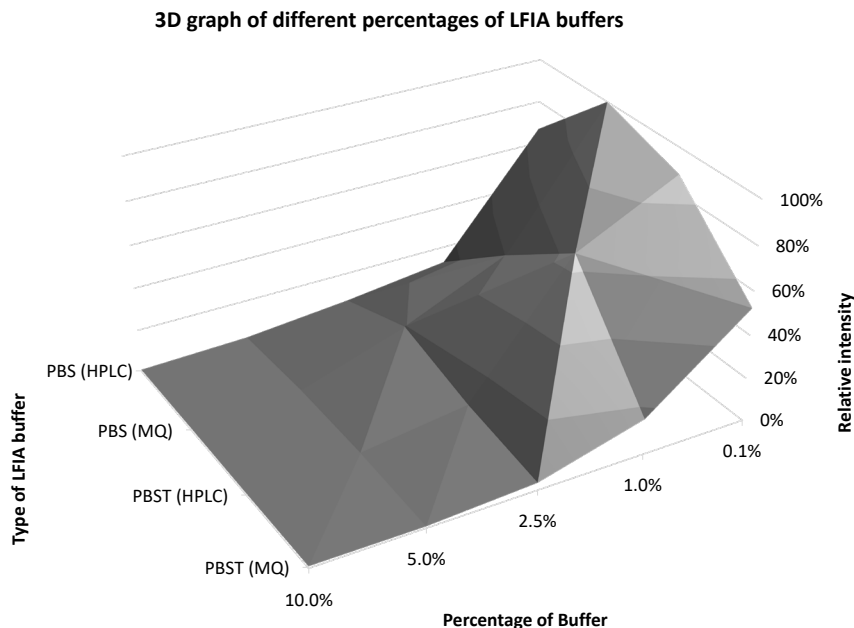


**Figure 2.7.** The relative intensity of  $[M-H]^+$  of DON 1  $\mu\text{g/mL}$  in standard solutions of MeOH/NH<sub>3</sub> (2% v/v) containing different percentages of running buffer. The higher the percentage of the running buffer, the higher the ion suppression, regardless of the type and the purity of the buffer used.

### 2.3.5 Analysis of spiked and incurred samples

In the final Q-Orbitrap experiments, we chose to acquire deprotonated ions  $[M-H]^-$  in single ion monitoring (SIM) mode, followed by MS/MS measurement of the characteristic fragment ion of each analyte (Table 2.1.). Apart from a hybrid Q-Orbitrap MS we also used a QqQ-MS/MS, being the most frequently used MS technique in confirmatory food analysis (32–35). For negative ESI-MS/MS detection the MRM data acquisition mode was used, at the optimized conditions given in section 2.2.3.

Following the developed approach, both naturally contaminated and spiked samples were analyzed. In Q-Orbitrap MS, a blank certified reference wheat material extract was spiked at 200 ng/mL for DON-3G and 100 ng/mL for DON. The sample was analyzed 6 times to demonstrate the repeatability of the ID-LFIA Q-Orbitrap procedure. For the QqQ measurements, 6 different blank wheat samples were analyzed, as well as spiked versions thereof, at 200 ng/mL DON. Moreover, to demonstrate that the developed ID-LFIA MS protocol is independent of the running buffer composition and applicable to different sample matrices, we also analyzed ID-LFIAs developed with 1x PBST (0.05% v/v Tween-20), HEPES, the running buffer from the commercial Charm DON assay, and ID-LFIAs developed with barley extracts. Finally, naturally contaminated wheat and beer samples were analyzed in both instruments.

Using the extraction protocol described in section 2.2.4, DON was isolated from the blank and spiked samples, and the extract was analyzed in duplicate by both the DON LFIA with smartphone readout and the newly developed ID-LFIA direct MS analysis approach. Thanks to the smartphone camera and app, a semi-quantitative result is obtained, next to the visual readout, which can be compared with the MS analysis. The results are shown in *Table 2.2* and *Table 2.3*. In all cases, negative and suspect smartphone LFIA screening results were successfully confirmed by ID-LFIA MS analysis: blank samples did not show any DON or DON conjugate in the MS analyses, while ID-LFIA MS analysis of spiked and incurred samples showed characteristic deprotonated and fragment ions, allowing rapid confirmation of identity (*Figure 2.8* and *Figure 2.9*), based on accurate mass and area ion ratio data. From *Table 2.2* it can be seen that the repeatability of the DON signal for the six (identical) spiked wheat samples in ID-LFIA Q-Orbitrap MS was 7.2% RSD without correction for the IS  $^{13}\text{C}$ -DON. In ID-LFIA QqQ-MS/MS the robustness of the area ion ratio (the mean ratio of the absolute area of the DON MRM product ion at  $m/z$  247.1 to the area of the ion at  $m/z$  265.1) turned out to be excellent for confirmation of identity according to regulatory requirements (*Table 2.3*). Moreover, neither the stability of the ion ratio nor the stability of the response factor versus the  $^{13}\text{C}$ -DON quality control standard was affected by the sample matrix or the assay buffer composition.

Regarding the incurred beer, the screening LFIA smartphone app reported a positive DON result of more than 5.5 mg/kg. However, according to the ID-LFIA MS follow-up analysis, this beer sample was found to contain apart from DON also DON-3G, thereby underlining the added value of rapid MS identification of suspect LFIA screening assays. These results are in very good agreement with data from biochip spray MS and conventional confirmatory LC-MS/MS analysis, in which the same beer sample was found to contain 3.8 mg/mL of DON-3G and 2.8 mg/mL of DON (25).

In confirmatory techniques, four identification points (IPs) are required for substances with an established ML. The IPs are earned by measuring specific characteristics, as described in the legislation (2). In our ID-LFIA MS approach, when measuring in hybrid Q-Orbitrap MS, two ions, namely, the precursor ion and a product ion, are monitored, thus yielding 4 IPs. Even without chromatographic separation, the IP system can be applied to confirm the identity of the analyte causing the suspect LFIA screening result. With the QqQ, two product ions are monitored in MRM mode yielding 3 IPs. Apart from that, additional IPs might possibly be granted in future revision of the legislation because of the inherent "immuno-chromatography" nature of the ID-LFIA.

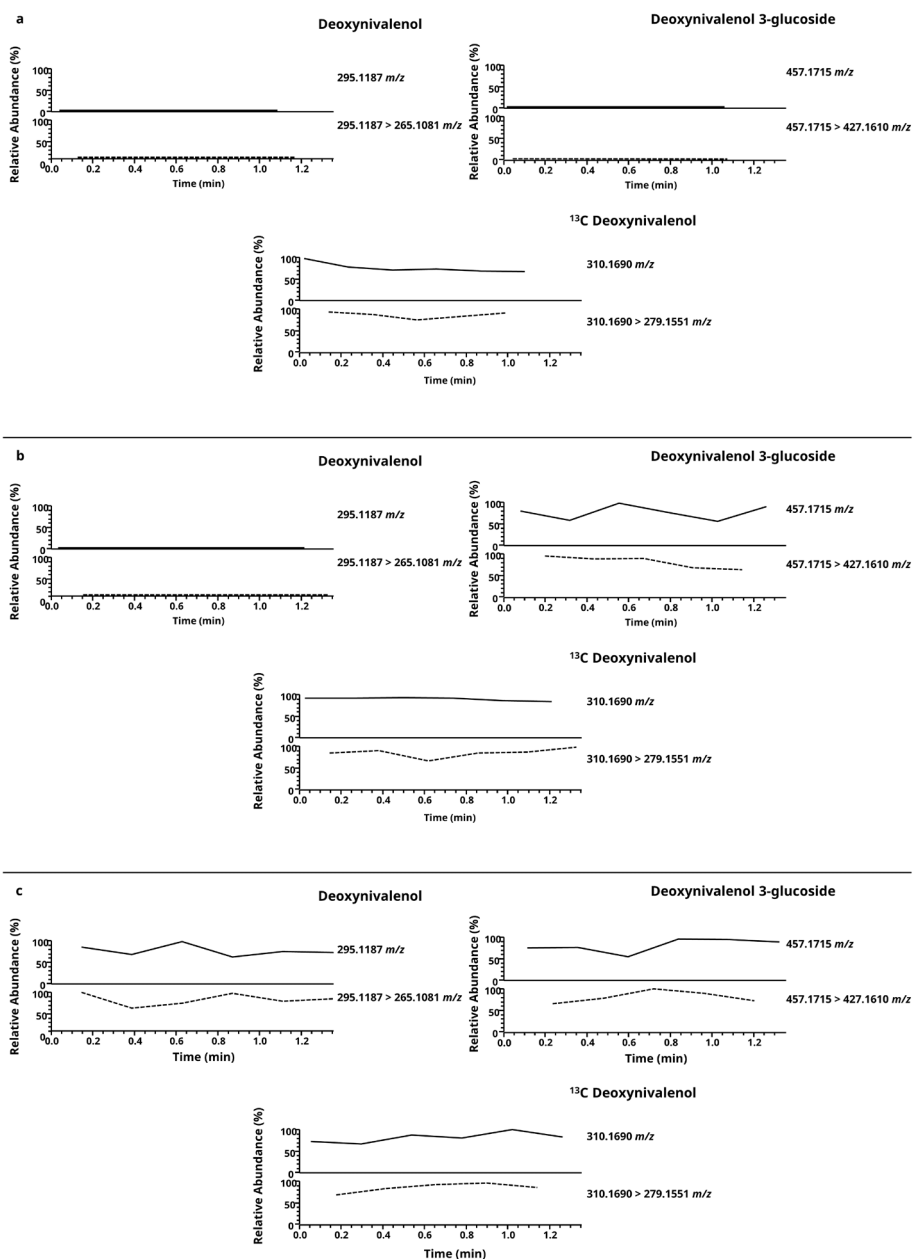


**Figure 2.8.** ID-LFIA Q-Orbitrap reconstructed ion currents for DON and DON-3G, and fragment ions thereof, in (a) blank wheat, (b) DON 3G spiked wheat and (c) an incurred beer sample.  $^{13}C$ -DON added as a quality control IS prior to MS analysis. The deprotonated ion is shown in continuous line and the main fragment ion in dashed line.

**Table 2.2.** Results from ID-LFIA Q-Orbitrap MS analysis of wheat and beer samples

Sample	mean absolute intensity of peak height ± SD				LFIA screening result (mg/kg, mean ± SD)
	DON		DON-3G		
<i>m/z</i>	295.1187	265.1081	457.1715	427.1610	
Blank wheat	-	-	-	-	<0.50(±0.00)
Spiked DON Wheat (1)	1045(±5.0)	338(±8.5)	-	-	2.63(±0.09)
Spiked DON Wheat (2)	1311(±29.0)	293(±5.5)	-	-	2.48(±0.01)
Spiked DON Wheat (3)	1046(±64.0)	291(±17.5)	-	-	2.57(±0.13)
Spiked DON Wheat (4)	1710(±250.0)	473(±22.5)	-	-	2.35(±0.00)
Spiked DON Wheat (5)	1665 (±130.0)	564(±3.5)	-	-	2.54(±0.04)
Spiked DON Wheat (6)	1550(±135.0)	507(±41)	-	-	2.56(±0.11)
Spiked DON Wheat – 1 week sta- bility of de- veloped ID- LFIA	1580(±50)	994(±47)	-	-	2.60(±0.01)
Incurred wheat DON	1165(±45)	287(±21)	-	-	2.57(±0.00)
Spiked DON-3G wheat	-	-	2230(±30)	983(±77)	2.64(±0.00)
Incurred beer UCT	3360(±220)	745(±34)	2900(±140)	820(±2)	>5.50(±0.00)

Conditions: duplicate infusions of the same final ID-LFIA dissociation solution in Q-Orbitrap MS. SD is the standard deviation of the duplicate measurement. The LFIA screening result was obtained with the *r-Biopharm* LFIA for DON and quantification with the associated smartphone application. SD is the standard deviation of duplicate reading of the same LFIA.

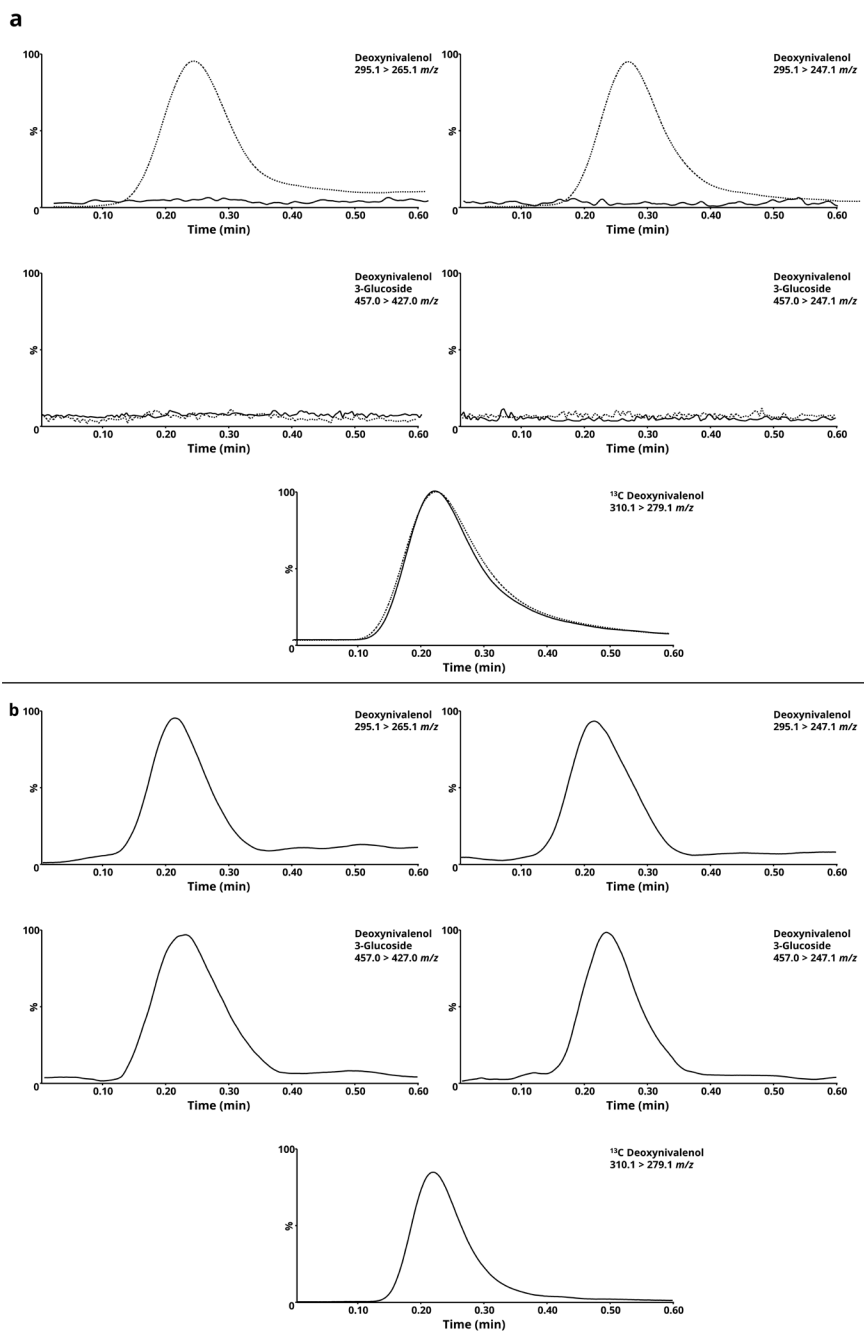


**Figure 2.9.** ID-LFIA MS/MS reconstructed MRM transition ion currents of DON and DON-3G in (a) spiked wheat (dashed line) overlaid with blank wheat (continuous line), (b) incurred beer sample.  $^{13}\text{C}$ -DON added as a quality control IS prior to MS analysis.

**Table 2.3.** Results from ID-LFIA ESI-QqQ-MS/MS analysis of wheat, barley, and beer samples

Sample	DON		DON-3G		LFIA screening result (mg/kg, mean $\pm$ SD)
	Mean area ion ratio $\pm$ SD	Response factor $\pm$ SD	Mean area ion ratio $\pm$ SD	Response factor $\pm$ SD	
Spiked DON Wheat (nr 798)	0.31 ( $\pm$ 0.03)	0.16( $\pm$ 0.011)	-	-	3.95( $\pm$ 0.10)
Spiked DON Wheat (nr 802)	0.31 ( $\pm$ 0.04)	0.16( $\pm$ 0.004)	-	-	3.88( $\pm$ 0.00)
Spiked DON Wheat (nr 803)	0.30 ( $\pm$ 0.05)	0.16( $\pm$ 0.003)	-	-	3.87( $\pm$ 0.03)
Spiked DON Wheat (CRM)	0.30 ( $\pm$ 0.02)	0.16( $\pm$ 0.005)	-	-	4.29( $\pm$ 0.17)
Spiked DON Wheat (nr 607)	0.30 ( $\pm$ 0.00)	0.16( $\pm$ 0.002)	-	-	3.88( $\pm$ 0.02)
Spiked DON Wheat (nr 670)	0.31 ( $\pm$ 0.06)	0.16( $\pm$ 0.004)	-	-	3.93( $\pm$ 0.19)
Spiked DON Barley (nr 797)	0.31 ( $\pm$ 0.01)	0.17( $\pm$ 0.021)	-	-	3.48( $\pm$ 0.10)
Spiked DON Wheat (CRM)/ 1x PBST (0.05% tween-20)	0.30( $\pm$ 0.05)	0.16( $\pm$ 0.001)	-	-	-
Spiked DON Wheat (CRM)/ 1x HEPES	0.29( $\pm$ 0.01)	0.17( $\pm$ 0.006)	-	-	-
Spiked DON Wheat (CRM)/ Charm Sc. r.b.	0.29( $\pm$ 0.00)	0.16( $\pm$ 0.009)	-	-	-
Incurred wheat DON	0.30( $\pm$ 0.01)	0.17( $\pm$ 0.008)	-	-	3.56( $\pm$ 0.18)
Incurred beer UCT	0.30( $\pm$ 0.04)	0.16( $\pm$ 0.005)	1.0( $\pm$ 0.02)	0.02( $\pm$ 0.007)	>5.5( $\pm$ 0.00)

Conditions: Duplicate injections of 10  $\mu$ L of the same final ID-LFIA dissociation solution were done in QqQ MS/MS with a flow rate of 80  $\mu$ L/min. SD is the standard deviation of the duplicate measurements, and response factor is the mean area ratio of DON/ $^{13}$ C DON of m/z 265.1 / 279.2, or DON-3G /  $^{13}$ C DON of m/z 427.1 / 279.2. The screening result was performed with the r-Biopharm LFIA and the quantification was done with the associated smartphone app. SD is the standard deviation of duplicate reading of the same LFIA.

### 2.4 Discussion

A simplified direct analysis of an LFIA with MS was developed allowing the rapid identification of low molecular weight analytes previously screened as suspect by regular or smartphone-based LFIA. Supported by SPR studies, selective capturing of the target analyte by a mAb on a newly developed ID-LFIA was achieved, followed by identification of the immuno-captured analyte, as well as any (un)expected cross-reacting conjugates, using either Q-Orbitrap MS or QqQ MS/MS. The developed ID-LFIA MS protocol was found to rapidly confirm the identity of the analytes based on accurate mass and/or robust ion ratios that were not affected by different sample matrices nor by different LFIA buffer compositions. The ion suppression caused was successfully managed, by introducing multiple lines of mAb and the addition of a washing step. Nonetheless, future experimentation with different types of porous substrates to capture the mAb and provide capillary flow, different types of rapid screening assays, and subsequent direct analysis of the analytes with MS could be tested to provide alternative direct analytical approaches.

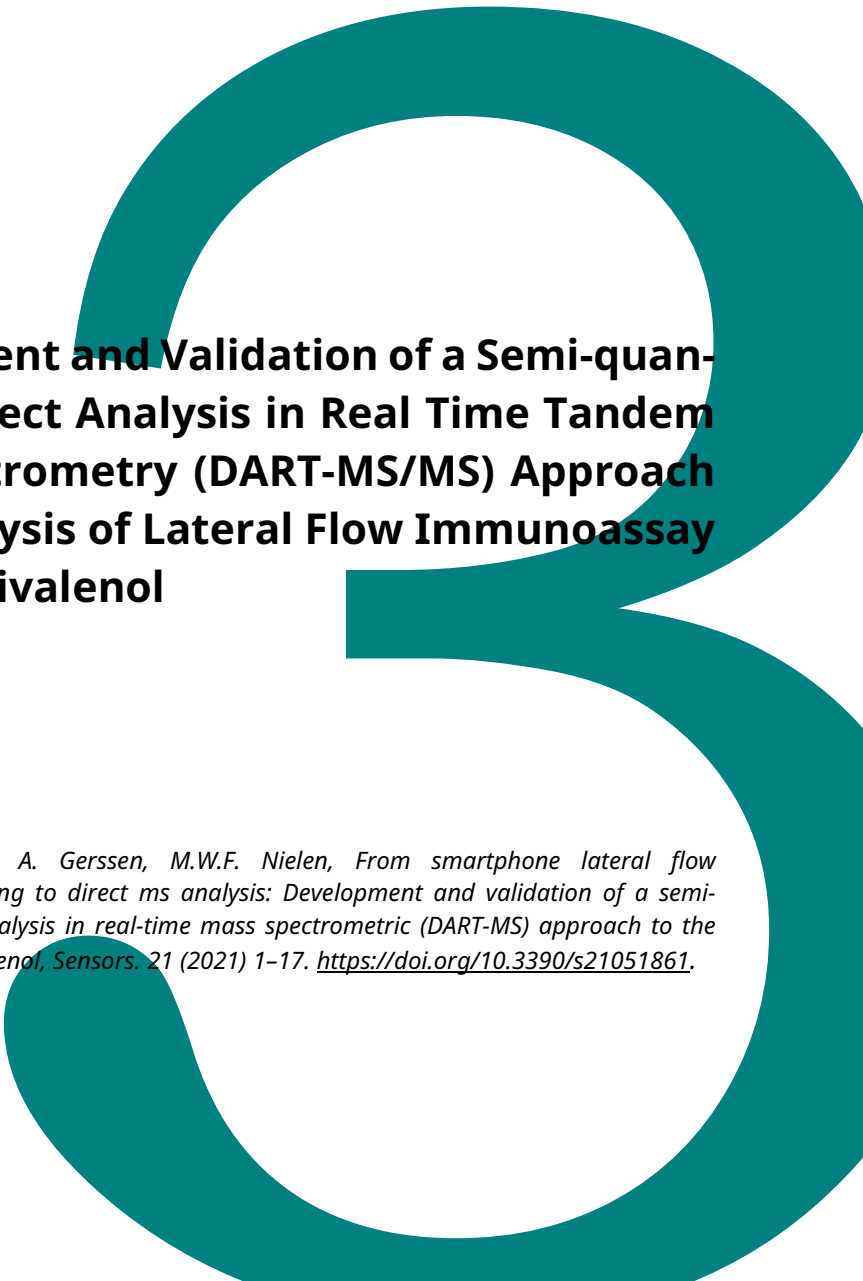
In the world of increasing numbers of simplified and smartphone-based food safety screening diagnostics, higher numbers of screening data will become available and, as a consequence, the number of results requiring a follow-up by instrumental analysis will increase as well, leading to more and more time-consuming confirmatory analysis needed. Even though conventional LC-MS/MS analysis has higher multiplexing and quantitative potentials (16, 22, 35), the developed ID-LFIA MS approach may act as an intermediate between the screening assays and the conventional quantitative confirmatory analysis by chromatographic separation followed by mass spectrometry, in order to moderate the increasing number of analyses. Following this concept, an individual performs a commercially available smartphone-based screening assay with LFIA format. In case of a suspect or ambiguous result, one would simply immerse our newly developed ID-LFIA in the same sample extract and send the developed ID-LFIA to the lab by courier, mail, or otherwise, for further processing. Following the wash and dissociation steps, the LFIA can be analyzed by direct MS in the lab, requiring less than a minute to either verify or reject the LFIA screening result as a false positive. Only if the result of this intermediate analysis is positive and further information or accurate quantification is needed, then conventional confirmatory analysis with LC-MS/MS would be necessary to be performed.



## 2.5 References

1. European Commission, *Off. J. Eur. Union*. **31**, 1–24 (2002).
2. European Commission. *Off. J. Eur. Union*. **180**, 84–109 (2021)
3. M. G. Lozano, Y.P. García, J.A.S. Gonzalez, C.V.O. Bañuelos, M.P.L. Escareño, N. Balagurusamy, *Enzymes in Food Biotechnology: Production, Applications, and Future Prospects*, **40**, 691–709 (2018).
4. R. Monosik, M. Stredansky, J. Tkac, E. Sturdik, *Food Anal. Methods*. **5**, 40–53 (2012).
5. M. S. Thakur, K. V. Ragavan, *J. Food Sci. Technol.* **50**, 625–641 (2013).
6. M. Han, L. Gong, J. Wang, X. Zhang, Y. Jin, R. Zhao, C. Yang, L. He, X. Feng, Y. Chen, *Sensors Actuators, B Chem.* **292**, 94–104 (2019).
7. J. Liu, S. Zanardi, S. Powers, M. Suman, *Food Control*. **26**, 88–91 (2012).
8. G. M. S. Ross, G. I. Salentijn, M. W. F. Nielen, *Biosensors*. **9**, 1–21 (2019).
9. Y. Lu, Z. Shi, Q. Liu, *Curr. Opin. Food Sci.* **28**, 74–81 (2019).
10. M. Rezazadeh, S. Seidi, S. Pedersen-Bjergaard, Y. Yamini, *TrAC*. **118**, 548–555 (2019).
11. G. Rateni, P. Dario, F. Cavallo, *Sensors*. **17**, 1453–1460 (2017).
12. K. M. Koczula, A. Gallotta, *Essays Biochem.* **60**, 111–120 (2016).
13. A. Chen, S. Yang, *Biosens. Bioelectron.* **71**, 230–242 (2015).
14. V. M. T. Lattanzio, B. Ciasca, S. Powers, C. von Holst, **76**, 137–144 (2016).
15. A. S. Tsagkaris, J.L.D. Nelis, G.M.S. Ross, S. Jafari, J. Guercetti, K. Kopper, Y. Zhao, K. Rafferty, J.P. Salvador, D. Migliorelli, G.I. Salentijn, K. Campbell, M.P. Marco, C.T. Elliot, M.W.F. Nielen, J. Pulkrabova, J. Hajslova, *TrAC*. **121**, 115688 (2019).
16. M. Sulyok, F. Berthiller, R. Krska, R. Schuhmacher, *Rapid Commun. Mass Spectrom.* **20**, 2649–2659 (2006).
17. E. De Dominicis, I. Commissati, M. Suman, *J. of Mass Spectrom.* **47**, 1232–1241 (2012).
18. B. Ciasca, M. Pascale, V.G. Altieri, F. Longobardi, M. Suman, D. Catellani, V.M.T. Lattanzio, *J. Mass Spectrom.* **53**, 743–752 (2018).
19. T. M. Annesley, *Clin. Chem.* **49**, 1041–1044 (2003).
20. European Commission. *Off. J. Eur. Union*, **364**, 558–577 (2006).
21. V. Nagl, G. Schatzmayr, *Curr. Opin. Food Sci.* **5**, 43–49 (2015).
22. R. Krska, M. Sulyok, F. Berthiller, R. Schuhmacher, *Mycotoxins*. **67**, 11–16 (2017).
23. S. Chen, Q. Wan, A. K. Badu-Tawiah, *J. Am. Chem. Soc.* **138**, 6356–6359 (2016).
24. K. M. Evans-Nguyen, T. L. Hargraves, A. N. Quinto, *Anal. Methods*. **9**, 4954–4957 (2017).
25. S. Joshi, H. Zuilhof, T. A. Van Beek, M. W. F. Nielen, *Anal. Chem.* **89**, 1427–1432 (2017).
26. Y. Zhao, M. Tang, F. Liu, H. Li, H. Wang, D. Xu, *Anal. Chem.* **91**, 13418–13426 (2019).
27. S. Joshi, A. Segarra-Fas, J. Peters, H. Zuilhof, T.A. Van Beek, M.W.F. Nielen, *Analyst*. **141**, 1307–1318 (2016).
28. V. Pagkali, P.S. Petrou, E. Makarona, G. Jobst, I. Moser, K. Gajos, A. Budkowski, A. Economou, K. Misiakos, I. Raptis, S.E. Kakabakos, *J. Hazard. Mater.* **359**, 445–453 (2018).
29. T. Mahmoudi, M. de la Guardia, A. Mokhtarzadeh, B. Baradaran, *TrAC*. **116**, 13–30 (2019).
30. T. Kadota, Y. Takezawa, S. Hirano, T. Nakajima, T. Tanaka, Y. Kamata, Y. Sugita-Konishi, *Anal. Chim. Acta*. **673**, 173–178 (2010).
31. K. L. Cox, V. Devanarayan, A. Kriauciunas, J. Manetta, C. Montrose, S. Sittampalam, *A Immunoassay methods. In: Assay Guidance Manual*, 1–39 (2014)
32. E. Beltrán, M. Ibáñez, J. V. Sancho, F. Hernández, *Rapid Commun. Mass Spectrom.* **23**, 1801–1809 (2009).
33. Y. Ren, Y. Zhang, Z. Cai, L. Feng, H. Pan, Z. Wang, *J. Chromatogr. A*. **1143**, 48–64 (2007).
34. X. Xu, Z. Cai, J. Zhang, Q. Chen, B. Huang, Y. Ren, *Food Control*. **71**, 393–402 (2017).
35. D. Steiner, R. Krska, A. Malachová, I. Taschl, M. Sulyok, *J. Agric. Food Chem.* **68**, 3868–3880 (2020).





## **Development and Validation of a Semi-quantitative Direct Analysis in Real Time Tandem Mass Spectrometry (DART-MS/MS) Approach to the Analysis of Lateral Flow Immunoassay for Deoxynivalenol**

*Adapted from:*

*A. Geballa-Koukoulou, A. Gerssen, M.W.F. Nielen, From smartphone lateral flow immunoassay screening to direct ms analysis: Development and validation of a semi-quantitative direct analysis in real-time mass spectrometric (DART-MS) approach to the analysis of deoxynivalenol, *Sensors*. 21 (2021) 1–17. <https://doi.org/10.3390/s21051861>.*

### *Abstract*

In current food safety monitoring, lateral flow immunoassays (LFIAs) are widely used for rapid food contaminant screening. Recent advances include smartphone readouts, offering semi-quantitative analysis of LFIAs with time, location, and data transfer in case of on-site testing. Following the screening, the next step in the EU regulations is confirmation by, e.g., liquid chromatography-tandem mass spectrometry (LC-MS/MS). In this work, using direct analysis in real time ambient ionization and triple quadrupole MS/MS (DART-QqQ-MS/MS), we achieved rapid confirmation of the identity of the substance(s) leading to a positive LFIA readout. In the proposed workflow, an individual performs the (on-site) smartphone LFIA screening, and when the result is suspect, an identification LFIA (ID-LFIA) is developed with the same sample extract, thereby removing the need for additional sample preparation. The ID-LFIA can be dissociated and rapidly analyzed in a control laboratory with DART-QqQ-MS/MS. The ID-LFIA consists of multiple lines of monoclonal antibodies against the mycotoxin deoxynivalenol, acting as a bioaffinity trap. The ID-LFIA DART-QqQ-MS/MS approach has been developed and validated, along with the screening smartphone LFIA, and its applicability has been demonstrated by analyzing incurred and spiked samples. The developed approach has been critically compared with our previous direct electrospray ionization MS method and was found to provide complementary information on the total deoxynivalenol contamination in the sample

### 3.1 Introduction

According to the European Union (EU) regulation, the food needs to be monitored and tested to reassure the absence of contaminants (1). Contaminants, including mycotoxins, adversely affect human health when consumed (2). Mycotoxins, such as deoxynivalenol (DON), are produced in crops contaminated by *Fusarium* sp. fungi. Due to plant metabolism (acetylation or glycosylation), DON can be converted into conjugated forms, which makes analytical detection an intricate task (3). Mycotoxins threaten human health and challenge the food industry with millions of euros in economic losses because mycotoxin-contaminated food commodities must be withdrawn or destroyed before reaching the market (4).

The contaminants monitoring strategy in the EU usually consists of a two-step approach. The first step involves rapid screening assays using, for instance, lateral flow immunoassays (LFIAs). Screening assays provide a positive or negative result regarding the presence of a specific contaminant at a validated target level. When the screening result is positive or ambiguous, confirmatory analysis should be performed with liquid or gas chromatography and (tandem) mass spectrometry (LC- or GC-MS/MS) (5). In this structure, screening and confirmation act complementarily; screening is fast and easily performed, but it does not give any structural information on the contaminant, so, confirmation provides unequivocal detection of the contaminant at the level of interest. However, confirmation involves time-consuming chromatography and elaborate sample preparation, which could be considered a disadvantage for routine analysis laboratories when many samples must be analyzed.

Until now, food safety procedures solely rely on official controls from authorities and food producers (6). However, in recent years, significant progress has been made in fields that could affect how food safety analysis is performed. First, user-friendly diagnostic tests have been developed, some of which use smartphone readouts for semi-quantitative interpretation of the result and can even be used by non-experts as screening assays (7, 8). The screening tests with smartphone readout provide improved sensitivity, ease of use, fast analysis, and GPS location data for spatiotemporal mapping of contaminations. All those advantages allow individuals to grasp their food safety, and primarily agri-food businesses and regulatory bodies to improve food safety testing. Another progress is the development of ambient ionization MS (AIMS) techniques, i.e., MS ionization methods that ionize in ambient conditions without time-consuming chromatographic separation. Direct analysis in real time (DART), one of the first AIMS developed (9), is an atmospheric pressure chemical ionization (APCI)-like technique requiring a very low sample volume for analysis. DART is not included into confirmatory analysis regulation despite having many applications regarding food quality and safety analysis (10–12), including residue analysis of drugs in bovine tissue (13), aflatoxin detection in milk (14), and mycotoxins analysis in cereals (15).

In our recently published work (**Chapter 2**) (16), an approach for the direct MS analysis of screening LFIAs for DON was demonstrated. The approach uses an

identification LFIA (ID-LFIA), which acts as a bioaffinity trapping means. DON is retrieved from the ID-LFIA in the laboratory with a dissociation solution that is directly analyzed by electrospray ionization (ESI) followed by quadrupole-orbitrap (Q-Orbitrap) MS or triple quadrupole (QqQ) MS/MS. However, the ID-LFIA ESI-MS approach was restricted to the negative ion (–) mode due to ion suppression caused by residues from the LFIA buffers and nitrocellulose substrate residues. Consequently, ID-LFIA ESI-MS cannot detect the acetylated forms of DON (AcDON) (16).

In the present study, we developed a DART alternative to ionize the retrieved DON from the ID-LFIA. Because of its ionization mechanism, DART does not suffer from limitations faced by the ESI approach in the positive ion mode, which made AcDON detection possible. The ID-LFIA DART-MS/MS approach was validated in-house as a semi-quantitative confirmatory method for wheat sample extracts (spiked and incurred) with DON. The preceding screening LFIA with smartphone readout was also validated using the same extracts. The current ID-LFIA DART-MS/MS approach is complementary to the previous ID-LFIA ESI-MS/MS approach (**Chapter 2**) in the detection of DON and its conjugated forms. ID-LFIA ESI-MS/MS provides a fast direct food safety monitoring approach, thereby improving the overall efficiency and cost-effectiveness in industrial and regulatory routine laboratories.

## 3.2 Material and Methods

### 3.2.1 Chemicals and reagents

Methanol (MeOH) of UHPLC-MS purity and ammonia solution (NH<sub>3</sub>) (25% v/v) were purchased from Merck (Darmstadt, Germany). Milli-Q water of 18.3 MΩ/cm conductivity was obtained with a Merck (Amsterdam, The Netherlands) water purification system. Standard stock solutions of 100 µg/mL DON, 25 µg/mL <sup>13</sup>C-DON internal standard (IS), 100 µg/mL 3-AcDON, and 100 µg/mL 15-AcDON, all in ACN, were purchased from LGC standards (Wesel, Germany). Wheat flour blank certified reference material (CRM) from the Joint Research Centre was purchased via LGC standards (Wesel, Germany). Furthermore, mouse monoclonal antibodies (mAbs) for DON, clone 2, were purchased from Aokin AG (Berlin, Germany). For the in-house validation study, 17 blank wheat samples previously analyzed for the absence of DON by a validated LC-MS/MS method were provided in-house, and the remaining four blank samples were created by pooling eight of the 17 blank samples. Also, a contaminated corn starch sample, previously analyzed with the official LC-MS/MS method for mycotoxins, was provided in-house. For the screening assays, a smartphone-based LFIA kit, Rida Quick DON RQS Eco, including its dedicated DON extraction buffer, was obtained from r-Biopharm (Darmstadt, Germany).

### 3.2.2 ID-LFIA preparation

The mAb for DON were diluted with 1× phosphate buffer saline (PBS) to a concentration of 0.3 mg/mL. The diluted mAbs were used to construct the ID-LFIA as

described in the previous publication (16). In short, 15 identical lines of the diluted mAb, forming a bioaffinity trapping zone, are sprayed on top of the center of a nitrocellulose membrane (HiFlow Plus HF13502, Millipore, Carrigtwohill, Ireland) secured on a plastic backing (G & L, San Jose, CA, USA), using an XYZ3060 BioJet and AirJet instrument (Biodot Inc., Irvine, CA, USA). The nitrocellulose membrane is finally cut to 5 mm width, thus creating the ID-LFIAs, and stored in the fridge at 4 °C until further use.

### 3.2.3 Sample preparation

The extraction protocol from the r-Biopharm smartphone-based LFIA was used for all samples. First, 5 g of grounded wheat sample was extracted using 25 mL Milli-Q water. After adding water, manual agitation and centrifugation at 2000× *g* for 1 min were performed to enable rapid sedimentation of the solid particles. The resulting supernatant was used to develop both the smartphone-based screening LFIA and the ID-LFIA. For the smartphone-based screening LFIA, 100 µL of the sample extract was diluted with 500 µL of the assay running buffer, and from that dilution, 100 µL was used to run the smartphone-based LFIA. After 5 min, the screening result was read visually and semi-quantified using the smartphone r-Biopharm app. For the ID-LFIA, 100 µL of the sample extract was diluted (1:1) with assay running buffer, and 200 µL thus obtained was used to develop the ID-LFIA.

The protocol developed for direct MS analysis of the ID-LFIA (**Chapter 2**) (16) was further improved to achieve a more time-efficient procedure for retrieving the final solution from the ID-LFIA for subsequent MS analysis. First, the part of the ID-LFIA with the rectangular mAb trapping zone was cut and washed with 500 µL of Milli-Q water in an Eppendorf tube under slight manual agitation for 30 s. The rectangular mAb trapping zone was then placed in an Eppendorf with 200 µL of MeOH/NH<sub>3</sub> (2% *v/v*) dissociation solution, followed by vigorous manual agitation for 1 min only. Finally, the solution was spiked at 60 ng/mL with the IS, <sup>13</sup>C-DON, to compensate for any remaining ion suppression and sampling irreproducibility in the subsequent DART ionization (17).

### 3.2.4 Mass spectrometry

#### DART-Triple Quadrupole MS/MS Conditions

The MS/MS analysis was performed on a model Xevo TQ-XS Tandem Triple Quadrupole MS/MS system (Waters Corporation, Milford, MA, USA) equipped with a DART SVP ion source (IonSense, Saugus, MA, USA). Optimized conditions included: cone voltage 20 V, source temperature 120 °C, nanoflow nitrogen gas 0.30 bar, argon collision gas flow 0.16 mL/min, and nitrogen nebulizer gas 7.0 bar. Data were acquired in multiple reaction monitoring (MRM) mode with collision energies indicated in Table 3.1. The DART ionization source was used with helium plasma carrier gas at an optimized temperature of 350 °C and operated in positive ionization mode. DART sample introduction was performed using a 12-position metal mesh device at a rail

speed of 0.6 mm/s. The total runtime for the analysis of the 12 mesh positions was less than 3.5 min. MassLynx software v4.2 (Waters) was used for data acquisition and processing of the MS data. From the chromatograms acquired, ratio of area of DON to that of the IS, were used for semi-quantification, and ion ratio calculation of the two MRM transitions for each substance was used for unequivocal confirmation of the identity of each substance.

**Table 3.1.** MRM ion transitions for DON,  $^{13}\text{C}$ -DON, and AcDON in triple quadrupole MS/MS and respective optimized collision energies.

Analyte	MRM Ion Transition ( $m/z$ ) (positive ion mode)	Collision Energy (eV)
DON	297.1 > 249.2	10
	297.1 > 231.1	16
$^{13}\text{C}$ -DON	312.1 > 263.2	10
	312.1 > 245.1	16
AcDON	339.1 > 231.1	10
	339.1 > 203.1	16

### 3.2.5 In-house validation

For the in-house validation study, 21 blank wheat samples were extracted and portions of the blank sample extracts were spiked with a DON or 3-AcDON solution at three different target levels (TL) based on the maximum limit (ML) of 1750  $\mu\text{g/kg}$  for extracted DON in unprocessed durum wheat (18) to a final level of 175 ng/mL ( $0.5 \times \text{TL}$ ), 350 ng/mL ( $1 \times \text{TL}$ ), and 525 ng/mL ( $1.5 \times \text{TL}$ ).

Both the smartphone-based LFIA and the ID-LFIA DART-QqQ-MS/MS method were validated in-house according to the 2021/808 guidelines (5), as a semi-quantitative screening, and confirmatory method, respectively. For the specificity assessment, the 21 spiked and blank wheat sample extracts were analyzed to demonstrate a difference in the response between blank and positive samples. Moreover, the intra- and inter-day repeatability assessment was performed by measuring seven different samples at three different spiking target levels over three different days and assessing the calculated %RSD. Additionally, using one-way ANOVA, the within-laboratory reproducibility was calculated for the three validation days. The trueness of the measurements of the smartphone-based LFIA, was calculated based on the theoretical concentration and comparing it with the smartphone readout result, expressed in mg/kg. For the ID-LFIA DART-QqQ-MS/MS, the trueness was assessed using an estimate of the expected concentration (mg/kg) calculated based on each day's calibration curve and comparing it with the theoretical concentration. The decision limit for confirmation ( $\text{CC}\alpha$ ) and the decision limit for screening ( $\text{CC}\beta$ ) were calculated, using the concentration at the  $1 \times \text{TL}$  plus 1.64 times the standard deviation of the within-laboratory reproducibility at this level.



For the ID-LFIA DART-QqQ-MS/MS approach, blank CRM wheat extracts were spiked to evaluate the linearity across the TL range. The linearity range of interest included the three spiking levels ( $0.5 \times$  TL,  $1 \times$  TL, and  $1.5 \times$  TL) and a blank level sample (zero). Additionally, SPR results were used to assess the selectivity of the mAb used on the ID-LFIA DART-QqQ-MS/MS. For the selectivity testing, surface plasmon resonance (SPR) measurements were performed in a Biacore 3000 (GE Healthcare, Uppsala, Sweden) using a carboxymethylated dextran-coated gold chip (CM5) (GE Healthcare, Uppsala, Sweden) with a conjugate of DON with BSA (DON-BSA) (Aokin AG, Berlin, Germany) immobilized on the surface. HBS-EP was used as a running buffer at  $5 \mu\text{L}/\text{min}$  flow rate, and  $20 \mu\text{L}$  was injected of a 1:1 mixture of anti-DON mAb  $0.3 \text{ mg}/\text{mL}$ : mycotoxin  $0.3 \text{ mg}/\text{mL}$ . When the mycotoxin analyte interacts with the antibodies in the mixture, then no signal is observed since the mAbs are occupied and cannot bind to the immobilized DON-BSA conjugate. Contrary, when the antibodies do not interact with the analyte in the sample, an increase in the SPR signal is observed because of the antibodies binding with the DON-BSA immobilized on the chip. After the binding occurs, regeneration of the chip is performed with NaOH  $25 \text{ mM}$ .

## 3.3 Results

### 3.3.1 General concept

As described in our previously published work (**Chapter 2**) (16), we envisage a future of smartphone-based on-site screening of food quality and safety parameters that will unavoidably increase confirmatory analysis requirements. Several smartphone-based screening methods have been developed, some of which demonstrate great citizen science potential (19–21). An individual may perform a rapid and user-friendly screening assay on-site, for example, an LFIA with a smartphone readout. If the result is positive, the same sample extract is diluted and used to develop an ID-LFIA, ready to be sent to the lab for subsequent confirmatory MS analysis. Following such an approach, the cause of the positive screening result at the relevant ML can be detected, and even a semi-quantitative analysis can be performed. The present ID-LFIA DART-QqQ-MS/MS method can be used either independently or in combination with the previously developed ID-LFIA ESI method (16) (**Chapter 2**), as the former indicates the presence of both DON and AcDON (*Figure 2.1*), and the latter the presence of both DON and the DON-3G. It is important to note that the EU legislation does not currently regulate the conjugated forms of DON, but revised regulations are under discussion.

### 3.3.2 DART-QqQ-MS/MS method development

The previous ESI method of **Chapter 2** (16) was developed in negative ion mode to deal with the severe ion suppression caused by residues of assay buffers and nitrocellulose substrate in the final ID-LFIA dissociation solution. However, because DART is an APCI-like ionization source known to be less prone to ion suppression, we

selected the more commonly used positive ion mode to analyze mycotoxins (22). In Figure 3.2, full scan DART-Orbitrap-MS spectra of DON in MeOH/NH<sub>3</sub> (2% v/v) solution, containing 10% v/v LFIA buffer, can be seen in negative and positive ion mode.

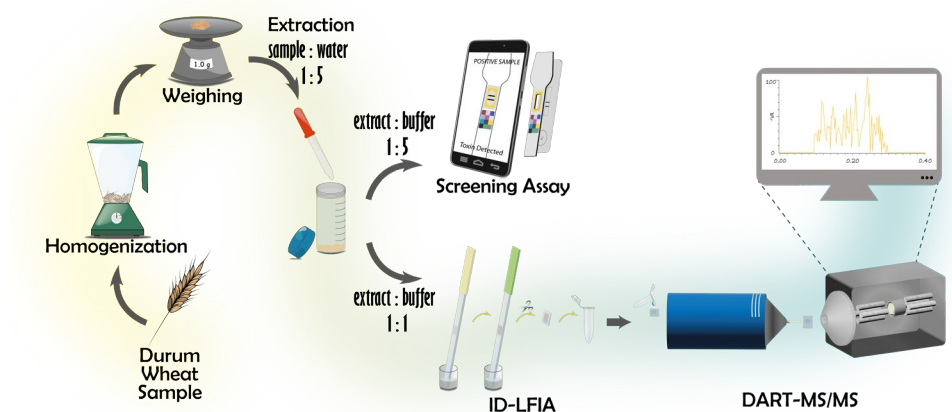


**Figure 3.1.** The general concept of the ID-LFIA DART-QqQ-MS/MS method. Wheat is selected and homogenized, and DON is extracted from grounded wheat. The extract is diluted with the running buffer on a 1:5 ratio. The extract is further diluted with the running buffer to develop the screening LFIA with smartphone readout. If the screening result is positive or ambiguous, the same sample extract is diluted with the running buffer to develop the ID-LFIA. The ID-LFIA can be further processed by washing and dissociating the bound DON and DON conjugates from the mAb. The final step is the rapid direct analysis by the newly developed and validated semi-quantitative DART-QqQ-MS/MS. In case further information is needed, e.g., absolute quantification over a different range or multitoxin analysis, conventional LC-MS/MS analysis may be considered a follow-up.

Both modes can detect DON using the DART ion source, contrary to the previously published ESI mode (16) that showed high interferences and ion suppression in positive ion mode. Although under ambient conditions, positive ion mode is in general characterized by a higher background compared to negative ion mode DART, the protonated ion of DON at  $m/z$  297.1344 at 5 ppm mass accuracy detection window can be easily detected in DART (Figure 3.2). Moreover, the positive ion mode allowed us to measure AcDON, which was impossible in the previous negative ion ID-LFIA ESI-MS approach (16). Preliminary DART experiments performed in a standard solution of 1  $\mu\text{g/mL}$  in MeOH/NH<sub>3</sub> (2% v/v) and using Orbitrap-MS in full scan negative ion mode suggested an ability to detect DON-3G as well through its deprotonated and its chlorine and formic acid adduct ions (Figure 3.3). Nevertheless, in agreement with previous DART attempts (15), the DART sensitivity was inadequate for DON-3G detection when trying to reach more food-safety-relevant levels.

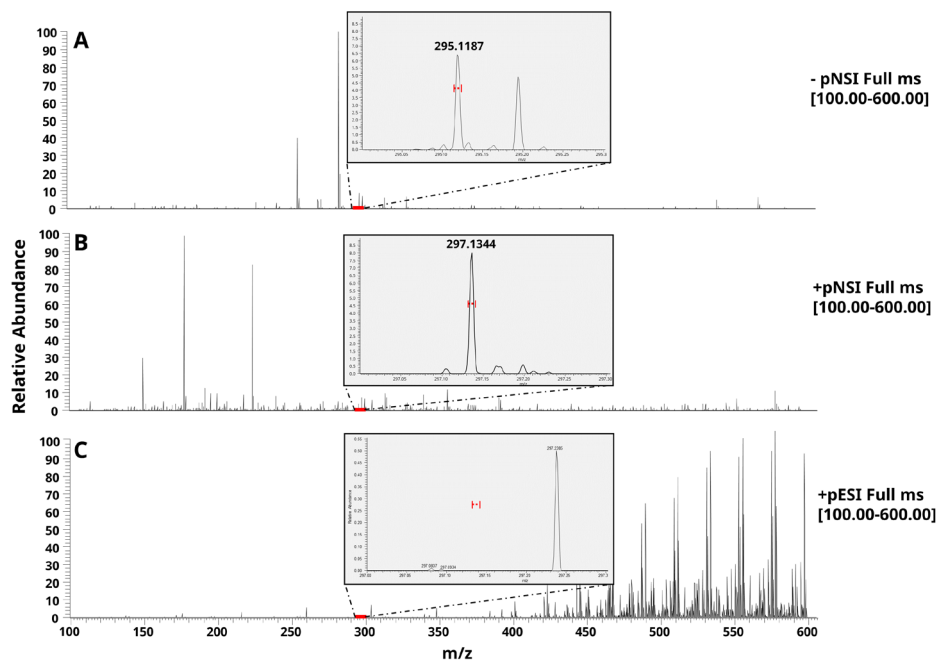


**Figure 3.2.** Comparison between full scan ( $m/z$  100–600) mass spectra of a MeOH/ $\text{NH}_3$  (2% v/v) solution of DON containing 10% v/v LFIA assay buffer in (A) negative (B) positive ion mode in DART-Orbitrap-MS and (C) positive ion mode in ESI-Orbitrap-MS. Inserted are the regions of deprotonated and protonated ions of DON, and marked in red are the expected  $m/z$  regions for the ions at 5 ppm mass accuracy.

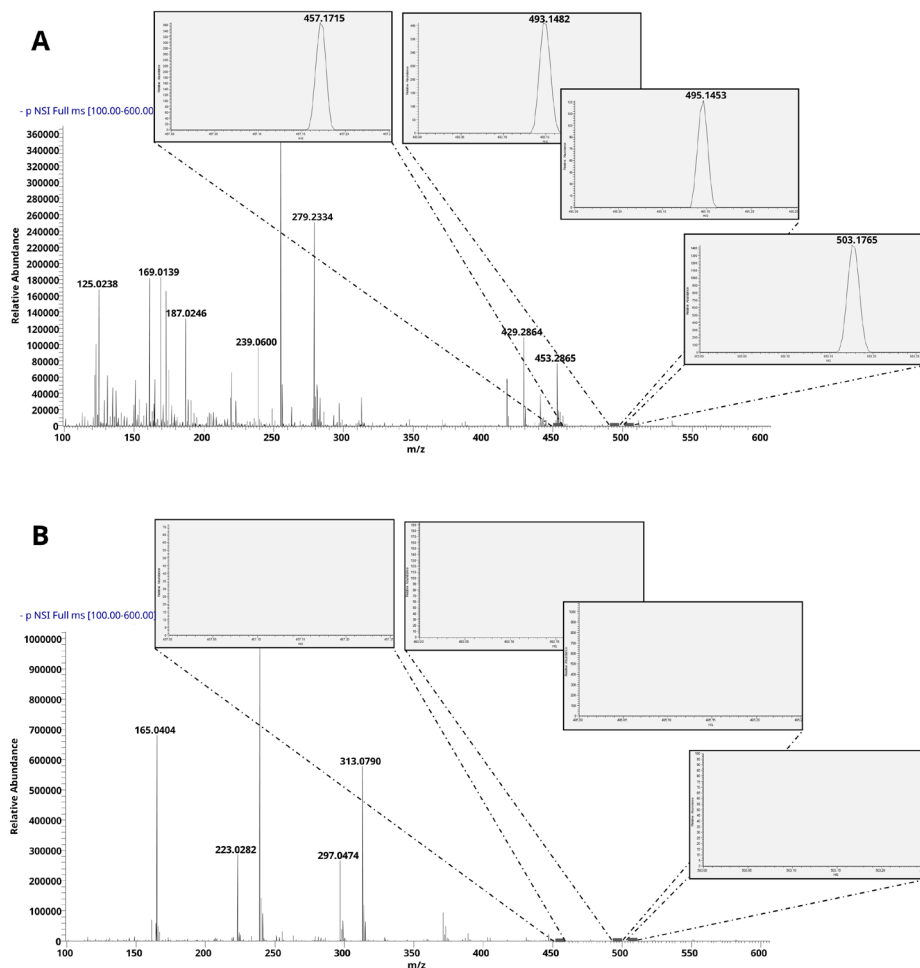


**Figure 3.3.** Ionization in DART-Orbitrap MS negative ion mode, full scan  $m/z$  100-600, of (A) DON-3G in MeOH/NH<sub>3</sub> (2% v/v) and (B) blank MeOH/NH<sub>3</sub> (2% v/v) solution. Detection of the characteristic deprotonated ion and adduct ions can be seen in the inserted zoomed-in mass spectra for  $m/z$  457.1715 [M-H]<sup>-</sup>,  $m/z$  493.1482/495.1453 [M+Cl]<sup>-</sup> and  $m/z$  503.1765 [M+FA-H]<sup>-</sup>. Note: formic acid (FA) and chloride are impurities in the solvents and/or the MS background.

To optimize the MS fragmentation conditions, the ion transition intensities were tested in MRM mode, following a stepwise increase in collision energy. DART is an open ion source, so we could not merely assess the fragment ions from a product ion scan because of ambient interferences biasing the optimum collision energy. To give an example, for the DON  $m/z$  297 > 249 MRM transition: the suggested optimum value of 30 eV was unable to differentiate between blank and spiked samples. In contrast, the second-best intense value in the absolute intensity signal versus the collision energy plot did successfully discriminate between spiked and blank samples

(Figure 3.4). Note that because of the lack of chromatographic separation and the production of common fragment ions from 3-AcDON and 15-AcDON, we cannot discriminate between them in AIMS methods such as DART due to the lack of chromatographic separation, and the same  $m/z$  values both have. Instead, the ID-LFIA DART-QqQ-MS/MS method detects apart from DON the total AcDONs. All the other MS/MS conditions were the same as in the previously developed ESI-QqQ-MS/MS approach (Chapter 2) (16), except for the cone voltage that was adjusted to 20 V, because it yielded more reproducible results in DART-QqQ-MS/MS.

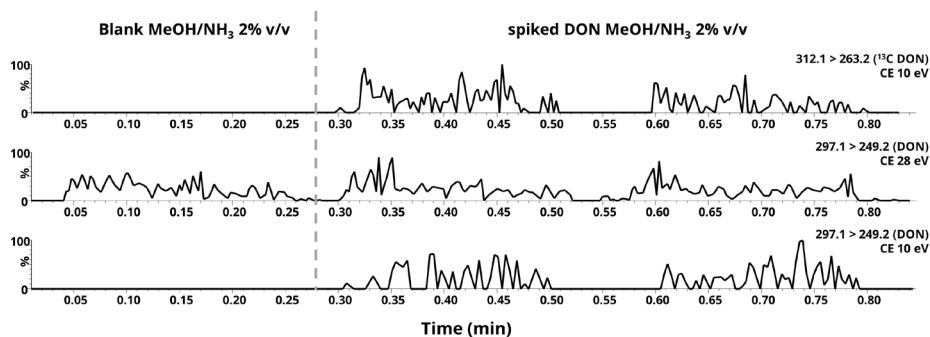


**Figure 3.4.** DART-QqQ-MS/MS chronograms of the selected ion transitions for DON and the  $^{13}\text{C}$ -DON. At first, a blank MeOH/NH<sub>3</sub> (2% v/v) solution is analyzed, followed by a duplicate sampling of a spiked DON plus  $^{13}\text{C}$ -DON of 60 ng/mL in MeOH/NH<sub>3</sub> (2% v/v), at two different collision energy (CE) settings, demonstrating the inability of the wrong CE setting at 28 eV to differentiate between blank and spiked sample.

Next, different compositions of ID-LFIA dissociation solutions were tested for DON in DART-MS/MS, such as MeOH or ACN with an organic modifier of HCOOH or NH<sub>3</sub> (2% v/v). As with the previously developed ESI approach in Chapter 2 (16), MeOH/NH<sub>3</sub> (2% v/v) showed the highest signal intensity for both DON and acetylated forms of DON (Figure 3.5).

Finally, optimization of the settings for the DART helium carrier gas was performed. Differences in DART gas temperature may lead to significant changes in the desorption/ionization efficiency and the method sensitivity (23–25). When the solution used for optimization was only MeOH/NH<sub>3</sub> (2% v/v), spiked with DON or 3-AcDON at 60 ng/mL, the optimum DART temperature was 300 °C for both analytes. In contrast, when a matrix-matched solution from ID-LFIA was developed with blank assay buffer and washed, and the final dissociation solution MeOH/NH<sub>3</sub> (2% v/v) was spiked, the optimum DART temperature was 350 °C. More importantly, the signal intensity doubles when the temperature increases from 300 to 350 °C, which underlines the importance of carrier gas settings optimization (Figure 3.6).

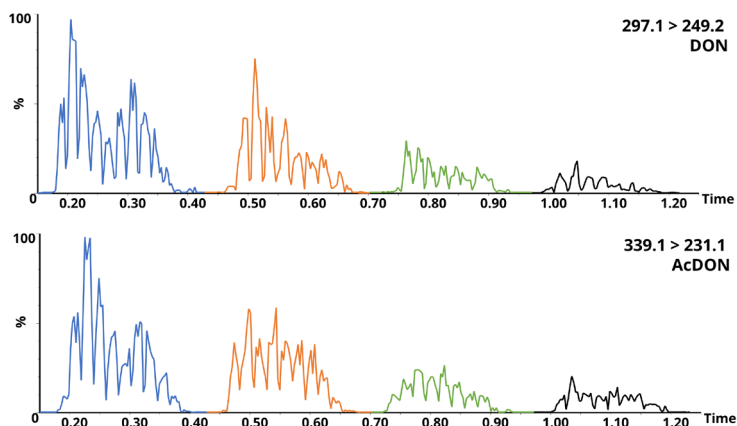


**Figure 3.5.** Chronograms of positive ionization DART-MS/MS of different dissociation solution compositions of 60 ng/mL,  $m/z$  297.1 > 249.2 for DON, and  $m/z$  339.1 > 231.1 for AcDON. MeOH/NH<sub>3</sub> (2% v/v) (blue), ACN/NH<sub>3</sub> (2% v/v) (orange), MeOH/HCOOH (2% v/v) (green), ACN/HCOOH (2% v/v) (black).

### Helium Temperature Optimization

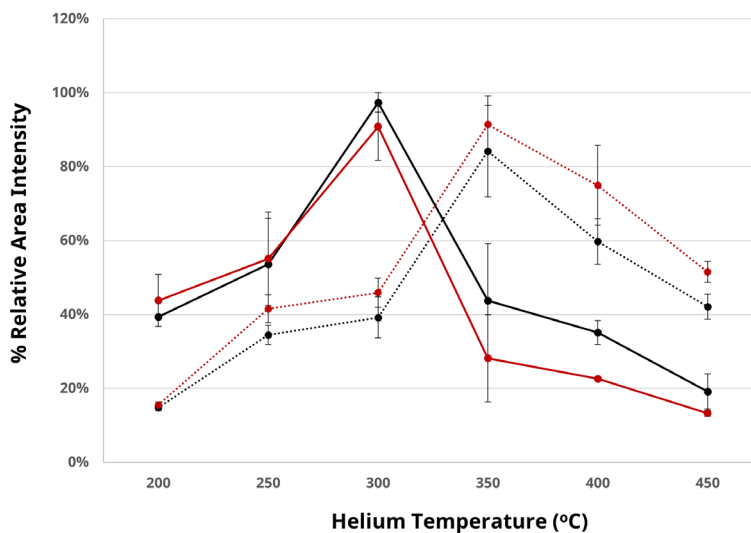


**Figure 3.6.** DART helium gas temperature optimization in QqQ-MS/MS for DON (black) and 3-AcDON (red) 60 ng/mL, in MeOH/NH<sub>3</sub> (2% v/v) (solid line) and MeOH/NH<sub>3</sub> (2% v/v) exposed to the ID-LFIA substrate (dotted line). Measurements were performed in duplicate by MRM monitoring of the ion transitions specified in Table 3.1. The standard deviation of the duplicate measurement is shown by the error bars. The results are presented as the relative (%) area intensity.

### 3.3.3 In-house method validation

#### Validation of Screening LFIA with Smartphone Readout

The specificity of the screening LFIA with smartphone readout was assessed by analyzing 21 blank wheat and spiked samples thereof. Based on the results, there was sufficient discrimination between blank and spiked samples from the 0.5× TL level onwards (Figure 3.7 and Table 3.2)

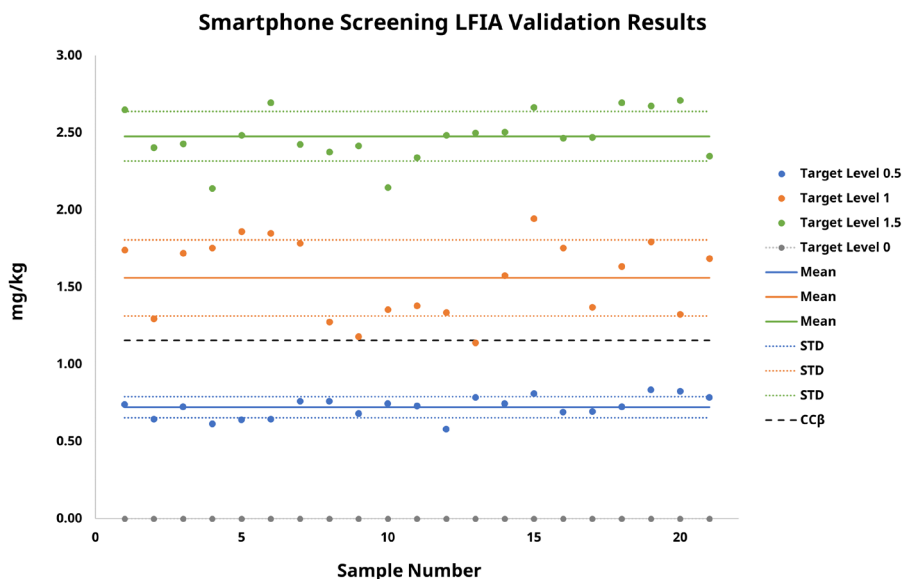


**Figure 3.7.** Data analysis of 21 blank wheat samples, and spiked versions thereof, at three target levels, demonstrating distinct differentiation between them in the screening LFIA. Quantification with the use of the smartphone *r-Biopharm* app.

Moreover, the repeatability, both intra-, and inter-day were assessed for the three validation levels. The intra-day repeatability results expressed as the %RSD were 7.9, 10.4, and 6.9% at 0.5× TL, 8.9, 10.1, and 4.9% at 1× TL, and 7.4, 12.7, and 5.2% at the 1.5× TL levels, respectively. The inter-day repeatability expressed by the %RSD was 9.4, 15.8, and 6.5% at 0.5×, 1×, and 1.5× TL, respectively. All RSD% values for the repeatability assessed were lower than 20% and within the acceptance range.

The %RSD to assess the within-laboratory reproducibility was calculated using one-way ANOVA for each TL. For the smartphone screening LFIA, the results were 10.0, 17.6, and 6.8% at 0.5×, 1×, and 1.5× TL, respectively. According to the quantitative performance criteria for the validation of substances with an established ML, %RSD should be not greater than the corresponding reproducibility at the 0.5× TL (5), which indicated that the calculated value for the 1× TL was not within the acceptance

range, and consequently, the smartphone-based LFIA should be considered as a semi-quantitative screening method.

For the trueness assessment of the smartphone screening LFIA, the theoretical concentration at each spiking level was compared to that of the smartphone readout result, expressed in mg/kg. The calculated trueness values were 83, 89, and 94% at the 0.5 $\times$ , 1 $\times$ , and 1.5 $\times$  TL, respectively, and within the acceptance range of 80 to 110% listed in the regulation (5). Finally, the CC $\beta$  was calculated at 1156  $\mu$ g/kg for 21 DON-spiked wheat samples at the ML level.

### Validation of ID-LFIA DART-QqQ-MS/MS

The linear range of the recovered DON from the ID-LFIA DART-QqQ-MS/MS was found to be 0–525 ng/mL, corresponding to a range of 0 to 1.5 $\times$  the ML of 1750  $\mu$ g/kg of DON in unprocessed durum wheat with a regression coefficient of 0.987, demonstrating semi-quantitative performance in the relevant range.

The ID-LFIA DART-QqQ-MS/MS selectivity is justified based on the use of specific antibodies that isolate the analyte of interest on the ID-LFIA. For assessment of the selectivity of the antibodies in the ID-LFIA, SPR measurements were performed. The results showed no interaction of the mAb with other mycotoxins produced by *Fusarium* sp. and likely to be present in wheat, such as T-2 toxin, fumonisin B2, and zearalenone (26). However, the mAb demonstrated binding with nivalenol and the conjugated forms of DON, such as AcDON and DON-3G (Figure 3.8)

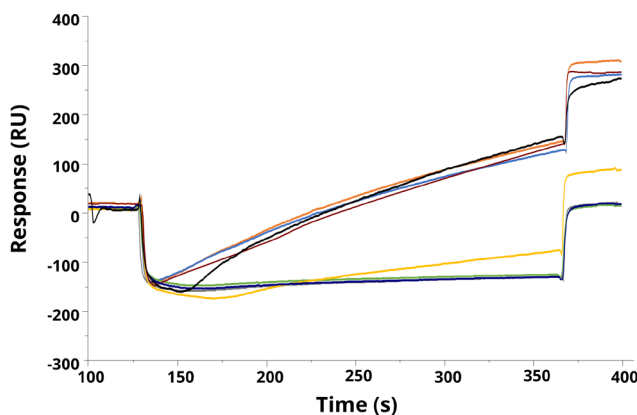


**Figure 3.8.** Overlay SPR sensograms from the inhibition measurements of *Fumonisin* sp. toxins: DON (dark blue), AcDON (grey), DON-3G (yellow), nivalenol (green), fumonisin B2 (light blue), T-2 toxin (dark red), zearalenone (orange) and blank (black).

Apart from the intrinsic and prominent biorecognition characteristic that the ID-LFIA adds to the overall selectivity, the MS analysis that follows can differentiate between DON and AcDONs. The selected MRM transitions monitored for each substance (Table 3.1), as well as the respective ion ratios (Table 3.2), demonstrated



robustness throughout the analysis of all samples and enabled the confirmation of the identity. More specifically, the mean ion ratio for the MRM transitions of DON was 0.29 (29%) with a %RSD of 9.2% for all the 21 spiked samples analyzed. This ratio is identical to the 0.29 ion ratio measured for DON standard solutions in MeOH/NH<sub>3</sub> (2% v/v) and in MeOH/NH<sub>3</sub> (2% v/v) exposed to the ID-LFIA substrate. As a result, neither the wheat sample matrix nor the ID-LFIA substrate affect the fragmentation of DON, and the ion ratio tolerance limit of the spiked wheat samples analyzed complies with the regulatory requirement of  $\pm 25\%$  for earning three identification points (IPs) (5). Also, the specificity of the method was assessed through the analysis of blank samples in MS. The 21 blank samples analyzed demonstrated no signal for the selected ion transitions, and the method is, thus, characterized as sufficiently specific to differentiate between blank and spiked real samples (*Figure 3.9* and *Table 3.2*).

Moreover, the repeatability, both intra-, and inter-day were assessed for the three validation levels. For the ID-LFIA DART-QqQ-MS/MS, the intra-day repeatability results expressed as the %RSD were 14.1, 13.9, and 8.7% at 0.5 $\times$  TL, 16.9, 3.7, and 4.5% at 1 $\times$  TL, and 9.6, 14.5, and 3.6% at the 1.5 $\times$  TL level, for day one, two, and three, respectively. The inter-day repeatability expressed by the %RSD was 16.9, 14.9, and 10.2% for the 0.5 $\times$ , 1 $\times$ , and 1.5 $\times$  TL, respectively, again underlining the performance of the developed ID-LFIA DART-QqQ-MS/MS approach, thus comparing nicely with the semi-quantitative smartphone screening assay. All RSD% values for the validation parameters assessed were lower than 20% and within the acceptance range.

Furthermore, to assess the within-laboratory reproducibility, the %RSD was calculated using one-way ANOVA, for each TL calculated at 18.4, 16.0, and 11.6% at 0.5 $\times$ , 1 $\times$ , and 1.5 $\times$  TL, respectively. According to the regulation, the %RSD should be not greater than the corresponding reproducibility at the 0.5 $\times$  TL for substances with defined ML (5), which means that all measurements were within the acceptance range. Moreover, the CC $\alpha$  was calculated at 2078  $\mu\text{g/kg}$  for 21 DON-spiked wheat samples at the ML level.

Finally, for the ID-LFIA DART-QqQ-MS/MS, an estimate of the expected mg/kg concentration was calculated, based on each day's calibration curve, and compared with the theoretical concentration at each spiking level to calculate the trueness of the measurements. The calculated trueness was 101, 91, and 104% for the 0.5 $\times$ , 1 $\times$ , and 1.5 $\times$  TL, respectively.

All measurements were within the acceptance range of the regulation (5). Therefore, the developed ID-LFIA DART-QqQ-MS/MS has been successfully validated as a semi-quantitative confirmatory method.

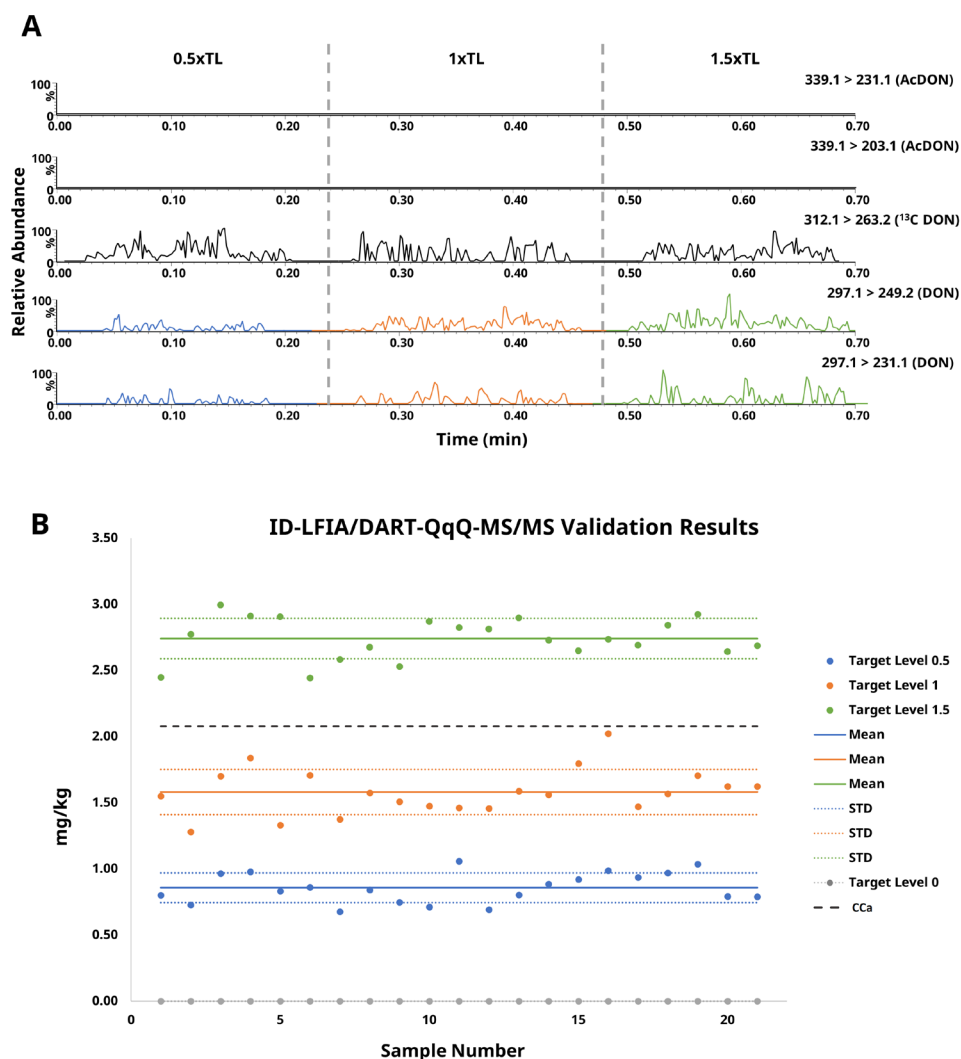


**Figure 3.9** (A). Representative chronograms for DON-spiked wheat samples used to develop the ID-LFIA, retrieved in dissociation solution and analyzed by DART-QqQ-MS/MS, demonstrating the three distinct spiking levels in blue 0.5× TL, orange 1× TL, and green 1.5× TL.  $^{13}\text{C}$ -DON is added as an IS before the MS/MS analysis. (B). Data analysis of 21 blank wheat samples, and spiked versions thereof in ID-LFIA DART-QqQ-MS/MS, at three target level concentrations in blue 0.5× TL, orange 1× TL, and green 1.5× TL.

**Table 3.2.** Results from ID-LFIA DART-QqQ-MS/MS analysis and the respective LFIA smartphone screening of 21 validation blank and spiked wheat samples at three different target levels and performed on three different days.

Day	Sample	ID-LFIA DART-QqQ-MS/MS (Response Factor)	LFIA Smartphone Screening Result (mg/kg, Mean Response $\pm$ SD)	ID-LFIA DART-QqQ-MS/MS		LFIA Smartphone Screening Result (mg/kg, Mean Response $\pm$ SD)	ID-LFIA DART-QqQ-MS/MS		LFIA Smartphone Screening Result (mg/kg, Mean Response $\pm$ SD)	ID-LFIA DART-QqQ-MS/MS		LFIA Smartphone Screening Result (mg/kg, Mean Response $\pm$ SD)
				Mean Ion Area Ratio of DON $\pm$ SD	Expected mg/kg $\pm$ SD			Mean Ion Area Ratio of DON $\pm$ SD	Expected mg/kg $\pm$ SD			Mean Ion Area Ratio of DON $\pm$ SD
1	1	0	<0.25	0.30 ( $\pm 0.03$ )	0.80 ( $\pm 0.01$ )	0.74 ( $\pm 0.01$ )	0.27 ( $\pm 0.03$ )	1.55 ( $\pm 0.06$ )	1.74 ( $\pm 0.01$ )	0.29 ( $\pm 0.05$ )	2.40 ( $\pm 0.02$ )	2.65 ( $\pm 0.00$ )
	2	0	<0.25	0.30 ( $\pm 0.00$ )	0.73 ( $\pm 0.01$ )	0.65 ( $\pm 0.02$ )	0.32 ( $\pm 0.01$ )	1.28 ( $\pm 0.03$ )	1.30 ( $\pm 0.01$ )	0.30 ( $\pm 0.03$ )	2.77 ( $\pm 0.01$ )	2.41 ( $\pm 0.01$ )
	3	0	<0.25	0.29 ( $\pm 0.02$ )	0.97 ( $\pm 0.06$ )	0.73 ( $\pm 0.01$ )	0.28 ( $\pm 0.01$ )	1.70 ( $\pm 0.03$ )	1.72 ( $\pm 0.02$ )	0.32 ( $\pm 0.01$ )	2.99 ( $\pm 0.03$ )	2.43 ( $\pm 0.02$ )
	4	0	<0.25	0.28 ( $\pm 0.04$ )	0.98 ( $\pm 0.01$ )	0.62 ( $\pm 0.01$ )	0.34 ( $\pm 0.00$ )	1.84 ( $\pm 0.04$ )	1.76 ( $\pm 0.01$ )	0.28 ( $\pm 0.00$ )	2.91 ( $\pm 0.11$ )	2.14 ( $\pm 0.03$ )
	5	0	<0.25	0.28 ( $\pm 0.01$ )	0.83 ( $\pm 0.03$ )	0.64 ( $\pm 0.00$ )	0.30 ( $\pm 0.02$ )	1.33 ( $\pm 0.01$ )	1.86 ( $\pm 0.02$ )	0.27 ( $\pm 0.00$ )	2.91 ( $\pm 0.12$ )	2.49 ( $\pm 0.03$ )
	6	0	<0.25	0.32 ( $\pm 0.01$ )	0.86 ( $\pm 0.02$ )	0.65 ( $\pm 0.01$ )	0.23 ( $\pm 0.00$ )	1.71 ( $\pm 0.04$ )	1.85 ( $\pm 0.03$ )	0.32 ( $\pm 0.02$ )	2.42 ( $\pm 0.00$ )	2.70 ( $\pm 0.03$ )
	7	0	<0.25	0.31 ( $\pm 0.02$ )	0.68 ( $\pm 0.02$ )	0.76 ( $\pm 0.00$ )	0.31 ( $\pm 0.02$ )	1.37 ( $\pm 0.00$ )	1.79 ( $\pm 0.02$ )	0.30 ( $\pm 0.01$ )	2.58 ( $\pm 0.06$ )	2.43 ( $\pm 0.01$ )

(Continued on next page)

Table 3.2 Continued

Day	Sample	ID-LFIA DART- QqQ- MS/MS (Re- sponse Factor)	LFIA Smartphone Screening Result (mg/kg, Mean Re- sponse $\pm$ SD)	ID-LFIA DART- QqQ-MS/MS		LFIA Smartphone Screening Re- sult (mg/kg, Mean Response $\pm$ SD)	ID-LFIA DART-QqQ- MS/MS		LFIA Smartphone Screening Re- sult (mg/kg, Mean Response $\pm$ SD)	ID-LFIA DART-QqQ- MS/MS		LFIA Smartphone Screening Result (mg/kg, Mean Response $\pm$ SD)
				Mean Ion Area Ratio of DON $\pm$ SD	Expected mg/kg $\pm$ SD		Mean Ion Area Ra- tio of DON $\pm$ SD	Expected mg/kg $\pm$ SD		Mean Ion Area Ra- tio of DON $\pm$ SD	Expected mg/kg $\pm$ SD	
2	8	0	<0.25	0.34 ( $\pm 0.00$ )	0.84 ( $\pm 0.02$ )	0.76 ( $\pm 0.00$ )	0.31 ( $\pm 0.02$ )	1.57 ( $\pm 0.02$ )	1.28 ( $\pm 0.01$ )	0.31 ( $\pm 0.02$ )	2.98 ( $\pm 0.01$ )	2.38 ( $\pm 0.02$ )
	9	0	<0.25	0.34 ( $\pm 0.01$ )	0.75 ( $\pm 0.02$ )	0.68 ( $\pm 0.01$ )	0.25 ( $\pm 0.00$ )	1.51 ( $\pm 0.03$ )	1.18 ( $\pm 0.01$ )	0.29 ( $\pm 0.03$ )	2.53 ( $\pm 0.01$ )	2.42 ( $\pm 0.00$ )
	10	0	<0.25	0.26 ( $\pm 0.01$ )	0.71 ( $\pm 0.03$ )	0.75 ( $\pm 0.01$ )	0.27 ( $\pm 0.02$ )	1.47 ( $\pm 0.06$ )	1.36 ( $\pm 0.01$ )	0.29 ( $\pm 0.02$ )	2.87 ( $\pm 0.07$ )	2.15 ( $\pm 0.02$ )
	11	0	<0.25	0.31 ( $\pm 0.02$ )	1.06 ( $\pm 0.01$ )	0.73 ( $\pm 0.00$ )	0.28 ( $\pm 0.05$ )	1.46 ( $\pm 0.02$ )	1.38 ( $\pm 0.00$ )	0.28 ( $\pm 0.04$ )	2.82 ( $\pm 0.00$ )	2.34 ( $\pm 0.07$ )
	12	0	<0.25	0.31 ( $\pm 0.01$ )	0.69 ( $\pm 0.00$ )	0.58 ( $\pm 0.01$ )	0.28 ( $\pm 0.01$ )	1.46 ( $\pm 0.00$ )	1.34 ( $\pm 0.01$ )	0.33 ( $\pm 0.02$ )	2.81 ( $\pm 0.01$ )	2.49 ( $\pm 0.05$ )
	13	0	<0.25	0.30 ( $\pm 0.04$ )	0.80 ( $\pm 0.01$ )	0.79 ( $\pm 0.01$ )	0.30 ( $\pm 0.02$ )	1.59 ( $\pm 0.01$ )	1.14 ( $\pm 0.01$ )	0.31 ( $\pm 0.04$ )	2.90 ( $\pm 0.05$ )	2.50 ( $\pm 0.00$ )
	14	0	<0.25	0.26 ( $\pm 0.01$ )	0.88 ( $\pm 0.00$ )	0.75 ( $\pm 0.01$ )	0.24 ( $\pm 0.00$ )	1.56 ( $\pm 0.00$ )	1.58 ( $\pm 0.03$ )	0.27 ( $\pm 0.01$ )	2.73 ( $\pm 0.00$ )	2.51 ( $\pm 0.00$ )

(Continued on next page)

Table 3.2. Continued

Day	Sample	ID-LFIA DART-QqQ-MS/MS (Response Factor)	LFIA Smartphone Screening Result (mg/kg, Mean Response $\pm$ SD)	ID-LFIA DART-QqQ-MS/MS		LFIA Smartphone Screening Result (mg/kg, Mean Response $\pm$ SD)	ID-LFIA DART-QqQ-MS/MS		LFIA Smartphone Screening Result (mg/kg, Mean Response $\pm$ SD)	ID-LFIA DART-QqQ-MS/MS		LFIA Smartphone Screening Result (mg/kg, Mean Response $\pm$ SD)
				Mean Ion Area Ratio of DON $\pm$ SD	Expected mg/kg $\pm$ SD		Mean Ion Area Ratio of DON $\pm$ SD	Expected mg/kg $\pm$ SD		Mean Ion Area Ratio of DON $\pm$ SD	Expected mg/kg $\pm$ SD	
2	15	0	<0.25	0.31 ( $\pm 0.03$ )	0.92 ( $\pm 0.02$ )	0.81 ( $\pm 0.00$ )	0.26 ( $\pm 0.03$ )	1.80 ( $\pm 0.07$ )	1.95 ( $\pm 0.02$ )	0.29 ( $\pm 0.02$ )	2.65 ( $\pm 0.01$ )	2.67 ( $\pm 0.02$ )
	16	0	<0.25	0.33 ( $\pm 0.02$ )	0.99 ( $\pm 0.03$ )	0.69 ( $\pm 0.01$ )	0.25 ( $\pm 0.02$ )	2.12 ( $\pm 0.02$ )	1.76 ( $\pm 0.02$ )	0.29 ( $\pm 0.05$ )	2.73 ( $\pm 0.03$ )	2.47 ( $\pm 0.03$ )
	17	0	<0.25	0.33 ( $\pm 0.01$ )	0.94 ( $\pm 0.01$ )	0.70 ( $\pm 0.02$ )	0.31 ( $\pm 0.03$ )	1.47 ( $\pm 0.03$ )	1.37 ( $\pm 0.01$ )	0.29 ( $\pm 0.01$ )	2.69 ( $\pm 0.04$ )	2.47 ( $\pm 0.01$ )
	18	0	<0.25	0.30 ( $\pm 0.04$ )	0.97 ( $\pm 0.03$ )	0.73 ( $\pm 0.05$ )	0.25 ( $\pm 0.00$ )	1.57 ( $\pm 0.01$ )	1.64 ( $\pm 0.02$ )	0.26 ( $\pm 0.01$ )	2.84 ( $\pm 0.07$ )	2.70 ( $\pm 0.03$ )
	19	0	<0.25	0.27 ( $\pm 0.02$ )	1.03 ( $\pm 0.01$ )	0.84 ( $\pm 0.04$ )	0.30 ( $\pm 0.03$ )	1.70 ( $\pm 0.02$ )	1.80 ( $\pm 0.01$ )	0.31 ( $\pm 0.01$ )	2.92 ( $\pm 0.07$ )	2.68 ( $\pm 0.01$ )
	20	0	<0.25	0.29 ( $\pm 0.00$ )	0.79 ( $\pm 0.02$ )	0.83 ( $\pm 0.06$ )	0.26 ( $\pm 0.02$ )	1.62 ( $\pm 0.01$ )	1.33 ( $\pm 0.01$ )	0.34 ( $\pm 0.00$ )	2.64 ( $\pm 0.01$ )	2.71 ( $\pm 0.03$ )
	21	0	<0.25	0.32 ( $\pm 0.00$ )	0.79 ( $\pm 0.03$ )	0.79 ( $\pm 0.01$ )	0.25 ( $\pm 0.00$ )	1.62 ( $\pm 0.06$ )	1.69 ( $\pm 0.05$ )	0.32 ( $\pm 0.01$ )	2.69 ( $\pm 0.05$ )	2.35 ( $\pm 0.25$ )

Conditions: a duplicate sampling of the same ID-LFIA dissociation solution in DART-QqQ-MS/MS. SD is the standard deviation of the duplicate measurements. The screening result was performed with the smartphone r-Biopharm LFIA, and the quantification with the smartphone app. SD is the standard deviation of duplicate reading of the same LFIA. The expected mg/kg is the concentration estimate calculated from each day's calibration curve based on the response factor (mean ratio of DON MRM product ion at m/z 249.2 to the  $^{13}\text{C}$ -DON MRM product ion at m/z 263.2). The DON ion ratio is the mean ratio of the absolute area of the DON MRM product ion at m/z 231.1 to the area of the ion at m/z 249.2.

### 3.3.4 Analysis of spiked and incurred samples

The applicability of the method is further demonstrated by the analysis of additional spiked and incurred samples. AcDON spiked samples were analyzed at the same spiking levels as the DON validation TL. The presence of AcDON was confirmed by the presence of the selected MRM ion transitions and the respective ion ratio compared with a standard spiked MeOH/NH<sub>3</sub> (2% v/v) solution. The mean ion ratio for AcDON in the spiked wheat samples analyzed was 0.71 (71%) with an %RSD of 12%, while the ion ratio of the standard spiked MeOH/NH<sub>3</sub> (2% v/v) solution was calculated at 0.76 (76%). As a result, the ion ratio tolerance limit of the AcDON-spiked wheat sample analyzed was within the regulatory requirements of  $\pm 20\%$ , and three IPs were obtained (5). The response factor of AcDON, i.e., the area ratio of AcDON and the IS, <sup>13</sup>C-DON, was used to differentiate between the three different spiking levels. The response factor for each spiking level clearly differentiates, as no overlapping can be observed between each mean response factor value ( $\pm$  standard deviation). This adds to the semi-quantitative attributes of the ID-LFIA DART-QqQ-MS/MS approach (Figure 3.10 and Table 3.3).

**Table 3.3.** Results from ID-LFIA DART-QqQ-MS/MS analysis and the respective LFIA smartphone screening of AcDON-spiked wheat samples at three target levels and the analysis of an incurred corn starch sample.

	TL	ID-LFIA DART-QqQ-MS/MS				LFIA Smartphone Screening Result (mg/kg, Mean Response $\pm$ SD)
		Mean Ion Area Ratio of DON $\pm$ SD	Response Factor $\pm$ SD	Mean Ion Area Ratio of AcDON $\pm$ SD	Response Factor $\pm$ SD	
AcDON	0.5	-	-	0.73 ( $\pm 0.06$ )	0.09 ( $\pm 0.01$ )	0.64 ( $\pm 0.01$ )
spiked	1	-	-	0.76 ( $\pm 0.03$ )	0.16 ( $\pm 0.02$ )	1.87 ( $\pm 0.04$ )
wheat	1.5	-	-	0.65 ( $\pm 0.02$ )	0.31 ( $\pm 0.01$ )	2.62 ( $\pm 0.03$ )
Contaminated corn starch		0.32 ( $\pm 0.09$ )	0.82 ( $\pm 0.08$ )	0.71 ( $\pm 0.08$ )	0.45 ( $\pm 0.05$ )	12.76 ( $\pm 0.07$ )

Conditions: duplicate sampling of the same final ID-LFIA dissociation solution in DART-QqQ-MS/MS. SD is the standard deviation of the duplicate measurements. The screening result was performed with the r-Biopharm LFIA, and the quantification was done with the associated smartphone app. SD is the standard deviation of duplicate reading of the same LFIA. The response factor for DON is the mean area ratio of the MRM product ion at m/z 249.2 and the <sup>13</sup>C-DON ion at m/z 263.2, and for AcDON the ratio of the MRM product ion at m/z 231.1 and the <sup>13</sup>C-DON ion at m/z 263.2. The DON ion ratio is the ratio of the absolute area of the DON MRM product ion at m/z 231.1 to the area of the ion at m/z 249.2 and for AcDON the ratio of the MRM product ions at m/z 203.1 and m/z 231.1

Moreover, a contaminated corn starch sample was analyzed, both with the ID-LFIA ESI-QqQ-MS/MS (16) and the ID-LFIA DART-QqQ-MS/MS approach. The smartphone-based LFIA screening revealed a highly contaminated sample (Table 3.3).

The ID-LFIA MS/MS results also indicated a high contaminated ( $>1.5\times$  TL) sample and were highly complementary, as the ESI method detected the presence of DON and DON-3G, and the DART method detected DON and AcDON (Figure 3.10). These results were also confirmed by an accredited LC-MS/MS confirmatory analysis method, demonstrating high contamination quantified as 13 mg/kg DON, 2.1 mg/kg 15-AcDON, 0.13 mg/kg 3-AcDON, and 0.52 mg/kg DON-3G.

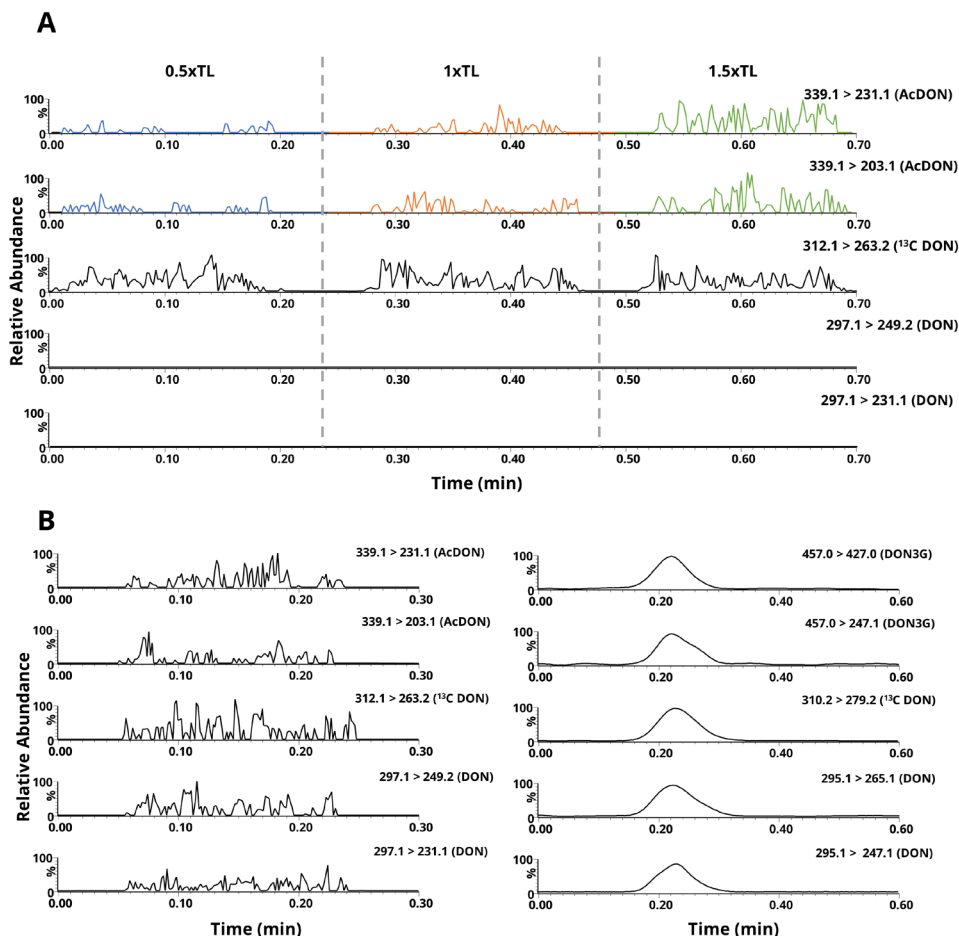


**Figure 3.10.** (A). Chronogram of AcDON-spiked wheat sample used to develop the ID-LFIA and retrieved in dissociation solution analyzed by DART-QqQ-MS/MS, demonstrating the three distinct TL in blue  $0.5\times$  TL, orange  $1\times$  TL, and green  $1.5\times$  TL.  $^{13}\text{C}$ -DON is added as an IS before the MS analysis. (B). Chronogram of the incurred corn starch sample used to develop the ID-LFIA and retrieved in dissociation solution analyzed in (+)DART-QqQ-MS/MS (left) and (-)ESI-QqQ-MS/MS in flow injection analysis mode (right).  $^{13}\text{C}$ -DON is added as an IS prior to MS analysis.

### 3.4 Discussion

In the modern world, people are highly dependent on their personal phones. Smartphones have endless possibilities, from monitoring our biorhythm to navigating us with accurate mapping (27). One of the emerging possibilities of smartphone use is monitoring food quality and safety (28). Soon, smartphone-based screening diagnostics in food safety analysis will be a reality, and the high demands for confirmatory analysis will overrun the routine analysis laboratories. Combining two techniques and using them to concentrate solely on the positives of each one, is the aim of many studies (29). Such technique is the presented ID-LFIA DART-QqQ-MS/MS. The developed and validated approach could be considered for application to any other low molecular weight contaminant for on-site screening and confirmation in future food control frameworks, provided antibodies are available, and the contaminant has a sufficient ionization efficiency.

At first, the method was optimized, and afterward, it was validated according to the EU 2021/808 guidelines (5). During the method optimization, we observed the significance of choosing the right temperature for the helium carrier gas and the collision energy in DART operation and AIMS, in general. Contrary to our previously published work, the ID-LFIA ESI-MS approach (**Chapter 2**) (16), the DART approach can deal more efficiently with the ion suppression caused by the LFIA buffer and nitrocellulose residues. Additionally, the DART-QqQ-MS/MS approach was validated as a semi-quantitative confirmatory method for DON in a limited but relevant concentration range around the regulatory limit. The number of lines of DON mAbs enables the binding of a limited amount of DON, which allows for a semi-quantitative approach around the relevant ML, but not for absolute quantification over an extensive linearity range. The robust ion ratios monitored showed a well-performing method for detecting DON and its acetyl forms. For the unambiguous confirmation of the identity of the target analytes selected, MRM transitions were monitored, and their respective ion ratios were calculated with robustness for all spiked and incurred samples. According to the confirmatory analysis performance criteria for group B substances (i.e., veterinary drugs and contaminants, including mycotoxins), four identification points (IPs) are required for substances' identification (5). With QqQ measurements, two product ions from the MRM ion monitoring yield three IPs for substances' identification. In the future revised regulation, additional IPs might be granted to this approach because of the immunochromatographic properties of the ID-LFIA. Moreover, the accompanied smartphone LFIA screening was also validated, leading to a complete validated approach for detecting DON: smartphone screening LFIA followed by ID-LFIA DART-QqQ-MS/MS analysis.

We acknowledge that our validated method is not the only LFIA or DART method published so far to detect DON. However, our method combines both LFIA and DART analysis, and it addresses several issues not coped with before. For instance, the screening (smartphone) LFIA methods published (30, 31) cannot discriminate between the DON and its conjugated forms that yield the positive result. On the other hand, the DART-MS method published (15), even though it measures a higher



number of mycotoxins, it does not yield enough IPs to be classified as a confirmatory approach according to the regulation, because of the full scan high-resolution detection of only a single  $m/z$  value for each mycotoxin. Finally, the conventional GC-MS or LC-MS/MS methods developed (32–35) require time-consuming sample preparation/pre-treatment, including derivatization in case of GC analysis and chromatographic separation, which can reach over 15 min per sample; and in case of LC-analysis, it consumes large amounts of solvents.

With the validated smartphone LFIA followed by ID-LFIA DART-QqQ-MS/MS approach, we can focus on each technique's positives and escape possible limitations. For this reason, the inability of the LFIA to discriminate the reason behind the positive result can be addressed with the following MS analysis, and the full scan monitoring can be addressed by the ID-LFIA, isolating only the mycotoxin group of interest. Other characteristics that make our method suitable for future use by routine confirmatory analysis laboratories and suitable to be incorporated in future food safety monitoring are its increased throughput, low sample and solvent volumes used, instrument operating time, and minimal sample preparation needed, as well as its robustness on the monitoring of the relevant ion transitions.

## 3.5 References

1. European Commission. *Off. J. Eur. Union*. **31**, 1–24 (2002).
2. R. S. Rodriguez, T.L. O’Keefe, C. Froehlich, R.E. Lewis, T.R. Sheldon, C.L. Haynes, *Anal. Chem.* **93**, 23–40 (2021).
3. L. T. Pedroso Pereira, P. Putnik, C. H. Tadashi Iwase, L. de Oliveira Rocha, *Curr. Opin. Food Sci.* **30**, 85–92 (2019).
4. A. P. Magnoli, V. L. Poloni, L. Cavaglieri. *Curr. Opin. Food Sci.* **29**, 99–108 (2019).
5. European Commission. *Off. J. Eur. Union*. **180**, 84–109 (2021).
6. A. de Boer. *Regul. Toxicol. Pharmacol.* **108**, 104437 (2019).
7. Y. Lu, Z. Shi, Q. Liu, *Curr. Opin. Food Sci.* **28**, 74–81 (2019).
8. J. L. D. Nelis, A. S. Tsagkaris, M. J. Dillon, J. Hajslova, C. T. Elliott, *TrAC*. **129**, 115934 (2020).
9. R. B. Cody, J. A. Laramée, H. D. Durst, *Anal. Chem.* **77**, 2297–2302 (2005).
10. H. Lu, H. Zhang, K. Chingin, J. Xiong, X. Fang, H. Chen, *TrAC*. **107**, 99–115 (2018).
11. X. Zhang, X. Ren, K. Chingin. *Rapid Commun. Mass Spectrom.* **35**, 1–13 (2021).
12. T. Guo, W. Yong, Y. Jin, L. Zhang, J. Liu, S. Wang, Q. Chen, Y. Dong, H. Su, T. Tan, *Mass Spectrom. Rev.* **36**, 161–187 (2017).
13. A. Khaled, J. R. Belinato, J. Pawliszyn, *Talanta*. **217**, 121095 (2020).
14. M. Busman, J. R. Bobell, C. M. Maragos, *Food Control*. **47**, 592–598 (2015).
15. L. Vaclavik, M. Zachariasova, V. Hrbek, J. Hajslova, *Talanta*. **82**, 1950–1957 (2010).
16. A. Geballa-Koukoula, A. Gerssen, M. W. F. Nielen, *Anal. Bioanal. Chem.* **412**, 7547–7558 (2020).
17. J. Hajslova, T. Cajka, L. Vaclavik. *TrAC*. **30**, 204–218 (2011).
18. European Commission. *Off. J. Eur. Union*, **364**, 558–577 (2006).
19. G. M. S. Ross, G. I. Salentijn, M. W. F. Nielen, *Biosensors*. **9**, 1–21 (2019).
20. A. S. Tsagkaris, D. Migliorelli, L. Uttl, D. Filippini, J. Pulkrabova, J. Hajslova, *Talanta*. **222**, 121535 (2021).
21. G. M. S. Ross, D. Filippini, M. W. F. Nielen, G. I. Salentijn, *Anal. Chim. Acta*. **1140**, 190–198 (2020).
22. D. Steiner, M. Sulyok, A. Malachová, A. Mueller, R. Krska, *J. Chromatogr. A*. **1629**, 461502 (2020).
23. J. H. Gross. *Anal. Bioanal. Chem.* **406**, 63–80 (2014).
24. L. Song, S. C. Gibson, D. Bhandari, K. D. Cook, J. E. Bartmess, *Anal. Chem.* **81**, 10080–10088 (2009).
25. L. Song, A. B. Dykstra, H. Yao, J. E. Bartmess, *J. Am. Soc. Mass Spectrom.* **20**, 42–50 (2009).
26. C. Juan, L. Covarelli, G. Beccari, V. Colasante, J. Mañes, *Food Control*. **62**, 322–329 (2016).
27. M. Rezazadeh, S. Seidi, M. Lid, S. Pedersen-Bjergaard, Y. Yamini, *TrAC*. **118**, 548–555 (2019).
28. G. Rateni, P. Dario, F. Cavallo, *Sensors*. **17**, 1453 (2017).
29. I. Domínguez, A. G. Frenich, R. Romero-González, *Anal. Methods*. **12**, 1148–1162 (2020).
30. V. M. T. Lattanzio, B. Ciasca, S. Powers, C. von Holst, **76**, 137–144 (2016).
31. Z. Liu, Q. Hua, J. Wang, Z. Liang, J. Li, J. Wu, X. Shen, H. Lei, X. Li, *Biosens. Bioelectron.* **158**, 1–8 (2020).
32. N. Broekaert, M. Devreese, T. De Mil, S. Fraeyman, S. De Baere, S. De Saeger, P. De Backer, S. Croubels, *J. Chromatogr. B*. **971**, 43–51 (2014).
33. V. M. T. Lattanzio, M. Solfrizzo, A. De Girolamo, S.N. Chulze, A.M. Torres, A. Visconti, *J. Chromatogr. B Anal. Technol. Biomed. Life Sci.* **879**, 707–715 (2011).
34. S. C. Cunha, J. O. Fernandes, *Food Chem. Toxicol.* **50**, 1019–1026 (2012).
35. J. Olsson, T. Börjesson, T. Lundstedt, J. Schnürer, *Int. J. Food Microbiol.* **72**, 203–214 (2002).







## **Immuno-Enriched Microspheres - Magnetic Blade Spray Tandem Mass Spectrometry for Domoic Acid in Mussels**

*Adapted from:*

A. Geballa-Koukoulou, A. Gerssen, M.H. Blokland, C.T. Elliott, J. Pawliszyn, M.W.F. Nielen, *Immuno-Enriched Microspheres - Magnetic Blade Spray-Tandem Mass Spectrometry for Domoic Acid in Mussels*, *Anal. Chem.* 93 (2021) 15736–15743.  
<https://doi.org/10.1021/acs.analchem.1c03816>

## **Abstract**

*Paramagnetic microspheres can be used in planar array fluorescence immunoassays for single or multiplex screening of food contaminants. However, no confirmation of the molecular identity is obtained. Coated blade spray (CBS) is a direct ionization mass spectrometry (MS) technique, and when combined with triple quadrupole MS/MS, it allows for rapid confirmation of food contaminants. The lack of chromatography in CBS, though, compromises the specificity of the measurement for unequivocal identification of contaminants, based on the European Union (EU) regulation. Therefore, a rapid and easy-to-use immunomagnetic blade spray (iMBS) method was developed in which immuno-enriched paramagnetic microspheres replace the coating of CBS. The iMBS-MS/MS method was fully optimized, validated in-house following the EU 2021/808 regulation, and benchmarked against a commercial lateral flow immunoassay (LFIA) for on-site screening of DA. The applicability of iMBS-MS/MS was further demonstrated by analyzing incurred mussel samples. The combination of immunorecognition and MS/MS detection in iMBS-MS/MS enhances the measurement selectivity, which is demonstrated by the rapid differentiation between the marine toxin domoic acid (DA) and its structural analog kainic acid (KA), which cannot be achieved with the LFIA alone. Interestingly, this first-ever reported iMBS-MS/MS method is generic and can be adapted to include any other immuno-captured food contaminant, provided that monoclonal antibodies are available, thus offering a complementary confirmatory analysis approach to multiplex immunoassay screening methods. Moreover, due to its speed of analysis, iMBS-MS/MS can bridge the logistics gap between future large-scale on-site testing using LFIAs and classical time-consuming confirmatory MS analysis performed in official control laboratories.*

## 4.1 Introduction

Liquid or gas chromatography (LC- or GC-) tandem mass spectrometry (MS/MS) is regarded as the gold standard in terms of European regulation on confirmatory analysis of food contaminants (1–3). However, chromatography is time-consuming, which is a drawback for routine laboratories when large numbers of samples often need to be analyzed (4). Ambient ionization mass spectrometry (AIMS)-based techniques can be used to shorten analysis time markedly. AIMS enables direct ionization of samples, with minimum or no sample pre-treatment, and induces ionization under ambient conditions without chromatographic separation (5) and many times directly from a surface (6). A few examples of such AIMS techniques are direct analysis in real time (DART) (7), desorption electrospray ionization (DESI) (8), and coated blade spray (CBS) (9). DESI and DART were the first AIMS techniques developed (7, 8) and support ionization using a constant flow of carrier liquid and gas, respectively. Contrary, CBS employs a coated (on the tip) conductive stainless steel strip, only requiring a small droplet of solvent for desorption and ionization, as in paper spray (10) and modified wooden-tip spray (11). The coating on CBS acts as a solid-phase microextraction (SPME) means to achieve selective enrichment of analytes from liquid samples or extracts. Following desorption of the compounds using a drop of organic solvent and high voltage application to the blade, spray ionization occurs without the requirement of additional gas or liquid flows (9). The simplicity of CBS enhances the possibilities for future portable CBS-MS applications in food testing (12, 13). The most recent evolutionary aspect of CBS is magnetic blade spray (MBS), where paramagnetic surface-functionalized microparticles have replaced the coating for easy extraction and sample handling (14).

In the EU food safety protocols, prior to the confirmatory analysis by LC- or GC-MS/MS, a rapid screening analysis is often performed (15). Screening methodologies include biorecognition-based assays with monoclonal antibodies (mAbs), which can provide a quick qualitative or semi-quantitative result for the presence of a targeted contaminant or a family of contaminants based on the cross-reactivity profile of the mAbs employed. However, screening assays do not provide any structural information on the contaminant detected; thus, confirmatory analysis with LC- or GC-MS/MS is needed in the case of a non-compliant screening result (15, 16). Apart from the well-known lateral flow immunoassay (LFIA) (17, 18), many other assay formats have been developed. Paramagnetic microspheres have been employed in fluorescent planar array screening bioassays. Carboxyl groups on the surface of paramagnetic microspheres allow for direct covalent coupling of biomolecules by EDC/NHS chemistry (19–21). Combining the features of biorecognition-based screening and AIMS may offer a novel and attractive rapid alternative workflow for confirmatory analysis. Only a few efforts have been made toward this direction of improved testing for contaminants (22–26), underlining both its novelty and potential applicability. However, no demonstrations of direct immuno-enrichment and magnetic blade spray MS (iMBS) for rapid analysis have been published so far.

The present study showcases the iMBS approach, where mAbs have been covalently coupled to surface-functionalized paramagnetic microspheres for selective biorecognition and capturing of targeted analytes. Subsequent blade spray and triple quadrupole (QqQ) MS/MS detection enable the ionization and unequivocal identification of the analytes without additional sample pre-treatment. As a proof of concept, the method was developed to detect the marine shellfish toxin domoic acid (DA) and its structural analog, kainic acid (KA) in mussels. DA is an analog of the amino acids glutamate and proline. Specific phytoplankton species produce DA, which bioaccumulates in filter feeders such as shellfish, including scallops, oysters, and mussels. Consumption of DA-contaminated commodities may lead to amnesic shellfish poisoning (ASP); thus, it can cause severe central nervous system symptoms, such as disorientation, seizures, memory loss, and even death (27, 28). The developed protocol of LFIA screening with smartphone-readout and subsequent iMBS confirmation for DA was validated according to the 2021 EU legislation (15) at three different target levels (TL) based on the maximum limit (ML) of 20 mg/kg (29) over the course of three days and benchmarked against a commercial LFIA for on-site testing of DA.

## 4.2 Material and Methods

### 4.2.1 Chemicals and reagents

Acetonitrile and methanol of UHPLC-MS purity grade and ammonia solution (25% v/v), formic acid (98% v/v), acetic acid (98% v/v), and DA and KA, were purchased from Merck (Darmstadt, Germany). Milli-Q water of 18.3 MΩ/cm conductivity was obtained using a water purification system from Merck (Amsterdam, The Netherlands). Solutions of 5 mM ammonium acetate and 5 mM ammonium formate (Merck) were prepared in Milli-Q water. Standard stock solutions of 1000 µg/mL DA, and 5000 µg/mL KA, were prepared in acetonitrile/water (10/90 v/v).

### 4.2.2 iMBS preparation

For iMBS, polystyrene/divinylbenzene coated blades provided by Restek Corp. (Bellefonte, Pennsylvania, USA) were sonicated at 40 °C in methanol/formic acid (50/50 v/v) for 40 min, to yield non-coated stainless steel blades. The non-coated blades were used for the entire optimization of DA ionization with standard solutions. For adherence of paramagnetic microspheres, a type N48 neodymium magnetic disc (3 mm×2 mm) from Supermagnete (Gottmadingen, Germany) was positioned under the tip of the non-coated blade. For the immuno-capturing part, MagPlex-C, paramagnetic carboxylated microspheres (MC10038, particle size 6.5 µm) were purchased from Luminex Corp. (Austin, Texas, USA), and mouse mAbs against DA were provided by Queen's University Belfast. These antibodies previously demonstrated a 24% cross-reactivity with KA but no cross-reactivity towards any naturally co-occurring toxins (30).



A carbodiimide covalent coupling procedure was followed for antibody immobilization on the paramagnetic microspheres, as described in the Luminex protocol (31). Briefly, 200  $\mu$ L of stock uncoupled paramagnetic microspheres were washed with Milli-Q water and activated using monobasic sodium phosphate ( $\text{NaH}_2\text{PO}_4$ ) (Merck), sulfo-NHS (N-hydroxysulfosuccinimide), and EDC (N-(3-dimethylaminopropyl)-N-ethylcarbodiimide hydrochloride) (Sigma-Aldrich, Zwijndrecht, The Netherlands). Next, mAbs for DA, 0.15 mg/mL in MES (2-(N-morpholino)ethanesulfonic acid) (Sigma Aldrich), were added to the activated paramagnetic microspheres for immobilization. After a 2 h incubation, the immuno-enriched paramagnetic microspheres were reconstituted in 200  $\mu$ L of PBS-TBN (phosphate-buffered saline with Tween-20, bovine serum albumin (BSA), and sodium azide), and stored in the refrigerator at 4 °C in a sealed dark Eppendorf tube. For the preparation of the PBS-TBN stock solution, a PBS solution containing 137 mM sodium chloride (NaCl), 2.7 mM potassium chloride (KCl), 10 mM sodium hydrogen phosphate ( $\text{Na}_2\text{HPO}_4$ ), and 1.8 mM potassium dihydrogen phosphate ( $\text{KH}_2\text{PO}_4$ ) (Merck, Darmstadt, Germany), having a pH of 7.4, was prepared in Milli-Q water. The final storage buffer, PBS-TBN, was prepared by tenfold dilution of the PBS stock solution in Milli-Q water containing (0.1% w/v) BSA, (0.02% v/v) Tween-20, and (0.05% w/v) sodium azide (Sigma-Aldrich).

For benchmarking, a commercially available LFIA screening test kit for DA, "Reveal® 2.0 for ASP", including LFIAs for DA and micro-perforated filter bags, was purchased from Neogen (Lansing, Michigan, USA).

For the in-house validation, 21 blank mussel samples (*Mytilus edulis*), and for the applicability study, three naturally contaminated (incurred) samples, homogenized and stored at -80 °C, previously analyzed for the presence of DA by validated and accredited routine LC-MS/MS and LC-UV methods, were provided in-house.

## 4.2.3 Mass spectrometry

### Triple Quadrupole MS/MS

The iMBS-MS/MS analysis was performed on a Micromass Quattro Ultima Pt QqQ-MS (Waters Corporation, Milford, MA, USA) equipped with a blade spray setup consisting of an x-y-z stage and high-voltage plug from a Waters nanoESI ion source. A plastic clamp was used to secure the blade in place (Figure 4.1). Optimized operating conditions included positive ionization mode with 3.7 kV spray voltage, 50 V cone voltage, 100 °C cone temperature, and 0.16 mL/min argon collision gas flow. Data were acquired in multiple reaction monitoring (MRM) mode, and two transitions were monitored for DA and KA. For DA,  $m/z$  312.1 > 266.1 and  $m/z$  312.1 > 248.1 at 12 eV collision energy, and for KA  $m/z$  214.1 > 168.1 and  $m/z$  214.1 > 122.1, at 10 and 18 eV collision energies, respectively. The data were acquired and processed using MassLynx software (Waters). From the chronograms acquired, area ion ratios of the two fragment ions for DA and KA were calculated and used for unequivocal confirmation of the identity of each substance according to the criteria (15).

For the semi-quantitative evaluation of the screening assays, a Samsung Galaxy A50 smartphone (Samsung electronics, Suwon, South Korea) was used to retrieve

photographs using the OpenCamera app (v1.47.3) under controlled light, exposure, and focus conditions. The photographs were processed using ImageJ software, to split the photographs into their RGB (red, green, and blue) color channels.

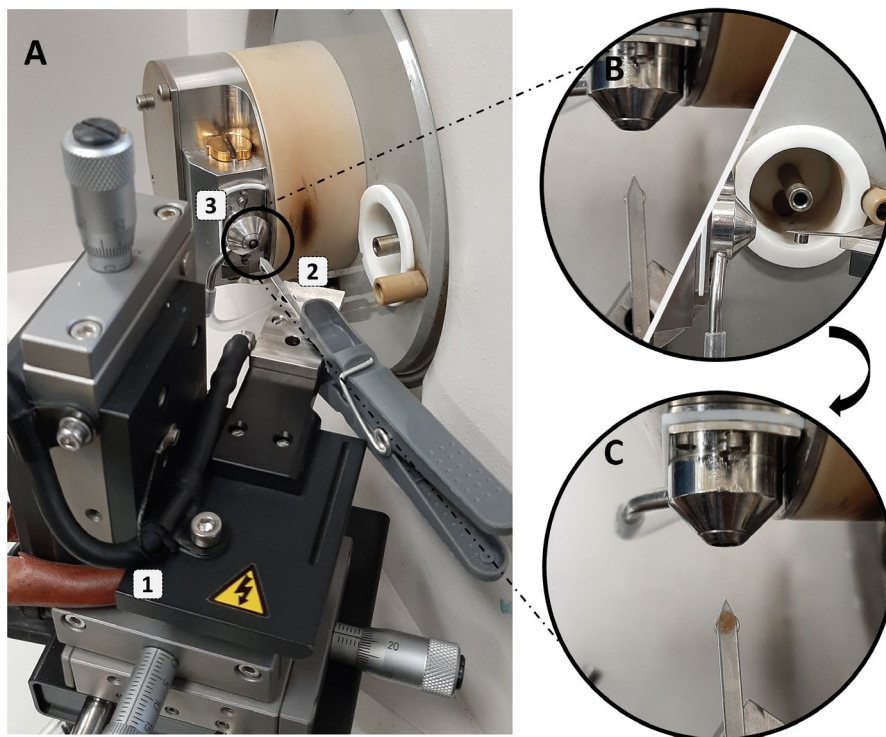


**Figure 4.1.** Photographs of the experimental setup of iMBS-MS/MS. (A) 1. x-y-z stage and high voltage plug from a Waters nanoESI ion source 2. blade secured with a plastic clamp and 3. inlet of the Micromass Quattro Ultima Pt QqQ-MS. Insert with zoomed-in parts of the setup where; (B) non-coated blades top and side view with the super magnet showing under the blade, and (C) top view of the non-coated blade with the sampling of 10  $\mu$ L of immuno-enriched paramagnetic microspheres.

### 4.2.4 Extraction and method development

For method development and in-house validation, mussel samples were extracted using the previously developed and commercialized Neogen screening assay extraction protocol for efficient extraction of DA from samples (32). In short, 1 g of the homogenized mussel sample was extracted using 30 mL of water. Vigorous manual agitation followed for 30 s, and afterward, a microperforated filter bag was used to extract further and remove the mussel residues. The final extract was stored in the refrigerator at 4 °C for further use.

For the LFIA screening assay, 100  $\mu\text{L}$  of the extracts was further diluted with the buffer provided in a vial in the assay kit. Finally, 100  $\mu\text{L}$  of the mixture thus obtained was used to develop the LFIA. The same spiked undiluted mussel extracts were also used for iMBS-MS/MS analysis. 10  $\mu\text{L}$  of the immuno-enriched paramagnetic microspheres suspension was mixed in a 96-well plate with 100  $\mu\text{L}$  of the undiluted mussel extract and 100  $\mu\text{L}$  of Milli-Q water. The mixture thus obtained was incubated at room temperature for 10 min. Then, a magnetic plate was positioned underneath the 96-well plate to induce fast sedimentation and adherence of the immuno-enriched paramagnetic microspheres at the bottom of the 96-well plate. The supernatant was discarded, and the magnetically trapped microspheres were washed three times with 100  $\mu\text{L}$  of Milli-Q water.

For the MS/MS analysis, the non-coated blade was placed at a  $\pm 6$  mm distance from the entrance cone of the ion source. While the spray voltage was at 0 kV, the incubated and washed paramagnetic microspheres were resuspended in 50  $\mu\text{L}$  of Milli-Q water and retrieved from the 96-well plate to be pipetted onto the non-coated metal blade at the tip of the blade with the magnet underneath. Next, after 30 s of adherence time of the paramagnetic microspheres, the excess supernatant liquid was removed by a clean tissue. Then, 4  $\mu\text{L}$  of methanol/formic acid (2.5% v/v) was pipetted on top of the immuno-enriched paramagnetic microspheres to dissociate the antigen from the immobilized antibodies. After 1 min, the binding of the DA from the mAb on the immuno-enriched paramagnetic microspheres was disrupted, and a second 4  $\mu\text{L}$  aliquot was pipetted because of evaporation of the first 4  $\mu\text{L}$ . Finally, the optimized spray voltage of 3.7 kV was applied to the non-coated blade to obtain an ESI-like spray, and the ions formed were analyzed by MS/MS (Figure 4.2).

## 4.2.5 Method validation

For the validation of the screening LFIA, a semi-quantitative assessment was performed using a custom-made 3D-printed holder (33), and a smartphone to retrieve photographs. The retrieved photographs were processed and splitted into their RGB (red, green, and blue) color channels. The blue color channel was used to measure the intensity of the background (B), the control (C) and the test (T) line. After subtracting the B from the T and C intensities, the corrected blue channel intensities (cBCI) were used to calculate the ratio between the T's cBCI and the C's cBCI. Finally, the T/C ratio was used for semi-quantitative assessment of the LFIAs performance.

To validate both the screening LFIA and the iMBS-MS/MS method, portions of the blank mussel extracts were spiked at three different TLs, namely 335 ng/mL (0.5 $\times$  TL), 670 ng/mL (1 $\times$  TL), and 1005 ng/mL (1.5 $\times$  TL). The TL were calculated based on the theoretically DA concentration in sample extracts from mussels contaminated at the ML of 20 mg/kg.

Both the screening LFIA and the iMBS-MS/MS methods, were validated according to the EU legislation 2021/808 (15), assessing the specificity, intra-day repeatability, inter-day repeatability, within-laboratory reproducibility, trueness, CC $\alpha$  and CC $\beta$ . To assess the specificity, differences in the signal between the lower 0.5 $\times$  TL spiking level onwards, and blank samples were assessed. Moreover, the intra-day and inter-

day repeatability results expressed as the %RSD was calculated and assessed for the 21 spiked samples. The within-laboratory reproducibility was calculated using one-way ANOVA. For the trueness assessment, the theoretical concentration at each spiking level was compared to that of the determined concentration, calculated based on each day's matrix-matched calibration curve expressed in mg/kg. Finally, the methods' compliance versus the performance criteria were assessed using the CC $\alpha$  and CC $\beta$  values. The CC $\alpha$  was calculated for the iMBS-MS/MS, using the concentration at the 1 $\times$ TL plus 1.64 times the standard deviation of the within-laboratory reproducibility at this level, whereas the CC $\beta$  value was calculated having the 0.5 $\times$ TL as screening target concentration (STC) and using the concentration at the STC plus 1.64 times the standard deviation of the within-laboratory reproducibility at the STC (15).

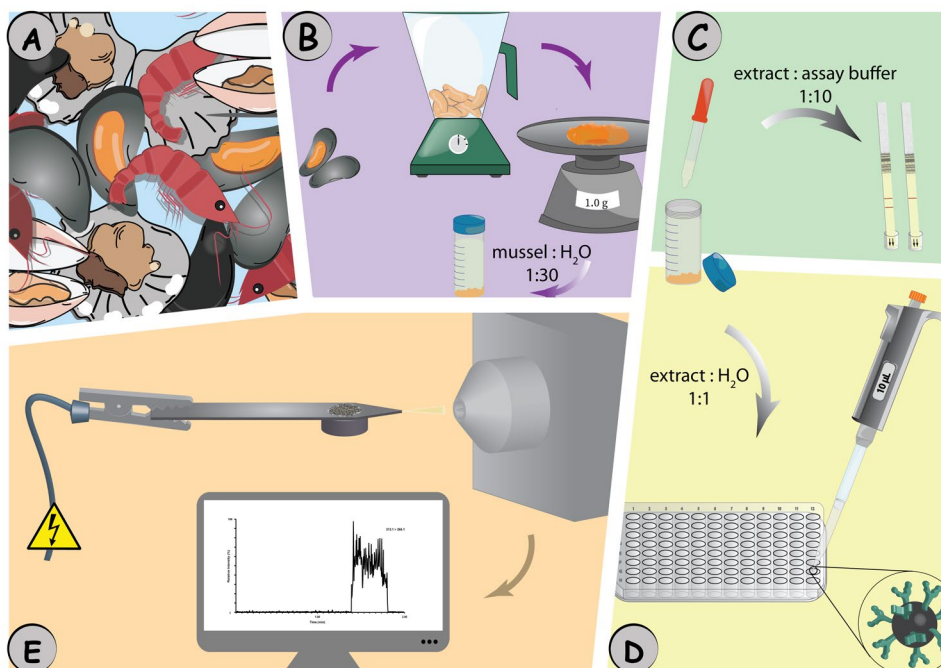


**Figure 4.2** Workflow application of iMBS-MS/MS for analysis of contaminated shellfish samples. (A) Samples are collected on-site. (B) The selected shellfish commodity, i.e., mussels, is homogenized, weighed, and 1 g is extracted with 30 mL of distilled water. (C) The sample extract is diluted with assay buffer for rapid on-site testing using a commercial screening LFIA, leading to a negative result (two lines) for any quantitative result lower than the ML of 20 mg/kg. In contrast, it provides a positive result (one line) for any readout of equal or more than 20 mg/kg. (D) For a positive or ambiguous result, the same sample extract from step (B) can be used for confirmation using the developed iMBS; the extract is diluted 1:1 with Milli-Q water, and 200  $\mu$ L of the diluted extract is incubated with 10  $\mu$ L of immuno-enriched paramagnetic microspheres. (E) After incubation, the final step is the deposition and fixation of the immuno-enriched paramagnetic microspheres on the blade tip using a super magnet, followed by dissociation with methanol/formic acid (2.5% v/v) and MS/MS confirmatory analysis.

## 4.3 Results

### 4.3.1 Method development

#### Optimization of Blade Spray and MS Conditions

Initial optimization was performed using DA solutions and non-coated blades aiming at optimum ionization and MS operating conditions. Ionization was performed at a distance of  $\pm 6$  mm between the tip of the blade and the cone inlet of the MS system, to prevent any loss of paramagnetic microspheres by vacuum suction at the final stage of the experimental design.

The optimum spray/desorption solution for DA ionization was tested by applying 10  $\mu$ L of 100 ng/mL DA in different desorption solutions and monitoring the intensity of the protonated ion in full scan positive ion mode ( $m/z$  200-400). The desorption solutions tested were mixtures of methanol or acetonitrile, with formic or acetic acid at a concentration of (0.5% v/v), and (80/20 v/v) mixtures of methanol/buffer and acetonitrile/buffer, with the buffer being 5 mM ammonium formate/ formic acid (0.5% v/v) or 5 mM ammonium acetate/ acetic acid (0.5% v/v). The rationale for testing these desorption solutions was based on the typical solvents applied for DA extraction and LC-MS/MS analysis (35–38). Apart from that, it is known that acidic or alkaline conditions and/or organic solvents are necessary to disrupt the binding of the analytes with mAbs. Acetonitrile showed a lower ionization efficiency than methanol, and the addition of buffers did not enhance the ionization efficiency. Among the spray solutions tested, sodium and potassium adducts were observed, next to the abundant protonated ion of DA. The solution that yielded the highest ionization efficiency for the protonated ion of DA was methanol/formic acid (0.5% v/v). Next, the formic acid concentration was further optimized, starting from (0.5% v/v) up to (5.5% v/v), with steps of (0.5% v/v) and monitoring in full scan mode ( $m/z$  200-400) the protonated ion of DA. At formic acid (2.5% v/v), the highest intensity of protonated ion of DA was observed. Clearly, a plateau was reached as increased formic acid concentrations did not further improve the intensity of the protonated DA (Figure 4.3).

Furthermore, the matrix interferences were briefly investigated using a methanol/formic acid solution fortified with 0, 0.1, and 1% v/v blank mussel extracts, to mimic an estimate of the matrix residue after three washing cycles of the paramagnetic microspheres at the final experimental iMBS setup. The presence of mussel matrix residues did not alter the resulting chronograms for any of the solutions tested.

Finally, the spray voltage, cone voltage, and collision energy were optimized using 10  $\mu$ L of 100 ng/mL DA in methanol/formic acid (2.5% v/v). Optimum conditions included 3.7 kV spray voltage, 50 V cone voltage and 12 eV collision energy for the MRM transitions  $m/z$  312.1 > 266.1 and  $m/z$  312.1 > 248.1 of DA, and 10 and 18 eV for the MRM transitions  $m/z$  214.1 > 168.1 and  $m/z$  214.1 > 122.1 of KA, respectively.

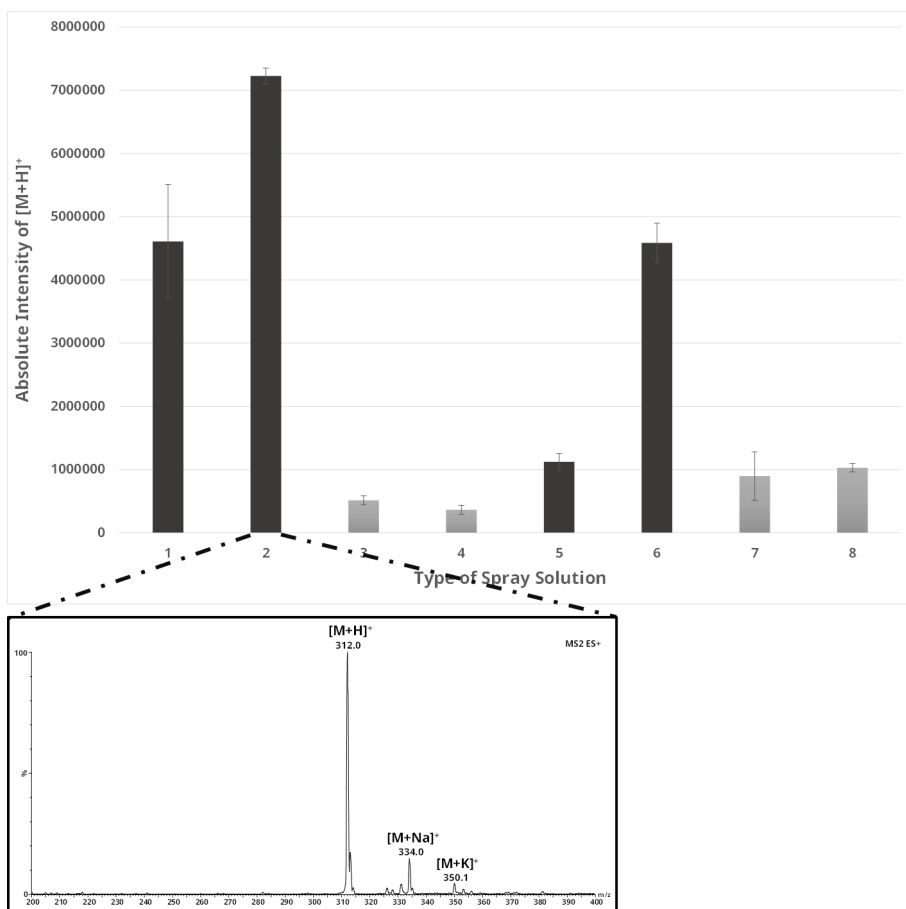


**Figure 4.3.** Spray solution optimization. Relative area intensity of the protonated ion of DA from non-coated blade spray measurements of DA 100 ng/mL in the following solutions (1) methanol/ acetic acid (0.5% v/v), (2) methanol/ formic acid (0.5% v/v), (3) acetonitrile/ acetic acid (0.5% v/v), (4) acetonitrile/ formic acid (0.5% v/v), (5) methanol/ 5 mM ammonium acetate/ acetic acid – (80/ 19.5/ 0.5 - v/v/v), (6) methanol/ 5 mM ammonium formate/ formic acid – (80/ 19.5/ 0.5 - v/v/v), (7) acetonitrile/ 5 mM ammonium acetate/ acetic acid – (80/ 19.5/ 0.5 - v/v/v), (8) acetonitrile/ 5 mM ammonium formate/ formic acid – (80/ 19.5/ 0.5 - v/v/v). Acetonitrile (light grey bars) showing lower ionization than methanol (dark grey bars). Conditions: full scan mode (200-400 m/z), 4 kV spray voltage for methanolic solutions, 4.5 kV for acetonitrile solutions. For methanol/formic acid (0.5% v/v), the mass spectrum with the adducts formed is inserted.

## iMBS-MS/MS of marine toxins in shellfish

When using the mussel extraction protocol (Figure 4.2), the calculated concentration of DA in the extract of a contaminated sample at the TL is approximately 670 ng/mL. Following a 1:1 dilution, 33 ng of DA will be theoretically available for incubation with the immuno-enriched paramagnetic microspheres. However, only a tiny fraction of DA is expected to bind due to the limited antibody capacity available.

Therefore, the limit of quantification (LOQ) and limit of detection (LOD) in direct MS/MS were assessed over a small dynamic range of 0-12 ng/mL only, using non-coated blades and DA spiked in methanol/formic acid (2.5% v/v) with a blank mussel matrix (0.1% v/v). The LOQ was determined at 2 ng/mL, and the LOD at 0.6 ng/mL.

Since no chromatography is applied with the iMBS-MS/MS approach, it could be argued that the selectivity of the method is compromised. According to the latest version of the EU legislation 2021/808 (15) for substances with an established ML, four identification points (IPs) are required for the unequivocal identification of contaminants, one of which is obtained from the chromatographic separation and three from the MS/MS detection when two ion transitions are being monitored. It is stated in the EU 2021/808 document that all MS analyses shall be combined with a separation technique "that shows sufficient separation power and selectivity for the specific application." It may be argued that the high selectivity of immuno-capturing is by far superior to a generic LC gradient separation using a C18 column, and therefore one IP point could be claimed for iMBS. In combination with the three IPs of MS/MS analysis, unequivocal identification of DA could be obtained using iMBS-MS/MS. To a further extent, according to Berendsen et al. (39), the selectivity of a direct MS/MS method is assessed by the probability of interference, i.e., P(I) value, which demonstrates the probability of the occurrence of another than the selected compound showing the same MS/MS characteristics. Having chosen the most selective MRM transitions for DA, P(I) is assessed at  $4.8 \times 10^5$ , which is still higher than the cut-off P(I) value of  $2 \times 10^7$  for achieving a selective MS/MS method without chromatography. Therefore, it is crucial that a direct MS/MS method features additional selectivity as provided by iMBS discussed in this paper. The immuno-capturing in iMBS adds selectivity to the overall MS/MS method, considering the use of mAbs that target only DA and structural analogs, which can be further differentiated in MS/MS based on their specific  $m/z$ .

### iMBS-MS/MS optimization

As a starting point to capture the immuno-enriched paramagnetic microspheres, prototype magnetic blades consisting of magnetic material with a copper strip for HV application were studied. These magnetic blades were provided by the Pawliszyn group and were previously used in the experimental setup described by Rickert et al. (14). It was noticed that for the same DA solutions tested in the range of 0-12 ng/mL, the signal was lower as compared to the non-coated metal blades used in our blade spray optimization experiments, and due to the lower signal, the ion ratios were less robust using these prototype magnetic blades compared to non-coated metal blades (Figure 4.4). The apparent differences between the prototype magnetic blades and the non-coated metal blades were the conductivity of the material and the tip angle. With the non-coated blade, the entire surface is conductive until the tip end. However, the magnetic prototype material is non-conductive, and to compensate for this lack of conductivity, a copper strip is connected to the blade material. However, the copper strip does not cover the entire surface and, instead, ends a few millimetres away from the tip, resulting in reduced conductivity. In addition, the prototype

magnetic blades' material is not as resistant to deformation as the non-coated blades, causing the tip to be less well-defined and sharp.

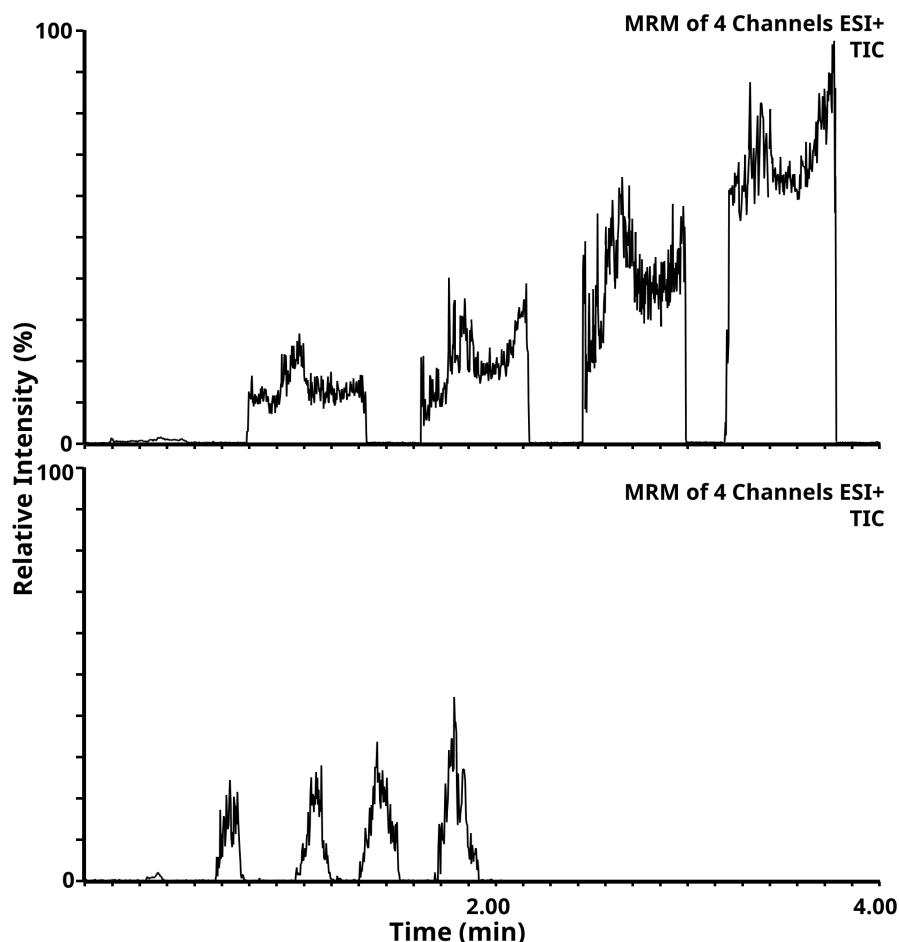


**Figure 4.4.** Comparison between non-coated blades and prototype magnetic blades. Total ion current (from four MRM transitions) chromatograms of consecutive sampling of 10  $\mu\text{L}$  of increasing DA standard concentrations of 0 ng/mL (blank), 2 ng/mL, 4 ng/mL, 6 ng/mL, and 12 ng/mL spiked into methanol/formic acid (2.5% v/v) – mussel extract solution (0.1% v/v). Metal non-coated blades (top) and prototype magnetic blades (bottom) from a previous publication<sup>8</sup>. Graphs have been normalized on the intensity (vertical) axis based on the highest intensity in the chromatograms.

The tip is where the voltage is concentrated at the vertex of the blade, according to the first description of CBS by Gómez-Ríos and Pawliszyn (9). Changes in the shape of the tip could result in alterations of the spray angle and the accumulation of the voltage; thus, applying the same voltage setting in both blades will yield differences in the effective voltage and electric field at the tip. Consequently, we only used



non-coated metal blades obtained by removing the coating from commercial CBS. Immuno-enriched paramagnetic microspheres were trapped onto these metal blades using a magnetic disc positioned under the tip. The trapping of the microspheres on the blade was characterized by SEM, where differences in the blade surface can be clearly seen between blank and paramagnetic microsphere-enriched surface (Figure 4.5).

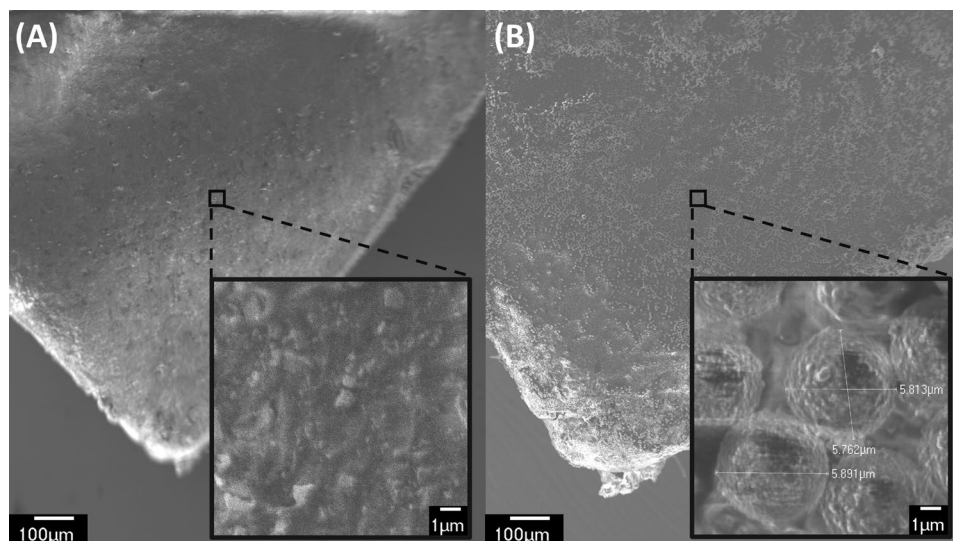


**Figure 4.5.** SEM images of (A) non-coated magnetic blades, and (B) non-coated magnetic blades with captured paramagnetic microspheres.

In order to develop the final iMBS-MS/MS method, the biorecognition part was optimized with respect to the incubation time needed for binding between the immuno-enriched paramagnetic microspheres and the DA in spiked sample extract. More specifically, 10  $\mu\text{L}$  of immuno-enriched paramagnetic microspheres were incubated with 200  $\mu\text{L}$  of a 1:1 water dilution of the mussel extract spiked with DA at a level of 670 ng/mL. The tested incubation times were 3, 5, 10, and 20 min. No signal was observed for the MRM transitions of DA when incubating for 3 min, indicating no binding between the mAb and DA. The 5 min incubation produced half the area intensities in the reconstructed MRM chronograms as compared to the 10 min incubation. The latter turned out to be sufficient for quantitative analysis of lower concentrations. No significant changes were observed in the area intensities of the DA MRM transitions for the 10 and 20 min incubation, possibly due to saturation of the immobilized mAbs; therefore, a 10 min incubation was invariably used in the optimized protocol (Figure 4.6).

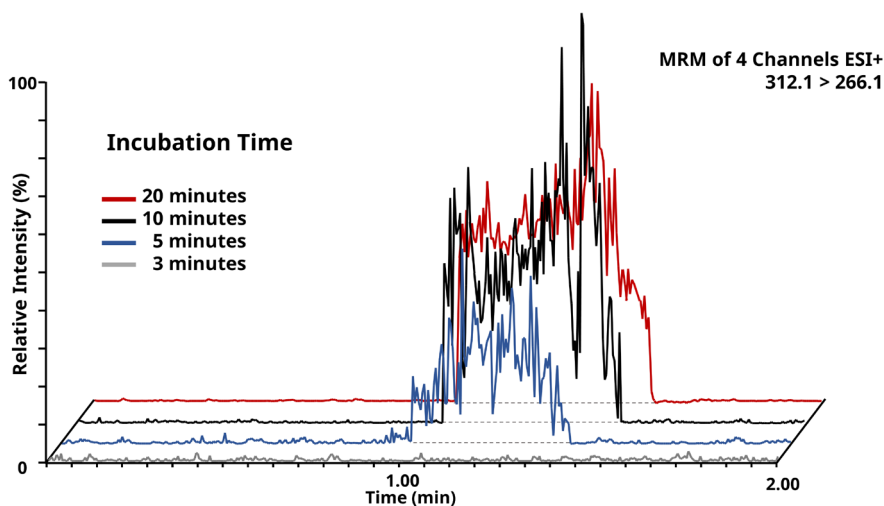


**Figure 4.6.** Overlay chromatograms of the  $m/z$  312.1 > 266.1 transition obtained following iMBS-MS/MS, varying in incubation time. For the exact conditions, see text.

Additionally, the amount of immuno-enriched paramagnetic microspheres to be used in each incubation was varied. Incubation for 10 min with 200  $\mu\text{L}$  of 1:1 diluted spiked (670 ng/mL) mussel extract and 5, 10, or 15  $\mu\text{L}$  of paramagnetic microspheres was tested. 5  $\mu\text{L}$  of paramagnetic microspheres produced lower area intensities of the DA MRM transitions than the other volumes tested. Between 10 and 15  $\mu\text{L}$ , similar results were obtained on the area intensities of the DA MRM transitions. However, using 10  $\mu\text{L}$  of immuno-enriched paramagnetic microspheres, one 4  $\mu\text{L}$  drop of dissociation/spray solution onto the blade was sufficient for quantitative dissociation of DA from the immuno-enriched paramagnetic microspheres, and repetitive desorptions did not yield additional signals showing the correct ion ratios. In contrast, with 15  $\mu\text{L}$  of immuno-enriched paramagnetic microspheres, multiple desorption steps are needed for quantitative dissociation. Therefore, 10  $\mu\text{L}$  was found to be the most cost-effective and appropriate volume to be used (Figure 4.7).

To illustrate the feasibility of the iMBS-MS/MS approach, a blank mussel extract was incubated with immuno-enriched paramagnetic microspheres. The same extract was spiked with DA at 670 ng/mL and next 200  $\mu\text{L}$  of both the blank and fortified 1:1 diluted sample extract were incubated with 10  $\mu\text{L}$  of unfunctionalized paramagnetic microspheres and 10  $\mu\text{L}$  of immuno-enriched paramagnetic microspheres. The results, as expected, showed no signal for the blank sample matrix, nor for the unfunctionalized paramagnetic microspheres. In contrast, DA MRM transition signals with the correct ion ratio of 0.29 (i.e., within the  $\pm 40\%$  relative deviation from the 0.34 ion ratio for DA (15)) were achieved for the immuno-enriched paramagnetic microspheres incubated with the spiked matrix sample (Figure 4.8).

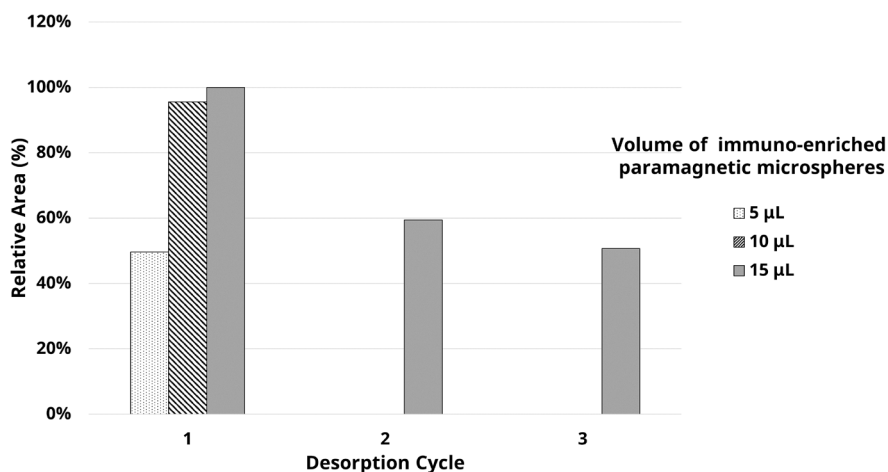


**Figure 4.7.** Bar graphs of the relative area for the MRM transition  $m/z$  312.1 > 266.1 versus the number of desorption cycles following iMBS-MS/MS, varying in the volume of immuno-enriched paramagnetic microspheres. For the exact conditions, see text.

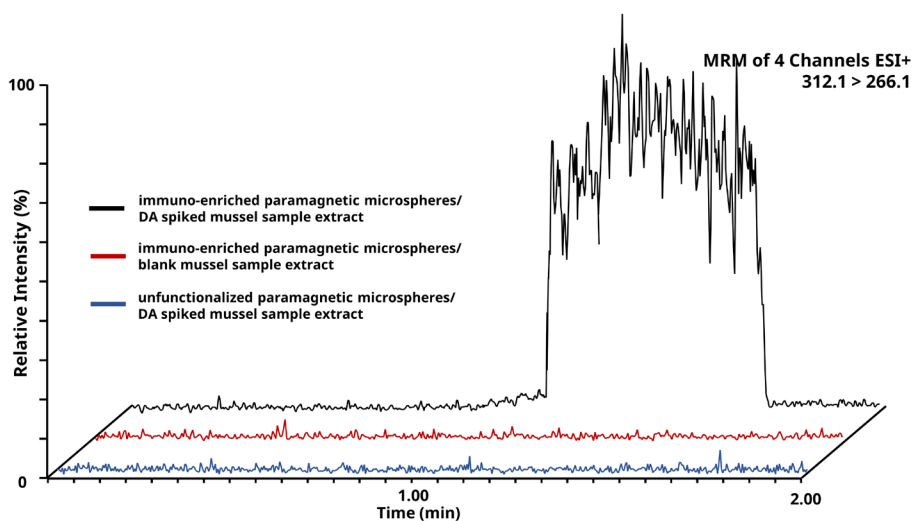


**Figure 4.8.** Overlay chromatograms of the  $m/z$  312.1 > 266.1 transition obtained following iMBS-MS/MS using immuno-enriched and unfunctionalized paramagnetic microspheres. For the exact conditions, see text.

### 4.3.2 In-house method validation

The optimized iMBS-MS/MS approach and a rapid screening LFIA were validated following the EU 2021/808 legislation. For the validation, 21 blank mussel samples were provided in-house, extracted with the LFIA protocol, and the extracts were spiked at three different levels ( $0.5\times$  TL,  $1\times$  TL, and  $1.5\times$  TL) and blank. Over three days, seven samples were analyzed each day, and the results of the statistical analysis were used to assess the performance of the methods.

#### Validation of the Screening LFIA Used for Benchmarking

For the LFIA validation, a qualitative assessment was performed by reading the LFIA results with the naked eye. According to the manufacturer's guidelines, the appearance of only the control line corresponds to a positive result of the contaminated sample containing equal or more than 20 ppm of DA, while two lines (test line and control line) correspond to a negative test result of less than 20 ppm. However, in contrast to the user manual and published results (32), a faded pink test line could be observed at all spiking levels by the naked eye. As an alternative, a semi-quantitative assessment was attempted using a custom-made 3D-printed holder (33), and a smartphone to retrieve photographs. The T/C ratio was used for semi-quantitative assessment of the LFIA's performance, as described in section 4.2.5, thereby overcoming the faded test line problem, and differentiating between positive/non-compliant ( $>20$  ppm) and negative samples (*Figure 4.9*).

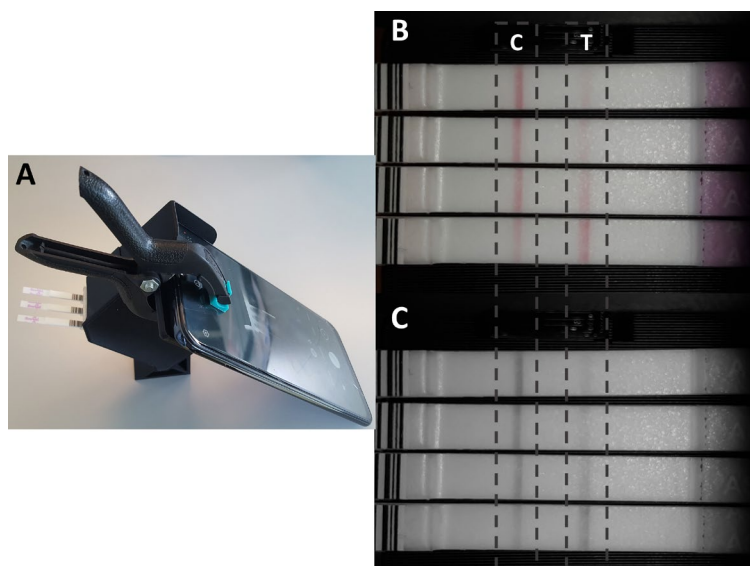


**Figure 4.9.** Photographs of the smartphone reading of commercial LFIA. (A) 3D printed holder with a smartphone attached. Representative (B) photographs and (C) processed blue channel images of the developed LFIA for different DA levels of  $0\times$ ,  $0.5\times$ ,  $1\times$ , and  $1.5\times$  TL, from bottom to top, respectively.

To validate the commercial screening LFIA the assessment levels were blank, 0.5×TL, and 1×TL, because of the inability to differentiate between 1 and 1.5×TL. Regarding the specificity/ sensitivity of the screening LFIA, sufficient discrimination was demonstrated between blank and spiked samples from the 0.5× TL level onwards (*Figure 4.10* and *Table 4.1*).

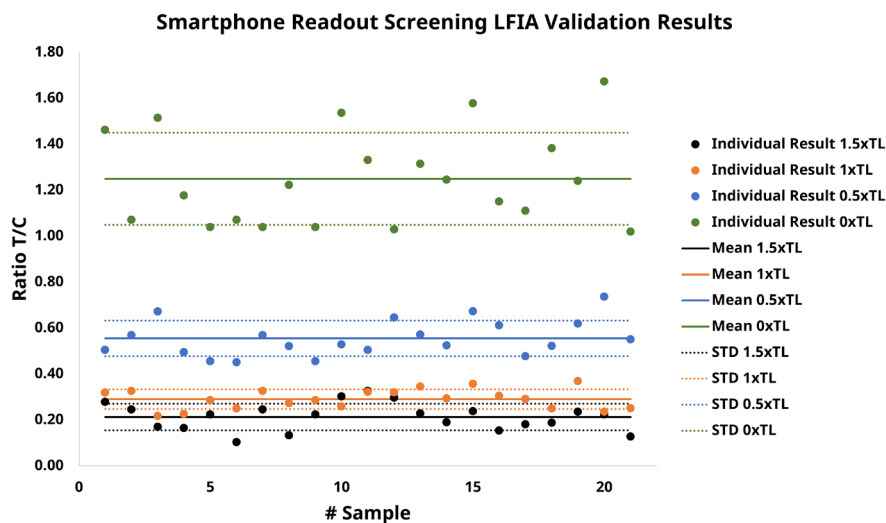


**Figure 4.10.** Data analysis of results from 21 blank mussel samples and spiked versions thereof in screening LFIA. On the vertical axis is the intensity of the isolated blue channel of the test line over the control line.

Further, based on the (semi-)quantitative smartphone reader, the intra-day repeatability results were 13.7, 10.3, and 13.9% at 0.5×TL, and 15.8, 9.4, and 16.8% at the 1×TL levels. The inter-day repeatability results were 14.0, and 14.6% at 0.5×, and 1× TL, respectively. Moreover, the within-laboratory reproducibility results were 13.9, and 15.8% at 0.5×TL, and 1×TL, respectively. The acceptable %RSD value for substances with an ML of >1000 µg/kg is <16%(15), which means that only one value on the third day of 1xTL measurements did not comply yet for a quantitative screening method. Consequently, for the time being our smartphone-based LFIA for DA should be considered as a semi-quantitative screening method. Moreover, the calculated trueness values were 91 and 112% at the 0.5×, and 1× TL, respectively, and within the acceptance range of 80 to 120% as stated in the legislation(15). Finally, the CCβ was calculated at 12.8 mg/kg (0.69 ratio T/C).

### Validation of the newly developed iMBS-MS/MS method

From the analysis of 21 blank mussel samples, no DA signal was observed, underlining the specificity of the iMBS-MS/MS approach. A clear signal was observed from the 0.5x TL spiking level onward (Figure 4.11 and Figure 4.12).

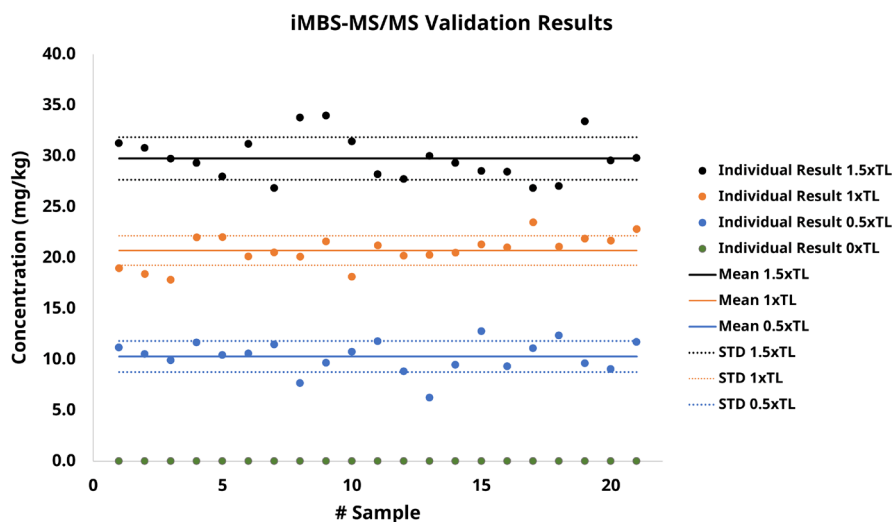


**Figure 4.11.** Data analysis of results from 21 blank mussel samples, and spiked versions thereof in iMBS-MS/MS.

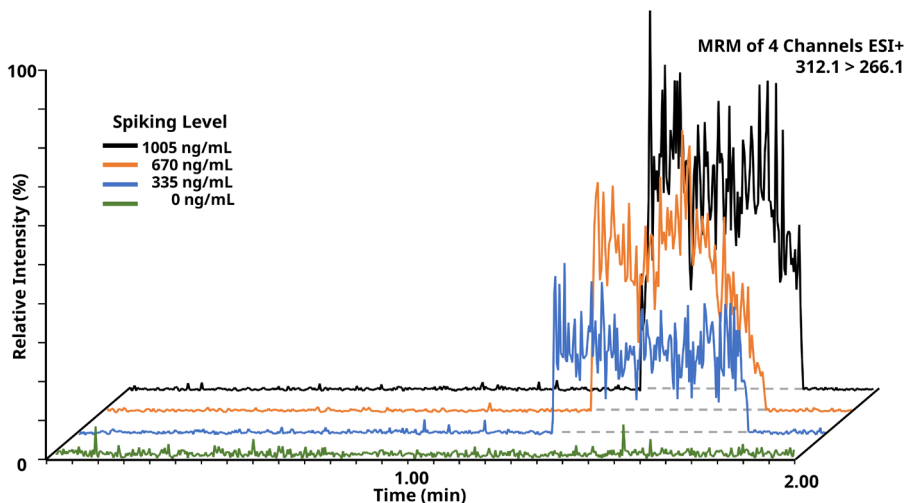


**Figure 4.12.** iMBS-MS/MS chromatograms of the  $m/z$  312.1 > 266.1 transition from paramagnetic microspheres/ DA spiked sample at different target level.

Moreover, the selected MRM transitions monitored and the respective ion ratios (Table 4.1) enable the confirmation of the identity of DA, without the need of an internal standard (IS) (Figure 4.13). The mean ion ratio for the MRM for DA was  $0.34 \pm 0.14$  ( $m/z$  248.1/266.1) for all the 21 spiked samples analyzed. This ratio is identical to the ion ratio measured for DA in standard methanol/formic acid/mussel solutions. As a result, the ion ratio tolerance limit of the spiked mussel samples analyzed complies with the regulatory requirement of  $\pm 40\%$  relative deviation allowed by the EU 2021/808 legislation(15). Thus, the method is demonstrated to be sufficiently specific/sensitive. The intra-day repeatability results were 5.4, 15.9, and 13.0% at  $0.5 \times TL$ , 7.7, 5.0, and 3.9% at TL, and 5.3, 7.6, and 7.0% at the  $1.5 \times TL$  level, for day one, two, and three, respectively. The inter-day repeatability results were 13.7, 7.0, and 7.1% for the  $0.5 \times$ ,  $1 \times$ , and  $1.5 \times TL$ , respectively. Furthermore, the within-laboratory reproducibility results were 13.9, 6.1, and 7.3% at  $0.5 \times$ ,  $1 \times$ , and  $1.5 \times TL$ , respectively. All RSD% values for the validation parameters assessed were lower than 16% and within the acceptance range (15), underlining the quantitative performance of the developed method in this range and a favorable comparison versus the LFIA screening assay. Moreover, the trueness values were calculated at 103, 104, and 99% for the  $0.5 \times$ ,  $1 \times$ , and  $1.5 \times TL$ , respectively, within the acceptance range of 80% to 120% (15). Finally, the CC $\alpha$  was 23.3 mg/kg, demonstrating that all samples of the  $1.5 \times TL$  and above were non-compliant. Therefore, the developed iMBS-MS/MS method has been successfully validated as a confirmatory method over a limited range around the relevant ML level.

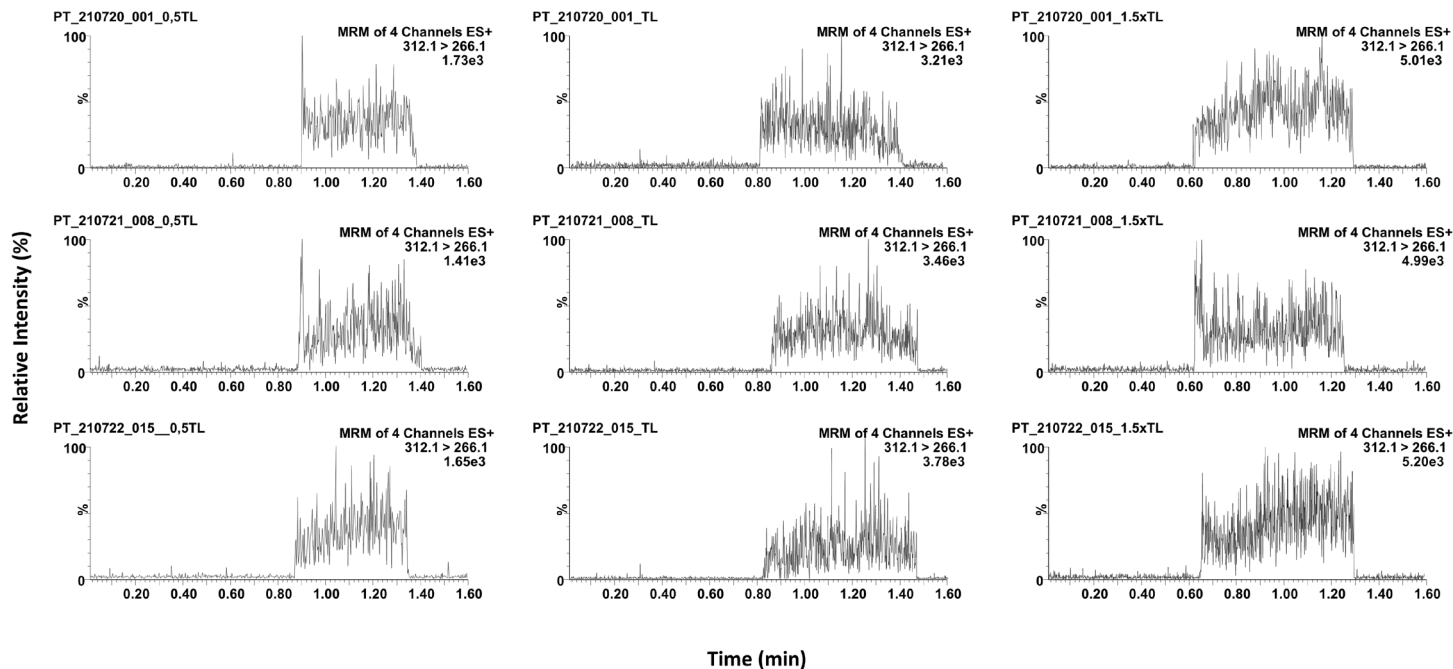


**Figure 4.13.** iMBS-MS/MS chronograms of the  $m/z$  312.1 > 266.1 transition from paramagnetic microspheres sampling of DA spiked mussel extracts at three different target level 335 ng/mL (0.5xTL), 670 ng/mL (1.0xTL), and 1005 ng/mL (1.5 xTL) (from left to right), and three different validation days (from top to bottom).



**Table 4.1.** Validation results from iMBS-MS/MS confirmatory analysis and LFIA screening of 21 blank and spiked mussel sample extracts at three different target levels and performed on three different days.

Day	Sample	0×TL		0.5×TL			1×TL			1.5×TL		
		iMBS-MS/MS Re-sponse	LFIA screening result (T/C)	iMBS-MS/MS		LFIA screening result (T/C)	iMBS-MS/MS		LFIA screening result (T/C)	iMBS-MS/MS		LFIA screening result (T/C)
				Ion ratio	Calculated Concentration (mg/kg)		Ion ratio	Calculated Concentration (mg/kg)		Ion ratio	Calculated Concentration (mg/kg)	
1	1	0	1.46	0.30	11.2	0.50	0.39	19.0	0.32	0.34	31.2	0.28
	2	0	1.07	0.37	10.5	0.57	0.37	18.4	0.33	0.39	30.8	0.24
	3	0	1.51	0.37	9.9	0.67	0.38	17.8	0.22	0.33	29.7	0.17
	4	0	1.18	0.37	11.7	0.49	0.33	22.0	0.23	0.29	29.3	0.16
	5	0	1.04	0.36	10.4	0.45	0.34	22.0	0.28	0.39	28.0	0.22
	6	0	1.07	0.34	10.6	0.45	0.38	20.1	0.25	0.34	31.2	0.10
	7	0	1.04	0.31	11.5	0.57	0.39	20.5	0.33	0.38	26.8	0.25
2	8	0	1.22	0.38	7.7	0.52	0.39	20.1	0.27	0.36	33.8	0.13
	9	0	1.04	0.36	9.7	0.45	0.39	21.6	0.28	0.35	34.0	0.22
	10	0	1.54	0.34	10.7	0.53	0.39	18.1	0.26	0.33	31.4	0.30
	11	0	1.33	0.29	11.8	0.50	0.33	21.2	0.32	0.35	28.2	0.33
	12	0	1.03	0.30	8.8	0.65	0.29	20.2	0.32	0.39	27.7	0.30
	13	0	1.31	0.30	7.2	0.57	0.36	20.3	0.34	0.39	30.0	0.23
	14	0	1.25	0.30	9.5	0.52	0.33	20.5	0.29	0.39	29.3	0.19

(Continued on next page)

**Table 4.1** *Continued.*

Day	Sample	0×TL		0.5×TL			1×TL			1.5×TL		
		iMBS-MS/MS Re- sponse	LFIA screen- ing re- sult (T/C)	iMBS-MS/MS		LFIA screen- ing re- sult (T/C)	iMBS-MS/MS		LFIA screen- ing re- sult (T/C)	iMBS-MS/MS		LFIA screen- ing re- sult (T/C)
				Ion ratio	Calcu- lated Con- centra- tion (mg/kg)		Ion ratio	Calcu- lated Con- centra- tion (mg/kg)		Ion ra- tio	Calcu- lated Con- centra- tion (mg/kg)	
3	15	0	1.58	0.38	12.8	0.67	0.33	21.3	0.36	0.38	28.5	0.24
	16	0	1.15	0.37	9.3	0.61	0.33	21.0	0.30	0.39	28.5	0.15
	17	0	1.11	0.36	11.1	0.48	0.35	23.5	0.29	0.35	26.9	0.18
	18	0	1.38	0.38	12.3	0.52	0.38	21.1	0.25	0.35	27.0	0.19
	19	0	1.24	0.33	9.6	0.62	0.39	21.9	0.37	0.36	33.4	0.23
	20	0	1.67	0.30	9.0	0.74	0.37	21.7	0.23	0.37	29.5	0.22
	21	0	1.02	0.38	11.7	0.55	0.31	22.8	0.25	0.36	29.8	0.13
	15	0	1.58	0.38	12.8	0.67	0.33	21.3	0.36	0.38	28.5	0.24
Conditions: The LFIA screening result was read using a smartphone camera equipped with a custom-made 3D-printed box to assure equal conditions of the reading of the LFIA. The LFIA screening result is corrected versus the blank and then the intensity of the test line is divided by the control line. iMBS-MS/MS, incubation with 10 μL of immuno-enriched paramagnetic microspheres, dissociation on the blade with 4 μL of methanol/formic acid 2.5% v/v. The ion ratio is the ratio of the absolute area of the DA MRM product ion at m/z 248.1 to the area of the ion at m/z 266.1												

### 4.3.3 Applicability of the method

The applicability of the method was further demonstrated by the analysis of KA spiked and DA incurred mussel samples. KA is a structural analog of DA but has lower toxicity, and hence the EU does not regulate it. However, KA might interfere with the immuno-capturing in LFIA and iMBS due to its structural similarity. Indeed, using blank mussel extract spiked with KA at 1005 ng/mL (corresponding to the 1.5× TL DA level), the LFIA screening test for DA, yielded a false-positive result because of the inability of the used mAb to differentiate between structural analogs. However, when using iMBS-MS/MS, it becomes clear that the positive LFIA test result is caused by the presence of KA only since the characteristic ion transitions and respective area ion ratio of 0.34 belonging to DA were absent in the MS/MS data. In contrast, the characteristic product ions belonging to KA were detected with their corresponding area ion ratio of 0.21 ( $m/z$  122.1/168.1) (Figure 4.14 and Table 4.2).

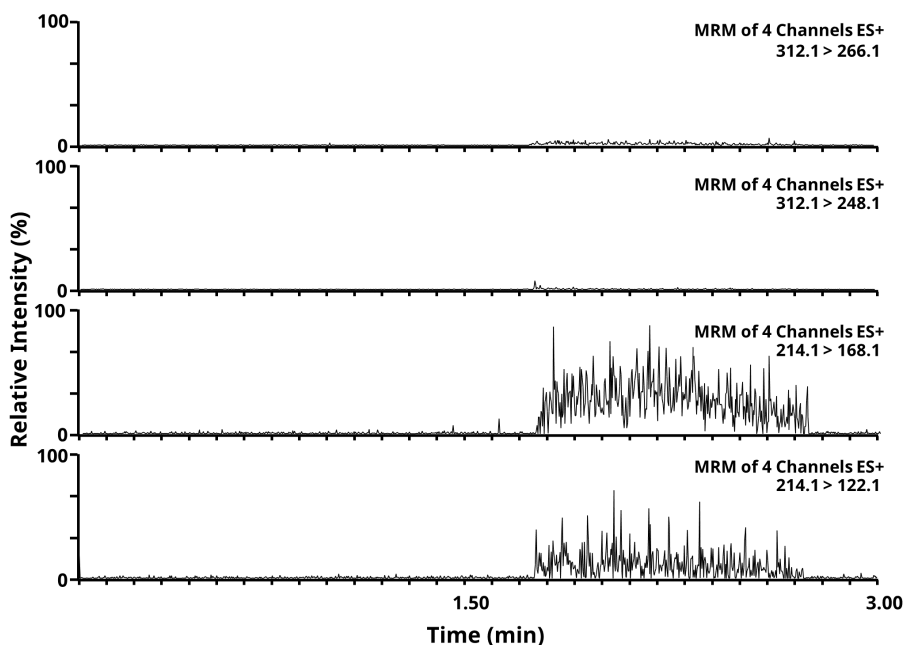


**Figure 4.14** Example of iMBS-MS/MS chromatograms of KA spiked mussel extract. For conditions, see text.

Finally, following the workflow described in Figure 4.2, three DA-incurred mussel samples originating from the Netherlands were analyzed by the screening LFIAs and the newly developed iMBS-MS/MS method. The results were similar to those of the accredited LC-MS/MS and LC-UV methods for DA. The LFIAs, showed positive

results and high contamination levels beyond  $1 \times \text{TL}$  according to semi-quantitative smartphone analysis. Also, the iMBS-MS/MS results were in accordance with previous results from the independent reference method. For incurred mussel samples #1 and #2, the estimated concentration was close to the analysis result of the reference method. For the incurred mussel #3, probably because of saturation of the immobilized mAbs on the paramagnetic microspheres, the estimated concentration according to iMBS-MS/MS was lower but in accordance with the limited dynamic range of an immuno-capturing method. In all cases, however, the iMBS-MS/MS results correctly characterized the analyzed samples as non-compliant and containing DA, confirmed by the respective ion ratio for DA ( $m/z$  248.1/266.1) within the  $0.34 \pm 40\%$  tolerance limit set by the legislation(15), and not containing the harmless KA (Table 4.2).

**Table 4.2.** Results from iMBS-MS/MS analysis and LFIA screening of KA spiked mussel sample and DA incurred mussel samples.

Sample	iMBS-MS/MS				LFIA screen- ing re- sult (T/C)	DA concentra- tion based on reference LC- MS/MS method (mg/kg)
	DA		KA			
	ion	calculated	ion ra-	calculated		
	ratio	concentra- tion (mg/kg)	tio	concentra- tion (mg/kg)		
KA spiked mussel extract	-	-	0.21	27.5*	0.21	-
Incurred mussel #1	0.37	23.5	-	-	0.23	20.0
Incurred mussel #2	0.36	31.5	-	-	0.17	39.0
Incurred mussel #3	0.39	35.6	-	-	0.09	46.6

*The screening result is corrected versus the blank and then the intensity of the test line is divided by the control line (Supporting Information). For exact conditions, see text.*

*\* The calculation of the KA concentration was done with the DA's calibration curve, under the estimation that the area intensity of DA's transition  $m/z$  312.1>266.1 is approximately 5x more intense than that of the KA's  $m/z$  214.1 > 168.1.*

## 4.4 Conclusion

AIMS methods are rapid tools for detecting numerous substances, as many applications demonstrate. However, their inherent lack of chromatographic separation leads to their exclusion as confirmatory methods in EU food safety protocols, as they do not meet the standards laid down in legislation. In this work, we have demonstrated the development of an iMBS-MS/MS confirmatory analysis method and its validation according to the recently revised EU regulation. Moreover, we showed that iMBS-MS/MS rapidly identifies false-positive LFIA screening results caused by harmless unregulated structure analogs. The iMBS exploits the use of mAbs for selective isolation of the analyte of interest, adding substantially to the overall specificity of the rapid direct MS/MS approach, thereby competing with time-consuming regulatory LC-MS/MS methods. An additional IP should be granted in future revisions of the

legislation because of the "immuno-chromatographic" nature of the iMBS-MS/MS approach.

The developed method is generic, reproducible, and quantitative without employing an IS, and could be applied to any MS-amenable analyte provided that a pair of antigen/antibodies is available. Moreover, different sets of immuno-enriched paramagnetic microspheres with antibodies aiming at different analytes, could lead to multiplex iMBS-MS/MS confirmatory analysis opportunities, complementary to multiplex planar array immunoassays used for parallel screening of routine samples.

## 4.5 References

1. S. J. Hird, B. P. Y. Lau, R. Schuhmacher, R. Krska, *TrAC*, **59**, 59–72 (2014).
2. B. Greer, O. Chevallier, B. Quinn, L. M. Botana, C. T. Elliott, *TrAC*, **141** (2021).
3. M. Silano, V. Silano, *Crit. Rev. Food Sci. Nutr.* **57**, 2162–2217 (2017).
4. A. S. Tsagkaris, J.L.D. Nelis, G.M.S. Ross, S. Jafari, J. Guercetti, K. Kopper, Y. Zhao, K. Rafferty, J.P. Salvador, D. Migliorelli, G.I. Salentijn, K. Campbell, M.P. Marco, C.T. Elliot, M.W.F. Nielen, J. Pulkrabova, J. Hajslova, *TrAC*, **121**, 115688 (2019).
5. M. Beneito-Cambra, B. Gilbert-López, D. Moreno-González, M. Bouza, J. Franzke, J.F. García-Reyes, A. Molina-Díaz, *Anal. Methods*, **12**, 4831–4852 (2020).
6. P.-K. So, B. Hu, Z.-P. Yao, *Mass Spectrom.* **3**, 1–28 (2014).
7. R. B. Cody, J. A. Laramée, H. D. Durst, *Anal. Chem.* **77**, 2297–2302 (2005).
8. Z. Takáts, J. M. Wiseman, B. Gologan, R. Graham Cooks, *Science*, **306**, 471–473 (2004).
9. G. A. Gómez-Ríos, J. Pawliszyn, *Angew. Chemie*, **53**, 14503–14507 (2014).
10. H. Wang, J. Liu, R. Graham Cooks, Z. Ouyang, *Angew. Chemie*, **49**, 877–880 (2010).
11. B. Hu, P.K. So, Y. Yang, J. Deng, Y.C. Choi, T. Luan, Z.P. Yao, *Anal. Chem.* **90**, 1759–1766 (2018).
12. M. H. Blokland, A. Gerssen, P. W. Zoontjes, J. Pawliszyn, M. W. F. Nielen, *Food Anal. Methods*, **13**, 706–717 (2019).
13. J. Jager, A. Gerssen, J. Pawliszyn, S.S. Sterk, M.W.F. Nielen, M.H. Blokland, *J. Am. Soc. Mass Spectrom.* **31**, 2243–2249 (2020).
14. D. A. Rickert, V. Singh, M. Thirukumaran, J.J. Grandy, J.R. Belinato, M. Lashgari, J. Pawliszyn, *Environ. Sci. Technol.* **54**, 15789–15799 (2020).
15. European Commission, *Off. J. Eur. Union*, **180**, 84–109 (2021).
16. S. Jafari, J. Guercetti, A. Geballa-Koukoulou, A.S. Tsagkaris, J.L.D. Nelis, M.-P. Marco, J.-P. Salvador, A. Gerssen, J. Hajslova, C. Elliott, K. Campbell, D. Migliorelli, L. Burr, S. Generelli, M.W.F. Nielen, S.J. Sturla, *Foods*, **10**, 1399 (2021).
17. B. Pérez-López, M. Mir, *Talanta*, **225**, 121898 (2021).
18. X. Xiao, S. Hu, X. Lai, J. Peng, W. Lai, *Trends Food Sci. Technol.* **111**, 68–88 (2021).
19. M. Fraga, N. Vilariño, M.C. Louzao, P. Rodríguez, K. Campbell, C.T. Elliott, L.M. Botana, *Anal. Chem.* **85**, 7794–7802 (2013).
20. H. Graham, D. J. Chandler, S. A. Dunbar, *Methods*, **158**, 2–11 (2019).
21. J. Qu, H. Xie, S. Zhang, P. Luo, P. Guo, X. Chen, Y. Ke, J. Zhuang, F. Zhou, W. Jiang, *Food Anal. Methods*, **12**, 877–886 (2019).
22. Y. Zhang, X. Li, H. Nie, L. Yang, Z. Li, Y. Bai, L. Niu, D. Song, H. Liu, *Anal. Chem.* **87**, 6505–6509 (2015).
23. S. Joshi, H. Zuilhof, T. A. Van Beek, M. W. F. Nielen, *Anal. Chem.* **89**, 1427–1432 (2017).
24. Y. Zhao, M. Tang, F. Liu, H. Li, H. Wang, D. Xu, *Anal. Chem.* **91**, 13418–13426 (2019).
25. A. Geballa-Koukoulou, A. Gerssen, M. W. F. Nielen, *Anal. Bioanal. Chem.* **412**, 7547–7558 (2020).
26. A. Geballa-Koukoulou, A. Gerssen, M. W. F. Nielen, *Sensors*, **21**, 1–17 (2021).
27. K. A. Lefebvre, A. Robertson, *Toxicon*, **56**, 218–230 (2010).
28. D. Schrenk *et al.*, *European Food Safety Authority Journal*, **19** (2021).
29. European Commission, *Off. J. Eur. Union*, **139**, 1–14 (2004).
30. B. J. Yakes, J. Buijs, C. T. Elliott, K. Campbell, *Talanta*, **156–157**, 55–63 (2016).
31. S. A. Dunbar, M. R. Hoffmeyer, *The Immunoassay Handbook*, 157–174 (2013).
32. W. Jawaid, J. Meneely, K. Campbell, M. Hooper, K. Melville, S. Holmes, J. Rice, C. T. Elliott, *Talanta*, **116**, 663–669 (2013).
33. G. M. S. Ross, D. Filippini, M. W. F. Nielen, G. I. J. Salentijn, *Anal. Chem.* **92**, 15587–15595 (2020).
34. V. Pagkali, P.S. Petrou, E. Makarona, J. Peters, W. Haasnoot, G. Jobst, I. Moser, K. Gajos, A.

- Budkowski, A. Economou, K. Misiakos, I. Raptis, S.E. Kakabakos, *J. Hazard. Mater.* **359**, 445–453 (2018).
35. A. Furey, M. Lehané, M. Gillman, P. Fernandez-Puente, K. J. James, *J. Chromatogr. A.* **938**, 167–174 (2001).
36. Z. Wang, K. L. King, J. S. Ramsdell, G. J. Doucette, *J. Chromatogr. A.* **1163**, 169–176 (2007).
37. O. Pardo, V. Yusà, N. León, A. Pastor, *J. Chromatogr. A.* **1154**, 287–294 (2007).
38. Z. Wang *et al.*, *Anal. Chim. Acta.* **715**, 71–79 (2012).
39. B. J. A. Berendsen, L. A. M. Stolker, M. W. F. Nielen, *J. Am. Soc. Mass Spectrom.* **24**, 154–163 (2013).







# **Immunoaffinity Plastic Blade Spray Mass Spectrometry for Rapid Confirmatory Analysis of Food Contaminants**

*Adapted from:*

*A. Geballa-Koukoulou, A. Gerssen, M.H. Blokland, M.W.F. Nielen, Immunoaffinity Plastic Blade Spray Mass Spectrometry for Rapid Confirmatory Analysis of Food Contaminants, JASMS. 33 (2022) 2038-2045. <https://doi.org/10.1021/jasms.2c00149>.*

## **Abstract**

*The lack of chromatographic separation in ambient and direct mass spectrometry (MS) ionization techniques jeopardizes the overall selectivity of the developed methods. Incorporating a biorecognition element at the ionization source could compensate for that inherent lack of selectivity. Thus, a simplified immunoaffinity – direct MS technique was developed, immunoaffinity blade spray (iBS), featuring a conductive polystyrene blade material. In iBS, the generic coating used in conventional coated blade spray (CBS) is replaced with a layer of highly specific monoclonal antibodies (mAbs), while the stainless steel is replaced with conductive polystyrene to allow for simple ELISA plate-like hydrophobic immobilization of mAbs. Due to its high relevance for climate change-induced food safety issues, the mycotoxin deoxynivalenol (DON) was chosen as a model substance. Following a rapid extraction from wheat flour, DON is immuno-captured, and the blade is positioned in front of the MS for direct iBS-MS/MS analysis. The method's applicability was demonstrated by analyzing spiked and incurred wheat flour samples omitting the need for time-consuming chromatographic separation. Apart from DON, cross-reacting DON conjugates could be successfully analyzed as well. The direct iBS-MS/MS method is generic and adaptable to detecting any analyte in sample extracts, provided that specific mAbs are available.*

## 5.1 Introduction

Coated blade spray (CBS) has emerged as a straightforward ambient ionization mass spectrometry (AIMS) method, utilizing a sharp-tipped stainless steel sheet that is coated with a biocompatible solid phase microextraction (SPME)-like sorbent (1). CBS combines sample clean-up and ionization directly from the same surface; the blade acts as a solid-substrate electrospray ionization (ESI) source and the coating as an extraction/preconcentration agent. Ionization in CBS occurs by applying a desorption/spray solution and a high voltage (2). CBS allows high throughput analysis and reduced matrix effects in complex sample mixtures analyses while consuming minimal sample and solvent volumes, thus contributing to a greener analytical chemistry (3). In only six years since its development in 2014, various applications of CBS in different fields have been reported in the literature (4–6). A typical CBS protocol consists of preconditioning the coated surface, extracting the analytes of interest from the sample, washing to minimize interferences, and desorption/ionization, all from the same blade (2). This simplified protocol leads to an analysis time that can be as short as 10 s per sample (7), which in comparison to the classic approach of liquid or gas chromatography to separate the analytes in time (8, 9), is a great improvement for a prompt analytical response. Nonetheless, when it comes to the unequivocal identification of substances, apart from the selective multiple reaction monitoring (MRM) transitions from a tandem MS method, also the retention time acts as an identification criterion (10, 11), especially in terms of food safety regulation (12). Still, the retention time is lacking, by definition, in all AIMS techniques (13).

To counterbalance the lack of chromatographic separation, antibodies have been employed for specific extraction/separation of the targeted analyte, followed by ambient or direct ionization and fast MS identification (14, 15). The latest development combines CBS with antibody enrichment in the developed iMBS (**Chapter 4**), in which the coating of the blades has been replaced by mAbs-enriched paramagnetic microspheres, held on the blade by a magnet (16). This method has demonstrated the added specificity and selectivity in the direct MS/MS analysis of analytes in complex sample matrices. However, the paramagnetic microspheres and the magnet increase the cost and complexity of the analysis: iMBS requires a rather extensive protocol for microsphere and blade preparation based on a covalent immobilization protocol entailing an EDC/NHS amine coupling procedure (17). Generally, in immunoassays, the choice of the immobilization strategy is greatly affected by the physicochemical properties of the surface and the antibodies, and physical immobilization can be a simple alternative to circumvent time-consuming covalent coupling reactions. Physical immobilization includes direct adsorption on a surface, and despite the weak attachment and random orientation of antibodies, it is more straightforward compared to the other immobilization methods (18). Physical adsorption on solid polystyrene (i.e., plastic) substrate by hydrophobic interactions has been employed traditionally in enzyme-linked immunosorbent assay (ELISA) (19). In such a case, the biorecognition element is diluted in a coating buffer and then deposited on the polystyrene substrate

while incubating to enable immobilization, without any additional reagents needed (20).

In the current study, we develop an immunoaffinity conductive polystyrene blade spray (iBS) approach. iBS utilizes conductive polystyrene sheets shaped at the dimensions of the stainless steel blades used in CBS. Previous research on CBS applications that employed different substrates, i.e., magnetic blades, required an adhesive copper tape for electric conductivity (21). However, the conductive polystyrene allows for simplified mAbs immobilization by adsorption while enabling ionization. The mAbs allow for the selective mining of a targeted analyte, adding selectivity and specificity to the overall AIMS method. The sample extract is incubated with the immunoaffinity blades, followed by washing to remove non-specifically bound analytes. The final step is the direct spray ionization by applying the optimized dissociation/spraying solution and the high voltage.

The method was developed to detect the mycotoxin deoxynivalenol (DON) as a proof of principle. DON is found in *Fusarium* sp. contaminated cereals, and DON's presence in food commodities risks human health (22). For this reason, DON is strictly monitored in the EU, with a maximum level (ML) of 1750  $\mu\text{g}/\text{kg}$  in unprocessed durum wheat (23). Moreover, the societal relevance of DON is eminent because of the climate change-related increase in worldwide mycotoxin production, which issues the increased need for monitoring in the near future (24, 25). DON is thermally stable and water-soluble (22), but its presence in its conjugated/masked forms due to plant metabolism makes its analytical detection elaborate. The developed iBS method can precisely and reproducibly monitor DON and its conjugated form of 3-Acetyldeoxynivalenol (3-AcDON). iBS is the first approach for a simplified online immuno-capture and successive blade spray MS detection, all from the same solid surface, without intricate chemical antibody immobilization.

## 5.2 Material and Methods

### 5.2.1 Chemicals and reagents

Solvents purchased included acetonitrile, methanol, and water, all of UHPLC-MS purity grade, and ammonia solution (25% v/v), formic acid (98% v/v), from Merck (Darmstadt, Germany), and Milli-Q water of 18.3 M $\Omega$ /cm conductivity was produced by a water purification system from Merck (Amsterdam, The Netherlands). A stock solution of 10 $\times$  phosphate buffered saline (PBS) with salts from Merck (Darmstadt, Germany) was prepared in Milli-Q water. Dilution of the stock solution to 1 $\times$  PBS in Milli-Q water and 0.05% v/v Tween-20 (Sigma-Aldrich, Zwijndrecht, The Netherlands) or 1% w/v bovine serum albumin (BSA) (Sigma-Aldrich, Zwijndrecht, The Netherlands), yielded the assay buffers PBST and PBS-BSA, respectively.

Standard stock solutions of 100  $\mu\text{g}/\text{mL}$  DON and 3-AcDON and 25  $\mu\text{g}/\text{mL}$   $^{13}\text{C}$ -DON internal standard (IS), and DON blank wheat flour certified reference material (CRM) (Joint Research Centre) were all purchased from LGC standards (Wesel, Germany). Fluorescent labeled fluorescein-DON was purchased from Aokin (Berlin,

Germany). A naturally incurred wheat flour (2900  $\mu\text{g}/\text{kg}$ ) sample was purchased from Trilog Analytical Laboratories (Arnhem, The Netherlands).

Conductive polystyrene blades were prepared by laser-cutting conductive polystyrene sheets of 1 mm thickness (Merck, Darmstadt, Germany) at the detailed dimensions of *Figure 5.1*. For the immuno-capturing, monoclonal antibodies for DON (mouse, clone 2) (Aokin AG, Berlin, Germany) were used.

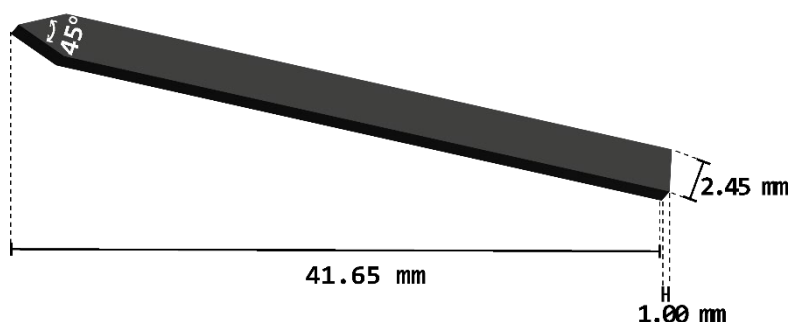


**Figure 5.1** Detailed illustration and dimensions of the conductive polystyrene blade.

## 5.2.2 Mass spectrometry

The iBS-MS/MS analysis was performed with a Micromass Quattro Ultima Pt QqQ-MS system (Waters Corporation, Milford, MA, USA) equipped with a blade spray setup consisting of a modified x-y-z stage and high-voltage plug from a Waters nanoESI ion source. Chronograms were acquired in positive ionization MRM mode, and two transitions were monitored for each analyte; for DON,  $m/z$  297.1 > 231.1 and  $m/z$  297.1 > 249.1 at 10 and 8 eV collision energies respectively, for 3-AcDON,  $m/z$  339.10 > 203.10 and  $m/z$  339.10 > 231.10 at 10 and 8 eV collision energy, respectively, and  $^{13}\text{C}$ -DON 312.10 > 263.10, at 8 eV collision energy, respectively. From the two fragments ions, ion ratios were calculated and used for unequivocal identification of each substance according to the EU criteria for confirmatory analytical methods (12). Operating conditions included 4.2 kV spray voltage, 50 V cone voltage, 120 °C cone temperature, and 0.16 mL/min argon collision gas flow. MassLynx software (Waters) was used for data acquisition and processing. A Voltcraft 7910 multimeter was used for conductivity measurement, and two microscopes, namely an Olympus BX51 fluorescence microscope and a Dino-lite AM4115T-GFBW digital microscope, were used for fluorescence imaging.

## 5.2.3 iBS preparation and method

Using Zeba™ Spin desalting columns (Thermo Fisher Scientific, San Jose, CA, USA), the storage buffer of the crude mAbs from Aokin is removed, and the mAbs are reconstituted in UHPLC-MS purity grade water. The mAbs are then diluted with

UHPLC-MS purity grade water to a 0.3 mg/mL final concentration. Finally, 7.5  $\mu$ L are simply pipetted on top of the conductive polystyrene blade the nearest possible to the sharp tip, and the prepared immunoaffinity blades are left to air-dry and are stored in the fridge at 4 °C until further use.

The simplified extraction method described previously for DON (**Chapters 2 and 3**) was applied without further optimization (26). Briefly, 1 g of grounded wheat sample is extracted using 5 mL Milli-Q water. Followed by manual agitation and centrifugation to fasten sedimentation, the supernatant is collected and used in case of incurred wheat or, in case of blank wheat, spiked at 350 ng/mL (corresponding to the DON concentration in the extract following extraction of contaminated commodities at the ML of 1750  $\mu$ g/kg). For iBS analysis, 200  $\mu$ L of the sample extract is diluted 1:1 Milli-Q water, placed in an Eppendorf tube with a single immunoaffinity blade, and incubated for 2 min. Next, the immunoaffinity blade is washed with 500  $\mu$ L of Milli-Q water for 30 s. Both immuno-extraction and washing are performed in an Eppendorf ThermoMixer C apparatus (Eppendorf SE, Hamburg, Germany) at 1200 rpm. For the iBS-MS/MS detection, the immunoaffinity blade is positioned at approx. 6 mm distance from the ion source cone. Then, the optimized dissociation/spray solution is pipetted on top of the mAbs of the blade twice. Firstly, 4  $\mu$ L methanol/ammonia solution (2% v/v) are pipetted to disrupt the binding between DON and mAbs. Secondly, after evaporation of the first aliquot, an additional 4  $\mu$ L of methanol/ammonia solution (2% v/v) spiked with the internal standard (IS)  $^{13}$ C-DON 10 ng/mL are pipetted, and the optimum spray voltage is applied to generate an ESI-like spray (*Figure 5.2*).

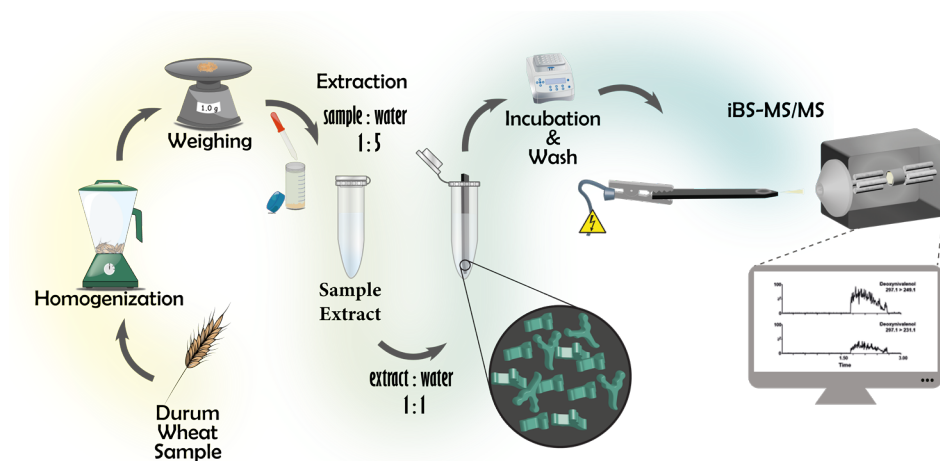


**Figure 5.2.** General concept of the iBS-MS/MS approach.

## 5.3 Results

### 5.3.1 Preparation and characterization of iBS

To produce the immunoaffinity blades, a large conductive polystyrene sheet was laser-cut in the desired size and shape (*Figure 5.1*). As discussed in previous CBS and iMBS studies, the angle of the blade is crucial for the ionization of substances; the tip of the blade is where the applied voltage is converged, leading to an ESI-like spray formation (1). Thus, the conductive polystyrene blades' selected shape is characterized by a pointed tip with an adequate surface for handling, mAbs immobilization, solvent deposition, and electrospray formation. After shaping the conductive polystyrene blades, mAbs for DON must be immobilized on the tip of the blade. The mAbs are stored in a buffer solution containing surfactants and salts that hinder ionization in MS. The Buffers residues in the immunoaffinity blade could pose a risk for the iBS-MS/MS method. So, the mAbs, prior to the immobilization, underwent buffer exchange using size-exclusion chromatography resin in desalting Zeba Spin columns to remove the excess buffer and reconstitute them in Milli-Q water. Then the mAbs were diluted to the desired concentration, pipetted on the conductive polystyrene tip of the blade, and immobilized on the surface after drying, simply by direct adsorption.

Unsurprisingly, the conductive polystyrene blades are characterized by an electric conductance 188000 times lower than the standard stainless steel blades. Nevertheless, the main voltage drop between the voltage application point and the inlet of the MS still occurs in the ambient air gap between the blade tip and the cone. The lower conductance is also apparent when comparing a standard solution of 10 ng/mL DON, 3-AcDON, and IS in methanol/ammonia solution (2% v/v) on the different blade materials. At 3.7 kV spray voltage, while the response factor (analyte/internal standard area ratio - A/IS area ratio) is identical between conductive polystyrene and stainless steel blades, the absolute area values in the MS/MS chronograms drop by 94%. Therefore, the high voltage setting had to be optimized for conductive polystyrene and was found to be 4.2 kV. It is worth mentioning that even with the optimum spray voltage for DON ionization on conductive polystyrene blades, the conductive polystyrene blades still yielded 65% lower ionization than the stainless steel blades at 3.7 kV (*Figure 5.3*). Most likely, this difference must be attributed to the different geometries of the blades; The tip angles are similar, but the thickness of the metal and polystyrene sheets differ by a factor of ten, so the polystyrene blade required a further manual adjustment to 0.1 mm with a scalpel.

Based on the overall sensitivity of the iBS-MS/MS method, the mAbs maximum theoretical loading capacity, and the regulatory limits for DON monitoring, a limited volume of 7.5  $\mu$ L 0.3 mg/mL mAbs solution per blade was fit-for-purpose; similar to the mAbs consumption in the identification lateral flow immunoassay (ID-LFIA) direct MS alternative approach of **Chapters 2 and 3** (27).

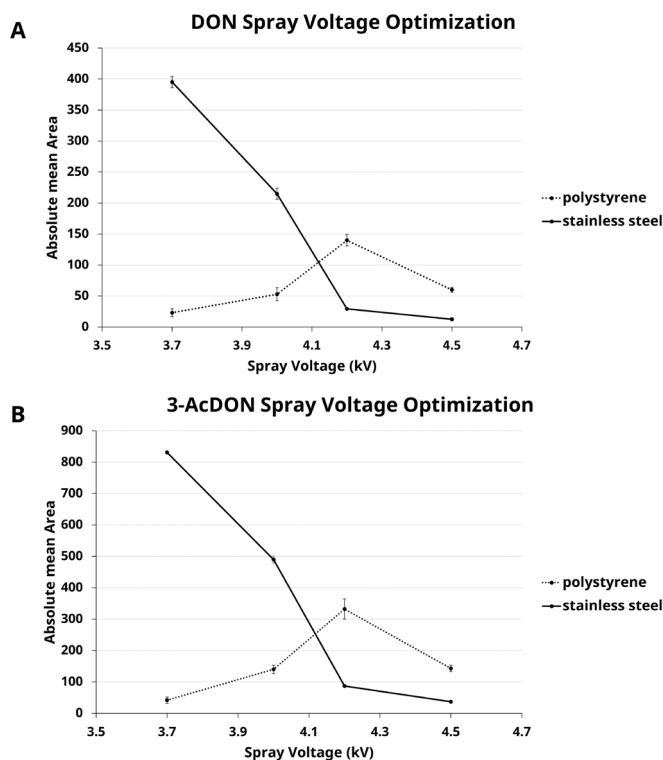


**Figure 5.3.** Comparison of conductive polystyrene and stainless steel blades for (A) DON and (B) 3-AcDON Conditions: 10 ng/mL concentration, 5  $\mu$ L sample application on the blade, MRM monitoring of fragments measuring the area. The comparison is done on different spray voltage intensities and based on the absolute mean values of the area ( $n=3$ ).

Fluorescence imaging was used to verify the coating at the immuno-enriched area on the conductive polystyrene blade. 5  $\mu$ L of fluorescein-DON were firstly deposited on the immunoaffinity blade and washed with Milli-Q water to remove the non-bound analyte, followed by the excitation and fluorescent imaging. As expected, only the immuno-enriched area of the blade was fluorescent. Moreover, the fluorescence intensity was increased at the edge of the immuno-enriched area suggesting a higher concentration of the mAbs; a typical characteristic of the so-called coffee-ring effect after evaporation of liquid from the center to the edge (28) (Figure 5.4). Using 200 $\times$  magnification, the surface of the conductive blade was observed to be not homogeneously coated but instead consisting of mAbs aggregations, resulting from the simplified but uncontrolled physical immobilization of antibodies. Finally, the immunoaffinity blades were cleaned by sonicating in methanol for 15 min and wiping the surface to remove the mAbs. The cleaning resulted in bare conductive polystyrene blades that could be re-used for immuno-enrichment in other iBS experiments. The



cleaning performance was demonstrated using the same process of fluorescein-DON addition, water washing, and fluorescence imaging. No fluorescence is observed on the cleaned blade, demonstrating the complete removal of mAbs and the effectiveness of the washing procedure for removing unbound analytes (*Figure 5.4*).

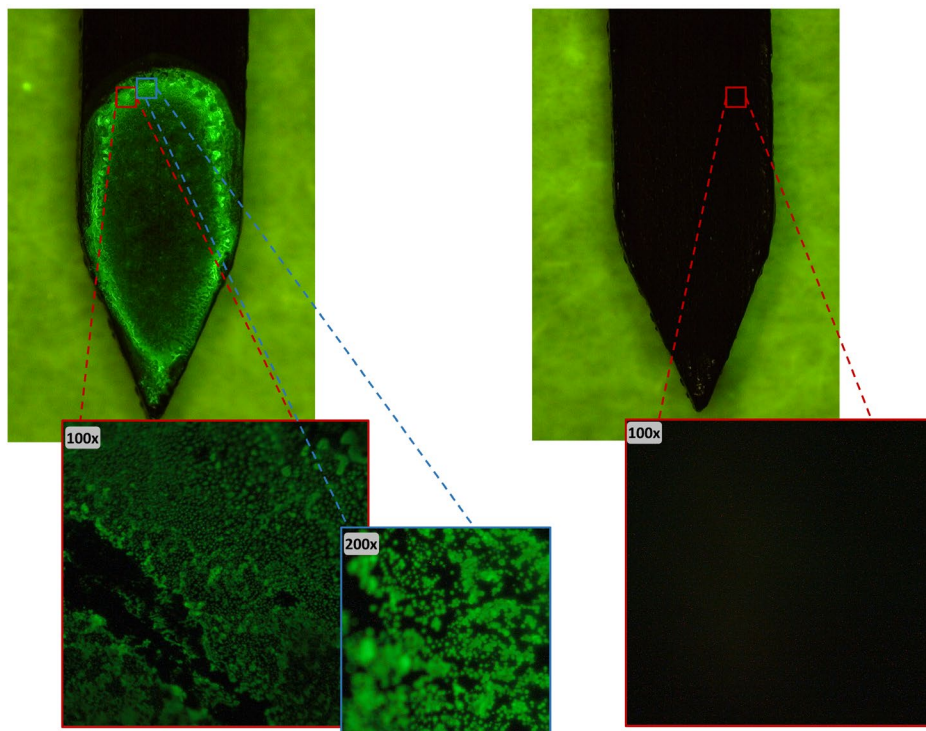


**Figure 5.4.** Fluorescence imaging with an excitation wavelength of 460-490 nm and an emission of 510-550 nm (before and after cleaning) of the immunoaffinity blade after adding fluorescein-DON, followed by washing with water. In the inserts, 100x and 200x magnifications are depicted.

### 5.3.2 iBS-MS/MS method development and application

The MS method optimization was performed at a distance of approx. 6 mm between the tip of the blade and the inlet of the MS; larger distances caused signal loss, while at a reduced distance, arcing occurred. The optimum spray/desorption solution was selected by applying on the conductive polystyrene blades, 5  $\mu$ L 200 ng/mL DON in various solutions, and monitoring the area in the chronograms for the protonated and deprotonated ions in full scan mode ( $m/z$  250-500) under different spray voltage settings in positive and negative ion mode. The solvents were selected to include a high percentage of organic solvent and alkaline or acidic modifier. The organic solvent reassures high ionization efficiency in the blade spray part, and the modifier supports the dissociation of the analyte from the antibodies in the final iBS-MS/MS

method. The optimized spray solution was similar to previously published results (27), i.e., methanol/ammonia solution (2% v/v) (Figure 5.5). However, regardless of the solvent used, negative ionization mode was not as efficient as positive ionization, contrary to previously published results (27); clearly, the different MS systems account for these differences. The optimum cone voltage and collision energy were investigated by applying 5  $\mu$ L 200 ng/mL DON in the optimum solution, methanol/ammonia solution (2% v/v). For the cone voltage, values were varied from 20 V to 110 V with a step of 10 V. Minor differences were observed in the area of the protonated ion of DON at different cone voltage settings; thus, the selected cone voltage was 50 V. Furthermore, the collision energy was optimized starting from 2 eV to 20 eV, with a step of 2 eV, and monitoring the area of the main fragment ions. The optimized MRM transitions were  $m/z$  297.1 > 231.1 at 10 eV and  $m/z$  297.1 > 249.1 at 8 eV collision energy for DON,  $m/z$  339.10 > 203.10 at 10 eV and  $m/z$  339.10 > 231.10 at 8 eV collision energy for 3-AcDON, and  $m/z$  312.10 > 263.10 at 8 eV collision energy for the IS,  $^{13}\text{C}$ -DON.

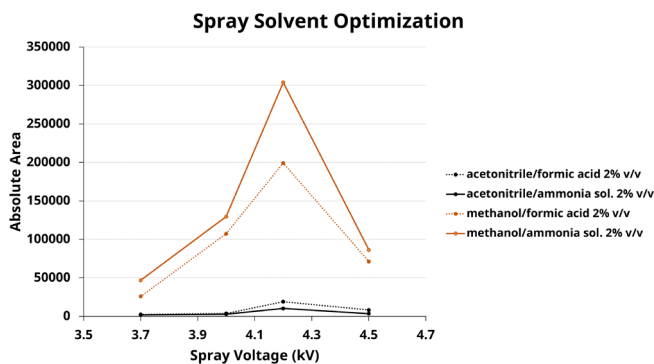


**Figure 5.5.** Spray solution optimization in different spray voltage values. Conditions: 200 ng/mL concentration, 5  $\mu$ L sample application, full scan mode monitoring the protonated ion of DON and measuring the area absolute value.

For the iBS protocol development, the approach was adapted from standard CBS methods, comprising of (i) conditioning of the blades; (ii) extraction/immunocapturing of the targeted analyte from the sample or sample extract; (iii), rinsing or washing the surface to remove interfering species; and (iv), the desorption/ionization of the analytes from the blade (2). The conditioning step was examined as part of the extraction step by using different buffers and Milli-Q water in 1:1 ratio with the 350 ng/mL DON spiked blank wheat extract and monitoring the A/IS area ratio in the chromatograms. Although assay buffers can be used to promote interactions between analytes and mAbs, the calculated A/IS area ratio revealed that 1 $\times$ PBS-T (0.05% v/v Tween-20) resulted in a 10% decrease in the mean area, and 1 $\times$ PBS 1% w/v BSA resulted in a 14% decrease in the mean area compared to Milli-Q water. The decrease in the mean area may result from some buffer residues leading to ion suppression. For the sample extraction, different undiluted volumes of sample extracts were

tested, namely, 200, 400, and 600  $\mu\text{L}$  of 350 ng/mL DON spiked wheat extract. There was a relative decrease in the A/IS area ratio with the volume increase. So, 200  $\mu\text{L}$  of sample extract was optimum for the extraction process (Figure 5.6).

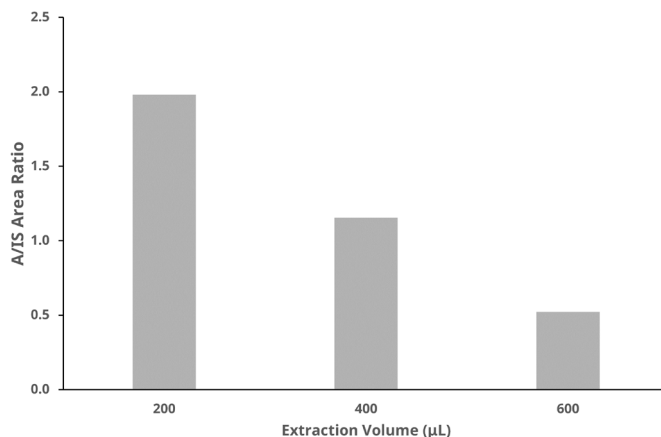


**Figure 5.6.** iBS-MS/MS method development. Extraction by immuno-capturing – extraction volume optimization.

Further, a comparison was made between 200  $\mu\text{L}$  of DON spiked undiluted wheat extract at 350 ng/mL and 200  $\mu\text{L}$  of DON spiked wheat extract at 350 ng/mL diluted 1:1 with Milli-Q water. In this case, the mean area was 50% decreased in the undiluted sampling, possibly due to matrix interferences hindering the biorecognition and causing ion suppression. For this reason, a 1:1 dilution of the wheat extract with Milli-Q water was chosen in the final protocol. Furthermore, the incubation time, i.e., the time of the immuno-capturing, was evaluated by assessing different incubation times from DON spiked sample extract at 350 ng/mL at 1:1 dilution with Milli-Q water and plotting them against the A/IS chromatogram area ratio obtained from the iBS-MS/MS analysis. The incubation was performed in an Eppendorf Thermomixer at room temperature, and 1200 rpm to reassure the reproducibility of the procedure (5.2.3). After 2 min incubation, a plateau was reached due to a limited capacity of the antibodies for the immuno-capturing to reach an equilibrium. Therefore, 2 min are used in the optimized extraction protocol (Figure 5.7).

Finally, various washing solution compositions and washing durations were tested for washing optimization, namely 500  $\mu\text{L}$  methanol/Milli-Q water in 0/100, 20/80, 50/50, and 80/20 % v/v and 10, 30, and 60 s with 500  $\mu\text{L}$  of Milli-Q water. A high percentage of organic solvent promotes denaturation of the mAbs and untimely dissociation of the analyte from the mAbs. As expected, the A/IS area ratio of 3.7 with 0/100 methanol/Milli-Q water decreased, by 37.8%, 94.3%, and 97.3%, with increasing percentages of methanol. Concerning the washing duration, 30 s produced the optimum result, which can be concluded as enough time to remove non-specifically bound analyte and remove matrix components from the wheat extract following

immuno-capturing. For that reason, 30 s were selected as the most efficient washing time (Figure 5.8).

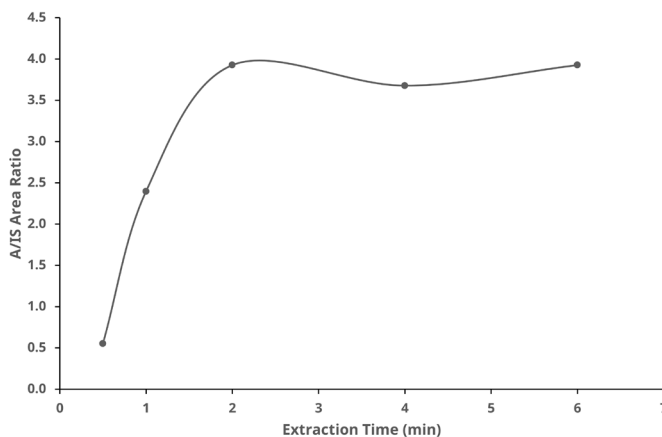


**Figure 5.7.** Extraction by immuno-capturing - time optimization during iBS-MS/MS method development

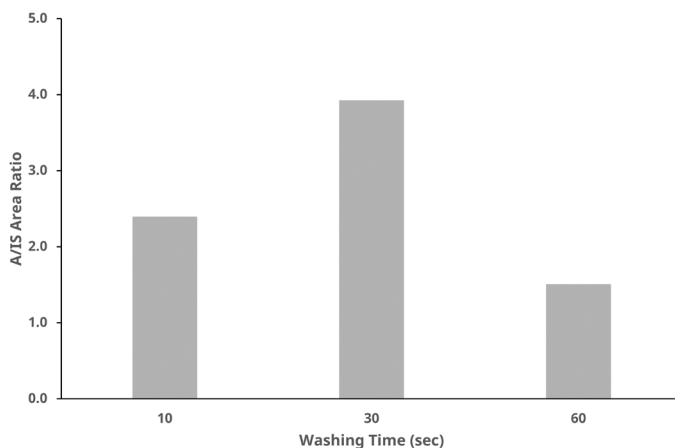


**Figure 5.8.** Washing time optimization during iBS-MS/MS method development

Next, the quantitative performance of the optimized protocol in the relevant range was evaluated by spiking blank wheat extract with DON at three different target levels (TL). The TL were based on the ML of 1750  $\mu\text{g/kg}$  for DON in unprocessed durum wheat to a final level of 175 ng/mL (0.5 $\times$  TL), 350 ng/mL (1 $\times$  TL), and 700 ng/mL (2 $\times$  TL). Good linear regression of 0.992 was observed (Figure 5.9).

The desorption step spray performance of iBS was examined using the optimized spray solution. 4  $\mu\text{L}$  was found to be the optimum applied volume when it comes to ionization from the iBS, as it creates a stable ESI-like spray, and it does not

elongate the ionization process beyond 50 s, as the 5  $\mu\text{L}$  used for method development did. The methanol/ammonia solution (2% v/v) has been examined in a previous publication to disrupt the binding of DON from the mAbs in surface plasmon resonance (SPR) (27). Due to differences in the surfaces between the blade and the SPR chip, the latter being in constant liquid flow contact, methanol/ammonia solution (2% v/v) did not quantitatively dissociate bound DON at once. Multi-desorption steps (6 in total for a sample of 350 ng/mL) are required for a complete desorption/ionization of the analyte bound with the mAbs. Despite that, the first single desorption already provides sufficient chronogram area counts for quantification in a reproducible manner, so multi-desorption steps were superfluous (Figure 5.10).

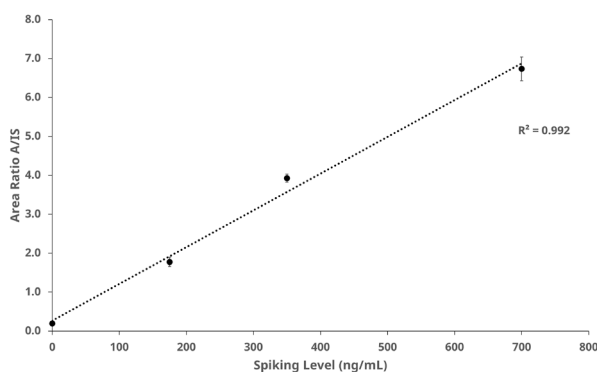


**Figure 5.9.** Quantitative analysis calibration curve of iBS-MS/MS method.

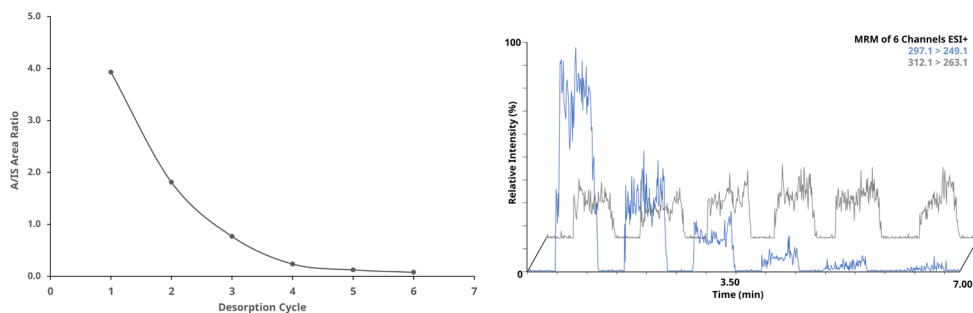


**Figure 5.10.** Multi-step desorption assessment, and respective representative overlay chronogram of  $m/z$  297.1 > 249.1 and  $m/z$  312.1 > 263.1. For detailed conditions and procedures, see text.

To illustrate the feasibility of the iBS-MS/MS approach, 200  $\mu\text{L}$  of blank wheat extract was spiked at 350 ng/mL, diluted 1:1 with Milli-Q water, and incubated for 2 min with: a. immuno-affinity blade (mAbs-enriched), b. BSA-enriched blade and c. bare conductive polystyrene blade. In addition, mAbs-enriched blade was incubated with unspiked blank wheat extract, diluted 1:1 with Milli-Q water. After 30 s of washing of the blades with 500  $\mu\text{L}$  of Milli-Q water and MS/MS analysis, results demonstrated, as anticipated, a positive signal for DON with ion ratio for  $m/z$  231.1/249.1 of

0.42 originated only from the immuno-affinity blade incubated with spiked sample extract, and from none of the other blades used. The ion ratio falls within the tolerance limit of the EU criteria for confirmatory methods (12) for ion ratio, since ion ratio  $m/z$  231.1/249.1 for DON in standard solutions was 0.47. This clearly demonstrates the added value of the mAbs for selective immuno-capturing and extraction since the positive signal resulted from the immuno-affinity blades and not from DON adsorbed on the bare conductive polystyrene surface (*Figure 5.11*).

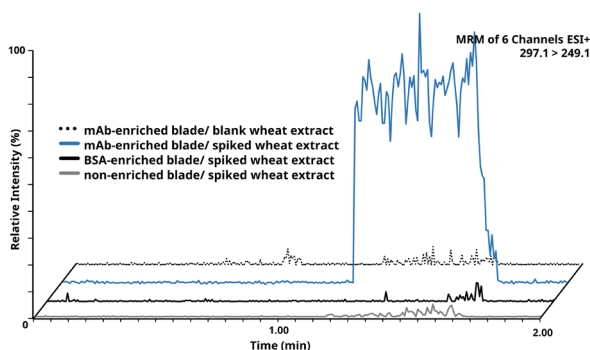


**Figure 5.11.** Feasibility of the iBS-MS/MS method. Overlay chronograms of the  $m/z$  297.1 > 249.1 transition obtained following the iBS-MS/MS extraction, immuno-capture, and ionization protocol using mAbs-enriched, BSA-enriched, and non-enriched blades.

Further, it was noticed that after repeated use, the polystyrene blades start to have differences in the tip sharpness, probably because of the extraction step performed with the blades' tip facing downwards and pressing against the bottom of the Eppendorf tube. For this reason, the reproducibility of the immunoaffinity blades was assessed by analyzing ten individual blades following DON immuno-capturing from the same wheat extract spiked at 350 ng/mL. Results of the absolute area values of the MS/MS chronograms had a  $\pm 22\%$  RSD, which is above the permitted by the EU regulation (12). Nonetheless, the corrected value used, i.e., the A/IS chronogram area ratio, was within  $\pm 4\%$  RSD for all the ten blades analyzed. As in many AIMS methods, an IS is necessary for reproducibility during ionization. However, for a quick qualitative confirmation of identity, the absolute areas also yielded a positive result with a stable ion ratio (*Figure 5.12* and *Table 5.1*).

Finally, the applicability of the optimized method described in *Figure 5.2* was illustrated by the analysis of different additional spiked and incurred samples. The samples included a blank CRM wheat flour, the same extract but spiked with 3-AcDON at 175 ng/mL ( $1\times$  TL for DON), and a 2900  $\mu\text{g/kg}$  ( $\approx 1.6\times$  TL for DON) incurred wheat sample. The mean ion ratio for  $m/z$  203.1/231.1 of 3-AcDON was 0.62 ( $\pm 0.04$ ), a ratio identical to that of the standard solution of 3-AcDON in methanol/ammonia solution (2% v/v), and within the regulatory EU criterion of 20% RSD. Moreover, the response factor A/IS for the chronogram area of 3-AcDON versus  $^{13}\text{C}$ -DON was 3.1 ( $\pm 0.1$ ) for two individual measurements of iBS-MS/MS, thereby clearly differentiating the spiked

from the blank CRM wheat sample. For the contaminated wheat sample, iBS-MS/MS results showed an A/IS area ratio for DON of 4.4 ( $\pm 0.4$ ), corresponding to a quantitative result of 535.6 ng/mL ( $\pm 14.2$ ), for two individual iBS-MS/MS measurements, calculated from the calibration curve and pointing to a level of 2678  $\mu\text{g/kg}$  in the contaminated wheat sample analyzed (Figure 5.13).

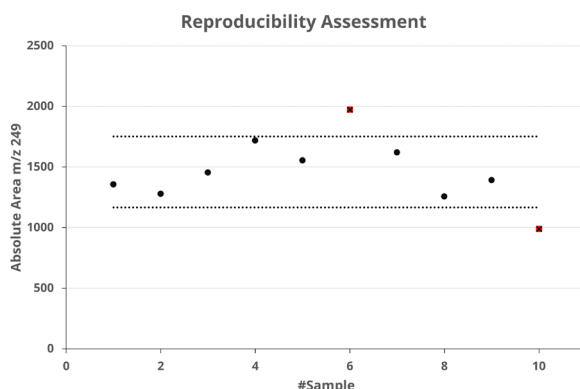


**Figure 5.12.** Reproducibility of the iBS-MS/MS method. Results within the acceptable 20% RSD% are within the dotted lines, except for blades #6 and #10 which are outliers. For detailed conditions and procedures, see text.

**Table 5.1.** Reproducibility assessment of 10 individual immunoaffinity blades using iBS-MS/MS analysis.

# of immunoaffinity blade	absolute area values				Response Factor (A/IS)
	DON		Ion ratio	<sup>13</sup> C DON	
	m/z 297.1 > 249.1	m/z 297.1 > 231.1		m/z 312.1 > 263.1	
#01	1358	603	0.44	339	4.00
#02	1280	560	0.44	305	4.19
#03	1455	605	0.42	376	3.87
#04	1719	717	0.42	448	3.84
#05	1556	740	0.48	396	3.93
#06	1974	906	0.46	482	4.10
#07	1622	675	0.42	380	4.27
#08	1257	594	0.47	301	4.18
#09	1392	597	0.43	354	3.93
#10	990	386	0.39	242	4.09
					RSD 4%

RSD 4%

Conditions: single measurement of 10 individual immunoaffinity blades, following extraction with immuno-capture, wash, and iBS-MS/MS analysis. RSD is the relative standard deviation of the ten measurements. The ion ratio is the area ratio of the two ion transitions for DON, m/z 231.1/249.1.

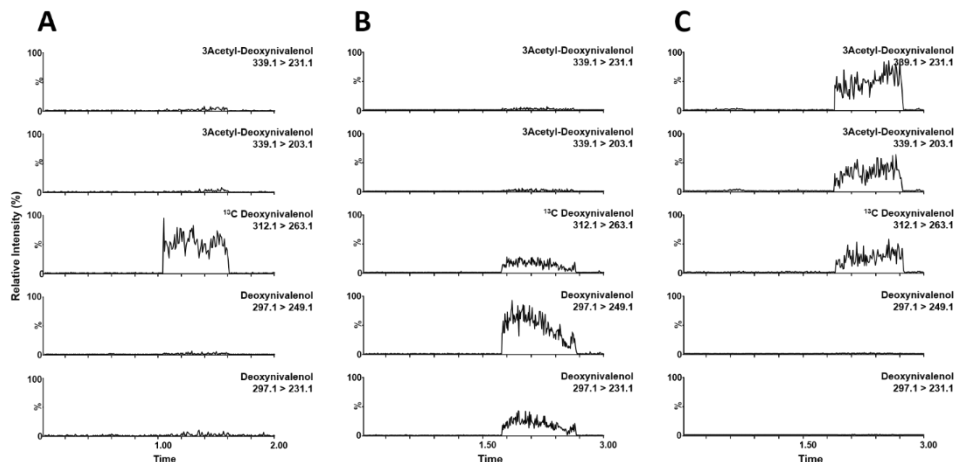


**Figure 5.13.** Representative chronograms from the analysis of (A) blank wheat (B) incurred wheat, and (C) 3-AcDON spiked wheat. The intensities are normalized on based on the highest intensity of each individual chrono-gram. For the exact conditions of the iBS-MS/MS analysis, see text.

## 5.4 Conclusion

Combining antibodies with direct MS analysis is an undoubtful advantage in raising the specificity of a rapid MS method. In this work, a simplified iBS-MS/MS method was presented, exploiting; first, the ease of antibody adsorption on polystyrene surfaces, second, the commercial availability of conductive polystyrene, and third, direct MS measurements. iBS-MS/MS is generic, enables semi-quantitative and reproducible analysis, and can be used for a fast, more secure screening or confirmation of substances, given the high specificity of mAbs. iBS-MS/MS results suggest that the mAbs activity is not compromised on the polystyrene blade and mAb lead to a selective immuno-extraction. Further, iBS-MS/MS highlights the opportunity to use alternative conductive surfaces for direct MS approaches. The conductive polystyrene blades can be cleaned to remove the mAbs and re-used following immobilization of new mAbs. Moreover, it can straightforwardly confirm the identity of the analyte bound on the mAbs of the blade, with a total time from sample to MS analysis that does not exceed 5 min, leading to high-throughput analysis. Theoretically, apart from DON, iBS-MS/MS can be modified to detect any other low molecular weight analyte in a similar integrated approach, provided that mAbs are available, also paving the road to multiplex iBS-MS/MS opportunities.



## 5.5 References

1. G. A. Gómez-Ríos, J. Pawliszyn, *Angew. Chemie*, **53**, 14503–14507 (2014).
2. G. A. Gómez-Ríos, M. Tascon, J. Pawliszyn, *Bioanalysis*, **10**, 257–271 (2018).
3. G. A. Gómez-Ríos, M. Tascon, N. Reyes-Garcés, E. Boyaci, J. Poole, J. Pawliszyn, *Sci. Rep.* **7** (2017).
4. A. Kasperkiewicz, J. Pawliszyn, *Food Chem.* **339**, 16104 (2021).
5. A. Khaled, G. A. Gómez-Ríos, J. Pawliszyn, *Anal. Chem.* **92**, 5937–5943 (2020).
6. J. J. Poole, G. A. Gómez-Ríos, E. Boyaci, N. Reyes-Garcés, J. Pawliszyn, *Environ. Sci. Technol.* **51**, 12566–12572 (2017).
7. A. Kasperkiewicz, G. A. Gómez-Ríos, D. Hein, J. Pawliszyn, *Anal. Chem.* **91**, 13039–13046 (2019).
8. O. Vendl, F. Berthiller, C. Crews, R. Krska, *Anal. Bioanal. Chem.* **395**, 1347–1354 (2009).
9. M. Cao, Q. Li, Y. Zhang, J. Wang, H. Zhai, J. Ma, L. Sun, X. Wan, Y. Tang, *Bull. Environ. Contam. Toxicol.* **107**, 248–254 (2021).
10. T. H. Kuo, E. P. Dutkiewicz, J. Pei, C. C. Hsu, *Anal. Chem.* **92**, 2353–2363 (2020).
11. B. J. A. Berendsen, L. A. M. Stolker, M. W. F. Nielen, *J. Am. Soc. Mass Spectrom.* **24**, 154–163 (2013).
12. European Commission. *Off. J. Eur. Union*. **180**, 84–109 (2021).
13. R. Javanshad, A. R. Venter, *Anal. Methods*, **9**, 4896–4907 (2017).
14. S. Joshi, H. Zuilhof, T. A. Van Beek, M. W. F. Nielen, *Anal. Chem.* **89**, 1427–1432 (2017).
15. K. M. Evans-Nguyen, T. L. Hargraves, A. N. Quinto, *Anal. Methods*, **9**, 4954–4957 (2017).
16. A. Geballa-Koukoula, A. Gerssen, M. H. Blokland, C. T. Elliott, J. Pawliszyn, M. W. F. Nielen, *Anal. Chem.* **93**, 15736–15743 (2021).
17. J. Peters, M. Bienenmann-Ploum, T. De Rijk, W. Haasnoot, *Mycotoxin Res.* **27**, 63–72 (2011).
18. N. G. Welch, J. A. Scoble, B. W. Muir, P. J. Pigram, *Biointerphases*, **12**, 301–317 (2017).
19. Q. Yu, Q. Wang, B. Li, Q. Lin, Y. Duan, *Crit. Rev. Anal. Chem.* **45**, 62–75 (2015).
20. Pichler H, Palme S, E. M. Binder, Krska R, *Mycotoxin Res.* **17**, 202–205 (2001)
21. D. A. Rickert, V. Singh, M. Thirukumaran, J. J. Grandy, J. R. Belinato, M. Lashgari, J. Pawliszyn, *Environ. Sci. Technol.* **54**, 15789–15799 (2020).
22. P. Sobrova, V. Adam, A. Vasatkova, M. Beklova, L. Zeman, R. Kizek, *Interdiscip. Toxicol.* **3**, 94–99 (2010).
23. European Commission. *Off. J. Eur. Union*. **58**, 1–398 (2008).
24. R. S. Chhaya, J. O'Brien, E. Cummins, *Trends Food Sci. Technol.* **126**, 126–141 (2021).
25. M. Eskola, G. Kos, C. T. Elliott, J. Hajšlová, S. Mayar, R. Krska, **60**, 2773–2789 (2019).
26. A. Geballa-Koukoula, A. Gerssen, M. W. F. Nielen, *Sensors*, **21**, 1–17 (2021).
27. A. Geballa-Koukoula, A. Gerssen, M. W. F. Nielen, *Anal. Bioanal. Chem.* **412**, 7547–7558 (2020).
28. D. Mampallil, H. B. Eral, *Adv. Colloid Interface Sci.* **252**, 38–54 (2018)



A large, stylized teal number '6' that serves as a background for the text.

## **General Discussion & Future Perspectives**



## 6.1 General Discussion

External influences and prevalent changes outlined in **Chapter 1**, including socioeconomic transformation, population growth, increased environmental awareness, and citizen science, will affect the lives of people worldwide. It is safe to assume that existing monitoring protocols will be unable to cope with the increased demand due to those changes. So, the current monitoring procedures must be adjusted in preparation for the future (*Figure 6.1*).

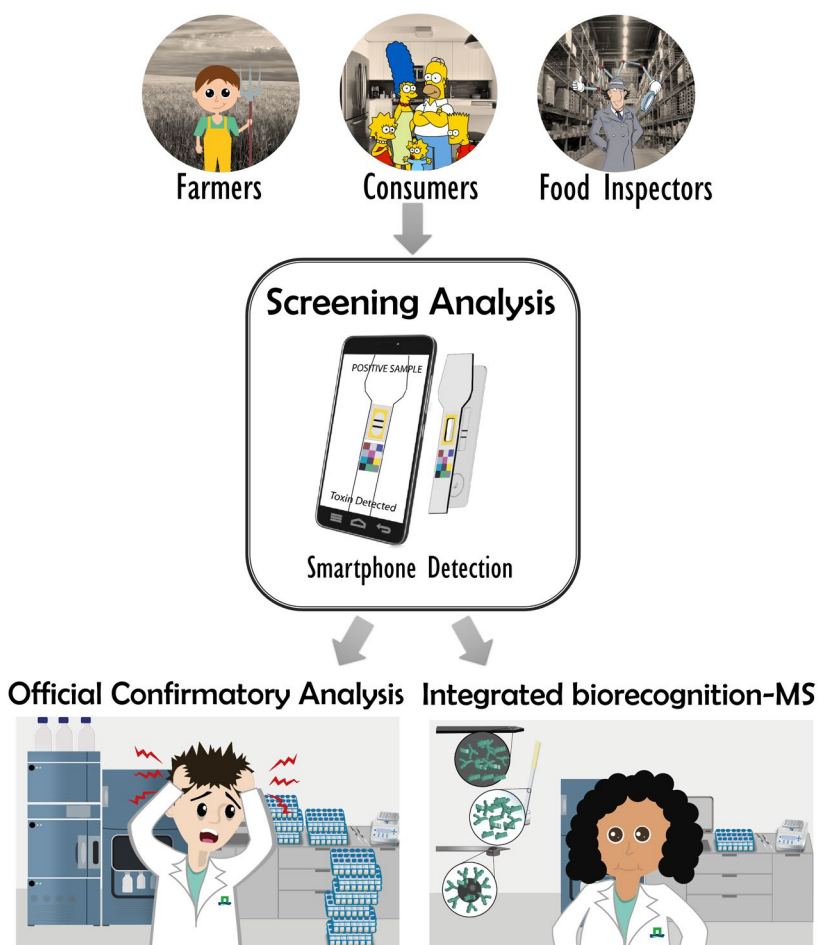


**Figure 6.1** Illustration of the future of food safety monitoring laboratories due to the changes in socio-economic parameters, including smartphone-based screening assays performed by citizens, leading to an overload in the confirmatory analysis that needs to be performed. A solution to this prospect is the broader development and application of integrated biorecognition-mass spectrometry approaches.

The vision of the presented research was to adapt the current methodologies to lay the foundation for a resilient, sustainable, and equitable monitoring system. In that line, alternative integrated approaches were developed, which combine modified versions of screening and confirmation technologies conventionally used in food safety-related protocols to offer easy and versatile detection methods. Tailored bioassays focusing on biorecognition-based isolation were crafted to replace the screening part. Additionally, mass spectrometry (MS) with ambient ionization sources was used for the confirmation. The presented approaches improve the selectivity of AIMS while eliminating the more significant drawbacks of confirmatory methods; extensive sample preparation for analyte isolation and time-consuming chromatographic separation. As proof of principle, the developed methods detected food contaminants (toxins) with high societal relevance. In this final chapter of the thesis, the core elements comprising the developed integrated methods, i.e., biorecognition and MS, are revisited, and the challenges, solutions, and future considerations are discussed (summarized in *Table 6.1*).

**Table 6.1.** Challenges for achieving an integrated biorecognition-mass spectrometry method, the approach taken to tackle the challenge and future suggestions for further improvements.

Challenge	Approach Taken	Future suggestion
Choice of a biorecognition element that is fit-for-purpose.	Use of highly specific animal-derived monoclonal antibodies.	Experimentation with alternative biorecognition elements (e.g. non-animal derived antibodies, recombinant antibodies, or synthetic biorecognition alternatives (MIPs)).
Incompatibility of the biorecognition assays with mass spectrometry detection.	Raise the MS detection sensitivity by adjusting the format of the bioassay.	Further investigation of MS-compatible assay buffers and evaluation of different MS ionization sources (fit-for-purpose for other approaches).
Selection of the appropriate target analyte.	Targeted monitoring of food safety-related contaminants and their analogs.	Testing of multiplexing possibilities by using biorecognition elements aiming at detecting different analytes.
Use of the appropriate mass spectrometry detection mode.	Primarily utilized multiple reaction monitoring (MRM) mode for targeted analysis.	Further explore different high resolution MS instrumentation in full scan mode to test potentials for retrospective analysis and monitoring emerging contaminants.
Limited accessibility of the integrated biorecognition-mass spectrometry approaches	Mainly use of Triple Quadrupole, which is the most frequently used in regulatory settings benchtop MS instrumentation.	Portable MS instrumentation – potential on-site applications.
Inconsistency in mass spectrometry ionization	Use of internal standards to correct for irreproducible ionization.	Use of 3D-printed attachments for reproducible sample handling (e.g. isolation of the mAb part of the ID-LFIA) and mass spectrometry ionization (e.g. in blade spray MS).
Integration possibilities of the integrated biorecognition-mass spectrometry approaches	Detection of an MS amenable analyte after its dissociation from the antibody (the antibodies act as an isolation/immuno-extraction mean).	hrMS measurement of the non-disrupted antibody/analyte complex.

## 6.2 Biorecognition

### 6.2.1 Immunorecognition

Immunoglobins (antibodies) have been the biorecognition element of choice for bioassays for decades. The reign of antibodies is evident; apart from the variety of published methods and applications, the antibody market size (excluding therapeutics) is greater than 1 billion dollars annually (1). Antibody usage in bioassays is justified because of their well-known sensitivity, selectivity, and variety of fit-for-purpose options (e.g., monoclonal-polyclonal). However, choosing antibodies for bioassays is sometimes based on personal preference; scientists who have gained substantial expertise after years of experimentation with antibodies choose them as a rationalized choice (2). So, the biorecognition element of choice in the applications presented in the thesis was highly specific monoclonal antibodies (mAbs).

Nevertheless, antibodies require an elaborate production, which entails scientific and ethical concerns. From a scientific point of view, animal-generated antibodies present batch-to-batch irreproducibility and require a lengthy and costly purification procedure (3). Regarding the moral stand, animal use in science is questionable even though almost one million animals are being used for antibody production each year in the European Union (EU) (1). Since 2010, in the EU, it has been valued to replace, reduce, or refine laboratory animal use to improve the quality of research. This trend is underlined in the 2010/63/EU directive, which aims to move towards animal-free testing, especially during the development of antibody-based assays (4). Even with the significant effort from governmental investments in development programs and the emergence of improved technologies, the EU Reference Laboratory for alternatives to animal testing (EURL-ECVAM) reported an increase in animals used for antibody production between 2015-2017 (5). The increase in the use of laboratory animals, despite the 2010/63/EU directive, emphasizes the demand for biorecognition-based reagents and stresses the mismatch between policymakers' decisions and scientific, industry-related, and clinical practices (2, 6).

In general, multiple issues impede the development and implementation of animal-free technologies, including education, political influence, and data sharing (2). Moving towards more ethical and sustainable alternatives is challenging. For instance, alternative recombinant non-animal derived technologies have not been broadly adopted, leading to an adaptation challenge to be resolved among scientific institutions. Recombinant methods replicate antibody genes from donor B cells by precisely designing synthetic gene sequences in yeast or phage (7). Those technologies face criticism, especially regarding the quality and validity of the produced antibodies; however, they provide the possibility for targeted sequences, enabling reliable identification and reproduction (8). Additionally, regarding the industry-related and clinical practices, practical application of the 2010/63/EU directive will lead to an immense shift in the market, causing drastic commercial and, thus, economic shifts (8). So, investing in alternative technologies and adapting thereof is of utmost importance in preparation for future monitoring procedures.



## 6.2.2 Compatibility of bioassays with mass spectrometry

At first glance, biorecognition assays are incompatible with mass spectrometry; the detection sensitivity of the MS part is greatly affected by the constituents of the biorecognition part. For this reason, in all the developed integrated approaches in this thesis, apart from optimizing the detection parameters of the MS instrumentation, additional points of reflection for method optimization were (i) the presence and type of bioassay buffers, (ii) the immobilization practice of the biorecognition element, and (iii) the dissociation efficiency of the analyte from the biorecognition element.

Regarding the effect bioassay buffers have on MS detection, the major complication is ion suppression. Ion suppression, i.e., the reduction in the ionization efficiency of the target analytes due to interference from components in the sample, such as salts, detergents, or other non-volatile residues, is a critical challenge in most MS analyses. In bioassays, buffers are used for various purposes, and they consist primarily of non-volatile salts (such as sodium or potassium chloride) and detergents (such as Triton-X or Tween-20). So, inevitably, bioassay buffer components hinder ionization leading to ion suppression. With conventional MS approaches, LC separates non-volatile and interfering compounds (9). However, chromatographic separation does not exist by default in the integrated approaches because ambient ionization mass spectrometry (AIMS) sources were used. So, alternative approaches were examined to cope with ion suppression. **Chapter 2** extensively reports on LFIA residues and bioassay buffers consisting of standard non-volatile bioassay buffers causing ion suppression. In **Chapters 2 through 4**, a simple water washing step during sample preparation dealt sufficiently with ion suppression-causing buffer residues. Alternatively, it is suggested in the literature the use of MS-compatible buffers, i.e., ammonium acetate and ammonium bicarbonate (10). In the tested configuration of **Chapter 2**, ammonium acetate/acetic acid buffer did not improve the ionization; chromatographic separation might be enhanced using buffers, but an increased percentage of organic solvent is favored in AIMS. Moreover, bioassay buffers are claimed to retain antibodies in their 3D shape and improve binding efficiency (11). However, in **Chapter 5**, mAbs reconstituted in water led to higher ionization than when bioassay buffers were used, suggesting that mAbs remain active even in non-ideal conditions, while buffers induce MS signal suppression. So, the middle ground between MS compatibility and bioassay development should be targeted.

Additionally, the effect of the analyte dissociation from the antibodies on the MS detection sensitivity was examined in terms of the effect of the dissociation solution. The dissociation solution acts simultaneously as a desorption/ ionization spray solution in the integrated approaches, enabling direct analysis. Thus, an increased percentage of organic solvent and an acidic or basic modifier are preferred (12), always considering that increasing the amount of the additives could have reversed results, minimizing ionization (9). In **Chapter 2**, the binding efficiency of the mAbs for all presented deoxynivalenol-related applications is demonstrated. Using surface plasmon resonance (SPR) measurements, the strong binding of the selected mAbs was established, and the efficiency of dissociation of the optimized solution was

demonstrated. In the case of the ID-LFIA format (**Chapters 2 and 3**), the optimized ionization solution of methanol/ammonia solution (2% v/v) allows for quantitative dissociation as demonstrated by the SPR measurements. In **Chapters 4 and 5**, the dissociation efficiency is demonstrated in terms of the number of dissociation cycles in the MS measurements.

The last point of reflection was the orientation of immobilization of the antibodies, which affects the available Fab active sides for binding, thus impacting antibody performance and biological activity (13) and influencing the analyte available for MS detection. In the case of physical adsorption on surfaces, such as nitrocellulose or plastic (**Chapters 2, 3, and 5**), the mAbs orientation cannot be controlled. Similarly, covalent immobilization on carboxylated paramagnetic microspheres employing EDC/sulfo-NHS leads to randomly but more strongly immobilized mAbs (**Chapter 4**). Using specific linkers when a covalent binding is implemented, antibodies can be immobilized on a surface from the fragment crystalline (Fc) region, leading to a site-specific immobilization (14, 15). On the biorecognition part of the integrated approaches, an increased amount of antibodies (compared to conventional bioassays) is necessary so that the trapped analyte produces (after dissociation) a signal sufficient to reach the concentrations within the detection range of the MS instrument. So, site-specific immobilization of mAb could potentially increase the performance of the mAb and lead to smaller volumes of mAb required for quantitative analysis in integrated approaches. For LFIA preparation (**Chapters 2 and 3**), the most common practice is that of physical adsorption. However, covalent immobilization can be employed to improve immobilization efficiency and performance of mAbs on plastic (**Chapter 5**). Nonetheless, employing more intricate chemistry for covalent immobilization would drastically increase the required time to prepare the bioaffinity plastic blades, eliminating the primary advantage of this integrated approach (16).

### 6.2.3 Immunorecognition alternatives

The broad spectrum of reactive chemical groups on antibodies provides options for structural modification to increase their selectivity and binding affinity. Selective post-translational modifications could include; alterations at cysteine residues and glycosylation sites, amino acid modification via free amines and carboxyl groups, or even engineering to include non-natural-derived amino acids. Despite achieving increased selectivity, those methods necessitate additional resources and knowledge, leading to an additional investment that needs to be made in science (13, 17).

Apart from naturally derived biorecognition elements, synthesized alternatives have been designed, studied, and tested in a scientific setting and even reached the market. Molecularly imprinted polymers (MIPs) are synthetic polymers with biorecognition properties, frequently referred to as "plastic antibodies." The biorecognition-like properties of MIPs are formed by non-covalent bonding (e.g., electrostatic interactions), size inclusion, or size exclusion patterns between the analyte and the cavities embedded in the polymer matrix. The polymer-based biorecognition is built in situ when a functional monomer is prearranged and then polymerized with a cross-linker around the targeted analyte to create active cavities (18, 19) (*Figure 6.2*). Despite the

advantages of using MIP, most MIP applications in literature concern sample preparation and clean-up usage as packing material in solid-phase extraction and liquid chromatography columns (20, 21), but limited use has been reported in assays and sensors (22–24).

For the developed approaches in **Chapters 2 through 5** animal-derived mAbs were used, either commercially available or prepared in-house. The antibodies were highly specific, exemplified by SPR (**Chapter 3**) and cross-reactivity testing (**Chapters 2 through 5**). It is evident, though, that broad adaptation of the developed integrated biorecognition-mass spectrometry approaches in future regulatory settings will require additional adjustment to using non-animal derived antibodies under the current 2010/63/EU directive.

To investigate an alternative to mAbs in the integrated approaches, MIPs were employed as the coating in coated blade spray (CBS) ionization MS. In our setup, a MIP for  $\beta$ -agonists was used to achieve selective and specific adsorption and subsequent ionization of the targeted analytes.  $\beta$ -agonists are a class of molecules used for therapeutic purposes in the symptomatic treatment of asthma (25). However,  $\beta$ -agonists are also abused to increase athletes' oxygen intake and muscle growth (26). Therefore, it is crucial to have a selective, specific, fast, easy-to-use, high throughput method for the routine monitoring of  $\beta$ -agonists, especially in large athletic events with an increased demand for sample analysis.

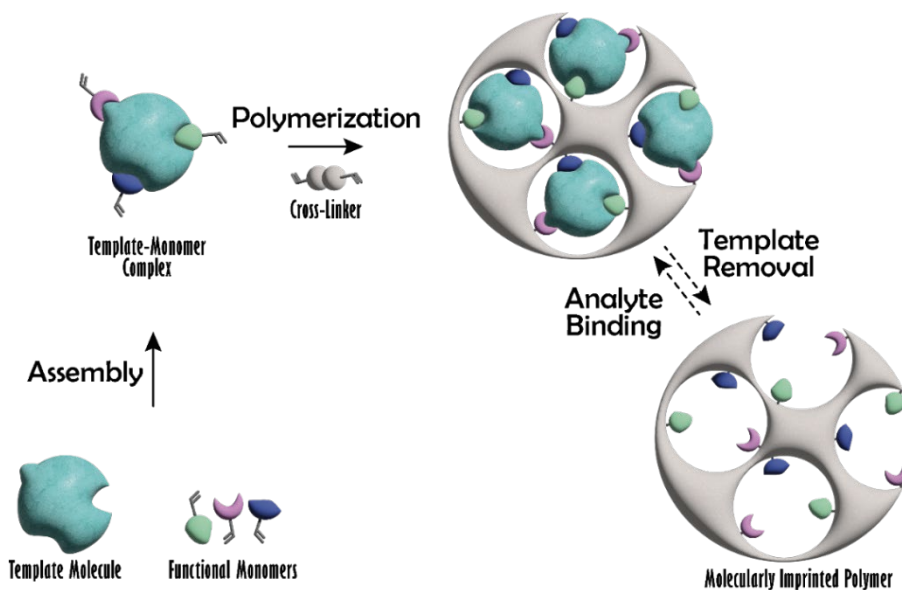


**Figure 6.2.** *Molecularly Imprinted polymers preparation. The functional monomers interact with the template molecule. The complex is then polymerized with cross-linkers. After removal of the template molecule, the MIP with characteristic binding sites is formed.*

The MIP-blade was prepared following the coating procedure described in the literature (27, 28). Briefly, the non-coated stainless steel blades were activated by

sonicating in concentrated hydrochloric acid for 60 minutes, followed by washing with UHPLC water and drying in the oven at 150°C. The activated blades were cooled at room temperature. Next, a mixture of 10% w/w polyacrylonitrile (PAN) in N, N-Dimethylformamide (DMF) was prepared by heating in the oven at 90 °C for 60 minutes. The mixture was allowed to cool at and to room temperature, and MIP material retrieved from commercial SPE cartridges (Sigma-Aldrich) was brought into suspension. MIP final concentration in the mixture was 10% w/w. The activated tip of the blade was dipped into the MIP-PAN-DMF mixture and then cured in the oven at 180 °C for 2 minutes. The dipping/curing process was repeated twice to achieve homogeneous tip coverage. For the extraction of  $\beta$ -agonists from human urine using the MIP-blade, the  $\beta$ -agonists extraction protocol from commercial MIP cartridges was adapted. The activation, sampling, washing, and elution/ionization steps were optimized to achieve higher ionization in MIP-blade spray MS and minimize the steps to lead to a shorter extraction time (Figure 6.3).

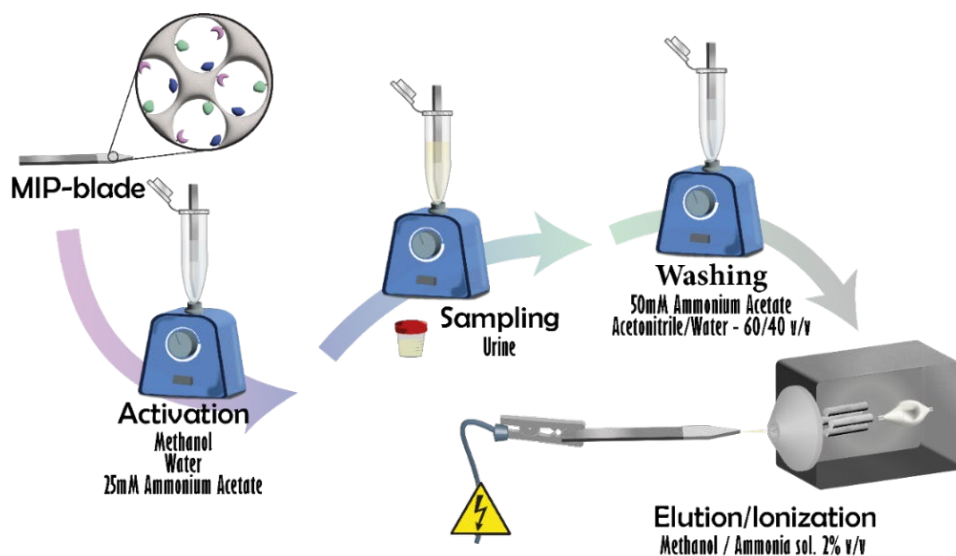


**Figure 6.3.** Optimized MIP-blade extraction process, including activation, extraction of  $\beta$ -agonists from urine (sampling), washing to remove non-specifically bound analytes, and direct elution of the analytes and blade spray ionization Q-Orbitrap MS.

MIP-blade spray performance was assessed by analyzing a blank and a spiked human urine sample. Characteristic  $m/z$  values for  $[M+H]^+$  precursor ions and fragment ions thereof for formoterol, clenbuterol, or salmeterol were absent in blank urine analysis. In contrast, detection at a level of 20 ng/mL in spiked urine was achieved for all substances, suggesting MIP-specific recognition (Figure 6.4). According to WADA, a 20 ng/mL concentration corresponds to inhaled formoterol of 1600  $\mu\text{g}/24\text{ h}$ , which is consistent with therapeutic use. However, for salmeterol, the detection at 20 ng/mL is above the WADA limit of 2.0 ng/mL, and for clenbuterol,

being a zero tolerance substance (29), the detection limit of 20 ng/mL is high compared to other MS methods in literature (30–32).

CBS is a high throughput method (33), suggesting the potential to monitor formoterol in anti-doping control, especially in large athletic events. MIP-blade spray could provide an alternative to the immuno-enriched microsphere magnetic blade spray (iMBS) approach (**Chapter 4**), with a more straightforward enrichment method, with high specificity.

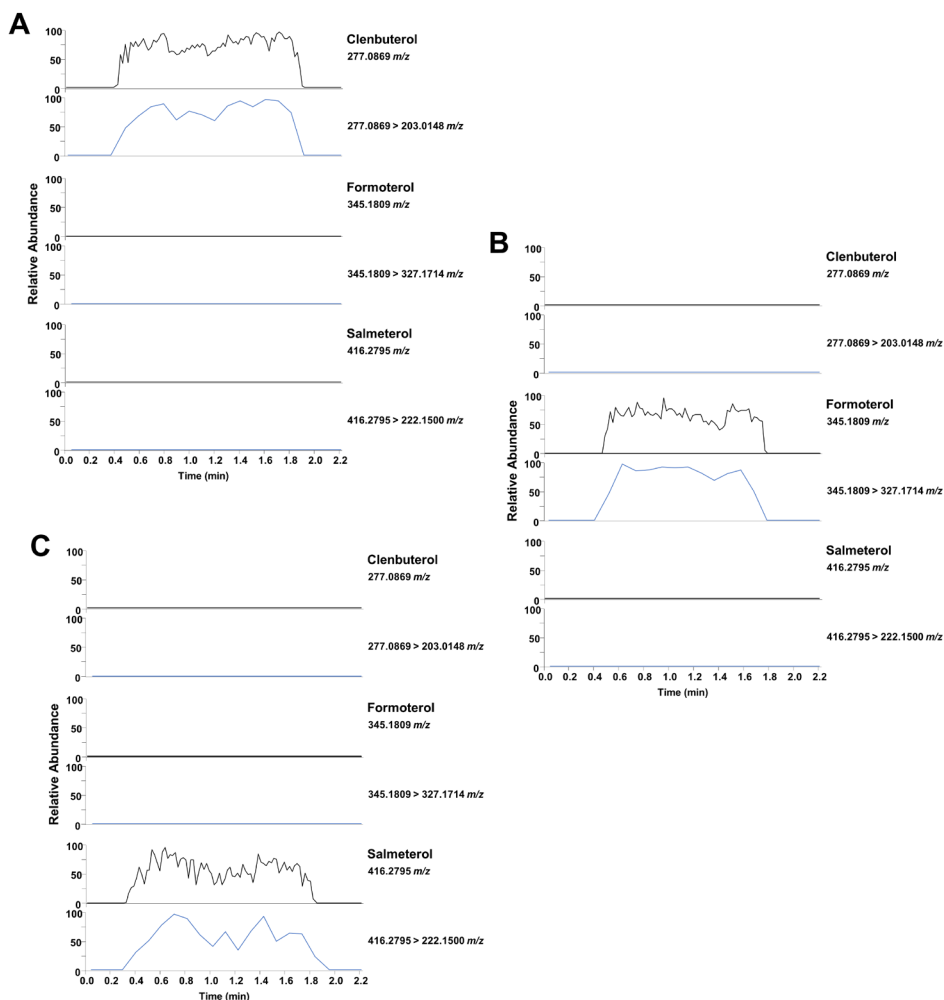


**Figure 6.4.** MIP-blade spray hrMS chronograms for clenbuterol, formoterol, and salmeterol monitoring the protonated ion in full scan mode and a characteristic fragment in parallel reaction monitoring (PRM) in (A) clenbuterol spiked urine, (B) formoterol spiked urine and (C) salmeterol spiked urine.

As described earlier, MIPs exploit a template molecule with distinct functional groups and stereochemistry to create binding cavities when the monomer binds around it. However, if the template molecule is insufficiently removed before use, leakage of the template molecule leads to false positive results (34). The MIP-blade spray setup revealed a false positive salbutamol signal when blank urine samples were analyzed using the adapted method (Figure 6.5). The false-positive salbutamol signal suggests its use as a template molecule, which is not surprising, given that the  $\beta$ -agonists share the same backbone structure. In literature, such an issue is eliminated using "dummy template molecules", i.e., structural analogs that replace the target analyte as a template during MIP synthesis (35). So, despite the variety of bio-recognition alternatives, each application requires good optimization to eliminate occurring problems.

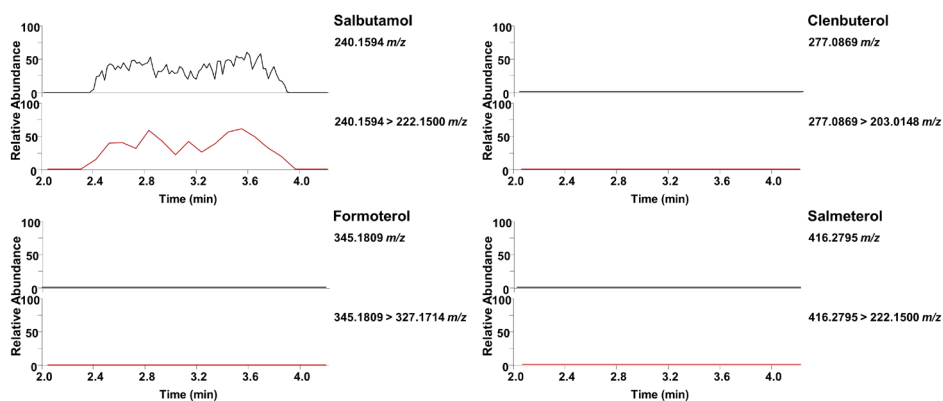


**Figure 6.5.** Chronograms of blank urine monitoring the protonated ion in full scan mode and a characteristic fragment in parallel reaction monitoring (PRM) for salbutamol, clenbuterol, formoterol and salmeterol.

## 6.3 Mass spectrometry

### 6.3.1 On-site mass spectrometry

In the field of food safety, where the integrated biorecognition-mass spectrometry approaches were developed, MS is primarily used for confirmatory analysis following a suspect screened sample. However, in terms of EU food safety regulation (EU 2021/808), MS can be used for screening, too (36). MS mostly outperforms bioassays on sensitivity and selectivity. However, MS is the method of choice for confirmation because of the high operation cost, extensive sample preparation needed, and the preceding time-consuming chromatographic separation. The point that confirmatory MS analysis lacks, and at the same time, the main advantage of screening bioassays is the possibility of on-site testing, especially by non-specialists without extensive training (37).

In response to the inability for on-site confirmatory testing with the conventional MS instrumentation, progress has been made in developing (trans)portable MS systems allowing on-site detection. Since 1942, when the first portable mass spectrometer was developed by John Hipple (38), portable MS systems have evolved to the point of a palm-sized MS system that weighs less than 2 kg, with a volume of less than 2 L, and runs on a 5 W battery (39, 40). For broad on-site MS analysis applications, all the benchtop instrumentation limitations, i.e., large size, high power consumption, and high price, need to be addressed. The ion source, vacuum system, energy supply, and sample preparation need to be miniaturized and adjusted to be compatible with on-site applications while at the same time remaining capable of performing equally to the benchtop instrumentation (41). Regarding the mass analyzers, quadrupole and ion trap mass analyzers are mainly used in portable instruments, but also, miniaturization of the magnetic sector and the TOF mass analyzers has been achieved, despite their resolution depending on the path the ions travel. For the ion sources, those operating at atmospheric pressure (ESI, APCI, and AP-MALDI) and AIMS sources are preferred because of the ease of hyphenation (39, 42). AIMS methods do not require time-consuming chromatography and are well compatible with on-site analysis because of the minimal sample preparation employed. Also, AIMS that do not require liquid or gas carriers, such as CBS, are exceptionally compatible with on-site applications (43, 44).

However, the (trans)portable MS analysis field is not yet ideal. The bottleneck of on-site testing is the risk of variable operating conditions. AIMS might be susceptible to ambient contamination because of the open interface, which could even lead to signal suppression. Additionally, AIMS sources that operate under the desorption principle could present instability of the spraying or even susceptibility of the spray to ambient air conditions (e.g., evaporation) (45). Further improvement could be made to the ease of operation; end-users value simplicity, but (trans)portable mass spectrometers are still high-end instruments that are expensive compared to bioassays, and require extensive training to use, hindering further adaptations.

Regardless of the limitations, (trans)portable MS instrumentation could pave the way for further developments with on-site confirmatory analysis. For instance, miniaturization of the triple quadrupole mass analyzer, which is the gold standard in routine analysis of food contaminants, highlights the potential for adaptation of standard routine methods to on-site analysis. Also, for the integrated biorecognition-mass spectrometry approaches presented in this thesis, all ionization sources, ESI (46), DART (47), and CBS (48), have been combined with (trans)portable instrumentation in literature. The transition from the benchtop to a portable MS analysis could open the path for on-site confirmatory analysis in future regulatory settings. This way, transportation and long-term sample storage in the monitoring laboratories will be minimized, for instance, in the food safety sector, and samples requiring analysis will be moderated (49).

### 6.3.2 General considerations in mass spectrometry

#### Use of Internal Standard

Internal standard (IS) use, i.e., structurally identical isotopically-labeled analyte, is required for absolute quantification in MS-based analysis methods. IS corrects for losses that potentially occur throughout the entire analytical method, especially during sample pre-treatment. IS is required in soft ionization methods because specific analytes ionize more efficiently than others; therefore, absolute quantification cannot be established only by signal intensity measurement. However, use of isotopically-labeled IS raises the cost per individual analysis because of their high purchase cost, which could be challenging for large-scale and routine testing. Also, commercial unavailability of IS, might lead to limit adaptation of analytical methods (50).

In the developed integrated biorecognition-MS approaches, the IS cannot be added for the compensation of sample handling because of the limited capture capability of the biorecognition element. A minimal and quantified amount of mAbs is used (as discussed in 1.2.2), for which the analyte will compete for the binding with the IS, leading to loss of sensitivity. The competition with the IS, could be exploited in a complementary bioassay for an integrated approach, for a quick screening of big-sized molecules, as has been done in literature, but in that case the following bioassay-MS method, would require the avoidance of IS usage (51).

Adding IS at the desorption stage is only used to compensate for irreproducibility in desorption/ionization and not irreproducibility caused by handling. Regarding the developed integrated approaches, irreproducibility in the desorption/ionization stage was noticed in the ID-LFIA methods (**Chapters 2 and 3**) due to LFIA residues causing ion suppression. Also, the iBS-MS/MS method (**Chapter 5**) required IS for quantitative analysis due to the shape of the plastic blade, which required manual shaping leading to irregularities between different blades. As observed from the experimental results of the iBS-MS/MS method, if IS is not employed, then quantification is compromised. When target quantification must be achieved for a regulatory purpose, the requisite use of IS is obvious. It is worth mentioning, though, that the use of IS in the developed approaches is not the exception but the rule; most AIMS suffer from ionization irreproducibility and require IS for quantification. Future adaptations of the developed approaches might eliminate the need for IS, leading to a more applicable and less expensive method. For instance, for the iBS-MS/MS method, plastic blades having a robust shape would be beneficial because they might eliminate the requirement of IS.

#### High Resolution Mass Analyzers (hrMS)

The gold standard in routine analysis is that of low-resolution MS, such as triple quadrupole MS. Those instrumentation allow for targeted analysis and monitoring of specific substances with high certainty and is relatively cheaper than the high resolution MS (hrMS) instrumentation. However, full scan non-targeted monitoring with hrMS can assist in monitoring emerging, unexpected or non-regulated contaminants and induce subsequent prompt mitigating measures. Using hrMS requires efficient



data evaluation from trained personnel for correct mass spectra interpretation to facilitate compound identification. Additionally, storage, managing, and sharing of the hrMS data retrieved, can ease open science and improve scientific communication and dissemination of the results (52, 53).

In the developed integrated biorecognition-mass spectrometry approaches, mAbs provide a tight window for molecule isolation compared to the generic liquid chromatography that would be used with a conventional approach. In **Chapter 2** use of hrMS (Q-Orbitrap) is showcased, where the DON-targeting mAbs, also detect DON-3G. The most appropriate use of hrMS is in full scan mode and retrospective analysis. For instance, after the specific antibody-aided separation, hrMS could recognize cross-contamination of co-occurring masked forms of the targeted mycotoxin (54, 55). Despite being counterintuitive, antibodies not too highly specific should be used if a retrospective detection with the help of integrated approaches and hrMS is aimed for. The use of non-highly-specific antibodies would help isolate a broader range of emerging contaminants compared to the approach now taken.

### Mass spectrometry of intact analyte-antibody complexes

For a successful integrated approach, a pair of a biorecognition element with an MS amenable analyte is a prerequisite; the biorecognition element binds with the analyte, and after dissociation, the analyte is detected with MS. In the case of a pair consisting of an antibody and a small-sized molecule that cannot be ionized easily, such as a highly non-polar compound, measurement of the native state of the antibody-analyte complex, is an alternative to dissociating and measuring only the free analyte. Additionally, native MS could ease the detection of analytes that cannot be retained using chromatography columns, such as highly polar compounds with a conventional C18 chromatographic column. To sustain the non-covalent contacts while ionizing, only soft ionization methods that enable MS analysis of intact molecules are compatible. ESI and Matrix-Assisted Laser Desorption Ionization (MALDI) allow complete biomolecule ionization with limited fragmentation (56–60). Therefore, native MS could be presented as a theoretically exceptional alternative. Additionally, qualitative and quantitative assessments have been reported using native MS (61).

However, native MS usually operates with hrMS instrumentation, mainly hybrid (quadrupole) time-of-flight hybrid ((Q)-TOF) (62). The integrated biorecognition-mass spectrometry approaches presented in this thesis use a triple quadrupole, which is the gold standard for routine analysis. Employment of hrMS instrumentation might restrict broader adaptation in routine analysis because hrMS instrumentation is relatively more intricate in use and requires more extensive training for data interpretation.

## 6.4 Accessibility of the developed approaches

Improvement of accessibility of both bioassays and MS can be achieved using custom-made 3D-printed attachments. The rise in the development of 3D printers, related computer-aided design (CAD) software, and consumables, including polymer

cartridges and raisins of different properties (63), has enabled applications in a variety of fields (64–66). The relatively low cost of 3D printing, custom designs, and user-friendliness encourage the adoption of 3D printing-related applications (67).

With 3D printing, adaptable modules for the smartphone camera can be created to evaluate the result of bioassays using a smartphone. Subsequently, images can be retrieved, processed, and rendered to a quantitative result using the smartphone camera. Such processing benefits the user by eliminating ambient light conditions that could hinder correct optical evaluation (68–70). In **Chapter 4**, such a 3D-printed module was used to assess a domoic acid screening assay with a smartphone; photos were retrieved and later processed offline using Image J. This process added semiquantitative potential and a more secure evaluation of the screening result, especially in cases of borderline to the regulatory limit contamination. However, this offline processing defeats the purpose of easy, on-site screening. This issue was considered earlier, in **Chapter 3**, where a (semiquantitative) evaluation of the screening result was performed without a 3D-printed attachment but with a commercial smartphone application (app). In that case, images could be acquired in ambient light conditions, but the app was only compatible with a few selected smartphone models (71). Considering the increased demand and production in the smartphone market, the broad adoption of smartphone usage, the increasing number of available smartphone brands in the market (72, 73), and the variety in smartphone operating systems, the development of apps that are compatible only with a limited fraction of the smartphones in the market, restricts wide adoption of the use of screening assays in a very narrow market (74–76).

In MS applications, 3D-printed modules can be generally employed throughout the entire analytical workflow (77–80). 3D-printed modules can ease sample preparation by facilitating sample collection, storage, and pre-treatment (including extraction and solvent mixing), both online and offline (81). Additionally, a valuable input of 3D printing is the improvement of reproducibility and efficiency in MS workflows by employing 3D-printed modules during sample preparation, targeting selective enrichment of complex samples and direct appliance in the ionization source by desorption or ionization. In all cases, chemical compatibility, ease of production, and cost issues must be addressed (82). The increasing demand for 3D printing is based on the customization and integration, ability to rapidly produce prototypes, uniformity of CAD data format despite the variety of software and printers, improved precision, reproducibility of printing, and type of functional materials (83).

Regarding the integrated biorecognition-mass spectrometry approaches, 3D-printed modules could be used in the future adaptation of **Chapters 2 and 3**, setups to more efficiently handle the ID-LFIA cut and isolation of the immuno-affinity trapping zone. Also, in **Chapters 4 and 5**, 3D-printed attachment in the inlet of the MS could secure similar iMBS and iBS ionization distance, eliminating the need for IS (see also section 6.3.2) and minimizing irreproducibility caused by the use of a modified in-house system. Nonetheless, the overall accessibility of MS systems is limited; besides the specialized software to obtain, analyze, and interpret the data, MS adaptation necessitates expert knowledge of apparatus handling and proper sample

preparation, so developing reliable MS procedures is more complex, expensive, and time-consuming than screening approaches, such as LFIA (37). In the future, specialized systems (84, 85) taking advantage of the developed easy-to-use biorecognition-mass spectrometry interfaces could be developed for targeted applications for citizen science.

## 6.5 General considerations and future perspectives

Numerous scientific challenges were addressed and tackled, highlighting the path for further future experimentation with integrated biorecognition-mass spectrometry approaches (summarized in *Table 6.1*). First and foremost, the overall incompatibility of (lateral flow) immunoassays with ESI-like ionization MS was successfully mitigated. Primarily, the signal suppression due to involatile buffer residues was eliminated with a water-aided washing step, and the insufficient amount of MS amenable analyte in conventional assays was addressed to achieve a higher absolute number of bound analytes. Additionally, it was demonstrated that different ionization sources are appropriate for the targeted applications. It was shown that various substrates, i.e., nitrocellulose, microspheres, and polystyrene, could be employed for biorecognition element immobilization and subsequent MS detection. Future applications exploring different bioassay substrates (45, 86, 87) could be explored in combination with several biorecognition elements (24, 88).

The biorecognition part employed in the integrated approaches acts more like a trapping zone for the targeted contaminant rather than a conventional screening assay consisting of additional labeled and conjugated molecules for signal attainment. Apart from incorporating the biorecognition part with MS and having an online biorecognition-dissociation-ionization process (**Chapter 5**), the biorecognition and dissociation of the analyte from the bioassay can be performed offline, followed by ionization (**Chapters 2 and 3**) or combine offline biorecognition followed by online analyte dissociation and ionization (**Chapter 4**). Provided that a bioassay is stable when the storage conditions are appropriate (12), when the biorecognition is performed offline, it allows for an indirect collaboration between experts and non-specialists; the bioassay is performed by untrained individuals, followed by the MS analysis in the lab. Of course, this is based on the fact that bioassays are by default more user-friendly and easy to perform, so even laypeople can use them without excessive training. The basis of such a future scenario is given in **Chapter 2**, where short-term storage of ID-FLIA (1 week) is examined, followed by intra-day dissociation and MS analysis. The results demonstrated that the ID-LFIA remained stable, and the MS analysis quantitative results were comparable with those of freshly developed and analyzed ID-LFIA samples.

Additionally, the detection of more than one analyte simultaneously, i.e., multiplexing properties, can be attributed to the integrated approaches using mAbs targeting different analytes (89). Following the rationality of developing conventional multiplex LFIAs, multiplexing ID-LFIAs could be achieved in two ways (90). First, using individual ID-LFIAs, each dedicated to detecting a different analyte. All strips would

be arranged in a customized holder to collect and distribute the same sample extract between the different ID-LFIAs. Alternatively, multiplexing can be achieved from a singular ID-LFIA by spraying bioaffinity trapping zones of mAbs dedicated to a different analyte. Nonetheless, each approach has its limitations; multiple strips require additional consumables, increasing the production cost, but multiple bioaffinity trapping zones are limited by the physical length of the assay. Similarly, multiplexing the iMBS and iBS, will require immobilizing mAbs on different microspheres or the polystyrene surface, respectively. In multiplexing, full scan and multiple reaction monitoring (MRM) mode can be employed for identification, with full scan mode helping to monitor emerging contaminants. However, a significant challenge is the sample preparation; analytes of a broad chemical nature must be extracted efficiently to reach legal or detectable limits, eliminating potential cross-reactivity (91, 92).

Another challenge that could be addressed to improve the broad future adaptation of the integrated biorecognition-mass spectrometry approaches is the regeneration of the biorecognition part. Regeneration restores the bioassay to its baseline, creating a reusable system (93). The iMBS and iBS approaches (**Chapters 4 and 5**) could accommodate modifications to achieve a reusable system. For a reusable system, the dissociation of the analytes from the mAbs has to be quantitative, and the immobilization of the mAbs should not be disrupted, just like an SPR immunosensor chip is reusable for a few cycles of regenerations (94, 95). Such an approach requires broad experimentation and fine-tuning between immobilization, dissociation, and ionization. Nevertheless, regeneration would create a more cost-efficient method, which will be appreciated in the industrial setting, primarily because of the increased amount of mAbs used in the integrated biorecognition-mass spectrometry approaches, which raises the cost per analysis.

The thesis included screening assays with smartphone readout validation and benchmarking against the developed integrated approaches (**Chapters 3 and 4**). Interpreting the screening result with a smartphone has advantages over optical evaluation, such as the possibility of quantification and automatic storing of the result on cloud servers or sharing the result among public platforms (96). Such a citizen science approach entails ethical issues; data handling, storage, and management security (97) are not reassured for the consumer. Also, it is unclear who bears the legal liability in case of a wrong (smartphone) interpretation of the screening result, leading to a negative outcome in the life of the individual (e.g., a false-negative result for the presence of allergens, allowing an allergic individual to consume allergen containing food, leading to anaphylaxis). Further guidelines protecting the consumers should be laid down.

Furthermore, the validation of the method under the criteria of confirmatory methods proves that the integrated biorecognition-mass spectrometry approaches are better than the conventional screening assays in terms of selectivity, while they are equal in performance to the officially recognized confirmatory methods. It is important to note that in the food safety sector, where the presented applications were developed, the current EU 2021/808 regulation requires four identification points for confirmatory methods, one of which is dictated by the chromatography retention time (36). Thus, by definition (98), AIMS are excluded from the EU 2021/808 regulation.

Despite this, the specificity of mAbs supports isolation of the targeted contaminant with higher certainty than generic retention in chromatographic columns, so the developed integrated approaches could be considered for inclusion as confirmatory methods in future revisions of food safety regulations.

## 6.6 Conclusions

This thesis presented the development (and validation) of different integrated biorecognition-mass spectrometry approaches. Under the impact of widespread changes that will affect peoples' lives in the future, the integrated biorecognition - mass spectrometry approaches could be employed to regulate the increased demand for confirmatory analysis from monitoring laboratories. Bridging the gap between those two orthogonal techniques (biorecognition and mass spectrometry) is undoubtedly an advantage; they offer identification based on the characteristic  $m/z$  values as a confirmatory method, maintaining the benefits of screening, i.e., immunorecognition-based specific isolation. Different substrates for biorecognition immobilization and MS instrumentation were employed, demonstrating the improvement in the specificity of the acquired data from ambient MS. The applications of the developed methods focused on food safety-related contaminants, but in future adaptations, the approaches could be expanded to a plethora of targeted applications.

## 6.7 References

1. A. C. Gray, A.R.M. Bradbury, A. Knappik, A. Plückthun, C.A.K. Borrebaeck, S. Dübel, *Nat. Methods*. **17**, 755–756 (2020).
2. S. Bressers, H. van den Elzen, C. Gräwe, D. van den Oetelaar, P.H.A. Postma, S.K. Schoustra, *Res. Integr. Peer Rev.* **4**, 1–9 (2019).
3. A. Gray, A.R.M. Bradbury, A. Knappik, A. Plückthun, C.A.K. Borrebaeck, S. Dübel, *Nat. Biotechnol.* **38**, 1234–1239 (2020).
4. European Commission. *Off. J. Eur. Union*. **276**, 33–79 (2010).
5. J.F. Viegas Barroso, M.E. Halder, M. Whelan. EURL ECVAM Recommendation on Non-Animal-Derived Antibodies (available at: <https://publications.jrc.ec.europa.eu/repository/handle/JRC120199>)
6. S. J. More, *Front. Vet. Sci.* **6**, 382 (2019).
7. K. Basu, E. M. Green, Y. Cheng, C. S. Craik, *Curr. Opin. Biotechnol.* **60**, 153–158 (2019).
8. Á. González-Fernández, F.J. Bermúdez Silva, M. López-Hoyos, C. Cobaleda, L. Montoliu, M. Del Val, K. Leech, *Nat. Methods*. **17**, 1069–1070 (2020).
9. A. Furey, M. Moriarty, V. Bane, B. Kinsella, M. Lehane, *Talanta*. **115**, 104–122 (2013).
10. A. Steckel, G. Schlosser, *Molecules*. **24**, 611 (2019).
11. K. L. Cox, V. Devanarayan, A. Kriauciunas, J. Manetta, C. Montrose, S. Sittampalam, A. *Immunoassay methods. In: Assay Guidance Manual*, 1–39 (2014)
12. R. Reverberi, L. Reverberi, *Blood Transfus.* **5**, 227–240 (2007).
13. M. Shen, J. F. Rusling, C. K. Dixit, *Methods*. **116**, 95–111 (2017).
14. S. Smith, K. Goodge, M. Delaney, A. Struzyk, N. Tansey, M. Frey, *Nanomater.* **10**, 2142 (2020).
15. S. Gao, J. M. Guisán, J. Rocha-Martin, *Anal. Chim. Acta*. **1189**, 338907 (2022).
16. D. Kim, A. E. Herr, *Biomicrofluidics*. **7**, 041501 (2013).
17. A. Makaraviciute, A. Ramanaviciene, *Biosens. Bioelectron.* **50**, 460–471 (2013).
18. M. Cieplak, W. Kutner, *Trends Biotechnol.* **34**, 922–941 (2016).
19. G. Zhang, M. M. Ali, X. Feng, J. Zhou, L. Hu, *TrAC*. **144** (2021).
20. L. X. Yi, R. Fang, G. H. Chen, *J. Chromatogr. Sci.* **51**, 608–618 (2013).
21. Y. Cui, L. Ding, J. Ding, *TrAC*. **147**, 116514 (2022).
22. J. R. J. Y. Choi, K. W. Yong, J. R. J. Y. Choi, A. C. Cowie, *Sensors*. **19**, 2–19 (2019).
23. M. Dagar, S. Yadav, V. V. R. Sai, J. Satija, H. Bhatia, *Talanta*. **238**, 123048 (2022).
24. I. Bazin, S. A. Tria, A. Hayat, J. L. Marty, *Biosens. Bioelectron.* **87**, 285–298 (2017).
25. H. S. Nelson. *Prim. Care Respir. J.* **15**, 271–277 (2006).
26. M. Thevis, G. Opfermann, W. Schänzer, *J. Mass Spectrom.* **38**, 1197–1206 (2003).
27. M. L. Musteata, F. M. Musteata, J. Pawliszyn, *Anal. Chem.* **79**, 6903–6911 (2007).
28. F. S. Mirnaghi, J. Pawliszyn, *Anal. Chem.* **84**, 8301–8309 (2012).
29. World Anti-Doping Agency (WADA), TD2022DL (2022).
30. F. Guan, C.E. Uboh, L.R. Soma, Y. Luo, R. Li, E.K. Birks, D. Teleis, J.A. Rudy, D.S. Tsang, *Rapid Commun. Mass Spectrom.* **16**, 1642–1651 (2002).
31. S. Yang, X. Liu, Y. Xing, D. Zhang, S. Wang, X. Wang, Y. Xu, M. Wu, Z. He, J. Zhao, *J. Chromatogr. Sci.* **51**, 436–445 (2013).
32. W. F. Duvivier, T.A. Van Beek, T. Meijer, R.J.P. Peeters, M.J. Groot, S.S. Sterk, M.W.F. Nielsen, *J. Agric. Food Chem.* **63**, 493–499 (2015).
33. A. Kasperkiewicz, G. A. Gómez-Ríos, D. Hein, J. Pawliszyn, *Anal. Chem.* **91**, 13039–13046 (2019).
34. M. Gao, Y. Gao, G. Chen, X. Huang, X. Xu, J. Lv, J. Wang, D. Xu, G. Liu, *Front. Chem.* **8**, 1142 (2020).
35. H. Santos, R. O. Martins, D. A. Soares, A. R. Chaves, *Anal. Methods*. **12**, 894–911 (2020).
36. European Commission, *Off. J. Eur. Union*. **180**, 84–109 (2021).

37. A. S. Tsagkaris, J.L.D. Nelis, G.M.S. Ross, S. Jafari, J. Guercetti, K. Kopper, Y. Zhao, K. Rafferty, J.P. Salvador, D. Migliorelli, G.I. Salentijn, K. Campbell, M.P. Marco, C.T. Elliot, M.W.F. Nielsen, J. Pulkrabova, J. Hajslova, *TrAC*. **121**, 115688 (2019).
38. J. A. Hipple, *Nature*. **150**, 111–112 (1942).
39. Z. Yang, Z. Ren, Y. Cheng, W. Sun, Z. Xi, W. Jia, G. Li, Y. Wang, M. Guo, D. Li, *Vacuum*. **199**, 110889 (2022).
40. M. Yang, T.-Y. Y. Kim, H.-C. C. Hwang, S.-K. K. Yi, D.-H. H. Kim, *J. Am. Soc. Mass Spectrom.* **19**, 1442–1448 (2008).
41. Z. Ouyang, R. G. Cooks, *Annu. Rev. Anal. Chem.* **2**, 187–214 (2009).
42. D. T. Snyder, C. J. Pulliam, Z. Ouyang, R. G. Cooks, *Anal. Chem.* **88**, 2–29 (2016).
43. S. Rankin-Turner, L. M. Heaney, W. H. Fein, *Anal. Sci. Adv.* **2**, 193–212 (2021).
44. X.-Y. Y. Guo *et al.*, *Chinese J. Anal. Chem.* **47**, 335–346 (2019).
45. S. R. Kumbhani, L. M. Wingen, V. Perraud, B. J. Finlayson-Pitts, *Rapid Commun. Mass Spectrom.* **31**, 1659–1668 (2017).
46. E. Sokol, R.J. Noll, R.G. Cooks, L.W. Beegle, H.I. Kim, I. Kanik, *Int. J. Mass Spectrom.* **306**, 187–195 (2011).
47. G. A. Gomez-Rios, T. Vasiljevic, E. Gionfriddo, M. Yu, J. Pawliszyn, G.A. Gómez-Ríos, T. Vasiljevic, E. Gionfriddo, M. Yu, J. Pawliszyn, *Analyst*. **142**, 2928–2935 (2017).
48. M. H. Blokland, A. Gerssen, P. W. Zoontjes, J. Pawliszyn, M. W. F. Nielsen, *Food Anal. Methods*. **13**, 706–717 (2019).
49. S. Jafari, J. Guercetti, A. Geballa-Koukoulou, A.S. Tsagkaris, J.L.D. Nelis, M.-P. Marco, J.-P. Salvador, A. Gerssen, J. Hajslova, C. Elliott, K. Campbell, D. Migliorelli, L. Burr, S. Generelli, M.W.F. Nielsen, S.J. Sturla, *Foods*. **10**, 1399 (2021).
50. J. G. van der Gugten, *Clin. Mass Spectrom.* **15**, 36–43 (2020).
51. P. Aqai, E. Cevik, A. Gerssen, W. Haasnoot, M. W. F. Nielsen, *Anal. Chem.* **85**, 3255–3262 (2013).
52. J. Hollender, B. van Bavel, V. Dulio, E. Farmen, K. Furtmann, J. Koschorreck, U. Kunkel, M. Krauss, J. Munthe, M. Schlabach, J. Slobodnik, G. Stroomberg, T. Ternes, N.S. Thomaidis, A. Togola, V. Tornero, *Environ. Sci. Eur.* **31**, 1–11 (2019).
53. M. Kunzelmann, M. Winter, M. Åberg, K.E. Hellenas, J. Rosen, M. Åberg, K.E. Hellenäs, J. Rosén, *Anal Bioanal Chem.* **410**, 5593–5602 (2018).
54. L. Righetti, T. Damiani, E. Rolli, G. Galaverna, M. Suman, R. Bruni, C. Dall'Asta, *Phytochemistry*. **170**, 112194 (2020).
55. A. Narváez, L. Castaldo, L. Izzo, N. Pallarés, Y. Rodríguez-Carrasco, A. Ritieni, *Food Control*. **132**, 108521 (2022).
56. S. Rogstad, A. Faustino, A. Ruth, D. Keire, M. Boyne, J. Park, *J. Am. Soc. Mass Spectrom.* **28**, 786–794 (2017).
57. F. Zubair, *Drug Discov. Today Technol.* **40**, 29–35 (2021).
58. W. S. Sawyer, N. Srikumar, J. Carver, P.Y. Chu, A. Shen, A. Xu, A.J. Williams, C. Spiess, C. Wu, Y. Liu, J.C. Tran, *Proc. Natl. Acad. Sci. U. S. A.* **117**, 9851–9856 (2020).
59. M. Källsten, R. Hartmann, K. Artemenko, S.B. Lind, F. Lehmann, J. Bergquist, *Analyst*. **143**, 5487–5496 (2018).
60. J. Chen, S. Yin, Y. Wu, J. Ouyang, *Anal. Chem.* **85**, 1699–1704 (2013).
61. A. J. R. Heck, *Nat. Methods* **5**, 927–933 (2008).
62. A. Murisier, B.L. Duivelshof, S. Fekete, J. Bourquin, A. Schmudlach, M.A. Lauber, J.M. Nguyen, A. Beck, D. Guilleme, V. D'Atri, *J. Chromatogr. A*. **1655**, 462499 (2021).
63. U. Kalsoom, P. N. Nesterenko, B. Paull, *TrAC*. **105**, 492–502 (2018).
64. P. Agrawal, J. G. Reifemberger, K. D. Dorfman, *ACS Omega*. **5**, 20817–20824 (2020).
65. C. T. Tracey, A. L. Predeina, E. F. Krivoschapkina, E. Kumacheva, *Trends Food Sci. Technol.* (2022).

66. G. M. S. Ross, D. Filippini, M. W. F. Nielen, G. I. Salentijn, *Anal. Chim. Acta.* **1140**, 190–198 (2020).
67. A. Jadhav, V. S. Jadhav, *Mater. Today Proc.* (2022).
68. T. Liu, S. Chen, K. Ruan, S. Zhang, K. He, J. Li, M. Chen, J. Yin, M. Sun, X. Wang, Y. Wang, Z. Lu, H. Rao, *J. Hazard. Mater.* **426**, 128091 (2022).
69. D. Calabria *et al.*, *Sensors Actuators B Chem.* **305**, 127522 (2020).
70. A. Roda, M. Mirasoli, M. Guardigli, P. Simoni, M. Zangheri, P. Severi, C. Caliceti, A. Roda, *Anal. Chem.* **86**, 7299–7304 (2014).
71. K. Pumpa, M. Lacorn, M. Mättner, D. Steinmann, J. Wolf, *J. AOAC Int.* **104**, 49–52 (2021).
72. Statista, Penetration rate of smartphones in selected countries 2020, (available at <https://www.statista.com/statistics/539395/smartphone-penetration-worldwide-by-country/>).
73. Statista, Number of smartphone users from 2016 to 2021, (available at <https://www.statista.com/statistics/330695/number-of-smartphone-users-worldwide/>).
74. J. L. D. Nelis, A. S. Tsagkaris, M. J. Dillon, J. Hajslova, C. T. Elliott, *TrAC*. **129**, 115934 (2020).
75. G. Rateni, P. Dario, F. Cavallo, *Sensors*. **17**, 1453 (2017).
76. Y. Zhao, S.Y. Choi, J. Lou-Franco, J.L.D. Nelis, H. Zhou, C. Cao, K. Campbell, C. Elliott, K. Rafferty, *Proc. IEEE Sensors*. (2019).
77. X. Huang, D. Wang, B. He, Q. Liu, L. Hu, G. Jiang, *Chem. Commun.* **56**, 1637–1640 (2020).
78. M. M. Wang, P. Laborda, L.P. Conway, X.C. Duan, K. Huang, L. Liu, J. Voglmeir, *Carbohydr. Res.* **433**, 14–17 (2016).
79. M. Tascon, V. Singh, M. Huq, J. Pawliszyn, *Anal. Chem.* **91**, 4762–4770 (2019).
80. G. Scotti, S.M.E. Nilsson, V.P. Matilainen, M. Haapala, G. Boije af Gennäs, J. Yli-Kauhaluoma, A. Salminen, T. Kotiaho, *Heliyon*. **5**, 1–7 (2019).
81. F. Li, M.R. Ceballos, S.K. Balavandy, J. Fan, M.M. Khataei, Y. Yamini, F. Maya, *J. Sep. Sci.* **43**, 1854–1866 (2020).
82. M. Grajewski, M. Hermann, R. D. Oleschuk, E. Verpoorte, G. I. Salentijn, *Anal. Chim. Acta.* **1166**, 338332 (2021).
83. S. Waheed, J.M. Cabot, N.P. Macdonald, T. Lewis, R.M. Guijt, B. Paull, M.C. Breadmore, *Lab Chip*. **16**, 1993–2013 (2016).
84. Z. Ouyang, *LCGC North Am.* **23**, 104–112 (2014).
85. C. J. Pulliam, R. M. Bain, J. S. Wiley, Z. Ouyang, R. G. Cooks, *J Am Soc Mass Spectrom.* **26**, 224–230 (2015).
86. M. Song, X. Lin, Z. Peng, S. Xu, L. Jin, X. Zheng, H. Luo, *Front. Mater.* **7**, 438 (2021).
87. Y. Jung, J. Y. Jeong, B. H. Chung, *Analyst*. **133**, 697–701 (2008).
88. M. A. Morales, J. M. Halpern, *Bioconjug. Chem.* **29**, 3231–3239 (2018).
89. S. Rebe Raz, W. Haasnoot, *TrAC Trends Anal. Chem.* **30**, 1526–1537 (2011).
90. L. Anfossi, F. Di Nardo, S. Cavallera, C. Giovannoli, C. Baggiani, *Biosensors*. **9**, 2–19 (2019).
91. M. K. Araz, A. M. Tentori, A. E. Herr, *J. Lab. Autom.* **18**, 350–366 (2013).
92. T. Guan, Z. Xu, J. Wang, Y. Liu, X. Shen, , *Compr. Rev. Food Sci. Food Saf.* **21**, 1627–1656 (2022).
93. N. An, K. Li, Y. Zhang, T. Wen, W. Liu, G. Liu, L. Li, W. Jin, *Talanta*. **231**, 122361 (2021).
94. J. Zhou, Q. Qi, C. Wang, Y. Qian, G. Liu, Y. Wang, L. Fu, *Biosens. Bioelectron.* **142**, 111449 (2019).
95. A. Azzouz, L. Hejji, K.H. Kim, D. Kukkar, B. Souhail, N. Bhardwaj, R.J.C. Brown, W. Zhang, *Biosens. Bioelectron.* **197**, 113767 (2022).
96. S. Kanchi, M. I. Sabela, P. S. Mdluli, Inamuddin, K. Bisetty, *Biosens. Bioelectron.* **102**, 136–149 (2018).
97. N. A. Maher, J.T. Senders, A.F.C. Hulsbergen, N. Lamba, M. Parker, J.P. Onnela, A.L. Bredenoord, T.R. Smith, M.L.D. Broekman, *Int. J. Med. Inform.* **129**, 242–247 (2019).
98. C. W. Klampfl, M. Himmelsbach, *Anal Chim Acta.* **890**, 44–59 (2015).







**Summary**





## Summary

Shifts in socioeconomic, environmental, and ethical issues shape the monitoring methods of the future because they could increase in the need for confirmatory analysis from official routine laboratories. To cope with this increased demand, alternative approaches are developed, which combine modified versions of screening and confirmation technologies conventionally used in food safety-related protocols in EU regulatory settings. First, modified bioassays based on monoclonal antibodies (mAbs) were crafted to replace the conventional screening by providing a biorecognition-based isolation. Second, ambient ionization mass spectrometry (AIMS) is used in the place of the cumbersome processes involved with liquid or gas chromatography-tandem mass spectrometry (LC- or GC- MS/MS) employed as classic confirmatory analysis. Integrating biorecognition to AIMS leads to an increase in selectivity, making the techniques of potential use in future regulatory settings. This framework of the thesis is explained in more details in **Chapter 1** after introducing the relevant information on the techniques used in the thesis.

In **Chapter 2**, the development of an identification lateral flow immunoassay (ID-LFIA) is presented in combination with high resolution mass spectrometry (hrMS). The ID-LFIA, i.e., a custom-made LFIA consisting of multi-lines of mAb that acts as a biorecognition trapping zone, was an ingenious way of dealing with the immunoassay buffers that are non-compatible with electrospray ionization (ESI) MS. The ID-LFIA targets the mycotoxin deoxynivalenol (DON) giving rise to high societal importance of the approach, because of the relevance of monitoring DON in food safety-related schemes. For the analysis, DON is retrieved from the mAb with a dissociation solution, which is subsequently analyzed with ESI-hrMS to rapidly confirm the presence of DON and any cross-reacting species.

In **Chapter 3**, the newly introduced ID-LFIA was further combined with direct analysis in real time (DART) ionization triple quadrupole MS/MS, demonstrating that alterations in the setup lead to ionization of different analytes, not detectable with the previous setup. Meanwhile, the validation of the developed approach demonstrates the fitness-for-purpose. In the proposed workflow, an individual performs the (on-site) smartphone LFIA screening, and when the result is suspect, an ID-LFIA is developed with the same sample extract, thereby removing the need for additional sample preparation. In the setups of **Chapters 2 and 3**, the biorecognition and dissociation are performed offline, and then the isolated analyte is ionized and detected with MS.

For the following approach in **Chapter 4**, namely immuno-enriched paramagnetic microspheres magnetic blade spray (iMBS), the biorecognition is performed offline, but the dissociation, ionization, and MS detection are performed online. Coated blade spray (CBS) as an AIMS technique allows for easy-to-use, high throughput analysis, but it lacks specificity for unequivocal identification according to the EU regulation. In iMBS the coating of CBS is replaced with highly specific mAb, by using immuno-enriched paramagnetic microspheres conventionally used in screening planar array immunoassays. In the workflow, a neodymium supermagnet is used to secure

the microspheres on the stainless steel blade, and dissociation, ionization, and MS/MS detection, lead to a highly specific and reproducible method.

Despite the advantages of the iMBS, the requirement of an extensive covalent mAb immobilization is a limitation, which, is addressed at the final approach of immunoaffinity blade spray (iBS). In iBS described in **Chapter 5**, the generic coating used in CBS is replaced by a layer of highly specific mAb, while the stainless steel is replaced with conductive polystyrene to allow for simple physical adsorption of mAb. With iBS, biorecognition, dissociation, and ionization are performed on the same surface (online), leading to a potential high throughput method. The presented approaches improve the selectivity of AIMS while eliminating confirmatory methods' more significant drawback; extensive sample preparation for analyte isolation and time-consuming chromatographic separation. The novel integrated biorecognition - mass spectrometry approaches have application in food safety contaminant detection and potential application in a variety of fields.

**Chapter 6** provides a general discussion on the results obtained in **Chapters 2-5** in retrospect of the points introduced in **Chapter 1**, and also includes future perspectives and suggestions for further research, also supported by preliminary data.

## **Acknowledgments**







## Acknowledgments

So far, this thesis highlights the scientific path of my PhD studies. However, this path was carved not only by science but also by many people I came across during those years of research. So, it is important to thank all those who made this journey special with their support, motivation, help, and friendship. When I started this journey four years ago, I was anticipating the time I would start writing the acknowledgments. Now that I am actually writing, the feeling is bittersweet as this part signifies the end.

To begin, I have to thank my promotor, **Michel Nielen**. The opportunity to collaborate and learn a lot from an expert in the field of Analytical Chemistry has been the most valuable lesson of my PhD journey. Our communication had been a bumpy road; you pushed me a lot and made me question what I knew, but in the end, you made me an improved version of my scientific self. During those years, I learned to appreciate your directness, guidance, and even your Dutch humor, which I will certainly miss. Next in line is, admittedly, my co-promotor, **Arjen Gerssen**. The first time we met during my interview for the PhD position, I thought, "wow! He's awake at 4 am while in the USA for a conference to interview me? What a dedication!". And I was not wrong... This dedication was your main characteristic; working late hours but always being open for a chat somewhere in between meetings! I learned a lot from your professionalism. I will never forget the discussions we had, both scientific and more personal, and your support when I was undertaken by the pressure of reaching the end of my PhD.

Also, **Gert IJ Salentijn**, apart from being an outstanding scientist, you have been a great company in the office. I have to admit that I secretly self-declared you my third supervisor. You never refused giving me a piece of advice, or help, and I am grateful for that! Thank you for provoking interesting discussions on every topic and for never thinking badly of the weird way I express myself. I will never understand your (bad) jokes, but I will always laugh at how proud you are of those. Speaking of (bad) jokes, another person comes to mind... **Marco Blokland**. You always put a smile on my face, even during a difficult day. Thank you for your significant input during our weekly meetings, your help with the experiments, and our overall interaction.

I wish you all enjoyed our collaborations, as I did... I will be glad to collaborate again in the future!

To my beloved paranymphs and closest friends:

**Clementina Vitali** and **Anouk Bosman**; I'm delighted to see you both making fantastic progress, and I am glad to have you by my side on the day of my defense! **Clementina**, when you joined WFSR, it was a breeze! Finally, a Mediterranean PhD candidate at WFSR with a similar mentality on hospitality, appreciation for tasty food, funny and approachable to make me feel at home. I will always cherish the fun we had trying to pronounce the Dutch GGGGGGG, in our failed attempt to learn the Dutch language. Thank you for being my paranymph, and apologies that I couldn't find a

## Acknowledgments

relevant SOP for this assignment. **Anouk**, I really admire your confidence and honesty. Sharing an office with you has been one of my drives for coming to work because I was sure that I would have an enjoyable time. Your joyful and upbeat personality made me appreciate our time in and out of the office. I am happy to see your fast scientific growth during our latest co-authorship and I wish you only the brightest future.

**Yao Zhou**. Thank you for your kind words, for pushing me for excellence, and for your magic touch with the TQ-XS. You taught me Chinese food and culture, and I miss you too much! I wish I could have you near me to celebrate after my defense. You are a sincerely kind-hearted person, always eager to help, and I am happy to be your friend. I look back at the photos from our excursion at Maastricht with great content. I hope you achieve all your goals and aspirations because you truly deserve it!

To my Turkish crew: **Sevil Şahin**, **Fatima Akin**, and **Canan Aksoy**. I greatly appreciate you not talking in your native language despite me being the only non-Turkish-speaking person in the group. Even though I met each of you under different time frames and conditions, we quickly bonded and enjoyed dinners of endless laughter. **Sevil**, you are the most endearing person I know, and simultaneously you are a good scientist, doing great at your defense and excelling during your post-doc. Truly inspirational! Also, thank you for being my go-to person for the technicalities during the thesis submission. **Fatma**, I was miserable about losing another friend from Wageningen because of stupid bureaucracies, so I was thrilled that you managed to stay! You are a true fighter, never losing your smile or giving up, despite any difficulty. Your positive vibes are enough to make me forget my insignificant problems. **Canan**, I enjoy every conversation with you. You are very open and honest, and I appreciate your sense of humor. Thank you for inviting me to your wedding, despite receiving a nasty present afterward – my first COVID-19 infection. You are doing very well in your PhD, so keep up the hard work!

To my friends from WFSR:

**Fatima Lakraoui**, with your kind personality and vibrant smile, thank you for always being there for me to whine and vent. You, **Etsuko Nakashima**, **Lieke van Meijer**, **Ningjing Liu**, and **Ashraf Intersaaf** had been the perfect company throughout my first year, from sushi eating to squash playing. **Anand Gavai**, thank you for your support when everything felt like it was failing, and you were there to tell me that it's not the end of the world. Your support and advice transformed my perspective on things I consider too complicated. **Joost Memelink**, **Eelco Sijtsma**, and **Arnoud Langen** thank you for making my first months in the lab fun and memorable! **Suzann Ludwig**, thank you for the brainstorming session that inspired the latest project I worked on. Our conversations during the monthly meetings were always exciting and motivating. **Ane Arrizabalaga-Larrañaga**, **Nico Grimblat**, **Clementina Vitali**, and **Serena Rizzo**, thank you for the 4-hour "dinner" during which we discussed all my propositions (that were later discarded by my promotor).

Moreover, many thanks to the wonderful **team of Bioassays and Biosensor - BB** (i.e., my new WFSR home). Since immunoassays have been a critical part of my PhD, working closely with this team was educational and reassuring. **Gina Ross**, I first met you during my 3<sup>rd</sup> round of interviews in Wageningen. Then, I was sure I would have a great, easy-going PhD buddy. Thank you for the help during my first year, especially regarding the countless EU reports and WFSR paperwork. I will never forget our time of endless banter. Thank you for choosing me as your paranymp, and best of luck with all your future endeavors. **Nathalie Smits** and **Jeroen Peters**, thank you for always having your office door open to ask anything I needed; antibodies, samples, and scientific questions. I was excited to attend your defense and see you gain this well-desired and deserved doctorate title. Also thank you for helping me with the numerous questions I had during the submission of my thesis. **Toine Bovee**, thank you for welcoming me to your team and allowing me to transfer the knowledge I obtained during my PhD and grow even further by learning even more! **Liza Portier**, **Richard van Hoof**, **Astrid Hamers**, and **Alexander Elferink**, thank you for the pleasant environment in the lab. **Linda Willemsen**, **Erik Beij**, **Qiofeng Li**, **Xiaodi Hong** and **Yoran Weide**, thank you for the lovely time in and after work (trying to escape a crazy farmer, among others). Special thanks to **Erik Beij** for helping me during a very stressful time with my thesis scan! Finally, to previous members of the BB group that have been great companions during my PhD trajectory and helped me adjust quickly to a new environment, thank you, **Vangela Xu Mang**, **Esmee van den Bossche**, **Adil Bouslim**, and **Ben Potter**. **Vangela**, I will never forget the endless fun we had during the countless dinners you organized at your place. **Esmee**, thank you, among others, for showing me a glimpse of Dutch culture by playing the Sinterklaas dice game.

### To my FoodSmartphone peers:

Having the opportunity to participate in an EU-funded H2020 project was a lifetime achievement and an unforgettable experience. This experience would not have been possible without the people behind this project. The coordinator, **Michel Nielsen** and the project secretaries **Wim Beek** and **Ingeborg van Leeuwen-Bol** for organizing everything and reminding us of deadlines. Thanks to all the project partners from **WFSR**, **QUB**, **UCT**, **CSIC**, **LIU**, **Aquamarijn**, **CSEM**, **Barilla** and **Zeulab** for the great organizations of summer schools, conferences, and the overall collaborations. Special thanks to **Katrina Campbell** and her lab for providing me with the antibodies used in the 4<sup>th</sup> chapter of my thesis, and to **Chris Elliott**, for the collaboration during publications. To **all FoodSmartphone ESRs**: it is delightful to see most of you already completing this challenging chapter by getting your doctorate. Thank you for the shared time during our project meetings, well... basically after the meetings with the dinners and drinks! Especially **Klaudia Kopper**, **Julian Guercetti** and **Javier Lou Franco**; thank you for the awesome 2-day exploration of Prague...

### To my ORC network:

Finally, looking back, I want to thank all **ORC people: academic and non-academic staff and PhDs**. Despite not seeing my face every day, thank you all for the

## Acknowledgments

welcoming environment at ORC. It was a great opportunity to present my work to you in Monday morning seminars. **Han Zuilhof, Hans-Gerd Janssen, Maurice Franssen** and **Fedor Miloserdov** thank you for your feedback during those Monday morning seminars. My deepest appreciation goes to **Frank Claassen** - your enormous patience with me and all the MS troubleshooting was valuable. It is true what they say that technicians are the ones holding the lab together. **Sidharam (Sidu) Pujari**, thank you for providing me with the SEM imaging used in chapter 4 of my thesis.

Moreover, many thanks to all of my fellow ORC PhDs, who had made this journey an enjoyable experience, especially with the laughing until tears at the "LFOTM" drinks. During Monday morning seminars, I felt overwhelmed (at best) with all your fancy chemistry. Still, I appreciate you coming to my elementary presentations, asking questions, and providing me with valuable input, despite the non-organic chemistry-related project I was working on. Thank you all!

To the previous PhD fellows, and now Drs; **Jorick Bruins, Jordi Keijzer, Ian de Bus, Esther Roeven, Pepijn Beekman**, and **Milou Santbergen**; seeing your hard work and the satisfying end result was extra motivational. **Freddie van Geenen**, thank you for your help with the MS at the beginning of my PhD. **Alice Guarneri**, you are a lovely person who always made me feel comfortable when you were around. I hope you always keep smiling. **Andriy Kuzmyn**, I got to know you better during our FoodSmartphone trip to Belfast, and ever since, I feel we have grown to be friends. Thank you for accepting me as I am, you "cool kid"... **Kaustub Singh**, I remember first meeting you - well, I remember you scarring me - an evening at Helix around 9 pm, when I thought the building was empty. It didn't take us long to appreciate each other's weird sense of humor, which I will never forget from our shared time.

Also, the guys that we started our PhD journeys almost the same time, **Allysa van den Boom, Ellen Dautzenberg, Sybren Schoustra, Lucas Teunissen**, and **Jay Gamaethiralalage**; we shared the same struggles and worries, especially during this last year, and I am looking forward to seeing you defend your thesis. Thank you for all the moments of laughter and fun! **Si Huang**, it was a pleasure to spend more time with you during RAFA 2022, during which I got to appreciate your humor and kind personality even more! **Michel de Haan**, I had a fantastic time roaming around Athens with you and Kylie. ORC has not been the same ever since you left...

Finally, I wish the best of luck to the "next generation" of Drs; **Daniele Chinello, Natassa Lional, Irene Shajan, Boudewijn Hollebrands, Bas Scheepmaker, Jasper van de Sande** and **Xuecong Li**, which I got to know better during my visits at ORC, lunch and coffee breaks, and boardgame-playing dinners. **Julian Engelhardt**, I look forward to your defense with a party similar to that on 24.06.2022 (and you wearing similar attire). **Stijn Pauluma**, thank you for helping me with my questionnaire for the anti-doping project. Much appreciated.

Thanks to **VLAG** for supporting all PhDs and helping me with my TSP submission during one of the many stressful breakdowns I had when reaching the end of my PhD.

Lastly, my sincere appreciation goes to the **scientific committee** for accepting to evaluate the entirety of my thesis.

### To my family:

Ending the acknowledgments, I would like to devote this thesis to my **family**; without their support, I wouldn't be able to achieve this goal of mine.

**Χαλήλ** ή μάλλον **Dr. Χαλήλ**... Είμαι η περήφανη μικρή σου αδερφή. Είμαι χαρούμενη που μοιραστήκαμε αυτό το ταξίδι την ίδια περίοδο, και είχαμε τις ίδιες ανησυχίες, τις ίδιες δυσκολίες και συναγωνιζόμασταν ποιος περνάει πιο δύσκολα. Σε ευχαριστώ για όλη την συμπαράσταση, τις συμβουλές, και όλες τις φορές που με πήρες τηλέφωνο απλά για να δεις πως είμαι (και καταλήγαμε να μιλάμε 2 ώρες). Επίσης, **μαμά, μπαμπά**, σας ευχαριστώ για την υποστήριξη και που πάντα πιστεύετε σε μένα. Σας ευχαριστώ που με εμψυχώσατε να έρθω στην Ολλανδία, όσο τρομακτικό και αν φαινόταν στην αρχή. Δεν θα ήμουν εδώ χωρίς εσάς. Ακόμα και όταν αναγκάστηκα να λείψω από την καθιερωμένη Δεκεμβριανή επίσκεψή μου λόγω των πειραμάτων, δεν με αποθαρρύνετε, αλλά ήσασταν δίπλα μου. **Θεία** μου, δεν θα ξεχάσω την επίσκεψή σου τον πρώτο χρόνο που ήμουν στην Ολλανδία. Είδαμε όμορφα μέρη, και με παρότρυνες να συνεχίσω να εξερευνώ την Ολλανδία όσο περισσότερο μπορώ. Σε ευχαριστώ για την συνεχή ερώτηση "και αυτό που κάνεις τώρα που μπορείς να το εφαρμόσεις", γιατί υπήρξε κινητήρια ώθηση στο να αποφασίσω με τι θέλω να ασχοληθώ περαιτέρω επαγγελματικά.

Finalement, la meilleure chose qui me soit arrivée, depuis que je me suis installé à Wageningen, a été de te rencontrer, **Osseni**. Tu es la personne la plus intelligente et la plus attentionnée que je connaisse. Un mot de cinq lettres serait trop court pour décrire ce que mon cœur ressent pour toi. T'avoir à 6000 km de distance a été l'une des plus grandes épreuves que j'ai subies pendant mon parcours de doctorat, alors, merci d'avoir cru en nous... Merci d'avoir cru en moi! Pour m'avoir soutenu et encouragé, même lorsque je manquais de confiance en moi. Je te transmets mes profondes gratitude, non seulement pour les innombrables heures où tu m'as aidé à préparer et à m'entraîner mes présentations, mais aussi pour tes conseils dans les moments où le doute a envahi mes sentiments et pensées. Ce genre de soutien était tout ce dont j'avais besoin, et je sais que c'est vrai quand je dis que ça n'aurait pas été pareil sans toi dans ma vie.



**Curriculum Vitae**







## Curriculum Vitae

Ariadni Geballa-Koukoula was born and raised in Athens, Greece. In 2010, she started a 5-year integrated master program in the School of Pharmacy at University of Athens (UoA), supported by a competitive scholarship. This program included a one-year internship, and a 6-month experimental thesis, which she conducted in the field of pharmaceutical nanotechnology. Having received her degree, she pursued postgraduate studies in UoA to further expand her knowledge into the more specialized field of “pharmaceutical analysis and quality control”. In the meantime, she received the professional pharmacist license. For her M.Sc. thesis, she handled HPLC-ESI-MS for the quantification of metronidazole and fluconazole in human breast milk and contributed to ongoing projects in the laboratory of pharmaceutical analysis. Ariadni excelled her M.Sc. studies, and afterwards, she was enrolled as a PhD candidate of the Marie Skłodowska-Curie Actions (MSCA) FoodSmartphone project. The objective of her project was the development of methods that combine biorecognition-based isolation, and direct mass spectrometry analysis, with an application on the detection of food contaminants. Results obtained from this research are presented in this thesis. Since 2022, Ariadni has been employed as a researcher by Wageningen Food Safety Research in the Bioassays & Biosensors group.

## List of Publications

- **Geballa-Koukoula, A.**, Gerssen, A., Blokland, M. H. & Nielen, M. W. (2022). Immunoaffinity Blade Spray Mass Spectrometry. *Journal of the American Society for Mass Spectrometry*. <https://doi.org/10.1021/jasms.2c00149>.
- **Geballa-Koukoula, A.**, Gerssen, A., Blokland, M. H., Elliott, C. T., Pawliszyn, J., & Nielen, M. W. (2021). Immuno-Enriched Microspheres - Magnetic Blade Spray-Tandem Mass Spectrometry for Domoic Acid in Mussels. *Analytical Chemistry*, 93(47), 15736–15743. <https://doi.org/10.1021/acs.analchem.1c03816>
- **Geballa-Koukoula, A.**, Gerssen, A., & Nielen, M.W.F. (2021). From Smartphone Lateral Flow Immunoassay Screening to Direct MS Analysis: Development and Validation of a Semi-Quantitative Direct Analysis in Real-Time Mass Spectrometric (DART-MS) Approach to the Analysis of Deoxynivalenol. *Sensors*, 21(5), 1861. <https://doi.org/10.3390/s21051861>
- Jafari, S., Guercetti, J., **Geballa-Koukoula, A.**, Tsagkaris, A. S., Nelis, J. L. D., Marco, M. P., Salvador, J. P., Gerssen, A., Hajslova, J., Elliott, C., Campbell, K., Migliorelli, D., Burr, L., Generelli, S., Nielen, M. W. F., & Sturla, S. J. (2021). ASSURED Point-of-Need Food Safety Screening: A Critical Assessment of Portable Food Analyzers. *Foods*, 10(6), 1399. <https://doi.org/10.3390/foods10061399>
- **Geballa-Koukoula, A.**, Gerssen, A., Nielen, M.W.F. (2020). Direct analysis of lateral flow immunoassays for deoxynivalenol using electrospray ionization mass spectrometry. *Analytical and Bioanalytical Chemistry*. 412 (27), 7547-7558. <https://doi.org/10.1007/s00216-020-02890-4>

- **Geballa-Koukoura, A.**, Panderi, I., Zervas, K., Geballa-Koukoulas, K., Kavvalou, E., Panteri-Petratou, E., Vourna, P., Gennimata, D. (2018). A porous graphitized carbon LC-ESI/MS method for the quantification of metronidazole and fluconazole in breast milk and human plasma. *Journal of Chromatography B*. 1084, 175-185. <https://doi.org/10.1016/j.jchromb.2018.03.034>
- Machairas, G., Panderi, I., **Geballa-Koukoura, A.**, Rozou, S., Antonopoulos, N., Charitos, C., Vonaparti, A. (2018). Development and validation of a hydrophilic interaction liquid chromatography method for the quantification of impurities in fixed-dose combination tablets containing rosuvastatin and metformin. *Talanta* 183, 131-141. <https://doi.org/10.1016/j.talanta.2018.02.068>
- **Geballa-Koukoura, A.**, Geballa-Koukoulas, K., Vourna, P., Gennimata, D., Panderi, I. (2018). Medication and breastfeeding: Compatibility and Concerns. *Pharmakeftiki* 30(2), 64-75. [ISSN: 1105-4999](#)



## **Overview of Completed Training Activities**



## Overview of Completed Training Activities

Discipline Specific Activities	Organizer	Year
NVMS fall meeting - Bioanalysis	NVMS	2019
Advanced Food Analysis	VLAG	2019
NVMS-BSMS international congress on Mass Spectrometry	NVMS-BSMS	2019
FAST - Forum for Analytical Science and Technology	Ti-COAST	2019
Summer School on Software Design and FoodSmartphone Exploitation*	QUB, CSEM, ZEU, Aquamarijn	2019
9 <sup>th</sup> International symposium on Recent Advances in Food Analysis (RAFA2019) *	UCT, WUR	2019
Final FoodSmartphone Network Conference - Smart tech for food*	CSIC (Nb4D)	2020
Workshop - Threats to our food system	QUB	2021
Advanced Organic Chemistry (AOC)	ORC research group	2021
American Society for Mass Spectrometry (ASMS) Annual Conference*	ASMS	2021
13 <sup>th</sup> Rapid Methods Europe (RME 2021) - Rapid Analysis & Diagnostics	WUR	2021
FAST - Forum for Analytical Science and Technology*	Ti-COAST	2021
European Forum on Analytical Sciences and Technology (EuroFAST) 2022	COAST, KNCV, SAC, EuChemS	2022
World Mycotoxin Forum virtual preconference on Analysis*	QUB, BOKU, Barrilla	2022
International Mass Spectrometry Conference (IMSC) 2022*	IMSF	2022
10 <sup>th</sup> International symposium on Recent Advances in Food Analysis (RAFA2022) *	UCT, WUR	2022
e-NVMS meeting: 10-minute pitches by PhD students*	NVMS	2022
General Courses	Organizer	Year
Presenting with Impact	WGS	2019
VLAG PhD week	VLAG	2019
Brain Training	WGS	2019
Efficient Writing Strategies	WGS	2019
Project and Time Management	WGS	2019
Scientific Artwork - Vector Graphics and Images	WUR Library	2019
Competence Assessment	WGS	2020

(Continued on next page)

## Training Activities

General Courses	Organizer	Year
Industrial Business Training	Barilla	2020
Searching and organizing literature for PhD candidates	WUR Library	2020
Scientific Writing	WGS	2020
How to present online	VLAG	2021
Reviewing a Scientific Manuscript	WGS	2021
Writing Grant Proposals	WGS	2022

Other Activities	Organizer	Year
Preparation of research proposal	ORC	2018
Weekly group meetings*	ORC	2018- 2022
BU & EG meetings of WFSR*	WFSR	2018- 2022
MSCA Falling walls lab*	Falling Walls Foundation	2019
Ethical Aspects of Research	CSIC (Nb4D)	2019
LabAnalyse*	FHI Laboratorium Technologie	2022

*\*oral presentation*





The research described in this thesis was funded by the European Union's Horizon 2020 research and innovation program under the Marie Skłodowska-Curie grant agreement No 720325.

Financial support from Wageningen Food Safety Research for printing this thesis is gratefully acknowledged.

Cover design and layout by Ariadni Geballa-Koukoula

Printed by proefschriftenprinten.nl



